

**Multiplexed Mass Spectrometric Approaches for Protein
Cross-linking Analysis and Protein Functional Studies**

by

Bo Wang

**A dissertation submitted in partial fulfillment
of the requirements for the degree of
Doctor of Philosophy
(Chemistry)
in The University of Michigan
2010**

Doctoral Committee:

**Associate Professor Kristina I. Håkansson, Chair
Professor David M. Lubman
Professor Michael D. Morris
Associate Professor Anna K. Mapp**

Copyright. Bo Wang

2010

To my parent, my wife, and my son

Acknowledgments

First I would like to express my greatest appreciation to my advisor Professor Kristina Håkansson, whose guidance, encouragement, and support make this thesis possible. Her passion for scientific research always inspires me. I also would like to thank my committee members, including Professor David Lubman, Professor Anna Mapp, and Professor Michael Morris, for the extremely valuable advice and guidance for my study.

My sincerely gratitude goes to all former and current members in Håkansson's group: Haichuan, Jason, Hye Kyong, Jiong, Julie, Natasa, Jingjie, Liping, Hyun Ju, Wen, Hangtian, Chris, Yibing, Ashley, Di, and Ning for the precious help and support.

I would like to thank all my collaborators: Professor Anna Mapp, Dr. Chinmay Majmudar, Professor Philip Andrews, and Billy Clifford-Nunn in Department of Chemistry, Professor David Sherman, Professor Janet Smith, Dr. Gu Liangcai, and Dr. Dheeraj Khare in Life Science Institute for the wonderful collaborations, encouragement, and thought-provoking discussions.

I am grateful for one-term dissertation fellowship from Rackham Graduate School at University of Michigan and teaching assistantship from Department of Chemistry at University of Michigan.

Last, but most importantly, I would like to thank my parents for the continuous and unconditional support. I like to express my deepest gratitude to my beloved wife, Yanni, for her love, care and support.

Table of Contents

Dedication-----	ii
Acknowledgments -----	iii
List of Tables -----	xii
List of Figures-----	xiii
List of Schemes -----	xxiv
Abstract -----	xxv

Chapter

1. Introduction-----	1
1.1 Chemical Cross-linking and Mass Spectrometry -----	1
1.1.1 Mass Spectrometry for Protein Analysis-----	1
1.1.2 Combining Chemical Cross-linking with Mass Spectrometry for Protein Structural and Protein-protein Interaction Analysis -----	3
1.1.3 Reactive Groups of Chemical Cross-linkers-----	5
1.1.4 Modifications of Chemical Cross-linkers -----	10

1.1.5	Other Methods to Facilitate the Detection of Cross-linked Products -----	13
1.2	Fourier Transform Ion Cyclotron Resonance Mass Spectrometry (FT-ICR MS)-----	
	-----	15
1.2.1	The Basic Theory of FT-ICR MS -----	15
1.2.2	FT-ICR Instrumentation -----	17
1.3	Tandem Mass Spectrometry (MS/MS) -----	23
1.3.1	CID and IRMPD: Slow Heating Methods to Produce Fragmentation-----	23
1.3.2	ECD, ETD, and EDD: Radical-driven Fragmentation Techniques -----	27
1.4	Application of FT-ICR MS to Investigate Natural Product Biosynthetic Pathways--	
	-----	31
1.4.1	Natural Product Biosynthesis by NRPS and PKS Catalysis -----	31
1.4.2	The Role of FT-ICR MS in Investigating NRPS and PKS Biosynthesis-----	32
1.5	Dissertation Overview -----	33
1.6	References-----	37
2.	Photo-cross-linking and Complementary Use of ESI and MALDI Mass	
	Spectrometry to Map Interaction Sites between Transcriptional Activators and	
	Mediator 15 -----	53
2.1	Introduction -----	53

2.2	Experimental-----	58
2.3	Results and Discussion -----	59
2.3.1	Identified Binding Sites between Med15 and Gcn4/Gal4/VP2 -----	59
2.3.2	Gas-phase cleavage of Bpa photo-crosslinker in MALDI TOF/TOF CID-----	73
2.4	Summary -----	74
2.5	References-----	75

3 Gas-Phase Cleavage of Sulfur-Sulfur and Sulfur-Carbon Bonds in Tandem

Mass Spectrometry of Peptides Linked by Disulfide-Containing Cross-linkers

	-----	78
3.1	Introduction-----	78
3.2	Experimental-----	82
3.2.1	Reagents and Cross-linking Reactions.-----	82
3.2.2	Mass Spectrometry and Data Analysis -----	82
3.2.3	Nomenclature for ICPs and their fragments in MS and MS/MS spectra-----	84
3.3	Results and Discussion -----	86
3.3.1	ECD and AI-ECD of TCC products from BN, MSH, and ubiquitin proteolytic peptides -----	86
3.3.2	Negative ion CID of BN-TCC, MSH-TCC, α_1 TCC β_1 , and α_2 TCC β_2 -----	92
3.3.3	EDD of BN-TCC and MSH-TCC-----	96

3.3.4 MALDI TOF/TOF CID of BN-TCC, MSH-TCC, α_1 TCC β_1 , and α_2 TCC β_2 -----	98
3.4 Summary -----	102
3.5 References-----	102
4. Selective C-I Bond Cleavage in ECD: Prospects for Designing a Novel Chemical Cross-linker and Mechanistic Implications-----	106
4.1 Introduction -----	106
4.2 Experimental-----	111
4.2.1 Sample Preparation and Iodination Reaction-----	111
4.2.2 Mass Spectrometry-----	112
4.3 Results and Discussion -----	115
4.3.1 Selective Iodination of His ⁶ or Tyr ² in MSH -----	115
4.3.2 C-I Bond Cleavage Behavior in ECD of Doubly and Triply Protonated His ⁶ - and Tyr ² -iodinated MSH -----	118
4.3.3 ECD of Ca ²⁺ -adducted Histidine- and Tyrosine-Iodinated MSH -----	120
4.3.4 ECD of Doubly Protonated and Calcium-Adducted Doubly Iodinated AAGF and Singly Iodinated BE -----	122
4.3.5 C-I Bond Cleavage in ECD: Implications for the ECD Mechanism -----	124
4.3.6 ETD and ECD Comparison of Doubly and Triply Protonated Histidine and	

Tyrosine Singly Iodinated MSH-----	124
4.3.7 MALDI TOF/TOF CID of His ⁶ Singly Iodinated MSH-----	129
4.4 Summary -----	130
4.5 References-----	131
5. Enhancing the Detection of Chemically Cross-linked Peptides in Mass Spectrometry: Enabling Selective Metal Dioxide-based Enrichment for a Novel Homobifunctional Peptide-based Cross-linker -----	137
5.1 Introduction -----	137
5.2 Experimental-----	139
5.2.1 Cross-linker I -----	139
5.2.2 Cross-linker II -----	140
5.2.3 Mass Spectrometry Analysis-----	141
5.3 Results and Discussion -----	141
5.3.1 Cross-linker I -----	141
5.3.2 Cross-linker II -----	146
5.4 Summary -----	151
5.5 References-----	152

6.	Improved Detection of Ions below m/z 700 with Quadrupole Fractionation (QF) in Hybrid Q-FT-ICR Mass Spectrometry -----	154
6.1	Introduction -----	154
6.1.1	Linear Quadrupole -----	154
6.1.2	Linear Quadrupole and FT-ICR MS -----	156
6.2	Experiment -----	157
6.3	Results and Discussion -----	159
6.3.1	Improved Detection of Non-cross-linked Peptides by QF -----	159
6.3.2	Improved Detection of Cross-linked Peptides by QF -----	164
6.3.3	Comparison of QF and DI After Compensating for the Extra Time Needed for QF -----	166
6.4	Summary -----	170
6.5	References -----	171
7.	Characterization of Enzyme Function and Functional Differentiation in <i>Curacin A</i> and <i>Jamaicamide</i> Biosynthesis by FTICR MS and IRMPD -----	174
7.1	Introduction -----	174
7.2	Experimental -----	177
7.2.1.	Protein Expression -----	177

7.2.2. FT-ICR MS for Functional Analysis of Proteins from the Cur and Jam	
Pathways -----	178
7.2.3 IRMPD-based Quantification of Cur ER, Jam ER, and Cur Hal Catalytic	
Efficiency -----	179
7.3 Results and Discussion -----	181
7.3.1 Functional analysis of GNAT in the initiation module of CurA biosynthesis----	
-----	181
7.3.2 Fuctional determination of Cur Hal, ECH ₁ S, ECH ₂ S, and ERs from Cur and	
Jam -----	186
7.3.3 Functional differentiation of ERs from Cur and Jam -----	192
7.3.4 Application of IRMPD to reveal crucial residues for Cur Hal catalysis -----	194
7.3.5 Characterization of products from ST and TE catalysis in the termination	
module of CurA biosynthesis-----	196
7.4 Summary -----	197
7.5 References-----	199
8. Summary and Prospects for Future Studies-----	202
8.1 Summary and Conclusion-----	202
8.1.1 The Goals of the Dissertation-----	202
8.1.2 Summary of Experimental Results-----	204

8.2	Prospects for Future Studies -----	206
8.2.1	Photo-cross-linking and Mass Spectrometry -----	206
8.2.2	Fragmentation Patterns of Cross-linked Peptides with Disulfide Bond Linkage- -----	207
8.2.3	Design of a Novel Cross-linker with Metal Dioxide Enrichment Potential or Unique Fragmentation Pattern-----	208
8.2.4	Study of Quadrupole Fractionation Mechanisms -----	210
8.2.5	MS/MS-based Approach to Study Enzyme Catalytic Efficiency -----	210
8.3	References-----	211

List of Tables

Table 1.1. Computer Programs for Cross-linked Peptide Identification-----	15
Table 2.1. Sequence and monoisotopic mass of three activators applied in this study ---	55
Table 2.2. Med15 binding sites for activators determined and verified by ESI and MALDI.-----	61
Table 6.1. BSA (without DTT/IAA treatment) tryptic peptides identified in QF and DI analysis, respectively. -----	160
Table 6.2. BSA (with DTT/IAA treatment) tryptic peptides that identified in QF and DI analysis-----	162
Table 7.1. Precursor and PPant ejection ions observed in FT-ICR MS and IRMPD of <i>apo</i> - and <i>holo</i> -ACP before and after incubation with AR-GNAT- <i>apo</i> -ACP and acetyl- or malonyl-CoA, and of NH ₂ -ACP after incubation with AR-GNAT- <i>apo</i> -ACP and acetyl-CoA (top), and of the trypsin digested AR-GNAT- <i>apo/holo</i> -ACP tridomain before and after incubation with malonyl-CoA.--	183
Table 7.2. ESI FT-ICR MS and IRMPD analysis of various ACP _{II} products. -----	189

List of Figures

- Figure 1.1.** Schematic diagram of a typical ICR trapping cell, which includes trapping electrodes, detection electrodes, and excitation electrodes. The direction of ion motion and the magnetic field are indicated with arrows.----- 19
- Figure 1.2.** Diagram of 7T FT-ICR mass spectrometer used in this work.-----21
- Figure 1.3.** Peptide product ion nomenclature in MS/MS. Cleavage of C_α-C, C-N, and N-C_α backbone bonds yields *a*-/*x*-, *b*-/*y*-, and *c*-/*z*-type product ions, respectively. Side chain losses (mainly in high-energy CID) produce *d*-, *v*-, and *w*-type ions. -----25
- Figure 1.4.** Structure and biological functions of some natural products derived from NRPS and PKS biosynthesis.-----31
- Figure 2.1.** Partial ESI FT-ICR mass spectra from top-down analysis of unreacted Med15 107-255 (top) and Med15 107-255 cross-linked with Gcn4 (bottom). Charge states +28-+31 of unmodified Med15 107-255 are observed in both cases. The arrows 1-3 indicate *m/z* regions where the cross-linked product (Med15 and Gcn4) should be observed in its +32, +33, and +34 charge state, respectively.-----57

- Figure 2.2.** Chemical structure of BHPDP.-----58
- Figure 2.3.** Binding sites identified in Med15 for Gal4, Gcn4 and VP2.-----60
- Figure 2.4.** MALDI-TOF (top) and ESI FT-ICR MS (positive mode, middle; negative mode, bottom) analysis of VP2/Med15 cross-linked products. Here, α represents the activator VP2, β_1 corresponds to Med15 345-348, β_2 to Med15 74-78, β_3 to Med15 79-85, β_4 to Med15 207-217, β_5 to Med15 222-231, and β_6 to Med15 160-174. Cross-linked products were verified by MS/MS. -----62
- Figure 2.5.** MALDI TOF (top) and ESI FT-ICR MS (positive ion mode, bottom) analysis of cross-linked products involving Gcn4 and Med15. Here, α_1 represents the activator tryptic peptide Gcn4 119-134; α_2 represents Gcn4 105-134, β_1 corresponds to Med15 74-78, and β_2 to Med15 207-217.-----63
- Figure 2.6.** MALDI-TOF (top) and ESI FT-ICR MS (positive ion mode, bottom) analysis of cross-linked products involving Gal4 and Med15. Following photo-cross-linking, samples were subjected to proteolysis and purification as described in the experimental section. Here, α represents the activator Gal4, β_1 corresponds to Med15 74-78, β_2 to Med15 160-174, and β_3 to Med15 207-217. -----64
- Figure 2.7.** MALDI-TOF/TOF CID MS/MS (top) and ESI FT-ICR MS/MS (negative ion low-energy CID, bottom) of a potential cross-linked product: VP2:Med15 207-217. Peaks 1 and 2 can be assigned as C-S bond cleavages, assuming that cross-linking occurred at Met213 in Med15 207-217. In MALDI TOF/TOF CID, extensive peptide fragmentation is observed but in negative

ion mode ESI FT-ICR MS/MS, only neutral losses of water and ammonia were seen, precluding confident verification of this cross-linked product with the latter technique (* = unidentified peaks). Here, α represents VP2 and β corresponds to Med15 207-217. -----67

Figure 2.8. ESI FT-ICR MS/MS (positive ion mode, top) and MALDI TOF/TOF high-energy CID MS/MS (bottom) of the potential cross-linked product Gal4:Med15 207-217. A series of backbone cleavages was observed in ESI MS/MS and, based on the fragmentation along the Med15 207-217 peptide backbone, the pBpa cross-linking site can be localized to Met 213. In MALDI TOF/TOF MS/MS, only a limited number of product ion peaks are observed.-----69

Figure 2.9. MALDI TOF-TOF CID MS/MS (top) and ESI FT-ICR MS/MS (positive ion mode, bottom) of the potential cross-linked product involving Gal4 and Med15 74-78. (β = free tryptic peptide VAVMR; * = unidentified peak).--70

Figure 2.10. ESI FT-ICR MS/MS (positive ion mode) of the potential cross-linked product involving Gal4 and Med15(160-174). Several peaks were not identified, perhaps due to imperfect precursor ion isolation. Here, α represents Gal4 and β corresponds to Med 15(160-174). -----71

Figure 3.1. ECD and AI-ECD of TCC products from BN (panels a and b), MSH (panels c and d), and ubiquitin; α_1 TCC β_1 (panels e and f), and α_2 TCC β_2 (panels g and h). For BN, S-S bond cleavage was observed in AI-ECD (inset in panel b) but not in ECD alone (inset in panel a). * = unidentified peaks.-----

-----92

Figure 3.2. Negative ion CID of TCC products from BN (panel a), MSH (panel b), and ubiquitin; α_1 TCC β_1 (panel c) and α_2 TCC β_2 (panel d). Abundant peaks corresponding to S-S and C-S bond cleavages are observed for BN and MSH but such cleavage is absent for α_1 TCC β_1 . For α_2 TCC β_2 , S-S and C-S bond cleavage is observed but at low abundance. * = unidentified peaks. -----96

Figure 3.3 EDD of TCC products from BN (panel a) and MSH (panel b). S-S and C-S bond cleavages are observed, along with backbone fragments, including y -, z -, and c -type ions. However, the fragmentation efficiency is low. In EDD of BN-TCC, a y_9 ion with - 17 Da (NH_3) and - 129 Da mass shift is observed. The latter shift corresponds to neutral loss from the tryptophan side chain, as previously reported [10]. * = unidentified peaks. -----98

Figure 3.4 MALDI TOF/TOF CID of TCC products from BN (panel a), MSH (panel b), and ubiquitin; α_1 TCC β_1 (panel c) and α_2 TCC β_2 (panel d). Abundant 66 Da doublets resulting from C-S bond cleavages are observed in all cases, along with significant backbone fragmentation. * = unidentified peaks. ----- 101

Figure 4.1. Sequences of peptides used in this study.----- 111

Figure 4.2. Positive ion mode ESI of MSH iodination product from condition I (panel A) and II (panel B). 1-3: triply protonated species; 4-6: doubly protonated species; 1,4: unmodified MSH; 2,5: singly iodinated MSH; 3,6: doubly iodinated MSH.----- 116

Figure 4.3. From the two different reaction conditions, PBS buffer followed by water (condition I) and the reverse order (condition II), His⁶ (panel A) and Tyr²

(panel B) in MSH could be selectively iodinated, respectively, as verified by CID. ----- 117

Figure 4.4. ECD of triply protonated His⁶-iodinated MSH (panel A) and Tyr²-iodinated MSH (panel B). In panel A, the most abundant fragment corresponds to iodine loss. The ratio of this iodine loss peak to the charge reduced species is ~2:1. Here, His⁶ is a likely protonation site, thus positive charge is very close to the C-I bond. In panel B, the most abundant fragment still corresponds to iodine loss but is less abundant than for His⁶-iodinated MSH. The ratio of this iodine loss peak to the charge reduced species is ~1:3. Series of backbone product ions are also observed. In the case of Tyr²-iodinated MSH, the C-I bond is a few residues away from the closest likely positive site (His⁶). ----- 119

Figure 4.5. ILE of triply protonated His⁶- and Tyr²- iodinated MSH (panel A). His⁶ iodination results in much higher ILE than that of Tyr². ILE of doubly protonated His⁶-and Tyr²-iodinated MSH are shown in panel B. His⁶ iodination results in slightly higher ILE than that of Tyr². Doubly protonated peptides are likely to have more folded gas-phase structures than triply protonated species. Thus, positive charge can be spatially close to the C-I bond in the Tyr²-iodinated species. ILE of doubly charged calcium-adducted His⁶-and Tyr²-iodinated MSH is shown in panel C. A likely calcium binding site is the acidic Glu⁵ residue between His⁶ and Tyr². Thus, positive charge may be close to the C-I bond in either iodinated form. Panel D represents the ILE of doubly protonated and calcium-adducted Tyr¹⁰

doubly iodinated AARF. Doubly protonated peptides may fold in the gas phase, placing the C-I groups on Tyr¹⁰ spatially close to the likely protonation sites (Arg1-2 near the N-terminus). The Ca²⁺ ion is likely to coordinate to the string of acidic residues N-terminal to Tyr¹⁰. ----- 121

Figure 4.6. ECD of doubly protonated and calcium-adducted His¹²-iodinated bombesin. For the doubly protonated species (top panel), the most abundant fragment corresponds to iodine loss whereas iodine loss is not dominant for the calcium-adducted species (bottom panel). In the doubly protonated species, His¹² is likely protonated, thus placing positive charge close to the C-I bond. In the Ca-adducted species, there is no obvious calcium binding site close to His¹². ----- 123

Figure 4.7. ILEs of triply protonated His⁶- and Tyr² singly-iodinated MSH from ECD and ETD on the SolariX FT-ICR instrument. ILEs from ECD on the Apex instrument are also shown for comparison. Very little variation is seen between ECD on the two instruments. ILEs from ETD are higher than the corresponding values from ECD because ETD results in more abundant charge reduced species and less peptide backbone fragmentation. ----- 125

Figure 4.8. ECD of triply protonated His⁶ singly iodinated MSH on a SolariX FT-ICR instrument. ----- 126

Figure 4.9. ETD of triply protonated His⁶ singly iodinated MSH on a SolariX FT-ICR instrument. ----- 127

Figure 4.10. ECD of triply protonated Tyr² singly iodinated MSH on a SolariX FT-ICR instrument. ----- 127

- Figure 4.11.** ETD of triply protonated Tyr² singly iodinated MSH on a SolariX FT-ICR instrument. ----- 128
- Figure 4.12.** ILEs of doubly protonated His⁶- and Tyr² singly-iodinated MSH from ECD and ETD on the SolariX FT-ICR instrument. ILEs from ECD on the Apex instrument are also shown for comparison. The SolariX instrument provided higher ILE values in ECD than the Apex instrument. ILEs from SolariX ECD and ETD are similar. ----- 129
- Figure 4.13.** MALDI TOF/TOF CID of His⁶ singly iodinated MSH. ----- 130
- Figure 5.1.** Synthesis of cross-linker I. ----- 142
- Figure 5.2.** Negative ion mode ESI-FT-ICR MS analysis of the yield of cross-linker I at different reaction times. Peptide I and GMBS were mixed at 1:4 molar ratio. 1: unmodified peptide I; 2: partial reaction product with one GMBS attached to peptide I; 3: the cross-linker Ac-C(GMBS)pSC(GMBS)-OH. Peaks 1-3 all correspond to singly charged ions. ----- 143
- Figure 5.3.** Positive ion mode ESI-FT-ICR mass spectra following cross-linking reaction of subP (panel A) and MSH (panel B) with cross-linker I, Ac-C(GMBS)pSC(GMBS)-OH. 1: singly charged un-reacted cross-linker; 2: doubly charged intramolecularly cross-linked subP; 3: doubly charged product from cross-linking of MSH (Lys¹¹) and an amine-reactive group in free excess GMBS ; 4: quadruply charged intermolecularly cross-linked product of two molecules of MSH; *=unidentified peak. ----- 144
- Figure 5.4.** ZrO₂ (top) and TiO₂ (bottom) treatment of Ac-C(GMBS)pSC(GMBS)-OH reacted with MSH. The intermolecularly cross-linked product observed

without metal oxide treatment (see Figure 5.3) was not detected, perhaps due to steric effects. The highlighted peaks all correspond to singly-charged impurities. ----- 146

Figure 5.5. Structure of cross-linker II. ----- 147

Figure 5.6. Comparison of Ziptip (top), TiO₂ (middle), and ZrO₂ (bottom) treatment of intramolecularly cross-linked product from subP with cross-linker II. 1: triply-deprotonated subP cross-linked product; 2: product (see Fig. 5.7) of reaction between the cross-linker and ammonium bicarbonate; 3: doubly-deprotonated cross-linked subP product. *=unidentified peak.----- 149

Figure 5.7. Deactivated cross-linker II from reaction with ammonium bicarbonate. -- 150

Figure 5.8. Negative ion CID of doubly deprotonated subP cross-linked with cross-linker II (peak 1). C-S bond cleavage on the reduced maleimide group is observed to yield products 2-4 as shown in the upper Scheme. Peaks 2-4 all correspond to singly charged ions. ----- 151

Figure 6.1. Improved BSA tryptic peptide detection by QF (top spectra in each panel) over DI (bottom spectra in each panel). Peptide sequences and charge states are: a) [Y⁴³⁴TR⁴³⁶ + H]⁺ ; b) [L⁴⁸³CVLHEK⁴⁸⁹ + 2H]²⁺ ; c) [K⁵⁴⁸QTALVELLK⁵⁵⁷ + 2H]²⁺ ; d) [A²³⁶WSVAR²⁴¹ + H]⁺ . Modified cysteine residue (from carbamidomethylation) in b) is indicated by italic font and is underlined. ----- 163

Figure 6.2. Sequence coverage of BSA obtained by DI, LC/MS, and by QF FT-ICR MS analysis.----- 164

Figure 6.3. Three intramolecularly cross-linked peptides that were observed with QF

	(top spectra in column a-c) but not in DI (bottom spectra).-----	165
Figure 6.4.	Ratios of peak abundances for BSA tryptic peptides from DI spectral acquisition with thirty vs. three scans, respectively. -----	167
Figure 6.5.	Ratio of peak abundances between QF (3 scans) and DI (21 scans) analysis of a peptide mixture in positive ESI mode. The mixture was obtained by digesting apomyoglobin with three enzymes (trypsin, chymotrypsin, and Glu C), respectively, and mixing the resulting peptides. Three replicates were carried out to obtain average and standard deviation. -----	168
Figure 6.6.	Ratio of peak abundances between negative ion mode QF and DI analysis of peptide mixtures obtained from three enzyme (trypsin, chymotrypsin, and Glu C) digestion of <i>apo</i> -myoglobin (panel A) and reduced and alkylated BSA (panel B). Three replicates were carried out to obtain average and standard deviation. -----	169
Figure 7.1.	Chemical structure of PPant. -----	175
Figure 7.2.	Chemical structures of Cur (top) and Jam (bottom). -----	176
Figure 7.3.	Enzymes (except KS and AT) that investigated in this thesis. The gene clusters that encoded those enzymes are also included. KS, β -ketoacyl-ACP synthase; AT, acetyl transferase. -----	177
Figure 7.4.	Nomenclature and chemical structures for substrates and products for Hal, ECH ₁ , ECH ₂ , and ER catalysis.-----	179
Figure 7.5.	Partial FT-ICR mass spectra of trypsin digested AR-GNAT-ACP in <i>apo</i> - (row A) and <i>holo</i> form (row B) and after incubation with malonyl-CoA (row C). An unmodified doubly protonated peptide (469-484) and its modified	

counterpart (PPant loaded) were observed at position 1 and 2, respectively.
Acetyl transfer product was observed in position 3. ----- 182

Figure 7.6. Partial FT-ICR mass spectra of *holo*-ACP-SH (left) and *holo*-ACP-NH₂ (right) incubated with the AR-GNAT-*apo*-ACP tridomain in the presence of malonyl-CoA. Acetyl transfer to *holo*-ACP-SH can be readily observed whereas no significant signal is seen for the NH₂ counterpart. ----- 184

Figure 7.7. IRMPD of the acetyl transfer product of *holo*-ACP-SH. The indicated PPant ejection ion was observed. ----- 185

Figure 7.8. FT-ICR MS comparison of the acetyl transfer efficiency of GNAT-*apo*-ACP didomain and GNATmonodomain from acetyl- and malonyl-CoA, respectively. The substrate and product are *holo*-ACP (1) and acetyl-*holo*-ACP (2), respectively.----- 186

Figure 7.9. FT-ICR MS analysis of 1-ACP_{II} and Cl-1-ACP_{II} after incubation with different combinations of Cur ECH₁, ECH₂, and ER/NADPH. ----- 188

Figure 7.10. FT-ICR MS analysis of Cl-1-ACP_{II} incubated with ECH₁, ECH₂, and ER from Cur or Jam.----- 191

Figure 7.11. IRMPD of products from 1-ACP_{II} (panels A and B) and Cl-1-ACP_{II} (panels C and D) incubated with Jam ECH₁ and ECH₂ (panels A and C) and Jam ECH₁, ECH₂, and ER (panels B and D). No significant change in peak abundance at the n + 2 position relative to the corresponding unsaturated PPant ejection ion was seen for Cl-1-ACP_{II}.----- 191

Figure 7.12. 3-ACP_{II}/4-ACP_{II} (panel A), Cl-3-ACP_{II}/Cl-4-ACP_{II} (panel B), and 4-ACP_{II}/5-ACP_{II} (panel C) were mixed at known ratios and quantified by

IRMPD. Each measurement was performed in triplicate to obtain a standard deviation. -----	193
Figure 7.13. Catalytic efficiencies for cyclopropanation and saturation of Cur and Jam ERs. All time-course studies were performed in triplicate under the same reaction conditions.-----	194
Figure 7.14. Catalytic efficiencies of WT Cur Hal and site-specific Hal mutants from IRMPD-based quantification.-----	196
Figure 7.15. FT-ICR MS analysis of <i>apo</i> -ACP _{III} (A), <i>holo</i> -ACP _{III} (B), and <i>holo</i> -ACP _{III} incubated with ST (C), and ST + TE (D). Peaks labeled with diamonds in A-D correspond to ACP _{III} lacking an N-terminal methionine relative to the heavier form of ACP _{III} . -----	197
Figure 8.1. A novel cross-linker design suggested by Prof. Larsen.-----	209

List of Schemes

Scheme 1.1. Reaction Scheme of NHS/sulfo-NHS ester with a primary amine (NHS: R=H; sulfo-NHS: R=SO ₃ Na)-----	6
Scheme 1.2. Reaction Scheme of sulfhydryl with maleimide. -----	7
Scheme 1.3. Photo-reaction of aryl azide. -----	8
Scheme 1.4. Photo-reaction of diazirine. -----	8
Scheme 1.5. Photo-reaction of benzophenone -----	9
Scheme 1.6. ECD process.-----	27
Scheme 1.7. EDD process.-----	30
Scheme 3.1. Structures, nomenclature, and mass increment of product ions observed in this work. R ₁ and R ₂ are specifically indicated for some peptides.-----	85

Abstract

Multiplexed Mass Spectrometric Approaches for Protein Cross-Linking Analysis and Protein Functional Studies

by

Bo Wang

Chair: Kristina I. Håkansson

Mass spectrometry (MS) alone, or combined with chemical cross-linking and proteolysis, is a valuable method in protein characterization. However, detection of cross-linked peptides remains challenging due to ion suppression and cross-linked peptide signals are difficult to differentiate from those of unmodified peptides. In this thesis, efforts to design a novel chemical cross-linker with metal oxide enrichment potential or unique gas-phase fragmentation pattern are presented. A series of biological studies, including mapping of protein-peptide interactions in the transcriptional machinery and determination of enzyme function and functional differentiation in natural product biosynthesis, were also performed.

Photo-cross-linking combined with multiplexed MS and biotin-avidin enrichment was employed to map binding sites between gene transcriptional activators and a co-activator (mediator) with resolution up to one amino acid residue. Unprecedented C-C and C-S bond cleavages were observed in matrix-assisted laser desorption/ionization

tandem time-of-flight collision induced dissociation (MALDI TOF/TOF CID) of photo-cross-linked products.

A novel phosphate-containing cross-linker was synthesized and demonstrated to have amine reactivity. The corresponding cross-linked product was selectively enriched by metal dioxides. Gas-phase fragmentation patterns of peptides linked with disulfide-containing cross-linkers were examined in electron capture dissociation (ECD), electron detachment dissociation (EDD), negative ion CID, and MALDI TOF/TOF CID, to find an optimal gas-phase cleavage method for identification of such cross-linked peptides. Iodinated peptides were subjected to ECD and electron transfer dissociation (ETD), showing highly selective C-I bond cleavage. A proximate, either through bond or through space, positive charge appears to facilitate C-I bond cleavage. These results provide a guide to design novel gas-phase cleavable cross-linkers and an additional model for elucidating the ECD/ETD mechanism. Quadrupole fractionation was also applied in this thesis to enhance detection in the 350-600 m/z region.

Fourier transform ion cyclotron resonance (FT-ICR) MS and infrared multiphoton dissociation (IRMPD) were applied to characterize the function and functional differentiation of enzymes from natural product biosynthetic pathways. GCN5-related *N*-acetyltransferase and enoyl reductase (ER) involved in Curacin A (Cur) biosynthesis were shown to have the unprecedented functions of dual decarboxylation/thiol acetyl transfer and cyclopropanation, respectively. Catalytic efficiencies of Cur and Jamaicamide ERs and site-specific mutants of Cur halogenase were measured by IRMPD. The role of a sulfotransferase in decarboxylative chain termination in Cur biosynthesis was also elucidated.

Chapter 1

Introduction

1.1 Chemical Cross-linking and Mass Spectrometry

1.1.1 Mass Spectrometry for Protein Analysis

With the development of modern proteomics came the realization that increasing the number of proteins isolated and characterized from cells or tissues is not sufficient to reveal the physiological complexity of living organisms, which involve specific higher order protein structure and networks of protein-protein interactions. It has been estimated that there are 35,000 protein-protein interactions in *Saccharomyces cerevisiae*, i.e., roughly six interactions for each protein [1, 2]. For human beings, the number of protein interactions is estimated to be even higher: 150,000-650,000 interactions from 26,000-38,000 protein-coding genes [3, 4]. After screening these possible interactions, ~6-25% have been confirmed or are under consideration, resulting in a number of ~38,000 [5]. The vast numbers of protein-protein interactions in living organisms indicate that: 1) the functions of each protein rely not only on its sequence and higher order structure, but also on its interaction network which can be either transient or stable; and 2) a certain protein may be involved in more than one interaction network to modulate related biological functions. Therefore, in order to fully understand a protein's biological function, it is

necessary to characterize its higher order structure and its protein-protein interaction network. In the latter case, the details of each interaction, including the identity, stoichiometry, interaction site, etc., should be determined.

Various techniques have been applied to characterize protein-protein interactions and protein complexes. Traditional approaches like X-ray crystallography [6-9], electron microscopy (EM) [10, 11], and nuclear magnetic resonance (NMR) [12-15] spectroscopy can characterize protein complexes with resolution up to the atomic level and therefore yield direct insight into protein-protein interactions. However, these approaches are laborious and have low sensitivity. Furthermore, highly purified protein complexes are required. Also, although proteins as large as 110 kDa have been characterized by NMR [16], that technique typically has size limitations around 30-35 kDa [17, 18].

The advent of mass spectrometry (MS) for biomolecular analysis by coupling to soft ionization sources, including electrospray ionization (ESI) [19] and matrix-assisted laser desorption/ionization (MALDI) [20, 21], has allowed progression towards characterization of multi-protein complexes. Advantages of MS include its high sensitivity for probing the real-time status of a protein complex, low sample requirements (as low as attomoles for proteins [22]), and high sample throughput. Meanwhile, high mass accuracy can be obtained from different mass analyzers, including 5-10 ppm for reflectron time of flight (TOF) [23], 1-5 ppm or sub-ppm for Fourier transform ion cyclotron resonance (FT-ICR) [23, 24], and less than 2 ppm for orbitrap [25].

MS can sometimes characterize protein complexes directly [26, 27] by assuming that interactions within the complex can be maintained from the liquid phase (prior to sample ionization) to the gas phase (inside the mass spectrometer). Typically, direct MS

analysis of protein complexes is conducted with ESI, which is the softest ionization for large non-volatile biomolecules, including proteins, carbohydrates, and oligonucleotides. ESI can generate multiply charged gaseous ions with little disturbance to the analyte structure. Many successful experiments involving application of ESI MS to characterize protein complexes have been reported. For example, MS can reveal protein-protein and protein-ligand interactions [28-30]. Application of tandem mass spectrometry (MS/MS) further allows binding sites to be localized [31, 32]. MS has been applied to reveal structures of protein complexes with mass up to MDa, including virus capsids [33, 34] and the intact ribosome [35].

1.1.2 Combining Chemical Cross-linking with Mass Spectrometry for Protein Structural and Protein-protein Interaction Analysis

Chemical cross-linking combined with MS is an emerging method for characterizing protein higher order structure and interactions. Detection by MS provides several advantages, including: 1) relatively high tolerance for the presence of un-cross-linked proteins/peptides in the sample; 2) the amount of sample required can be as low as femtomoles [36]; 3) no strict size limitation of cross-linked proteins, particularly when proteolysis is employed; 4) fast speed of analysis; 5) various approaches for identification and confirmation of cross-linked proteins/peptides, including accurate mass measurement and MS/MS analysis.

One strategy for applying chemical cross-linking to proteins is to target the side chains of certain amino acid residues, including amines [37, 38], sulfhydryls [39], and carboxylic acids [40] with specific reactive groups on chemical cross-linkers. Upon the

cross-linking reaction, targeted amino acid pairs are covalently linked by chemical cross-linkers with cleavable [41] or un-cleavable spacer arms of various lengths. Once the cross-linked products are identified, the proximity relationship of cross-linked residue pairs can be estimated. Another approach relies on photo-chemically reactive groups, including aryl azides [42, 43], diazirines [44, 45], and benzophenones [46, 47], to generate covalent linkage of chemical groups in spacial vicinity. A third method establishes covalent [48] or non-covalent [49] interaction between cross-linking reagents and specific chemical groups on amino acid side chains (e.g., amine groups of lysine). In this approach, “linkage” between two amino acid residues is not applicable.

Once cross-linking is accomplished, modified proteins can be analyzed by the so called top-down approach [50]. Another approach is to carry out proteolytic digestion and identify cross-linked proteolytic peptides by MS/MS, thereby providing a rough map of the protein structure and the interaction sites (when applicable). For cross-linking reagents based on non-covalent interactions, ESI MS is typically applied to detect a protein mass shift and thereby obtain the number of reagents that are involved in interaction. This approach is analogous to hydrogen/deuterium exchange but reveals the solvent accessibility of certain residue side chains rather than the protein backbone [49].

Efficient detection of cross-linked peptides, particularly for photo-cross-linking, still remains challenging due to: 1) the low yield and resulting ion suppression effect from an excess of non-cross-linked peptides (ion suppression can be reduced by selective enriching of cross-linked peptides (e.g. biotin-avidin affinity purification). 2) the formation (in some cases) of inter-, intra-, and dead-end products in the chemical cross-linking reaction [51], which makes spectra more complex. 3) the difficulty to

differentiate cross-linked peptide signals from those of unmodified peptides, particularly in LC/MS/MS analysis. Product ions from cross-linked peptides are either identical to their non-cross-linked counterparts, or bear a “mystery” mass shift (because the mass/identity of the other attached peptide is unknown prior to analysis). Database searching exhaustively against all possible peptide pair combinations is a huge challenge for computation and storage space [52]. Several efforts have been made to overcome these challenges and these are discussed in sections 1.1.4 and 1.1.5 below.

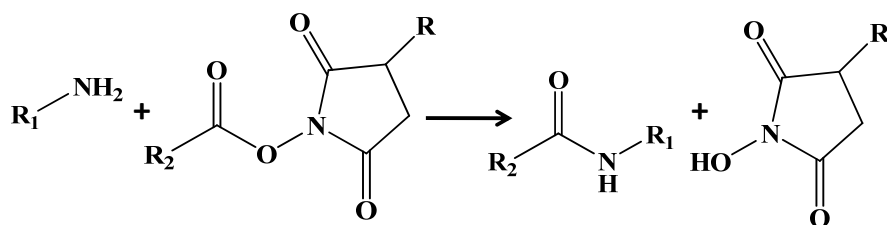
1.1.3 Reactive Groups of Chemical Cross-linkers

As mentioned above, chemical cross-linkers rely on their reactive groups to form covalent bonds between two amino acid residues in a protein and thereby map protein structure and interfaces in protein-protein interactions. Chemical cross-linkers can be classified as homobifunctional, i.e., targeting two identical residues (e.g., a lysine pair), heterobifunctional, i.e., comprising two different reactive groups targeting different residues, or trifunctional, i.e., including a third chemical group that can be used for, e.g., isolation or identification. Some of the most widely used cross-linking reactions and the corresponding chemical cross-linkers are discussed below.

1.1.3.1 Amine-reactive Groups

Amine-reactive groups target free amine groups, including protein N-termini and the ϵ -amino group in Lys side chains. The most widely used amine-reactive group is *N*-hydroxysuccinimide (NHS) ester, which was introduced in the 1970s [37, 38]. The NHS group is hydrophobic and insoluble in aqueous buffers. Therefore, organic solvent is required to carry out NHS reactions. In order to extend the application of NHS, sulfate

(SO₃) groups were introduced to produce a water-soluble analog, sulfo-NHS [53]. The reaction of NHS with primary amine group (-NH₂) is shown in Scheme 1. After the reaction, the NHS group is released and a stable amide bond is formed. Although NHS mainly targets amine groups, it also reacts with hydroxyl groups of serine and tyrosine and such products have been confirmed by MS/MS analysis [54]. The pH value for the NHS reaction is critical for controlling the specificity. For example, NHS reacts with N-termini and tyrosine OH under acidic conditions (pH 6.0). but, in basic conditions (pH 8.4), N-termini and Lys amine groups react with NHS [55].

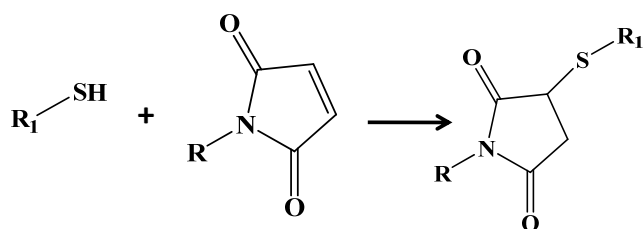


Scheme 1.1. Reaction Scheme of NHS/sulfo-NHS ester with a primary amine (NHS: R=H; sulfo-NHS: R=SO₃Na)

1.1.3.2 Sulfhydryl-reactive Group

Incorporation of a maleimide moiety into chemical cross-linkers targets sulfhydryl groups, i.e., Cys residues (with SH group on their side chain) in proteins or protein complexes. As shown in Scheme 1.2, a sulfhydryl group can insert into the maleimide moiety by Michael addition. The pH value is important for controlling the reaction between maleimide and an SH group, e.g., maleimide reacts specifically with SH group in the pH range 6.5 to 7.5 [39, 56] but demonstrates potential side reaction with NH₂

group at basic conditions [57]. In addition, one should be aware of the limitation of sulfhydryl-reactive chemical cross-linkers because: 1) Cys is a rare amino acid with the lowest frequency [58]; 2) the formation of disulfide (S-S) bonds between Cys pairs blocks the reaction between maleimide and SH group. If S-S bonds are reduced to release SH groups prior to the cross-linking reaction, the native conformation or interaction status is likely compromised and the original structure will be lost.



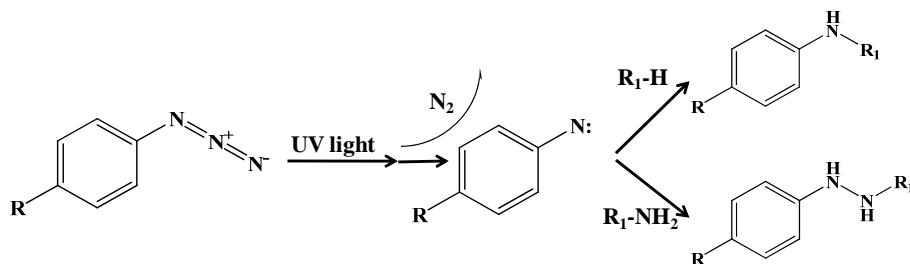
Scheme 1.2. Reaction Scheme of sulfhydryl with maleimide.

1.1.3.3 Photo-reactive Groups

Photo-reactive groups incorporated into chemical cross-linkers include aryl azide, diazirine, and benzophenone moieties. Photo cross-linking reactions are catalyzed by UV irradiation at specified wavelengths. In general, photo-reactive groups are incorporated into heterobifunctional cross-linkers with an additional amine- or sulfhydryl-reactive group [36].

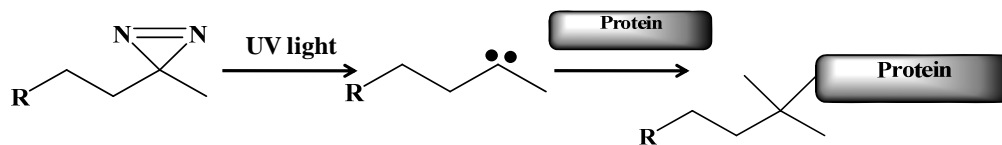
Studies of the photochemical properties of aryl azides started about 80 years ago [42]. Upon UV irradiation, aryl azide loses N_2 and forms short-lived singlet nitrene [42], which can undergo insertion into adjacent C-H or C-N bonds [59] (Scheme 1.3). Aryl azide has been the most commonly applied photo-cross-linking reagent [60] to

investigate protein-DNA [61], protein-RNA [62], and protein-protein interactions[63, 64]. One major limitation of applying aryl azides in protein characterization is the wavelengths (<280nm) [36] for inducing photo-activation, which may cause photolytic damage.



Scheme 1.3. Photo-reaction of aryl azide.

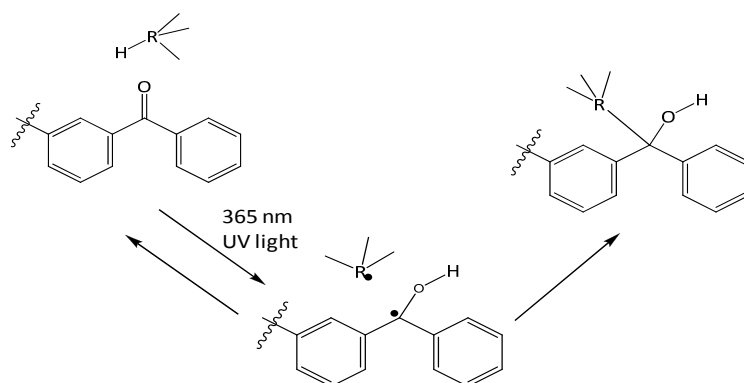
Diazirines can be activated at wavelengths longer than 350 nm to induce photo cross-linking reaction based on carbene chemistry [65]. The mechanism is shown in Scheme 1.4. It has been reported that activated diazirines may generate undesired diazo isomerization but the rearrangement can be avoided by introducing an CF_3 group into the diazirine moiety [66].



Scheme 1.4. Photo-reaction of diazirine.

Benzophenone (BP) is activated at 365 nm to form a triplet intermediate, which

induces hydrogen abstraction from any C-H bond within the right proximity. This process results in formation of a C-C bond between BP and the target molecule [46] (Scheme 1.5). At this wavelength for photo-activation, protein damage can be effectively minimized. Another favorable character of BP is its reversible photo-activation property: if the H abstraction process does not occur, BP can relax back to its ground state and be re-activated in the next round of irradiation [46]. BP-based photo cross-linkers have been widely used in the characterization of protein-protein interactions [67-71]. Specifically, p-benzoyl phenyl alanine (pBpa), which contains BP moiety, can be expressed as an unnatural amino acid in bacteria and induce photo-cross-linking reaction *in vivo* [72, 73].



Scheme 1.5. Photo-reaction of benzophenone (adopted from reference [46]).

1.1.3.4 Cross-linking through Non-covalent Interactions

18-crown-6 ether (18C6) was reported to exhibit non-covalent interaction with lysine [74]. 18C6 [49] and another analog, phenyl bis-crown (PBC) [75], were applied to structural determination of proteins, including cytochrome *c*, ubiquitin, and melittin. By examining the number of adducts in different charge states of the protein, solvent accessibility of side chains is inferred. Therefore, protein structural and conformational

changes can be monitored.

1.1.4 Modifications of Chemical Cross-linkers

In addition to the reactive groups, other chemical modifications can be introduced into chemical cross-linkers to facilitate detection of cross-linked products. Some strategies are described below.

1.1.4.1 Isotope-labeled Chemical Cross-linkers

A chosen number of deuterium atoms can be selectively incorporated into chemical cross-linkers and isotopically labeled cross-linkers are then mixed with their unmodified counterparts (1:1 w/w) to react with proteins or protein complexes. After the cross-linking reaction followed by proteolysis, cross-linked peptides demonstrate characteristic isotopic patterns (due to the existence of deuterium atoms), which will aid their identification [76-80].

Oxygen atoms in chemical cross-linkers can also be substituted by ^{18}O to yield di- ^{18}O -labeled species [81]. After reacting proteins with a mixture of labeled and unlabeled cross-linker followed by proteolysis, two sets of mass spectral peaks from intermolecularly cross-linked peptides can be observed with a mass difference of 4 Da [81].

1.1.4.2 Thiol-cleavable Chemical Cross-linkers

Thiol-cleavable cross-linkers (TCCs), such as 3,3'-dithiobis [sulfosuccinimidyl propionate] (DTSSP), were first synthesized in 1976 [38] and have been applied to map protein complex interfaces [41, 82, 83] as well as protein three-dimensional structure with low-resolution [84]. The strategy of identifying TCC products involves dividing the

product in half after the cross-linking reaction. One half (fraction 1) is subjected to disulfide bond reduction followed by thiol group alkylation [85] in solution phase and the other half, fraction 2, is left untreated. These two fractions are then subjected to proteolysis and peptide mapping by MS. Comparison of mass spectral peaks reveals potential inter-molecularly cross-linked products as they are observed in fraction 2 but not in fraction 1. Similarly, putative intra-molecularly cross-linked products demonstrate a +116 Da shift (due to reduction and alkylation) for fraction 1 compared to fraction 2. One drawback is that these manipulations prior to MS analysis increase sample consumption and operation time.

1.1.4.3 Gas-phase Cleavable Chemical Cross-linkers

Another way to differentiate cross-linked peptides from unmodified peptides is to design a cross-linker that is cleavable in the gas phase. The basic idea is to incorporate a specific moiety, which is labile upon IR irradiation [80, 86], UV irradiation [87], or collisions with neutral gas [88-92]. During MS/MS analysis, precursor ions containing a gas-phase cleavable cross-linker produce characteristic product ions, e.g., so called “reporter ions” [88], which identify cross-linked products. Gas-phase cleavable cross-linkers demonstrate promising prospects because multiple rounds of MS analysis or comparison of complex spectra from different liquid-phase treatments (e.g., such as described for DTSSP cross-linkers) is not necessary. Therefore, the time for sample preparation, the amount of sample, and time for analysis are reduced.

1.1.4.4 Enrichable Chemical Cross-linkers

To improve the detection of cross-linked products, trifunctional cross-linkers,

which contain two reactive groups and a biotin moiety, have been designed and applied in cross-linking research [70, 77, 93-95]. After the cross-linking reaction and proteolysis, cross-linked products can be selectively enriched by biotin-avidin affinity purification. However, incorporation of biotin into cross-linkers presents some problems: 1) Biotin must be sufficiently distant from the other two reactive groups to minimize interference. Therefore, a long chain, e.g., polyethylene glycol [96], is introduced to isolate the biotin group but this strategy makes the cross-linker bulky. The length of the spacer arm normally exceeds the preferred range of 8-15 Å [36, 81], which may influence the acquisition of meaningful information on protein structure and interactions. 2) Strong detergents, including SDS and urea, are normally required to dissociate biotin-avidin interactions. Such detergents are not compatible with MS analysis and removal of detergents may be challenging and cause sample loss.

An alternative approach for enriching cross-linked products, termed click-enabled linker for interacting proteins (CLIP) [97] was recently reported. The CLIP strategy involves a novel trifunctional cross-linker, which contains two reactive groups and one alkyne moiety. Proteolysis is carried out after the cross-linking reaction and the resulting peptides, cross-linked and unmodified ones, are mixed with biotin-azide enrichment tag. Cross-linked peptides can then be retained by alkyne-azide reaction and purified by biotin-avidin affinity purification.

1.1.4.5 Zero-length Chemical Cross-linkers

If a chemical cross-linker does not have a spacer arm between two reactive groups, it is referred to as a zero-length (ZL) species. One example of a ZL cross-linker is 1-

ethyl-3-[3-dimethylaminopropyl] carbodiimide hydrochloride (EDC), which can couple carboxyl groups to primary amines with [36, 98], or be used to synthesize the NHS group [99].

Protein footprinting techniques can also be classified as “zero-length” cross-linking because the utilized reagents only target one specific group, including amines [48] (Lys, N-termini) or carboxyl groups (Asp, Glu, and C-termini) [100], i.e., following the reaction, only one residue is modified. The corresponding products can be regarded as analogs of dead-end products [51]. By detecting these modified residues, the solvent accessible area of the target protein or protein complex can be deduced and that information translates into protein conformation or interface information.

1.1.5 Other Methods to Facilitate the Detection of Cross-linked Products

1.1.5.1 Separation Methods

Cross-linked protein complexes can be separated from un-reacted species by gel electrophoresis if the mass difference between them is big enough. Bands corresponding to cross-linked species can be identified by estimating the mass after cross-linking (e.g., the mass of protein A plus the mass of its binding partner, protein B) and excised for subsequent proteolysis and MS analysis [36]. In addition, the cross-linking yield can be estimated by examining the staining intensity of the corresponding gel bands.

Gel separation is mainly applied for cross-linked protein complexes. When cross-linking reactions are carried out on one specific protein (e.g., for structural analysis) or the mass difference between a cross-linked complex and its interacting units is not sufficient, the bottom-up method (to characterize peptide fragments from proteolysis) can

be directly applied by combining enrichment, LC/MS, and LC/MS/MS methods. To differentiate cross-linked peptides from unmodified peptides, either gas-phase cleavable cross-linkers that generate unique fragments, or computer programs with appropriate algorithms to identify cross-linked peptides can be used.

1.1.5.2 Computer-aided Identification of Cross-linked Peptides

Spectra obtained from LC/MS/MS analysis of proteolyzed cross-linked proteins or protein complexes are highly complex and vast in number. For intermolecular and dead-end cross-linked peptides, MS/MS identification can be accomplished with certain programs, including “in silico-digestion” programs (e.g., “Peptide Mass” from www.Expasy.org) and MS/MS fragmentation prediction programs (e.g. “MS-Product” from <http://prospector.ucsf.edu>). Any potential residues that undergo cross-linking to form intermolecularly cross-linked and dead-end products can be defined as modified residues with a specific mass shift caused by the cross-linking reaction. Generation of such lists is easily automated.

Detection of intermolecularly cross-linked peptides is much more difficult because the mass shift from inter-cross-linking is unknown prior to identification. Therefore, the strategies used for intramolecular and dead-end species are not applicable. Since 2000, a series of programs have been developed to aid the identification of intermolecularly cross-linked peptides. Some of these are summarized in Table 1.1.

Table 1.1 Computer Programs for Cross-linked Peptide Identification

Program Name	URL*	Reference
MS2Assign	http://roswell.ca.sandia.gov/~mmyang	[51]
MS2PRO	N/A	[101]
SearchXlinks	http://www.searchxlinks.de/cgi-bin/home.pl	[102]
C-MS3D	http://ms3d.org	[103]
xComb	http://phenyx.proteomics.washingto.edu/CXDB/index.cgi	[104]

* Obtained from the references and may have expired.

In addition to the open-source programs mentioned above, in-house programs have been developed to facilitate identification of cross-linked peptides [52, 105].

1.2 Fourier Transform Ion Cyclotron Resonance Mass Spectrometry (FT-ICR MS)

1.2.1 The Basic Theory of FT-ICR MS

The concept of obtaining mass-to-charge ratios via the measurement of ion cyclotron frequencies was introduced in the early 1950s [106]. With the development of FT-NMR, the concept and technique of FT-ICR MS was conceived and first introduced in 1974 by Comisarow and Marshall [107]. Since its inception, FT-ICR MS has become a powerful tool applied in numerous areas, including proteomics.

Unlike other types of mass analyzers, including magnetic sector (ion deflection), TOF (time for ions to travel a certain distance), and quadrupole/ion trap (ion stability in DC and RF fields), the FT-ICR mass analyzer, provides measurement of ion motion in a

fixed magnetic field. Once ions are generated from various ion sources, including ESI and MALDI, they are transferred into the ICR trapping cell (see Figure 1.1) in an ultra high vacuum environment (10^{-9} to 10^{-10} Torr) and a spatially uniform magnetic field (up to 21 Tesla) provided by cryogenic or turbomolecular pumps and superconducting coils, respectively. Ion motion in the ICR trapping cell is governed by the Lorentz force given by equation **1a** in which \mathbf{F} , m , \mathbf{a} , q , \mathbf{v} , \mathbf{B} stand for force, ion mass, acceleration, charge, velocity, and strength of magnetic field, respectively. Specifically, the direction of the Lorentz force is perpendicular to the plane of \mathbf{v} and \mathbf{B} and pointing inward to the center of the ICR trapping cell. If ions remain undisturbed, e.g. no collisions, their path is circular with a radius r , resulting in an outward directed centrifugal force F_c , with the magnitude shown in equation **2**. The centrifugal force balances the inward directed Lorentz force with the magnitude qvB (equation 1b). The linear velocity divided by the cyclotron radius, v/r , in equation **2** can be substituted by the angular velocity, ω , to yield equation **3**. Setting equation **1** equal to equation **3** and rearranging yields equation **4** in which ω is the ion cyclotron frequency.

$$\mathbf{F} = m\mathbf{a} = q\mathbf{v} \times \mathbf{B} \quad (1a) \quad \text{or} \quad F = qvB \quad (1b)$$

$$F_c = \frac{mv^2}{r} \quad (2)$$

$$F_c = m\omega v \quad (3)$$

$$\omega = \frac{Bq}{m} \quad (4)$$

Because B is constant, it is clear that ω is determined by only one variable: the charge-to-mass ratio (q/m). In other words, q/m , and thus m/z (m in units of u and z for the number of elementary charges) can be determined with ultra high accuracy because ω can be measured with high accuracy [108]. Unlike other mass analyzers, initial ion kinetic energy does not influence the measurement because ω is independent of it. In other words, ions with a certain m/z value will demonstrate exactly the same ω regardless of their kinetic energy although they will orbit at different radii.

1.2.2 FT-ICR Instrumentation

The previous section shows that measurement of ω in an ICR trapping cell provides highly accurate m/z values. To achieve that goal, designs of FT-ICR MS instrumentation are very important. Some related aspects are discussed below.

First of all, when ions enter the ICR trapping cell, the magnetic field governs radial ion motion via the Lorentz force. However, ion motion along the direction of the magnetic field is independent of the magnetic field strength and is not confined within the ICR trapping cell. Therefore, trapping electrodes have to be installed at both ends of the ICR trapping cell to provide an axial harmonic electric field preventing ions from escaping axially. By introducing this axial electric field, ions can be held in the ICR trapping cell oscillating between the two trapping electrodes and performing ion cyclotron motion in the radial direction. In addition, the combination of the added electric field and the magnetic field will cause ions to undergo magnetron motion in which the center of cyclotron motion precesses around the ICR trapping cell. The frequency of ion magnetron motion is far less than ω [108].

As ions enter the ICR trapping cell and are trapped, they demonstrate random cyclotron phases. Ions with a certain m/z value may start their cyclotron motion at any point along a circle inside the ICR trapping cell, which prevents detection of ω by measuring induced current between detector plates because currents on one side of the cell would be balanced to zero by currents induced on the opposite side of the cell. In addition, the initial cyclotron radius is much smaller than the ICR cell, precluding detection of induced currents. To solve these problems, RF excitation is applied to excitation electrodes incorporated into the ICR trapping cell (see Fig. 1.1) to provide a spatially uniform electric field oscillating perpendicular to the direction of the magnetic field. The radiofrequency of the excitation electric field can be controlled to match the cyclotron frequency of ions with a certain m/z value and thereby make those ions absorb energy, which expands their ion cyclotron radii, and synchronize their cyclotron motion coherently as an ion packet. Consequently, if an observation point is set on the ICR trapping cell wall, ion packets will approach and leave that point in an alternating manner. Detection electrodes (Fig. 1.1), which are positioned at opposite sides of the ICR trapping cell wall, record the differential current from the orbiting ion packets. This current is then amplified and digitized to generate a time-domain signal containing all ion frequencies (and hence m/z values) present in the ICR cell. By applying fast Fourier transformation, the time-domain signal can be converted to a frequency domain spectrum, which can be converted to an m/z spectrum by using equation 4. However, equation 4 does not take into account higher order effects due to the presence of the axial electric field. Thus, the modified equation 5 is typically used for frequency-to- m/z conversion in which ν_c is the observed cyclotron frequency [23]. It should be pointed out that

detectable image current between the two detection plates requires a certain number of charges, ~ 200 under typical conditions [109].

$$\frac{m}{z} = \frac{A}{v_c} + \frac{B}{v_c^2} \quad (5)$$

Ion excitation in the ICR trapping cell is not only required for detection but also important for ion fragmentation [110] and ejection [108].

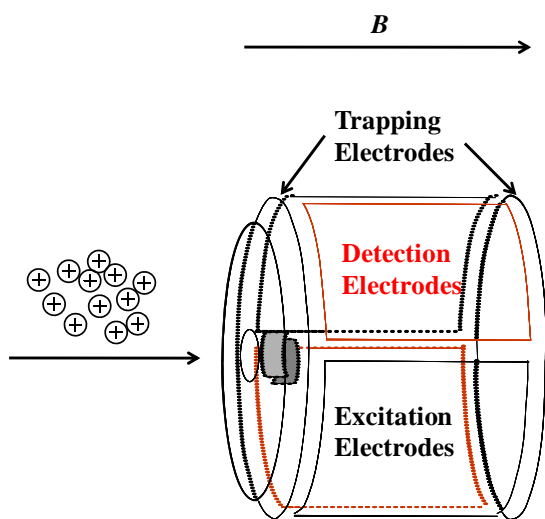


Figure 1.1. Schematic diagram of a typical ICR trapping cell, which includes trapping electrodes, detection electrodes, and excitation electrodes. The direction of ion motion and the magnetic field are indicated with arrows.

As mentioned above, the presence of the magnetic field in ICR MS is crucial for generating ion cyclotron motion. However, a strong magnetic field gradient between the

ICR trapping cell and other parts of the FT-ICR MS instrument causes problems regarding transmission of ions into the ICR trapping cell. This phenomenon is called the magnetic mirror effect [111]. If the ratio of ion axial to radial velocity along the path of motion to the ICR trapping cell is insufficient, ions may be radially ejected [111] or even reverse their direction [112]. Efforts have been made to prevent ions from leaving radially by applying quadrupole [113] or octopole [114] ion guides. In an alternative approach, electrostatic lenses [115] are used to increase ion axial velocity through the magnetic field gradient and then retarding the ions before trapping.

Most experiments described in this thesis were carried out with a 7T-ESI-quadrupole-FT-ICR mass spectrometer, shown in Figure 1.2. FT-ICR MS instruments are typically coupled with an ESI source, as first reported in 1989 [116] because: 1) ESI tends to provide multiply charged ions with m/z values typically below 2000 [112]. Limiting m/z values is important because the performance of FT-ICR MS decreases as m/z values increase [108]. For example, as shown in equation 6 [117], the resolving power (R) of FT-ICR MS is proportional to ion cyclotron frequency and the duration (T) of detection. Clearly, ions with lower m/z values (higher ω) give higher R . In order to get similar R values for ions with higher m/z , T must be longer [117].

$$R = \frac{\omega T}{2} \quad (6)$$

2) multiply charged ions are preferred in MS/MS analysis and specifically required in some FT-ICR MS/MS techniques, including electron capture dissociation (ECD) [118] in

positive ion mode and electron detachment dissociation (EDD) [119] in negative ion mode. MALDI typically generates singly charged ions with much higher m/z values than ESI and thus it is not applied as widely as ESI in FT-ICR MS.

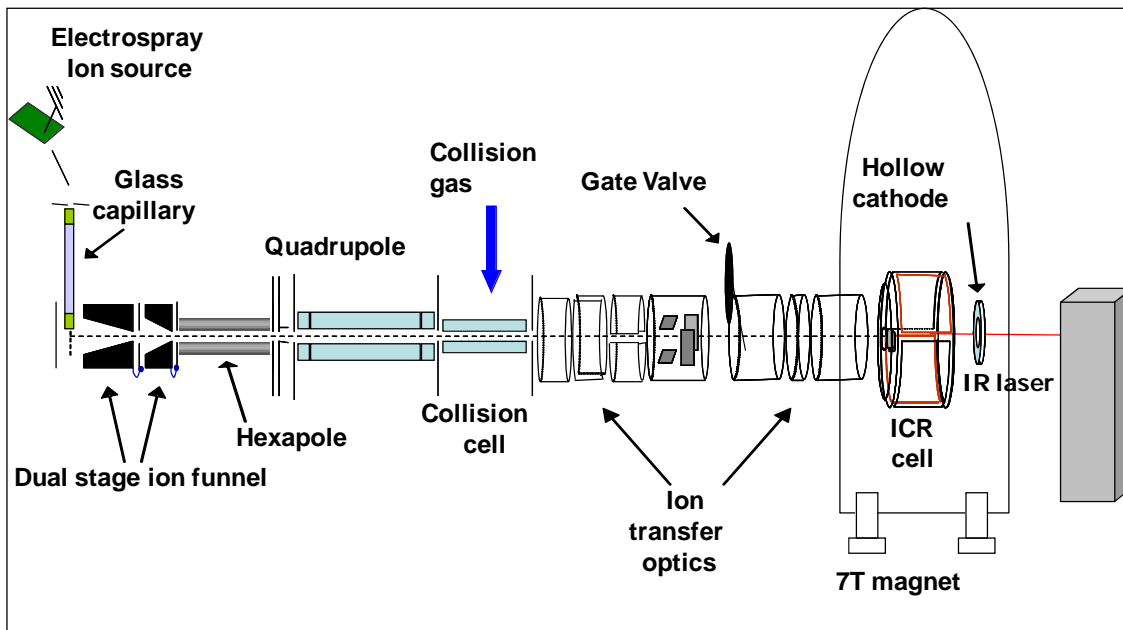


Figure 1.2. Diagram of 7T FT-ICR mass spectrometer used in this work.

Ions generated at atmospheric pressure by the ESI source are unavoidably experiencing collisions and repulsion between each other. Therefore, a dual stage ion funnel, as shown in Fig. 1.2, is located after the ESI source to accept a wide spatial distribution of ions and focus them into the mass spectrometer by a combination of RF fields and a gradient DC potential [120-122]. Ions are then subjected to a first round of external ion accumulation in a hexapole. A quadrupole mass filter is placed after this

hexapole to provide further ion focusing and precursor ion selection for MS/MS analysis. Mass-selective external ion accumulation is accomplished in a second hexapole (collision cell) located after the quadrupole. Mass-selective external ion accumulation provides improved sensitivity and dynamic range of ESI FT-ICR MS [123]. The collision cell can also be used for collision induced dissociation (CID) by adjusting its DC offset. Product ions are analyzed in the ICR trapping cell. A series of high voltage ion transfer optics are utilized as described above, to allow ions to overcome the magnetic mirror effect and enter the ICR cell.

Fig. 1.2 also shows two additional components: first, an indirectly heated dispenser cathode [124], which generates electrons for ion-electron reactions, including ECD, EDD, electron induced dissociation (EID) [125, 126], etc.; second, a 10.6 μm CO₂ laser, which provides photons for infrared multiphoton dissociation (IRMPD) [127, 128].

In summary, FT-ICR MS provides the highest mass resolving power, defined as $m/\Delta m_{50\%}$ (m is the mass of an ion and $\Delta m_{50\%}$ is the peak width of that ion at half maximum peak height) of all mass analyzers. Values of $\sim 4 \times 10^6$ at m/z 1,000 [23] and 8×10^6 for crude oil analysis [129] have been reported, and even 1.7×10^7 at m/z 1,087 by modifying the ICR trapping cell [130]. Purcell et al. reported the identification of more than 12,000 compounds from crude oil in a 400 Da mass window [131-133]. For biomolecules, FT-ICR MS can obtain unit protein resolution up to 142 kDa [134]. In addition, FT-ICR MS provides up to sub-ppm mass measurement accuracy for peptides [135] and better than 100-300 ppb in crude oil analysis [136]. Although ~ 200 charges are required to generate detectable image current in an ICR trapping cell (as mentioned above), those charges have to enter the cell if an external ion source is used.

Nevertheless, FT-ICR MS can still provide detection limits as low as ~6,000 molecules with external ion accumulation [123]. Also, single-molecule detection has been reported with up to 10^4 charges [137].

1.3 Tandem Mass Spectrometry (MS/MS)

The term tandem mass spectrometry (MS/MS) indicates two-stages of MS analysis. The first stage is to isolate precursor ions with specific m/z values for further analysis. In the case of the FT-ICR MS instrument shown in Figure 1.2, isolation can be achieved by the external quadrupole, or in the ICR trapping cell by using correlated harmonic excitation fields [138]. The second MS stage is to apply various ion activation techniques to dissociate precursor ions and generate product ions. Structural information of precursor ions can be deduced by analyzing these product ions. Similarly, MS analysis in more than two stages (e.g., MS^3 , MS^4 , etc.) [139, 140] is performed by further isolating a specific product ion and subjecting it to further fragmentation. In the work discussed in this thesis, utilized MS/MS techniques include CID, IRMPD, ECD, electron transfer dissociation (ETD) [141], and EDD. These techniques are discussed in detail below.

1.3.1 CID and IRMPD: Slow Heating Methods to Produce Fragmentation

Although the manner of generating precursor ion excitation is different in CID and IRMPD, they are classified into one category because they yield similar fragmentation pathways and generate comparable product ions after activation.

Gas-phase ion decomposition due to collisional activation was observed and explained in the beginning of the 20th century [142, 143]. The first set of CID spectra

were reported in the 1960s [144, 145]. Later on, McLafferty and co-workers [146] proposed that CID would be a powerful tool to characterize ion structure. After nearly four decades of research and development, CID has become the most widely applied MS/MS technique, typically performed in the low-energy regime, i.e. at less than 100 eV. Generally, low-energy CID can be considered as a two-step process [147, 148]. In the first step, a precursor ion ($A^{n+/-}$) collides with target neutral gas, e.g., N_2 or Ar, and obtains vibrational or electronic internal energy [147] by absorbing translational energy during the collision. Precursor ions are continually excited by multiple collisions to yield $A^{n+/-*}$. The interval of each collision is ~tens to hundreds of milliseconds [149]. Due to the relatively long time scale for excitation, low-energy CID is considered a slow-heating MS/MS method [150]. In the second step, internal energies distribute throughout the molecule and cause rupture of the most labile chemical bonds. Formation of product ions in CID is a result of competition between multiple dissociation pathways [151] and the dissociation starts with the channels of lowest dissociation energy [147].

The development of “soft” ionization techniques, including ESI and MALDI, allowed CID to be applied to large biomolecules. Peptide fragmentation behavior in CID is influenced by the collision energy. Low energy CID (1-100 eV) of peptide cations produces mainly *b*- and *y*-type product ions (Figure 1.3.) by “charge-directed fragmentation” [152], as further discussed below. In high-energy CID (keV collision energy), *v*-, *d*-, and *w*-type ions (Figure 1.3.) are also generated via “charge-remote fragmentation” [153]. CID fragmentation behavior for deprotonated peptides is more complicated, demonstrating the same product ion types as in positive ion CID (e.g., *b*- and *y*-type ions) but also other ions resulting from various backbone cleavages and side

chain losses [154].

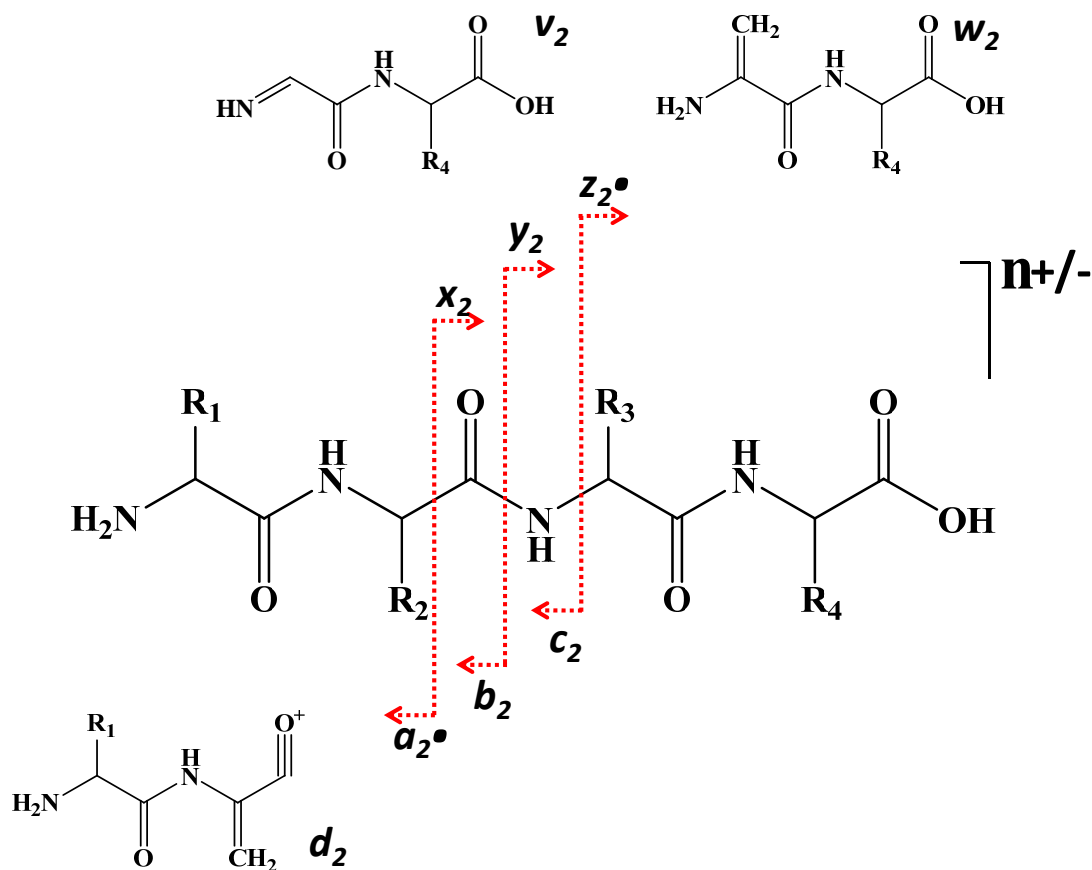


Figure 1.3. Peptide product ion nomenclature in MS/MS. Cleavage of C α -C, C-N, and N-C α backbone bonds yields a -/ x -, b -/ y -, and c -/ z -type product ions, respectively. Side chain losses (mainly in high-energy CID) produce d -, v -, and w -type ions.

In IRMPD, precursor ions with IR chromophore(s) are irradiated with a low power CO₂ laser (<100 W) and activated by absorbing photons. Because the energy

transferred to precursor ions by each photon is only about 0.1 eV [155], relatively long duration of IR irradiation (ten to hundreds of milliseconds, or more) is needed for generating effective activation and dissociation, thus IRMPD is also a slow-heating technique. Subsequently, activated precursor ions undergo internal energy redistribution and dissociations similar to those from CID. Therefore, IRMPD and CID provide similar spectra in most cases. One advantage of IRMPD over CID is the avoidance of the low mass cut-off limit in RF-based trapping instruments (e.g., ion trap) [155]. In addition, the amount of energy deposited into precursor ions can be adjusted more accurately than CID by varying laser power or irradiation time [155]. IRMPD can also provide higher fragmentation efficiency than CID for phosphate-containing molecules, including phosphopeptides [156, 157], products from a phosphate-containing cross-linker [86], and metabolites [158] due to the high gas-phase IR absorption of the phosphate group. Thus, such species can be differentiated from non-phosphate-containing analytes at low irradiation power for which phosphate-containing species will show reduced abundances (due to dissociation) and other species will not. Finally, IRMPD is preferred over in-cell CID in FT-ICR MS because introduction of collision gas, which decreases FT-ICR performance, is not required.

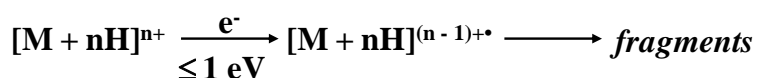
Fragmentation of protonated peptides in CID and IRMPD can be rationalized by the “mobile proton model” [159-162]. According to this theory, protons are originally located at basic sites, including N-termini and side chains of basic residues (if available). Protons may also associate with the oxygen atom of the amide carbonyl group or the backbone amide nitrogen atom by solvation. Following peptide activation from the energy imparted in CID or IRMPD, protons can migrate from their original locations to

backbone amide nitrogens. Protons initially located at strongly basic residues, i.e. arginine, are restricted from migrating effectively and, thus, the presence of arginines equal to or in higher number than the number of protons alters fragmentation behavior [159].

1.3.2 ECD, ETD, and EDD: Radical-driven Fragmentation Techniques

ECD, ETD, and EDD are categorized together because they all rely on the generation of gas-phase radical ions to induce dissociation. In addition, their peptide fragmentation patterns are completely different from those in CID and IRMPD. Therefore, radical-driven and slow-heating based dissociation methods yield complementary product ions. Combining these two kinds of MS/MS approaches extends the amount of structural information that can be generated for biomolecules, including proteins, peptides, and carbohydrates.

Since its inception [118], ECD has become a promising MS/MS technique. In ECD (see Scheme 1.6), low energy electrons (<1 eV) are captured by multiply charged precursor cations, resulting in the formation of a radical charge reduced cation and subsequent N-C_α backbone bond cleavage generates even-electron c- and radical z-type product ions [118] (Figure 1.3).



Scheme 1.6. ECD process.

One of the most exciting characteristics of ECD is the retention of protein post-translational modifications (PTMs) during backbone fragmentation. As a result, ECD is extremely useful for localizing PTMs, including phosphorylation [163-169], glycosylation [170-174], and sulfation [175, 176], which are labile in the gas phase and thus preferentially lost in slow-heating MS/MS. In addition, ECD provides preferential cleavage of disulfide (S-S) bonds [177], which demonstrate limited fragmentation in positive ion mode low-energy CID [178]. S-S bond rupture can also be achieved in several other MS/MS approaches, including negative mode CID [179] and IRMPD [180], EDD [180], and high-energy CID [92, 181, 182]. In some cases, ECD can retain and therefore characterize non-covalent interactions at protein-protein interfaces [31, 183]. Because CID and ECD produce different product ion types (*b*-/*y*- and *c*-/*z*-type ions, respectively) they can be combined to provide complementary sequential and structural information of proteins and peptides, which is particularly useful for peptide *de novo* sequencing [184]. Limitations of ECD include the charge state (*n*) requirement ($n \geq 2$, otherwise not applicable) and its low fragmentation efficiency [185, 186].

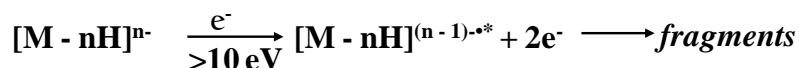
The exact mechanism of ECD is still under controversy. At present, there are two main theories: the first one for peptide ECD [118, 177, 187, 188] involves electron capture at protonated sites, including the side chains of basic residues (Arg, Lys, and His) or the N-terminal primary amine group, to yield neutralization and formation of a hypervalent radical center with subsequent energy release. A hot hydrogen atom (H•) is ejected and can attack an S-S bond (if present), or a backbone carbonyl group to form a labile aminoketyl intermediate. This hydrogen migration is followed by preferential S-S bond cleavage or non-selective cleavage of adjacent N-C_α bonds, respectively. In the

latter case, *c*- and *z*- type ions are generated (Figure 1.3). The second theory, referred to as the “superbase mechanism” was proposed by Turecek’s [189] and Simons’ groups [190, 191]. Here, S-S bonds or backbone carbonyl groups capture an electron directly into their antibonding orbitals, generating a highly basic site (superbase). Protons are then abstracted from nearby locations to yield charge neutralization, and subsequent N-C_α bond cleavage. In the superbase model, protons do not have to originate from protonated basic sites, thus, it can explain ECD of metal-adducted peptides, particularly because the acidity of C_α protons can be greatly increased in the presence of metals [189]. Simons and co-workers showed computationally that 90-99% of electrons are captured by positively charged sites but 1-10% are directly attached to either σ* (S-S bond) or π* (amide) orbitals assisted by Columbic stabilization from adjacent positively charged groups, rendering attachment exothermic [190, 191]. Further, electrons captured by positively charged groups can be released and transferred to S-S or N-C_α bonds [192].

ETD is believed to be analogous to ECD by sharing a similar mechanism and generating *c*- and *z*-type product ions [141, 192, 193]. One favorable characteristic of ETD over ECD is its direct compatibility with radio-frequency based ion storage without needing a magnetic field to confine electrons [194]. Because the electron transfer process in ETD relies on electron donation from radical reagent anions, some factors that influence ECD and ETD dissociation, including cross sections for electron capture/transfer, recombination energies, and the time scales of the electron capture/transfer processes, can be different [195]. For example, precursor ions absorb all electron energy in ECD but, in ETD, energy is partitioned between analyte ions and the remaining neutral reagent [192]. In addition, it has been reported that doubly protonated

precursor ions yield less backbone fragmentation than their triply protonated counterparts in ECD [196]. In ETD, doubly protonated species generally generate limited fragmentation unless supplementary activation methods, including collisional activation and pre-IR irradiation, are applied [194, 195].

EDD is an ion-electron based MS/MS approach for multiply charged anions. As shown in Scheme 1.7, precursor anions are irradiated with electrons with much higher energy (>10 eV) than in ECD. Upon irradiation, one electron is detached from precursor ions, leading to formation of charge reduced anions and subsequent dissociation. For peptides, mainly the backbone C_α-C bond is cleaved to produce *a*- and *x*-type ions (Figure 1.3). Because EDD operates in negative ion mode, it is an ideal approach for characterizing acidic biomolecules, including oligonucleotides [197-199] and oligosaccharides [200-202]. Similar to ECD, EDD retains PTMs, including phosphorylation [169] and sulfation [119].



Scheme 1.7. EDD process.

The mechanism of EDD has been studied by Simons' and Zubarev's groups [203, 204]. Briefly, formation of multiply charged anions is the result of deprotonation at acidic residues (aspartic and glutamic acids with carboxyl side chain), C-termini, and backbone amide nitrogens. In the latter case, electron ejection from the deprotonated site results in formation of a radical site on the nitrogen atom. Experimental observation [119,

205] as well as computational analysis [203, 204] revealed that backbone *N*-centered radicals induces C_{α} -C cleavage to produce even-electron *x*-type and radical *a*-type product ions.

1.4 Application of FT-ICR MS to Investigate Natural Product Biosynthetic Pathways

1.4.1 Natural Product Biosynthesis by NRPS and PKS Catalysis

Non-ribosomal peptide synthetases (NRPSs) and polyketide synthases (PKSs) are two enzyme families that catalyze the biosynthesis of a vast number of natural products with tremendous structural diversity. In addition, many natural products from PKS/NRPS biosynthesis demonstrate pharmacological potential, including antitumor[206], antimicrobial, and immunosuppressant [207, 208] properties. Some examples are shown in Figure 1.4.

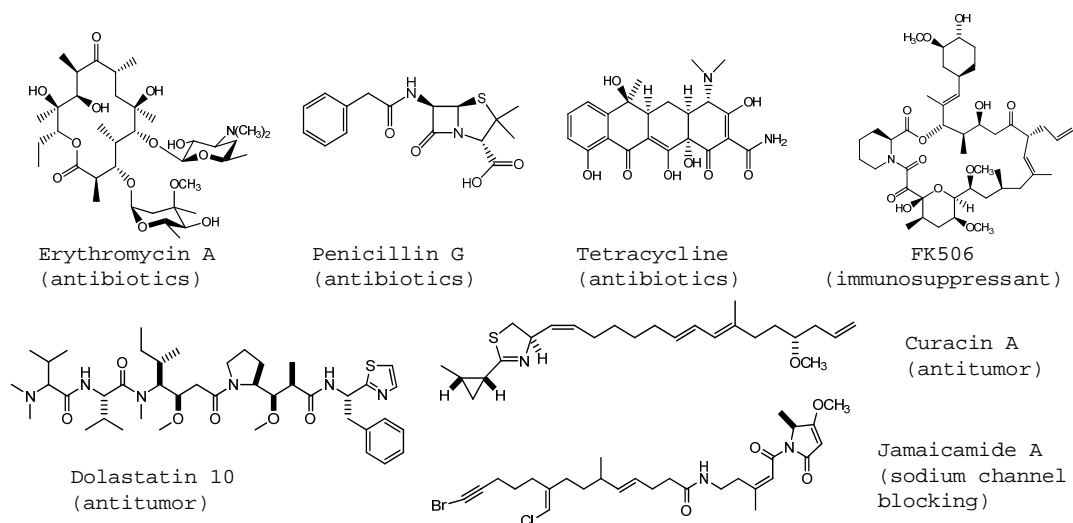


Figure 1.4. Structure and biological functions of some natural products derived from

NRPS and PKS biosynthesis.

During NRPS and PKS catalysis, substrates are covalently linked to a serine residue of a carrier protein through a phosphopantetheine (PPant) arm (chemical structure is shown in Chapter 7), which is introduced by a phosphopantetheinyl transferase [209, 210]. Substrates in NRPS/PKS catalysis are subjected to various chemical reactions (e.g., dehydration and decarboxylation) and undergo chain elongation to form intermediates of increasing length. These intermediates are transferred to downstream carrier domains for the next step of chain elongation and processing. Eventually, the natural product is released.

1.4.2 The Role of FT-ICR MS in Investigating NRPS and PKS Biosynthesis

The first application of FT-ICR MS to investigate the proteins of an NRPS biosynthetic pathway was reported in 1999 [211]. In that work, a proteolytic peptide with PPant moiety was detected by FT-ICR MS without HPLC purification.

In top-down analysis, the ultra high resolving power provided by FT-ICR MS can resolve isotopic peaks for a protein (e.g., carrier domains with loaded substrates or intermediates) in a specific charge state and, therefore, the correct charge state can be obtained from the m/z difference between isotopic peaks by a simple calculation [208]. Knowledge of the charge state corresponding to a particular mass spectral peak allows the mass of that protein to be measured with high accuracy. Based on this virtue of FT-ICR MS, NRPS/PKS catalytic reactions can be straightforwardly monitored by measuring the mass shift between carrier domain-loaded substrates and products and, thus, provide

insights into the function of specific catalytic domains. For example, - 18 Da shift between substrate and product indicates a dehydration reaction. We have successfully applied this strategy to interrogate NRPS/PKS catalysis as discussed in Chapter 7.

Under certain conditions, MS/MS approaches provided by FT-ICR MS can simplify the analysis of NRPS/PKS reactions. For example, application of IRMPD/CID has been shown to cleave the PPant arm of carrier domains [212]. Substrate conversion information (e.g., dehydration, decarboxylation, halogen addition) remains linked to the ejected low mass PPant ions and can be deduced from MS/MS. Therefore, the complex isotopic distributions of intact proteins in top-down analysis can be avoided.

1.5 Dissertation Overview

The main objectives for this thesis are 1) to apply chemical cross-linking, MS, and MS/MS techniques for investigation of protein-protein interactions; 2) to investigate the optimal conditions and approach for cleaving disulfide-containing chemical cross-linkers in the gas phase; 3) to study the MS/MS behavior of iodinated amino acid side chains for evaluating the prospective of designing a novel chemical cross-linker with a C-I bond; 4) to design a novel chemical cross-linker with metal-dioxide enrichment potential; 5) to apply the mass-selective interface in FT-ICR MS for improving detection in the low m/z area; 6) to apply FT-ICR MS and IRMPD for characterization of enzyme function and functional differentiation.

In Chapter 2, photo-cross-linking (BP-based), biotin-avidin affinity purification, and multiplexed mass spectrometric techniques, including ESI FT-ICR MS, MALDI MS,

low-energy CID, and high-energy MALDI TOF/TOF CID were combined to successfully map the binding sites between three gene transcriptional activators, including Gal4, Gcn4, and VP2, and the coactivator Med15. In some cases, resolution up to a single amino acid residue could be obtained. To our knowledge, this work includes the first report of BP-based photo cross-linking for peptides up to 5 kDa and identity confirmation by MS/MS. It also reports for the first time specific C-S/S-C and C-C bond cleavage of BP cross-linked products in MALDI TOF/TOF CID, thus presenting an additional tool for identification of such products. This work was a collaboration project with Professor Anna Mapp and has been published in *Angewandte Chemie* [71].

Chapter 3 presents efforts to find the optimal approach for dissociating disulfide-containing chemical cross-linkers in the gas phase and thereby facilitate and expedite the identification of cross-linked peptides. In this work, DTSSP, a commercial chemical cross-linker with a midpoint SS linkage, was reacted with model peptides as well as a protein (ubiquitin). Among the cross-linked peptides obtained from these reactions, five intermolecularly cross-linked peptides (ICPs) were subjected to ECD, activated ion (AI) ECD, MALDI TOF/TOF CID, negative ion CID, and EDD. The results demonstrate that ECD provides the most efficient S-S and C-S bond cleavage but, sometimes, IR pre-irradiation is required. Negative ion CID, which provides preferred S-S and C-S bond cleavages for peptides containing disulfide bonds, did not yield stable and consistent results in our work. EDD resulted in S-S and C-S bond cleavages but with low efficiency. MALDI TOF/TOF CID showed C-S bond cleavage to form a 66 Da doublet, which can aid the identification of ICPs. In addition, MALDI TOF/TOF CID does not require highly abundant precursor ions. Based on these results, it appears that the combination of

ECD and MALDI TOF/TOF CID may be the best choice for maximizing S-S and C-S bond cleavage in ICPs.

In Chapter 4, specific residues in peptides, including His and Tyr, were selectively iodinated. Iodinated peptides were subjected to ECD and ETD in their triply- and doubly protonated as well as calcium-adducted forms. For all iodinated peptides, carbon iodine (C-I) bond cleavage was observed in both ECD and ETD but with various efficiencies depending on the distance between the positive charge and the C-I bond, either through bond or through space: the closer the distance, the higher trend for efficient C-I bond cleavage in ECD/ETD. C-I bonds were not cleaved in MALDI TOF/TOF CID. These results provide new insights into the mechanism(s) of ECD and ETD for proteins/peptides. In addition, selective C-I bond rupture in ECD offers interesting prospects for designing novel C-I bond containing cross-linkers with unique iodine ejection in ECD.

Efforts to design a new phosphate-containing homobifunctional cross-linker are shown in Chapter 5. Based on previous reports, zirconium dioxide (ZrO_2) and titanium dioxide (TiO_2) enrichment can specifically enhance the detection of phosphopeptides in MS [213]. After incubating the designed phosphate-containing cross-linker with substance P, one intramolecularly cross-linked product was observed, which confirmed the reactivity of the new cross-linker. In addition, the cross-linked product, spiked into a proteolytic peptide mixture (trypsin digested apomyoglobin) could be selectively enriched by TiO_2 and ZrO_2 due to the presence of the phosphate group. CID demonstrated intriguing fragmentation patterns in which the labile phosphate group was retained.

In Chapter 6, we utilized an external quadrupole to improve the detection of peptides in FT-ICR MS, particularly within the 350-600 m/z region. Data show that application of quadrupole fractionation (QF) (i.e., use of consecutive 50 m/z isolation windows), increases peptide signals 2-11 fold compared to standard broadband mode detection. The additional time required for QF was considered and compensated for.

In Chapter 7, FT-ICR MS was successfully applied to characterize portions of the biosynthetic pathway of the natural products, curacin A (Cur) and jamaicamide (Jam). This work included elucidation of the functional differentiation of the highly similar Cur and Jam biosynthetic enzymes, and provided supporting information for enzyme functional determination based on crystal structures. The function of a GCN5-related *N*-acetyltransferase (GNAT) in the Cur pathway was characterized with FT-ICR MS and IRMPD, demonstrating the unprecedented function of transferring an acyl group to a free thiol group rather than the canonical amine group.

The functions of putative dehydratases (ECH₁) and decarboxylases (ECH₂) from the Cur and Jam pathways were also revealed. ECH₁ and ECH₂ from the Cur pathway generate a product with α,β C=C moiety whereas Jam ECH₁ and ECH₂ yield a β,γ C=C configuration. Coupled with Cur halogenase (Hal), Cur ECH₁ and ECH₂, Cur enoylreductase (ER) was revealed to catalyze an unprecedented cyclopropanation reaction. Meanwhile, Cur ER still retains the canonical function of reducing an α,β C=C bond. The saturation function of Jam ER is redundant in the Jam biosynthetic pathway due to generation of β,γ C=C and vinyl chloride group by upstream enzymes (Hal, ECH₁ and ECH₂). By applying IRMPD, the catalytic efficiency of Cur ER cyclopropanation as well as Cur ER and Jam ER saturation were evaluated. The results show that Cur ER

catalyzes cyclopropanation much faster, around 240-fold, than saturation. Jam ER still shows highly efficient catalytic ability for the saturation reaction. With a similar strategy, the function of a series of site-specific Hal mutants was also evaluated. Top-down FT-ICR MS and IRMPD were also applied to characterize intermediates after sulfotransferase (ST) and thioesterase (TE) treatments for elucidating the chain termination mechanism in the Cur pathway. The work in this Chapter is part of collaboration projects with Professors David Sherman and Janet Smith and has been published in *Science*, *Nature*, *Journal of the American Chemical Society*, and *Proceedings of the National Academy of Sciences of the United States of America* [214-217]. A summary of all results in this thesis as well as prospects for future work are provided in Chapter 8.

1.6 References

1. Hart, G.T.; Ramani, A.K.; Marcotte, E.M., How complete are current yeast and human protein-interaction networks? *Genome Biol.*, **2006**, *7*, 121-129.
2. Sharon, M., How Far Can We Go with Structural Mass Spectrometry of Protein Complexes? *J. Am. Soc. Mass Spectrom.*, **2010**, *21*, 487-500.
3. Stumpf, M.P.H.; Thorne, T.; de Silva, E.; Stewart, R.; An, H.J.; Lappe, M.; Wiuf, C., Estimating the size of the human interactome. *Proc. Natl. Acad. Sci. U. S. A.*, **2008**, *105*, 6959-6964.
4. Mohamed, T.P.; Carbonell, J.G.; Ganapathiraju, M.K., Active learning for human protein-protein interaction prediction. *Bmc Bioinformatics*, **2010**, *11*, S57.
5. Rual, J.F.; Venkatesan, K.; Hao, T.; Hirozane-Kishikawa, T.; Dricot, A.; Li, N.; Berriz, G.F.; Gibbons, F.D.; Dreze, M.; Ayivi-Guedehoussou, N.; Klitgord, N.; Simon, C.; Boxem, M.; Milstein, S.; Rosenberg, J.; Goldberg, D.S.; Zhang, L.V.; Wong, S.L.; Franklin, G.; Li, S.M.; Albala, J.S.; Lim, J.H.; Fraughton, C.; Llamas, E.; Cevik, S.; Bex, C.; Lamesch, P.; Sikorski, R.S.; Vandenhaute, J.; Zoghbi, H.Y.; Smolyar, A.; Bosak, S.; Sequerra, R.; Doucette-Stamm, L.; Cusick, M.E.; Hill, D.E.; Roth, F.P.; Vidal, M., Towards a proteome-scale map of the

- human protein-protein interaction network. *Nature*, **2005**, *437*, 1173-1178.
6. Geiger, J.H.; Hahn, S.; Lee, S.; Sigler, P.B., Crystal structure of the yeast TFIIA/TBP/DNA complex. *Science*, **1996**, *272*, 830-836.
 7. Tan, S.; Richmond, T.J., Crystal structure of the yeast MAT alpha 2/MCM1/DNA ternary complex. *Nature*, **1998**, *391*, 660-666.
 8. Schulman, B.A.; Carrano, A.C.; Jeffrey, P.D.; Bowen, Z.; Kinnucan, E.R.E.; Finnin, M.S.; Elledge, S.J.; Harper, J.W.; Pagano, M.; Pavietich, N.P., Insights into SCF ubiquitin ligases from the structure of the Skp1-Skp2 complex. *Nature*, **2000**, *408*, 381-386.
 9. Scott, F.L.; Stec, B.; Pop, C.; Dobaczewska, M.K.; Lee, J.J.; Monosov, E.; Robinson, H.; Salvesen, G.S.; Schwarzenbacher, R.; Riedl, S.J., The Fas-FADD death domain complex structure unravels signalling by receptor clustering. *Nature*, **2009**, *457*, 1019-1022.
 10. Milligan, R.A., Protein-protein interactions in the rigor actomyosin complex. *Proc. Natl. Acad. Sci. U. S. A.*, **1996**, *93*, 21-26.
 11. Goley, E.D.; Rammohan, A.; Znameroski, E.A.; Firat-Karalar, E.N.; Sept, D.; Welch, M.D., An actin-filament-binding interface on the Arp2/3 complex is critical for nucleation and branch stability. *Proc. Natl. Acad. Sci. U. S. A.*, **2010**, *107*, 8159-8164.
 12. Legault, P.; Li, J.; Mogridge, J.; Kay, L.E.; Greenblatt, J., NMR structure of the bacteriophage lambda N peptide/boxB RNA complex: Recognition of a GNRA fold by an arginine-rich motif. *Cell*, **1998**, *93*, 289-299.
 13. Banci, L.; Bertini, I.; Cantini, F.; Felli, I.C.; Gonnelli, L.; Hadjiliadis, N.; Pierattelli, R.; Rosato, A.; Voulgaris, P., The Atx1-Ccc2 complex is a metal-mediated protein-protein interaction. *Nat. Chem. Bio.*, **2006**, *2*, 367-368.
 14. Tang, C.; Iwahara, J.; Clore, G.M., Visualization of transient encounter complexes in protein-protein association. *Nature*, **2006**, *444*, 383-386.
 15. Betzi, S.; Restouin, A.; Opi, S.; Arold, S.T.; Parrot, I.; Guerlesquin, F.; Morelli, X.; Collette, Y., Protein-protein interaction inhibition (2P2I) combining high throughput and virtual screening: Application to the HIV-1 Nef protein. *Proc. Natl. Acad. Sci. U. S. A.*, **2007**, *104*, 19256-19261.
 16. Salzmann, M.; Pervushin, K.; Wider, G.; Senn, H.; Wuthrich, K., NMR assignment and secondary structure determination of an octameric 110 kDa protein using TROSY in triple resonance experiments. *J. Am. Chem. Soc.*, **2000**, *122*, 7543-7548.
 17. Yu, H.T., Extending the size limit of protein nuclear magnetic resonance. *Proc. Natl. Acad. Sci. U. S. A.*, **1999**, *96*, 332-334.
 18. Xu, Y.Q.; Zheng, Y.; Fan, J.S.; Yang, D.W., A new strategy for structure determination of large proteins in solution without deuteration. *Nat. Methods*, **2006**, *3*, 931-937.
 19. Fenn, J.B.; Mann, M.; Meng, C.K.; Wong, S.F.; Whitehouse, C.M., Electrospray Ionization for Mass-Spectrometry of Large Biomolecules. *Science*, **1989**, *246*, 64-71.
 20. Karas, M.; Bachmann, D.; Bahr, U.; Hillenkamp, F., Matrix-Assisted Ultraviolet-Laser Desorption of Nonvolatile Compounds. *Int. J. Mass Spectrom. Ion*

- Processes*, **1987**, 78, 53-68.
21. Tanaka, K.; Waki, H.; Ido, Y.; Akita, S.; Yoshida, Y.; Yoshida, T., Protein and polymer analyses up to m/z 100 000 by laser ionization time-of-flight mass spectrometry. *Rapid Commun Mass Spectrom*, **1988**, 2, 151-153.
 22. Valaskovic, G.A.; Kelleher, N.L.; Little, D.P.; Aaserud, D.J.; McLafferty, F.W., Attomole-Sensitivity Electrospray Source for Large-Molecule Mass-Spectrometry. *Anal. Chem.*, **1995**, 67, 3802-3805.
 23. Marshall, A.G.; Hendrickson, C.L., High-Resolution Mass Spectrometers. *Annu. Rev. Anal. Chem.*, **2008**, 1, 579-599.
 24. Zhang, L.K.; Rempel, D.; Pramanik, B.N.; Gross, M.L., Accurate mass measurements by Fourier transform mass spectrometry. *Mass Spectrom. Rev.*, **2005**, 24, 286-309.
 25. Makarov, A.; Denisov, E.; Kholomeev, A.; Baischun, W.; Lange, O.; Strupat, K.; Horning, S., Performance evaluation of a hybrid linear ion trap/orbitrap mass spectrometer. *Anal. Chem.*, **2006**, 78, 2113-2120.
 26. Loo, J.A., Studying noncovalent protein complexes by electrospray ionization mass spectrometry. *Mass Spectrom. Rev.*, **1997**, 16, 1-23.
 27. Benesch, J.L.P.; Ruotolo, B.T.; Simmons, D.A.; Robinson, C.V., Protein complexes in the gas phase: Technology for structural genomics and proteomics. *Chem. Rev.*, **2007**, 107, 3544-3567.
 28. Ganem, B.; Li, Y.T.; Henion, J.D., Detection of Noncovalent Receptor Ligand Complexes by Mass-Spectrometry. *J. Am. Chem. Soc.*, **1991**, 113, 6294-6296.
 29. Huang, E.C.; Pramanik, B.N.; Tsarbopoulos, A.; Reichert, P.; Ganguly, A.K.; Trotta, P.P.; Nagabhushan, T.L.; Covey, T.R., Application of Electrospray Mass-Spectrometry in Probing Protein-Protein and Protein Ligand Noncovalent Interactions. *J. Am. Chem. Soc.*, **1993**, 4, 624-630.
 30. Potier, N.; Rogniaux, H.; Chevreux, G.; Van Dorsselaer, A., Ligand-metal ion binding to proteins: Investigation by ESI mass spectrometry. *Biol. Mass Spectrom.*, **2005**, 402, 361-389.
 31. Xie, Y.M.; Zhang, J.; Yin, S.; Loo, J.A., Top-down ESI-ECD-FT-ICR mass spectrometry localizes noncovalent protein-ligand binding sites. *J. Am. Chem. Soc.*, **2006**, 128, 14432-14433.
 32. Yin, S.; Loo, J.A., Elucidating the Site of Protein-ATP Binding by Top-Down Mass Spectrometry. *J. Am. Soc. Mass Spectrom.*, **2010**, 21, 899-907.
 33. Uetrecht, C.; Versluis, C.; Watts, N.R.; Roos, W.H.; Wuite, G.J.L.; Wingfield, P.T.; Steven, A.C.; Heck, A.J.R., High-resolution mass spectrometry of viral assemblies: Molecular composition and stability of dimorphic hepatitis B virus capsids. *Proc. Natl. Acad. Sci. U. S. A.*, **2008**, 105, 9216-9220.
 34. Uetrecht, C.; Versluis, C.; Watts, N.R.; Wingfield, P.T.; Steven, A.C.; Heck, A.J.R., Stability and shape of hepatitis B virus capsids in vacuo. *Angew. Chem., Int. Ed.*, **2008**, 47, 6247-6251.
 35. Videler, H.; Ilag, L.L.; McKay, A.R.C.; Hanson, C.L.; Robinson, C.V., Mass spectrometry of intact ribosomes. *FEBS Lett.*, **2005**, 579, 943-947.
 36. Sinz, A., Chemical cross-linking and mass spectrometry to map three-dimensional protein structures and protein-protein interactions. *Mass Spectrom. Rev.*, **2006**, 25,

- 663-682.
37. Bragg, P.D.; Hou, C., Subunit Composition, Function, and Spatial Arrangement in Ca²⁺-Activated and Mg²⁺-Activated Adenosine Triphosphatases of Escherichia-Coli and Salmonella-Typhimurium. *Arch. Biochem. Biophys.*, **1975**, *167*, 311-321.
 38. Lomant, A.J.; Fairbanks, G., Chemical Probes of Extended Biological Structures - Synthesis and Properties of Cleavable Protein Cross-Linking Reagent [Dithiobis(Succinimidyl-S-35 Propionate). *J. Mol. Biol.*, **1976**, *104*, 243-261.
 39. Smyth, D.G.; Konigsberg, W.; Blumenfeld, O.O., Reactions of N-Ethylmaleimide with Peptides + Amino Acids. *Biochem. J.*, **1964**, *91*, 589-&.
 40. Hoare, D.G.; Koshland, D.E., A Procedure for Selective Modification of Carboxyl Groups in Proteins. *J. Am. Chem. Soc.*, **1966**, *88*, 2057-&.
 41. Bennett, K.L.; Kussmann, M.; Bjork, P.; Godzwon, M.; Mikkelsen, M.; Sorensen, P.; Roepstorff, P., Chemical cross-linking with thiol-cleavable reagents combined with differential mass spectrometric peptide mapping - A novel approach to assess intermolecular protein contacts. *Protein Sci.*, **2000**, *9*, 1503-1518.
 42. Schrock, A.K.; Schuster, G.B., Photochemistry of Phenyl Azide - Chemical-Properties of the Transient Intermediates. *J. Am. Chem. Soc.*, **1984**, *106*, 5228-5234.
 43. Krieg, U.C.; Walter, P.; Johnson, A.E., Photo-Cross-Linking of the Signal Sequence of Nascent Preprolactin to the 54-Kilodalton Polypeptide of the Signal Recognition Particle. *Proc. Natl. Acad. Sci. U. S. A.*, **1986**, *83*, 8604-8608.
 44. Goldman, D.W.; Pober, J.S.; White, J.; Bayley, H., Selective Labeling of the Hydrophobic Segments of Intrinsic Membrane-Proteins with a Lipophilic Photogenerated Carbene. *Nature*, **1979**, *280*, 841-843.
 45. Brunner, J.; Semenza, G., Selective Labeling of the Hydrophobic Core of Membranes with 3-(Trifluoromethyl)-3-(M-[I-125]Iodophenyl)Diazirine, a Carbene-Generating Reagent. *Biochemistry*, **1981**, *20*, 7174-7182.
 46. Dorman, G.; Prestwich, G.D., Benzophenone Photophores in Biochemistry. *Biochemistry*, **1994**, *33*, 5661-5673.
 47. Hino, N.; Okazaki, Y.; Kobayashi, T.; Hayashi, A.; Sakamoto, K.; Yokoyama, S., Protein photo-cross-linking in mammalian cells by site-specific incorporation of a photoreactive amino acid. *Nature Methods*, **2005**, *2*, 201-206.
 48. Sletten, E.M.; Bertozzi, C.R., Bioorthogonal Chemistry: Fishing for Selectivity in a Sea of Functionality. *Angewandte Chemie-International Edition*, **2009**, *48*, 6974-6998.
 49. Ly, T.; Julian, R.R., Using ESI-MS to probe protein structure by site-specific noncovalent attachment of 18-crown-6. *J. Am. Soc. Mass Spectrom.*, **2006**, *17*, 1209-1215.
 50. Kelleher, N.L.; Lin, H.Y.; Valaskovic, G.A.; Aaserud, D.J.; Fridriksson, E.K.; McLafferty, F.W., Top down versus bottom up protein characterization by tandem high-resolution mass spectrometry. *J. Am. Chem. Soc.*, **1999**, *121*, 806-812.
 51. Schilling, B.; Row, R.H.; Gibson, B.W.; Guo, X.; Young, M.M., MS2Assign, automated assignment and nomenclature of tandem mass spectra of chemically crosslinked peptides. *J. Am. Soc. Mass Spectrom.*, **2003**, *14*, 834-850.
 52. Rinner, O.; Seebacher, J.; Walzthoeni, T.; Mueller, L.; Beck, M.; Schmidt, A.;

- Mueller, M.; Aebersold, R., Identification of cross-linked peptides from large sequence databases. *Nat. Methods.*, **2008**, *5*, 315-318.
53. Staros, J.V., N-Hydroxysulfosuccinimide Active Esters - Bis(N-Hydroxysulfosuccinimide) Esters of 2 Dicarboxylic-Acids Are Hydrophilic, Membrane-Impermeant, Protein Cross-Linkers. *Biochemistry*, **1982**, *21*, 3950-3955.
 54. Swaim, C.L.; Smith, J.B.; Smith, D.L., Unexpected products from the reaction of the synthetic cross-linker 3,3'-dithiobis(sulfosuccinimidyl propionate), DTSSP with peptides. *J. Am. Soc. Mass Spectrom.*, **2004**, *15*, 736-749.
 55. Leavell, M.D.; Novak, P.; Behrens, C.R.; Schoeniger, J.S.; Kruppa, G.H., Strategy for selective chemical cross-linking of tyrosine and lysine residues. *J. Am. Soc. Mass Spectrom.*, **2004**, *15*, 1604-1611.
 56. Partis, M.D.; Griffiths, D.G.; Roberts, G.C.; Beechey, R.B., Cross-Linking of Protein by Omega-Maleimido Alkanoyl N-Hydroxysuccinimido Esters. *J. Protein Chem.*, **1983**, *2*, 263-277.
 57. Brewer, C.F.; Riehm, J.P., Evidence for Possible Nonspecific Reactions between N-Ethylmaleimide and Proteins. *Anal. Bioanal. Chem*, **1967**, *18*, 248-&.
 58. Brooks, D.J.; Fresco, J.R.; Lesk, A.M.; Singh, M., Evolution of amino acid frequencies in proteins over deep time: Inferred order of introduction of amino acids into the genetic code. *Mol. Biol. Evol.*, **2002**, *19*, 1645-1655.
 59. Gilchrist, T.L.; Rees, C.W., Carbenes, nitrenes, and arynes, studies in modern chemistry. **1969**, London: Nelson Publ. p 131.
 60. Kotzybahibert, F.; Kapfer, I.; Goeldner, M., Recent Trends in Photoaffinity-Labeling. *Angew. Chem. Int. Ed.*, **1995**, *34*, 1296-1312.
 61. Meisenheimer, K.M.; Koch, T.H., Photocross-linking of nucleic acids to associated proteins. *Crit. Rev. Biochem. Mol. Biol.*, **1997**, *32*, 101-140.
 62. Hanna, M.M., Photo-Cross-Linking Analysis of Protein-Rna Interactions in Escherichia-Coli Transcription Complexes. *Cell. Mol. Biol. Res.*, **1993**, *39*, 393-399.
 63. Persinger, J.; Bartholomew, B., Mapping the contacts of yeast TFIIB and RNA polymerase III at various distances from the major groove of DNA by DNA photoaffinity labeling. *J. Biol. Chem.*, **1996**, *271*, 33039-33046.
 64. McMahan, S.A.; Burgess, R.R., Use of Aryl Azide Cross-Linkers to Investigate Protein-Protein Interactions - an Optimization of Important Conditions as Applied to Escherichia-Coli Rna-Polymerase and Localization of a Sigma(70)-Alpha Cross-Link to the C-Terminal Region of Alpha. *Biochemistry*, **1994**, *33*, 12092-12099.
 65. Hashimoto, M.; Hatanaka, Y., Recent progress in diazirine-based photoaffinity labeling. *Eur. J. Org. Chem.*, **2008**, 2513-2523.
 66. Brunner, J.; Senn, H.; Richards, F.M., "3-Trifluoromethyl-3-Phenyldiazirine - a New Carbene Generating Group for Photolabeling Reagents. *J. Biol. Chem.*, **1980**, *255*, 3313-3318.
 67. Adams, A.E.; Pines, M.; Nakamoto, C.; Behar, V.; Yang, Q.M.; Bessalle, R.; Chorev, M.; Rosenblatt, M.; Levine, M.A.; Suva, L.J., Probing the Bimolecular Interactions of Parathyroid-Hormone and the Human Parathyroid-Hormone

- Parathyroid Hormone-Related Protein-Receptor .2. Cloning, Characterization, and Photoaffinity-Labeling of the Recombinant Human Receptor. *Biochemistry*, **1995**, *34*, 10553-10559.
68. Greenberg, Z.; Bisello, A.; Mierke, D.F.; Rosenblatt, M.; Chorev, M., Mapping the bimolecular interface of the parathyroid hormone (PTH)-PTH1 receptor complex: Spatial proximity between Lys(27) (of the hormone principal binding domain) and Leu(261) (of the first extracellular loop) of the human PTH1 receptor. *Biochemistry*, **2000**, *39*, 8142-8152.
 69. Ward, D.G.; Brewer, S.M.; Comes, M.P.; Trayer, I.P., A cross-linking study of the N-terminal extension of human cardiac troponin I. *Biochemistry*, **2003**, *42*, 10324-10332.
 70. Ahrends, R.; Kosinski, J.; Kirsch, D.; Manelyte, L.; Giron-Monzon, L.; Hummerich, L.; Schulz, O.; Spengler, B.; Friedhoff, P., Identifying an interaction site between MutH and the C-terminal domain of MutL by crosslinking, affinity purification, chemical coding and mass spectrometry. *Nucleic Acids Res.*, **2006**, *34*, 3169-3180.
 71. Majmudar, C.Y.; Wang, B.; Lum, J.K.; Hakansson, K.; Mapp, A.K., A high-resolution interaction map of three transcriptional activation domains with a key coactivator from photo-cross-linking and multiplexed mass spectrometry. *Angew. Chem. Int. Ed. Engl.*, **2009**, *48*, 7021-7024.
 72. Farrelli, I.S.; Toroney, R.; Hazen, J.L.; Mehl, R.A.; Chin, J.W., Photo-cross-linking interacting proteins with a genetically encoded benzophenone. *Nat. Methods*, **2005**, *2*, 377-384.
 73. Majmudar, C.Y.; Lee, L.W.; Lancia, J.K.; Nwokoye, A.; Wang, Q.; Wands, A.M.; Wang, L.; Mapp, A.K., Impact of Nonnatural Amino Acid Mutagenesis on the in Vivo Function and Binding Modes of a Transcriptional Activator. *J. Am. Chem. Soc.*, **2009**, *131*, 14240-+.
 74. Julian, R.R.;Beauchamp, J.L., Site specific sequestering and stabilization of charge in peptides by supramolecular adduct formation with 18-crown-6 ether by way of electrospray ionization. *Int. J. Mass spectrom.*, **2001**, *210*, 613-623.
 75. Ly, T.; Liu, Z.J.; Pujanauski, B.G.; Sarpong, R.; Julian, R.R., Surveying ubiquitin structure by noncovalent attachment of distance constrained bis(crown) ethers. *Anal. Chem.*, **2008**, *80*, 5059-5064.
 76. Muller, D.R.; Schindler, P.; Towbin, H.; Wirth, U.; Voshol, H.; Hoving, S.; Steinmetz, M.O., Isotope tagged cross linking reagents. A new tool in mass spectrometric protein interaction analysis. *Anal. Chem.*, **2001**, *73*, 1927-1934.
 77. Trester-Zedlitz, M.; Kamada, K.; Burley, S.K.; Fenyo, D.; Chait, B.T.; Muir, T.W., A modular cross-linking approach for exploring protein interactions. *J. Am. Chem. Soc.*, **2003**, *125*, 2416-2425.
 78. Petrotchenko, E.V.; Olkhovik, V.K.; Borchers, C.H., Isotopically coded cleavable cross-linker for studying protein-protein interaction and protein complexes. *Mol. Cell. Proteomics*, **2005**, *4*, 1167-1179.
 79. Ihling, C.; Schmidt, A.; Kalkhof, S.; Schulz, D.M.; Stingl, C.; Mechtler, K.; Haack, M.; Beck-Sickinger, A.G.; Cooper, D.M.F.; Sinz, A., Isotope-labeled cross-linkers and Fourier transform ion cyclotron resonance mass spectrometry for

- structural analysis of a protein/peptide complex. *J. Am. Soc. Mass Spectrom.*, **2006**, *17*, 1100-1113.
80. Petrotchenko, E.V.; Xiao, K.H.; Cable, J.; Chen, Y.W.; Dokholyan, N.V.; Borchers, C.H., BiPS, a Photocleavable, Isotopically Coded, Fluorescent Cross-linker for Structural Proteomics. *Mol. Cell. Proteomics*, **2009**, *8*, 273-286.
81. Collins, C.J.; Schilling, B.; Young, M.L.; Dollinger, G.; Guy, R.K., Isotopically labeled crosslinking reagents: Resolution of mass degeneracy in the identification of crosslinked peptides. *Bioorg. Med. Chem. Lett.*, **2003**, *13*, 4023-4026.
82. Davidson, W.S.; Hilliard, G.M., The spatial organization of apolipoprotein A-I on the edge of discoidal high density lipoprotein particles - A mass spectrometry study. *J. Biol. Chem.*, **2003**, *278*, 27199-27207.
83. Armengaud, J.; Dedieu, A.; Solques, O.; Pellequer, J.L.; Quemeneur, E., Deciphering structure and topology of conserved COG2042 orphan proteins. *Bmc Struct. Biol.*, **2005**, *5*, -.
84. Peterson, J.J.; Young, M.M.; Takemoto, L.J., Probing alpha-crystallin structure using chemical cross-linkers and mass spectrometry. *Mol. Vision*, **2004**, *10*, 857-866.
85. Gorman, J.J.; Wallis, T.P.; Pitt, J.J., Protein disulfide bond determination by mass spectrometry. *Mass Spectrom. Rev.*, **2002**, *21*, 183-216.
86. Gardner, M.W.; Vasicek, L.A.; Shabbir, S.; Anslyn, E.V.; Brodbelt, J.S., Chromogenic cross-linker for the characterization of protein structure by infrared multiphoton dissociation mass spectrometry. *Anal. Chem.*, **2008**, *80*, 4807-4819.
87. Yang, L.; Tang, X.T.; Weisbrod, C.R.; Munske, G.R.; Eng, J.K.; von Haller, P.D.; Kaiser, N.K.; Bruce, J.E., A Photocleavable and Mass Spectrometry Identifiable Cross-Linker for Protein Interaction Studies. *Anal. Chem.*, **2010**, *82*, 3556-3566.
88. Tang, X.T.; Munske, G.R.; Siems, W.F.; Bruce, J.E., Mass spectrometry identifiable cross-linking strategy for studying protein-protein interactions. *Anal. Chem.*, **2005**, *77*, 311-318.
89. Soderblom, E.J.; Goshe, M.B., Collision-induced dissociative chemical cross-linking reagents and methodology: Applications to protein structural characterization using tandem mass spectrometry analysis. *Anal. Chem.*, **2006**, *78*, 8059-8068.
90. Chowdhury, S.M.; Munske, G.R.; Tang, X.T.; Bruce, J.E., Collisionally activated dissociation and electron capture dissociation of several mass spectrometry-identifiable chemical cross-linkers. *Anal. Chem.*, **2006**, *78*, 8183-8193.
91. Lu, Y.L.; Tanasova, M.; Borhan, B.; Reid, G.E., Ionic Reagent for Controlling the Gas-Phase Fragmentation Reactions of Cross-Linked Peptides. *Anal. Chem.*, **2008**, *80*, 9279-9287.
92. King, G.J.; Jones, A.; Kobe, B.; Huber, T.; Movavadov, D.; Hume, D.L.; Ross, I.L., Identification of disulfide-containing chemical cross links in proteins using MALDI-TOF/TOF-mass spectrometry. *Anal. Chem.*, **2008**, *80*, 5036-5043.
93. Alley, S.C.; Ishmael, F.T.; Jones, A.D.; Benkovic, S.J., Mapping protein-protein interactions in the bacteriophage T4 DNA polymerase holoenzyme using a novel trifunctional photo-cross-linking and affinity reagent. *J. Am. Chem. Soc.*, **2000**, *122*, 6126-6127.

94. Hurst, G.B.; Lankford, T.K.; Kennel, S.J., Mass spectrometric detection of affinity purified crosslinked peptides. *J. Am. Soc. Mass Spectrom.*, **2004**, *15*, 832-839.
95. Zhang, H.Z.; Tang, X.T.; Munske, G.R.; Tolic, N.; Anderson, G.A.; Bruce, J.E., Identification of Protein-Protein Interactions and Topologies in Living Cells with Chemical Cross-linking and Mass Spectrometry. *Mol. Cell. Proteomics*, **2009**, *8*, 409-420.
96. Fujii, N.; Jacobsen, R.B.; Wood, N.L.; Schoeniger, J.S.; Guy, R.K., A novel protein crosslinking reagent for the determination of moderate resolution protein structures by mass spectrometry (MS3-D). *Bioorg. Med. Chem. Lett.*, **2004**, *14*, 427-429.
97. Chowdhury, S.M.; Du, X.X.; Tolic, N.; Wu, S.; Moore, R.J.; Mayer, M.U.; Smith, R.D.; Adkins, J.N., Identification of Cross-Linked Peptides after Click-Based Enrichment Using Sequential Collision-Induced Dissociation and Electron Transfer Dissociation Tandem Mass Spectrometry. *Anal. Chem.*, **2009**, *81*, 5524-5532.
98. Grabarek, Z.; Gergely, J., Zero-length Crosslinking Procedure with the Use of Active Esters. *Analytical Biochemistry*, **1990**, *185*, 131-135.
99. Staros, J.V.; Wright, R.W.; Swingle, D.M., Enhancement by N-Hydroxysulfosuccinimide of Water-Soluble Carbodiimide-Mediated Coupling Reactions. *Anal. Bioanal. Chem.*, **1986**, *156*, 220-222.
100. Wen, J.Z.; Zhang, H.; Gross, M.L.; Blankenship, R.E., Membrane orientation of the FMO antenna protein from *Chlorobaculum tepidum* as determined by mass spectrometry-based footprinting. *Proc. Natl. Acad. Sci. U.S.A.*, **2009**, *106*, 6134-6139.
101. Kruppa, G.H.; Schoeniger, J.; Young, M.M., A top down approach to protein structural studies using chemical cross-linking and Fourier transform mass spectrometry. *Rapid Commun. Mass Spectrom.*, **2003**, *17*, 155-162.
102. Wefing, S.; Schnaible, V.; Hoffmann, D., SearchXLinks. A program for the identification of disulfide bonds in proteins from mass spectra. *Anal. Chem.*, **2006**, *78*, 1235-1241.
103. Yu, E.T.; Hawkins, A.; Kuntz, I.D.; Rahn, L.A.; Rothfuss, A.; Sale, K.; Young, M.M.; Yang, C.L.; Pancerella, C.M.; Fabris, D., The Collaboratory for MS3D: A New Cyberinfrastructure for the Structural Elucidation of Biological Macromolecules and Their Assemblies Using Mass Spectrometry-Based Approaches. *J. Proteome Res.*, **2008**, *7*, 4848-4857.
104. Panchaud, A.; Singh, P.; Shaffer, S.A.; Goodlett, D.R., xComb: A Cross-Linked Peptide Database Approach to Protein-Protein Interaction Analysis. *J. Proteome Res.*, **2010**, *9*, 2508-2515.
105. Chen, Z.A.; Jawhari, A.; Fischer, L.; Buchen, C.; Tahir, S.; Kamenski, T.; Rasmussen, M.; Lariviere, L.; Bukowski-Wills, J.C.; Nilges, M.; Cramer, P.; Rappsilber, J., Architecture of the RNA polymerase II-TFIIF complex revealed by cross-linking and mass spectrometry. *EMBO J.*, **2010**, *29*, 717-726.
106. Sommer, H.; Thomas, H.A.; Hipple, J.A., The Measurement of E/M by Cyclotron Resonance. *Phys. Rev.*, **1951**, *82*, 697-702.
107. Comisaró, M.; Marshall, A.G., Fourier-Transform Ion-Cyclotron Resonance

- Spectroscopy. *Chem. Phys. Lett.*, **1974**, *25*, 282-283.
108. Marshall, A.G.; Hendrickson, C.L.; Jackson, G.S., Fourier transform ion cyclotron resonance mass spectrometry: A primer. *Mass Spectrom. Rev.*, **1998**, *17*, 1-35.
 109. Grosshans, P.B.; Marshall, A.G., Theory of Ion-Cyclotron Resonance Mass-Spectrometry - Resonant Excitation and Radial Ejection in Orthorhombic and Cylindrical Ion Traps. *Int. J. Mass Spectrom. Ion Processes*, **1990**, *100*, 347-379.
 110. Gauthier, J.W.; Trautman, T.R.; Jacobson, D.B., Sustained Off-Resonance Irradiation for Collision-Activated Dissociation Involving Fourier-Transform Mass-Spectrometry - Collision-Activated Dissociation Technique That Emulates Infrared Multiphoton Dissociation. *Anal. Chim. Acta*, **1991**, *246*, 211-225.
 111. Mciver, R.T., Trajectory Calculations for Axial Injection of Ions into a Magnetic-Field - Overcoming the Magnetic-Mirror Effect with an Rf Quadrupole Lens. *Int. J. Mass Spectrom. Ion Processes*, **1990**, *98*, 35-50.
 112. Hakansson, K.; Cooper, H.J.; Hudgins, R.R.; Nilsson, C.L., High resolution tandem mass spectrometry for structural biochemistry. *Curr. Org. Chem.*, **2003**, *7*, 1503-1525.
 113. Mciver, R.T.; Hunter, R.L.; Bowers, W.D., Coupling a Quadrupole Mass-Spectrometer and a Fourier-Transform Mass-Spectrometer. *International Journal of Mass Spectrometry and Ion Processes*, **1985**, *64*, 67-77.
 114. Senko, M.W.; Hendrickson, C.L.; PasaTolic, L.; Marto, J.A.; White, F.M.; Guan, S.H.; Marshall, A.G., Electrospray ionization Fourier transform ion cyclotron resonance at 9.4 T. *Rapid Commun. Mass Spectrom.*, **1996**, *10*, 1824-1828.
 115. Alford, J.M.; Williams, P.E.; Trevor, D.J.; Smalley, R.E., Metal Cluster Ion-Cyclotron Resonance - Combining Supersonic Metal Cluster Beam Technology with Ft-Icr. *Int. J. Mass Spectrom. Ion Processes*, **1986**, *72*, 33-51.
 116. Henry, K.D.; Williams, E.R.; Wang, B.H.; McLafferty, F.W.; Shabanowitz, J.; Hunt, D.F., Fourier-Transform Mass-Spectrometry of Large Molecules by Electrospray Ionization. *Proc. Natl. Acad. Sci. U. S. A.*, **1989**, *86*, 9075-9078.
 117. Amster, I.J., Fourier transform mass spectrometry. *J. Mass Spectrom.*, **1996**, *31*, 1325-1337.
 118. Zubarev, R.A.; Kelleher, N.L.; McLafferty, F.W., Electron capture dissociation of multiply charged protein cations. A nonergodic process. *J. Am. Chem. Soc.*, **1998**, *120*, 3265-3266.
 119. Budnik, B.A.; Haselmann, K.F.; Zubarev, R.A., Electron detachment dissociation of peptide di-anions: an electron-hole recombination phenomenon. *Chem. Phys. Lett.*, **2001**, *342*, 299-302.
 120. Shaffer, S.A.; Tang, K.Q.; Anderson, G.A.; Prior, D.C.; Udseth, H.R.; Smith, R.D., A novel ion funnel for focusing ions at elevated pressure using electrospray ionization mass spectrometry. *Rapid Commun. Mass Spectrom.*, **1997**, *11*, 1813-1817.
 121. Shaffer, S.A.; Prior, D.C.; Anderson, G.A.; Udseth, H.R.; Smith, R.D., An ion funnel interface for improved ion focusing and sensitivity using electrospray ionization mass spectrometry. *Anal. Chem.*, **1998**, *70*, 4111-4119.
 122. Shaffer, S.A.; Tolmachev, A.; Prior, D.C.; Anderson, G.A.; Udseth, H.R.; Smith, R.D., Characterization of an improved electrodynamic ion funnel interface for

- electrospray ionization mass spectrometry. *Anal. Chem.*, **1999**, *71*, 2957-2964.
123. Belov, M.E.N., E.N.; Anderson, G.A.; Udseth, H.R.; Conrads, T.P.; Veenstra, T.D.; Masselon, C.D.; Gorshkov, M.V.; Smith, R.D., Design and performance of an ESI interface for selective external ion accumulation coupled to a Fourier transform ion cyclotron mass spectrometer. *Anal. Chem.*, **2001**, *73*, 253-261.
 124. Tsybin, Y.O.; Witt, M.; Baykut, G.; Kjeldsen, F.; Hakansson, P., Combined infrared multiphoton dissociation and electron capture dissociation with a hollow electron beam in Fourier transform ion cyclotron resonance mass spectrometry. *Rapid Commun. Mass Spectrom.*, **2003**, *17*, 1759-1768.
 125. Cody, R.B.; Freiser, B.S., Electron-Impact Excitation of Ions in Fourier-Transform Mass-Spectrometry. *Anal. Chem.*, **1987**, *59*, 1054-1056.
 126. Budnik, B.A.; Haselmann, K.F.; Elkin, Y.N.; Gorbach, V.I.; Zubarev, R.A., Applications of electron-ion dissociation reactions for analysis of polycationic chitooligosaccharides in Fourier transform mass spectrometry. *Anal. Chem.*, **2003**, *75*, 5994-6001.
 127. Woodin, R.L.; Bomse, D.S.; Beauchamp, J.L., Multi-Photon Dissociation of Molecules with Low-Power Continuous Wave Infrared-Laser Radiation. *J. Am. Chem. Soc.*, **1978**, *100*, 3248-3250.
 128. Little, D.P.; Speir, J.P.; Senko, M.W.; O'Connor, P.B.; McLafferty, F.W., Infrared multiphoton dissociation of large multiply charged ions for biomolecule sequencing. *Anal. Chem.*, **1994**, *66*, 2809-2815.
 129. McKenna, A.M.; Purcell, J.M.; Rodgers, R.P.; Marshall, A.G., Heavy Petroleum Composition. 1. Exhaustive Compositional Analysis of Athabasca Bitumen HVGO Distillates by Fourier Transform Ion Cyclotron Resonance Mass Spectrometry: A Definitive Test of the Boduszynski Model. *Energy Fuels*, **2010**, *24*, 2929-2938.
 130. Brustkern, A.M.; Rempel, D.L.; Gross, M.L., An electrically compensated trap designed to eighth order for FT-ICR mass Spectrometry. *J. Am. Soc. Mass Spectrom.*, **2008**, *19*, 1281-1285.
 131. Purcell, J.M.; Hendrickson, C.L.; Rodgers, R.P.; Marshall, A.G., Atmospheric pressure photoionization Fourier transform ion cyclotron resonance mass spectrometry for complex mixture analysis. *Anal. Chem.*, **2006**, *78*, 5906-5912.
 132. Purcell, J.M.; Hendrickson, C.L.; Rodgers, R.P.; Marshall, A.G., Atmospheric pressure photoionization proton transfer for complex organic mixtures investigated by fourier transform ion cyclotron resonance mass spectrometry. *J. Am. Soc. Mass Spectrom.*, **2007**, *18*, 1682-1689.
 133. Purcell, J.M.; Rodgers, R.P.; Hendrickson, C.L.; Marshall, A.G., Speciation of nitrogen containing aromatics by atmospheric pressure photoionization or electrospray ionization Fourier transform ion cyclotron resonance mass spectrometry. *J. Am. Soc. Mass Spectrom.*, **2007**, *18*, 1265-1273.
 134. Ge, Y.; Rybakova, I.N.; Xu, Q.G.; Moss, R.L., Top-down high-resolution mass spectrometry of cardiac myosin binding protein C revealed that truncation alters protein phosphorylation state. *Proc. Natl. Acad. Sci. U. S. A.*, **2009**, *106*, 12658-12663.
 135. Conrads, T.P.; Anderson, G.A.; Veenstra, T.D.; Pasa-Tolic, L.; Smith, R.D., Utility

- of accurate mass tags for proteome-wide protein identification. *Anal. Chem.*, **2000**, *72*, 3349-3354.
136. Hughey, C.A.; Hendrickson, C.L.; Rodgers, R.P.; Marshall, A.G.; Qian, K.N., Kendrick mass defect spectrum: A compact visual analysis for ultrahigh-resolution broadband mass spectra. *Anal. Chem.*, **2001**, *73*, 4676-4681.
 137. Chen, R.D.; Cheng, X.H.; Mitchell, D.W.; Hofstadler, S.A.; Wu, Q.Y.; Rockwood, A.L.; Sherman, M.G.; Smith, R.D., Trapping, Detection, and Mass Determination of Coliphage T4 DNA Ions of 10(8) Da by Electrospray-ionization Fourier-transform Ion-cyclotron Resonance Mass Spectrometry. *Anal. Chem.*, **1995**, *67*, 1159-1163.
 138. de Koning, L.J.; Nibbering, N.M.M.; van Orden, S.L.; Laukien, F.H., Mass selection of ions in a Fourier transform ion cyclotron resonance trap using correlated harmonic excitation fields (CHEF). *Int. J. Mass spectrom.*, **1997**, *165*, 209-219.
 139. Nourse, B.D.; Cox, K.A.; Morand, K.L.; Cooks, R.G., Collisional Activation of Pyrene and Anthracene in an Ion-Trap Mass-Spectrometer. *J. Am. Chem. Soc.*, **1992**, *114*, 2010-2016.
 140. Cox, K.A.; Williams, J.D.; Cooks, R.G.; Kaiser, R.E., Quadrupole Ion Trap Mass-Spectrometry - Current Applications and Future-Directions for Peptide Analysis. *Biol. Mass Spectrom.*, **1992**, *21*, 226-241.
 141. Syka, J.E.P.; Coon, J.J.; Schroeder, M.J.; Shabanowitz, J.; Hunt, D.F., Peptide and protein sequence analysis by electron transfer dissociation mass spectrometry. *Proc. Natl. Acad. Sci. U. S. A.*, **2004**, *101*, 9528-9533.
 142. Thomson, J.J., Rays of positive electricity and their application to chemical analysis. *London: Longmans, Green*, **1913**.
 143. Aston, F.W., *Proc. Cambridge Philos. Soc.*, **1919**, *19*, 317.
 144. Haddon, W.F.; McLafferty, F.W., Metastable Ion Characteristics .7. Collision-Induced Metastables. *J. Am. Chem. Soc.*, **1968**, *90*, 4745-&.
 145. Jennings, K.R., Collision-induced decompositions of aromatic molecular ions. *Int. J. Mass Spectrom. Ion Phys.*, **1968**, *1*, 227-235.
 146. McLafferty, F.W.; Bente, P.F.; Kornfeld, R.; Tsai, S.C.; Howe, I., Collisional Activation Spectra of Organic Ions. *J. Am. Chem. Soc.*, **1973**, *95*, 2120-2129.
 147. McLuckey, S.A., Principles of Collisional Activation in Analytical Mass-Spectrometry. *J. Am. Soc. Mass Spectrom.*, **1992**, *3*, 599-614.
 148. Shukla, A.K.; Futrell, J.H., Tandem mass spectrometry: dissociation of ions by collisional activation. *J. Mass Spectrom.*, **2000**, *35*, 1069-1090.
 149. Wells, J.M.; McLuckey, S.A., Collision-induced dissociation (CID) of peptides and proteins. *Biol. Mass Spectrom.*, **2005**, *402*, 148-185.
 150. McLuckey, S.A.; Goeringer, D.E., Slow heating methods in tandem mass spectrometry. *J. Mass Spectrom.*, **1997**, *32*, 461-474.
 151. Mayer, P.M.; Poon, C., The Mechanisms of Collisional Activation of Ions in Mass Spectrometry. *Mass Spectrom. Rev.*, **2009**, *28*, 608-639.
 152. Summerfield, S.G.; Gaskell, S.J., Fragmentation efficiencies of peptide ions following low energy collisional activation. *Int. J. Mass spectrom.*, **1997**, *165*, 509-521.

153. Johnson, R.S.; Martin, S.A.; Biemann, K., Collision-Induced Fragmentation of (M+H)⁺Ions of Peptides - Side-Chain Specific Sequence Ions. *Int. J. Mass Spectrom. Ion Processes*, **1988**, *86*, 137-154.
154. Bowie, J.H.; Brinkworth, C.S.; Dua, S., Collision-induced fragmentations of the (M-H)⁻ parent anions of underivatized peptides: An aid to structure determination and some unusual negative ion cleavages. *Mass Spectrom. Rev.*, **2002**, *21*, 87-107.
155. Brodbelt, J.S.; Wilson, J.J., Infrared Multiphoton Dissociation in Quadrupole Ion Traps. *Mass Spectrom. Rev.*, **2009**, *28*, 390-424.
156. Flora, J.W.; Muddiman, D.C., Selective, sensitive, and rapid phosphopeptide identification in enzymatic digests using ESI-FTICR-MS with infrared multiphoton dissociation. *Anal. Chem.*, **2001**, *73*, 3305-3311.
157. Crowe, M.C.; Brodbelt, J.S., Infrared multiphoton dissociation (IRMPD) and collisionally activated dissociation of peptides in a quadrupole ion trap with selective IRMPD of phosphopeptides. *J. Am. Soc. Mass Spectrom.*, **2004**, *15*, 1581-1592.
158. Yoo, H.J.; Liu, H.C.; Hakansson, K., Infrared multiphoton dissociation and electron-induced dissociation as alternative MS/MS strategies for metabolite identification. *Anal. Chem.*, **2007**, *79*, 7858-7866.
159. Dongre, A.R.; Jones, J.L.; Somogyi, A.; Wysocki, V.H., Influence of peptide composition, gas-phase basicity, and chemical modification on fragmentation efficiency: Evidence for the mobile proton model. *J. Am. Chem. Soc.*, **1996**, *118*, 8365-8374.
160. Tsaprailis, G.; Nair, H.; Somogyi, A.; Wysocki, V.H.; Zhong, W.Q.; Futrell, J.H.; Summerfield, S.G.; Gaskell, S.J., Influence of secondary structure on the fragmentation of protonated peptides. *J. Am. Chem. Soc.*, **1999**, *121*, 5142-5154.
161. Wysocki, V.H.; Tsaprailis, G.; Smith, L.L.; Brechi, L.A., Special feature: Commentary - Mobile and localized protons: a framework for understanding peptide dissociation. *J. Mass Spectrom.*, **2000**, *35*, 1399-1406.
162. Paizs, B.; Suhai, S., Fragmentation pathways of protonated peptides. *Mass Spectrom. Rev.*, **2005**, *24*, 508-548.
163. Stensballe, A.; Jensen, O.N.; Olsen, J.V.; Haselmann, K.F.; Zubarev, R.A., Electron capture dissociation of singly and multiply phosphorylated peptides. *Rapid Commun Mass Spectrom.*, **2000**, *14*, 1793-1800.
164. Sweet, S.M.M.; Creese, A.J.; Cooper, H.J., Strategy for the identification of sites of phosphorylation in proteins: Neutral loss triggered electron capture dissociation. *Anal. Chem.*, **2006**, *78*, 7563-7569.
165. Creese, A.J.; Cooper, H.J., The effect of phosphorylation on the electron capture dissociation of peptide ions. *J. Am. Soc. Mass Spectrom.*, **2008**, *19*, 1263-1274.
166. Hengel, S.M.; Shaffer, S.A.; Nunn, B.L.; Goodlett, D.R., Tandem Mass Spectrometry Investigation of ADP-ribosylated Kemptide. *J. Am. Soc. Mass Spectrom.*, **2009**, *20*, 477-483.
167. Sweet, S.M.M.; Bailey, C.M.; Cunningham, D.L.; Heath, J.K.; Cooper, H.J., Large Scale Localization of Protein Phosphorylation by Use of Electron Capture Dissociation Mass Spectrometry. *Mol. Cell. Proteomics*, **2009**, *8*, 904-912.

168. Woodling, K.A.; Eyler, J.R.; Tsybin, Y.; Nilsson, C.L.; Marshall, A.G.; Edison, A.S.; Al-Naggar, I.M.; Bubb, M.R., Identification of single and double sites of phosphorylation by ECD FT-ICR/MS in peptides related to the phosphorylation site domain of the myristoylated alanine-rich C kinase protein. *J. Am. Soc. Mass Spectrom.*, **2007**, *18*, 2137-2145.
169. Kweon, H.K.; Hakansson, K., Metal oxide-based enrichment combined with gas-phase ion-electron reactions for improved mass spectrometric characterization of protein phosphorylation. *J. Proteome Res.*, **2008**, *7*, 749-755.
170. Mirgorodskaya, E.; Roepstorff, P.; Zubarev, R.A., Localization of O-glycosylation sites in peptides by electron capture dissociation in a fourier transform mass spectrometer. *Anal. Chem.*, **1999**, *71*, 4431-4436.
171. Kjeldsen, F.; Haselmann, K.F.; Budnik, B.A.; Sorensen, E.S.; Zubarev, R.A., Complete characterization of posttranslational modification sites in the bovine milk protein PP3 by tandem mass spectrometry with electron capture dissociation as the last stage. *Anal. Chem.*, **2003**, *75*, 2355-2361.
172. Adamson, J.T.; Hakansson, K., Infrared multiphoton dissociation and electron capture dissociation of high-mannose type glycopeptides. *J. Proteome Res.*, **2006**, *5*, 493-501.
173. Deguchi, K.; Ito, H.; Baba, T.; Hirabayashi, A.; Nakagawa, H.; Fumoto, M.; Hinou, H.; Nishimura, S.I., Structural analysis of O-glycopeptides employing negative- and positive-ion multi-stage mass spectra obtained by collision-induced and electron-capture dissociations in linear ion trap time-of-flight mass spectrometry. *Rapid Commun Mass Spectrom*, **2007**, *21*, 691-698.
174. Seipert, R.R.; Dodds, E.D.; Clowers, B.H.; Beecroft, S.M.; German, J.B.; Lebrilla, C.B., Factors that influence fragmentation behavior of N-linked glycopeptide ions. *Anal. Chem.*, **2008**, *80*, 3684-3692.
175. Kelleher, R.L.; Zubarev, R.A.; Bush, K.; Furie, B.; Furie, B.C.; McLafferty, F.W.; Walsh, C.T., Localization of labile posttranslational modifications by electron capture dissociation: The case of gamma-carboxyglutamic acid. *Anal. Chem.*, **1999**, *71*, 4250-4253.
176. Liu, H.; Hakansson, K., Electron capture dissociation of tyrosine O-sulfated peptides complexed with divalent metal cations. *Anal. Chem.*, **2006**, *78*, 7570-7576.
177. Zubarev, R.A.; Kruger, N.A.; Fridriksson, E.K.; Lewis, M.A.; Horn, D.M.; Carpenter, B.K.; McLafferty, F.W., Electron capture dissociation of gaseous multiply-charged proteins is favored at disulfide bonds and other sites of high hydrogen atom affinity. *J. Am. Chem. Soc.*, **1999**, *121*, 2857-2862.
178. Wells, J.M.; Stephenson, J.L.; McLuckey, S.A., Charge dependence of protonated insulin decompositions. *Int. J. Mass spectrom.*, **2000**, *203*, A1-A9.
179. Zhang, M.X.; Kaltashov, I.A., Mapping of protein disulfide bonds using negative ion fragmentation with a broadband precursor selection. *Anal. Chem.*, **2006**, *78*, 4820-4829.
180. Kalli, A.; Hakansson, K., Preferential cleavage of S-S and C-S bonds in electron detachment dissociation and infrared multiphoton dissociation of disulfide-linked peptide anions. *Int. J. Mass spectrom.*, **2007**, *263*, 71-81.

181. Bean, M.F.; Carr, S.A., Characterization of Disulfide Bond Position in Proteins and Sequence-Analysis of Cystine-Bridged Peptides by Tandem Mass-Spectrometry. *Anal. Bioanal. Chem.*, **1992**, *201*, 216-226.
182. Zhou, J.; Ens, W.; Poppeschriemer, N.; Standing, K.G.; Westmore, J.B., Cleavage of Interchain Disulfide Bonds Following Matrix-Assisted Laser-Desorption. *Int. J. Mass Spectrom. Ion Processes*, **1993**, *126*, 115-122.
183. Jackson, S.N.; Dutta, S.; Woods, A.S., The Use of ECD/ETD to Identify the Site of Electrostatic Interaction in Noncovalent Complexes. *J. Am. Soc. Mass Spectrom.*, **2009**, *20*, 176-179.
184. Horn, D.M.; Zubarev, R.A.; McLafferty, F.W., Automated de novo sequencing of proteins by tandem high-resolution mass spectrometry. *Proc. Natl. Acad. Sci. U. S. A.*, **2000**, *97*, 10313-10317.
185. Zubarev, R.A.; Haselmann, K.F.; Budnik, B.; Kjeldsen, F.; Jensen, F., Towards an understanding of the mechanism of electron-capture dissociation: a historical perspective and modern ideas. *Eur. J. Mass Spectrom.*, **2002**, *8*, 337-349.
186. Gorshkov, M.V.; Masselon, C.D.; Nikolaev, E.N.; Udseth, H.R.; Pasa-Tolic, L.; Smith, R.D., Considerations for electron capture dissociation efficiency in FTICR mass spectrometry. *Int. J. Mass spectrom.*, **2004**, *234*, 131-136.
187. Zubarev, R.A.; Horn, D.M.; Fridriksson, E.K.; Kelleher, N.L.; Kruger, N.A.; Lewis, M.A.; Carpenter, B.K.; McLafferty, F.W., Electron capture dissociation for structural characterization of multiply charged protein cations. *Anal. Chem.*, **2000**, *72*, 563-573.
188. Turecek, F., N-C-alpha bond dissociation energies and kinetics in amide and peptide radicals. Is the dissociation a non-ergodic process? *J. Am. Chem. Soc.*, **2003**, *125*, 5954-5963.
189. Syrstad, E.A.; Turecek, F., Toward a general mechanism of electron capture dissociation. *J. Am. Soc. Mass Spectrom.*, **2005**, *16*, 208-224.
190. Sobczyk, M.; Anusiewicz, W.; Berdys-Kochanska, J.; Sawicka, A.; Skurski, P.; Simons, J., Coulomb-assisted dissociative electron attachment: Application to a model peptide. *J. Phys. Chem. A*, **2005**, *109*, 250-258.
191. Anusiewicz, W.; Berdys-Kochanska, J.; Simons, J., Electron attachment step in electron capture dissociation (ECD) and electron transfer dissociation (ETD). *J. Phys. Chem. A*, **2005**, *109*, 5801-5813.
192. Simons, J., Mechanisms for S-S and N-C-alpha bond cleavage in peptide ECD and ETD mass spectrometry. *Chem. Phys. Lett.*, **2010**, *484*, 81-95.
193. Zhang, Z.Q., Prediction of Electron-Transfer/Capture Dissociation Spectra of Peptides. *Anal. Chem.*, **2010**, *82*, 1990-2005.
194. Swaney, D.L.; McAlister, G.C.; Wirtala, M.; Schwartz, J.C.; Syka, J.E.P.; Coon, J.J., Supplemental activation method for high-efficiency electron-transfer dissociation of doubly protonated peptide precursors. *Anal. Chem.*, **2007**, *79*, 477-485.
195. Sohn, C.H.; Chung, C.K.; Yin, S.; Ramachandran, P.; Loo, J.A.; Beauchamp, J.L., Probing the Mechanism of Electron Capture and Electron Transfer Dissociation Using Tags with Variable Electron Affinity. *J. Am. Chem. Soc.*, **2009**, *131*, 5444-5459.

196. Kalli, A.; Hakansson, K., Comparison of the electron capture dissociation fragmentation behavior of doubly and triply protonated peptides from trypsin, Glu-C, and chymotrypsin digestion. *J. Proteome Res.*, **2008**, *7*, 2834-2844.
197. Yang, J.; Mo, J.J.; Adamson, J.T.; Hakansson, K., Characterization of oligodeoxynucleotides by electron detachment dissociation Fourier transform ion cyclotron resonance mass spectrometry. *Anal. Chem.*, **2005**, *77*, 1876-1882.
198. Yang, J.; Hakansson, K., Fragmentation of oligoribonucleotides from gas-phase ion-electron reactions. *Journal of the American Society for Mass Spectrometry*, **2006**, *17*, 1369-1375.
199. Kinet, C.; Gabelica, V.; Balbeur, D.; De Pauw, E., Electron detachment dissociation (EDD) pathways in oligonucleotides. *Int. J. Mass spectrom.*, **2009**, *283*, 206-213.
200. Adamson, J.T.; Hakansson, K., Electron detachment dissociation of neutral and sialylated oligosaccharides. *J. Am. Soc. Mass Spectrom.*, **2007**, *18*, 2162-2172.
201. Wolff, J.J.; Amster, I.J.; Chi, L.L.; Linhardt, R.J., Electron detachment dissociation of glycosaminoglycan tetrasaccharides. *J. Am. Soc. Mass Spectrom.*, **2007**, *18*, 234-244.
202. Wolff, J.J.; Laremore, T.N.; Leach, F.E.; Linhardt, R.J.; Amster, I.J., Electron capture dissociation, electron detachment dissociation and infrared multiphoton dissociation of sucrose octasulfate. *Eur. J. Mass Spectrom.*, **2009**, *15*, 275-281.
203. Anusiewicz, I.; Jasionowski, M.; Skurski, P.; Simons, J., Backbone and side-chain cleavages in electron detachment dissociation (EDD). *J. Phys. Chem. A*, **2005**, *109*, 11332-11337.
204. Kjeldsen, F.; Silivra, O.A.; Ivonin, I.A.; Haselmann, K.F.; Gorshkov, M.; Zubarev, R.A., C-alpha-C backbone fragmentation dominates in electron detachment dissociation of gas-phase polypeptide polyanions. *Chem. Eur. J.*, **2005**, *11*, 1803-1812.
205. Haselmann, K.F.; Budnik, B.A.; Kjeldsen, F.; Nielsen, M.L.; Olsen, J.V.; Zubarev, R.A., Electronic excitation gives informative fragmentation of polypeptide cations and anions. *Eur. J. Mass Spectrom.*, **2002**, *8*, 117-121.
206. Wipf, P.; Reeves, J.T.; Balachandran, R.; Day, B.W., Synthesis and biological evaluation of structurally highly modified analogues of the antimetabolic natural product curacin A. *J. Med. Chem.*, **2002**, *45*, 1901-1917.
207. Schwecke, T.; Aparicio, J.F.; Molnar, I.; Konig, A.; Khaw, L.E.; Haydock, S.F.; Oliynyk, M.; Caffrey, P.; Cortes, J.; Lester, J.B.; Bohm, G.A.; Staunton, J.; Leadlay, P.F., The Biosynthetic Gene-Cluster for the Polyketide Immunosuppressant Rapamycin. *Proc. Natl. Acad. Sci. U. S. A.*, **1995**, *92*, 7839-7843.
208. Dorrestein, P.C.; Kelleher, N.L., Dissecting non-ribosomal and polyketide biosynthetic machineries using electrospray ionization Fourier-Transform mass spectrometry. *Nat. Prod. Rep.*, **2006**, *23*, 893-918.
209. Kealey, J.T.; Liu, L.; Santi, D.V.; Betlach, M.C.; Barr, P.J., Production of a polyketide natural product in nonpolyketide-producing prokaryotic and eukaryotic hosts. *Proc. Natl. Acad. Sci. U. S. A.*, **1998**, *95*, 505-509.
210. Reuter, K.; Mofid, M.R.; Marahiel, M.A.; Ficner, R., Crystal structure of the

- surfactin synthetase-activating enzyme Sfp: a prototype of the 4'-phosphopantetheinyl transferase superfamily. *EMBO J.*, **1999**, *18*, 6823-6831.
211. Shaw-Reid, C.A.; Kelleher, N.L.; Losey, H.C.; Gehring, A.M.; Berg, C.; Walsh, C.T., Assembly line enzymology by multimodular nonribosomal peptide synthetases: the thioesterase domain of E-coli EntF catalyzes both elongation and cyclolactonization. *Chem. Biol.*, **1999**, *6*, 385-400.
 212. Dorrestein, P.C.; Bumpus, S.B.; Calderone, C.T.; Garneau-Tsodikova, S.; Aron, Z.D.; Straight, P.D.; Kolter, R.; Walsh, C.T.; Kelleher, N.L., Facile detection of acyl and peptidyl intermediates on thiotemplate carrier domains via phosphopantetheinyl elimination reactions during tandem mass spectrometry. *Biochemistry*, **2006**, *45*, 12756-12766.
 213. Kweon, H.K.; Hakansson, K., Selective zirconium dioxide-based enrichment of phosphorylated peptides for mass spectrometric analysis. *Anal. Chem.*, **2006**, *78*, 1743-1749.
 214. Gu, L.C.; Geders, T.W.; Wang, B.; Gerwick, W.H.; Hakansson, K.; Smith, J.L.; Sherman, D.H., GNAT-like strategy for polyketide chain initiation. *Science*, **2007**, *318*, 970-974.
 215. Gu, L.; Wang, B.; Kulkarni, A.; Geders, T.W.; Grindberg, R.V.; Gerwick, L.; Hakansson, K.; Wipf, P.; Smith, J.L.; Gerwick, W.H.; Sherman, D.H., Metamorphic enzyme assembly in polyketide diversification. *Nature*, **2009**, *459*, 731-735.
 216. Gu, L.; Wang, B.; Kulkarni, A.; Gehret, J.J.; Lloyd, K.R.; Gerwick, L.; Gerwick, W.H.; Wipf, P.; Hakansson, K.; Smith, J.L.; Sherman, D.H., Polyketide decarboxylative chain termination preceded by o-sulfonation in curacin A biosynthesis. *J. Am. Chem. Soc.*, **2009**, *131*, 16033-16035.
 217. Khare, D.W., B.; Gu, L.; Razelun, J.; Sherman, D.H.; Gerwick, W.H.; Håkansson, K.; and Smith, J.L., Conformational Switch Triggered by α -Ketoglutarate in a Halogenase of Curacin A Biosynthesis. *Proc. Natl. Acad. Sci.*, **2010**, in press.

Chapter 2

Photo-cross-linking and Complementary Use of ESI and MALDI Mass Spectrometry to Map Interaction Sites between Transcriptional Activators and Mediator 15

2.1 Introduction

The process of eukaryotic gene expression, in which RNA is synthesized from a corresponding DNA template, is initiated by proteins termed transcriptional activators. Activators initially bind to specific DNA sequences upstream of the gene transcription starting site [1], then they recruit and assemble the transcriptional complex which includes RNA polymerase II (pol II) and associated general transcriptional factors. In addition, activators aid pol II to bind correctly at specific sequences in DNA and attract pol II to the starting point of transcription. The interaction between activators and pol II is indirect and relayed by an approximately 20 protein co-activator/mediator complex [2]. Due to their central role in gene transcription, malfunctioning or mis-regulated activators can cause many human diseases, such as diabetes [3], Huntington's disease [4], and cancers [5, 6]. Therefore, detailed understanding of the function and activation of activators, including mapping of the interaction/binding sites between activators and mediator, is desired. Such understanding will also provide necessary information for

designing artificial activators aiming at transcription-based therapeutics. Strong efforts have been made to reveal such binding interactions in detail [7-9]. However, the multiple binding areas shared by various activators [10, 11] make it difficult to localize specific binding sites for a particular activator, and the technical challenges of obtaining covalently cross-linked peptides in high yield makes the application of MS and MS/MS strategies for high resolution analysis challenging.

Nevertheless, photo-cross-linking followed by proteolytic digestion and mass spectrometric characterization of the covalently linked products has proven valuable for characterizing protein-protein interactions [12-15]. p-Benzoyl phenyl alanine (pBpa) is an unnatural amino acid that can be incorporated *in vivo* into transcriptional activators. pBpa has a benzophenone (BP) moiety that can be activated into a triplet state under 365 nm irradiation and thereby abstract a hydrogen atom from any closely located C-H bond to form a C-C bond [16]. The 365 nm wavelength used in pBpa photo-cross-linking minimizes protein damage. In addition, if H abstraction does not occur, pBpa can relax back to the ground state and be re-activated in the next round of irradiation [16]. This property is beneficial for reaction yield. However, challenges still exist in applying this strategy: first, the acid-rich sequences of many transcriptional activators make positive ESI mode difficult due to their low ionization efficiency and labile nature [17, 18]. The hydrophilic nature of activators also diminishes ESI efficiency due to their reduced surface activity [19, 20]. Second, the photo-cross-linking efficacy of pBpa depends on the stability and proper accessibility of the interacting partners [16] thus the yield may be very low [21, 22]. Third, cross-linked products generally need to be separated from non-cross-linked material prior to analysis. However, as shown in Table 2.1., the mass

increment of our Med15 construct (Med15 1-416; 47 kDa) after cross-linking is less than 4 kDa, rendering gel-based separation difficult.

Table 2.1. Sequence and monoisotopic mass of three activators applied in this study

Name	Sequence ^{1,2}	Monoisotopic Mass ³
Gcn4 (105-134)	TPMF EYENLEDNSKEW TS <i>LFD</i> NDIPVTTDD <u>C</u>	3770.5917
Gal4 (854-874)	<u>C</u> GMFNTT <i>MDDVYNYFD</i> DEDT	2712.0343
VP2	DFDL <i>DMLGD</i> FDL <i>DMLGC</i>	2036.8210

- 1: Phe in sequence marked by bold and italic font was substituted by pBpa.
- 2: Cys with underline is introduced to incorporate N-(6-(biotinamido)hexyl)-3'-(2'-pyridyldithio)-propionamide (BHPDP).
- 3: Mass of BHPDP is not included.

In collaboration with Prof. Mapp's group, *in vitro* cross-linking experiments with the activators VP2/Gcn4/Gal4 and the protein co-activator Med15 (residues 1-416) were performed. In order to verify the photo-cross-linking yield, top-down analysis of cross-linked product from a shorter Med15 fragment, 107-255 (average MW of 33,582) with Gcn4 was carried out (the binding activity with Gcn4 is similar for this construct as for Med15 1-416 [23]). As shown in Figure 2.1, the major mass spectral peaks both with and without cross-linking correspond to unmodified Med15. No detectable signals were observed for a cross-linked species. Therefore, it can be concluded that the photo-cross-linking yield was too low for direct analysis.

Efforts were made to overcome all these challenges. First, a reversible biotinylation reagent ((N-(6-(biotinamido)hexyl)-3'-(2'-pyridyldithio)-propionamide, BHPDP) was used to incorporate a biotin moiety into activators (at a Cys residue, located either at the N- or C-terminus, as shown in Table 2.1). As shown in Figure 2.2, BHPDP has a biotin moiety linked to an SH reactive group. Once the Cys residue is biotinylated, cross-linked products can be selectively bound to neutravidin beads for enrichment. The presence of a disulfide bond in BHPDP allows bound species to be released from the neutravidin by S-S reduction with dithiothreitol (DTT). This strategy is beneficial because use of detergents, which are not compatible with subsequent MS analysis and difficult to remove, can be avoided. Second, both MALDI and ESI (the latter was applied in both positive and negative ion modes) were utilized combined with corresponding MS/MS approaches. Briefly, the cross-linking reaction was carried out and the product was subjected to trypsin digestion, then cross-linked peptides were selectively isolated via biotinylation-avidin affinity purification, identified by ESI FT-ICR MS and/or MALDI-MS, and confirmed by MS/MS approaches, including ESI low-energy CID and MALDI TOF/TOF high-energy CID. MALDI and ESI have previously been shown to yield complementary information in proteomic analyses in that some proteins were identified with MALDI only whereas others for ESI only [24-27].

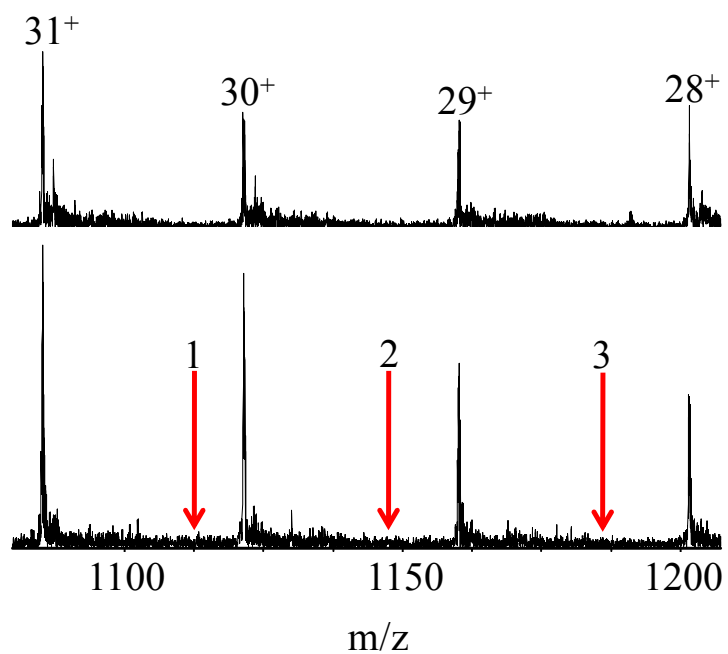


Figure 2.1. Partial ESI FT-ICR mass spectra from top-down analysis of unreacted Med15 107-255 (top) and Med15 107-255 cross-linked with Gcn4 (bottom). Charge states +28-+31 of unmodified Med15 107-255 are observed in both cases. The arrows 1-3 indicate m/z regions where the cross-linked product (Med15 and Gcn4) should be observed in its +32, +33, and +34 charge state, respectively.

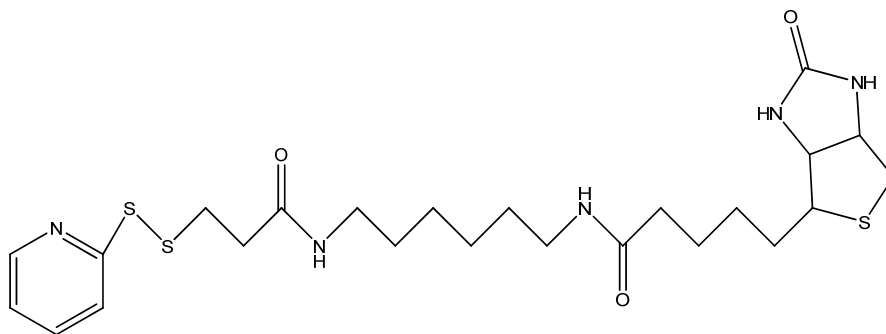


Figure 2.2. Chemical structure of BHPDP.

2.2 Experimental

All experiments involving sample preparation, including Med15 expression, synthesis of Gal4, Gcn4, and VP2, and BHPDP conjugation, were accomplished by Dr. Majmudar [28].

For ESI in both positive and negative ion mode, samples were analyzed with an actively shielded 7 Tesla quadrupole-Fourier transform ion cyclotron resonance mass spectrometer (APEX-Q, Bruker Daltonics, Billerica, MA). Target analytes in electrospray solution (1:1 CH₃CN:H₂O with 0.1% HCOOH for positive ion mode, and 1:1 CH₃CN:H₂O with 20 mM NH₄HCO₃ for negative ion mode) were directly infused into an ESI source (Apollo II, Bruker Daltonics) at a flow rate of 70 μ L/h. A counterflow of hot (240 $^{\circ}$ C) nitrogen gas was applied to assist desolvation of ESI droplets. Multiply charged ions generated by ESI were externally accumulated in a hexapole and transferred into an infinity ICR cell [29] through a series of high-voltage optics for m/z analysis. For external CID, precursor ions were mass-selectively accumulated in the hexapole collision cell at collision voltages ranging from -18-24 V. Argon was used as collision gas. All

data were acquired with XMASS software (version 6.1, Bruker Daltonics) in broadband mode from $m/z = 200$ to 2000 with 512k data points and summed up to 50 scans. Mass spectra were analyzed with MIDAS software [30].

For MALDI analysis (performed at the Michigan Proteome Consortium), 5 μL of alpha-cyano-4-hydroxycinnamic acid (5 mg/mL in 50% acetonitrile, 0.1% TFA, 2 mM ammonium citrate) were added to the avidin purified cross-linked tryptic peptides. Samples were taken to dryness and resuspended in 5 μL of 50% acetonitrile/0.1% TFA. 0.5 μL of this solution was hand-spotted onto a 192-well MALDI target and allowed to dry under atmosphere. MALDI mass spectra were acquired on an Applied Biosystems 4800 Proteomics Analyzer (TOF/TOF) in reflector positive ion mode. Peptide masses were acquired up to 8,000 Da. Mass spectra were obtained with 2000 laser (Nd-YAG laser operating at 355 nm and 200 Hz) shots. At least three trypsin autolysis peaks were used for internal calibration. MS/MS spectra were also acquired in positive ion mode. MS/MS spectra were accumulated based on 6,000 laser shots, or until up to five peptide product ions were observed at a signal-to-noise ratio of 100. Atmosphere, at a pressure of $\sim 6 \times 10^{-7}$ Torr was used as collision gas with a collision energy of 2 keV.

2.3 Results and Discussion

2.3.1 Identified Binding Sites between Med15 and Gcn4/Gal4/VP2

The identified binding sites of Gal4, Gcn4 and VP2 within Med15 (1-416) are shown in Figure 2.3. These results show that all three activators share two binding sites: residues 74-78 and 207-217 in Med15. Additionally, Gal4 and VP2 have one common

binding site: residues 160-174, and VP2 has three more unique binding sites; residues 79-85, 222-231, and 345-348.

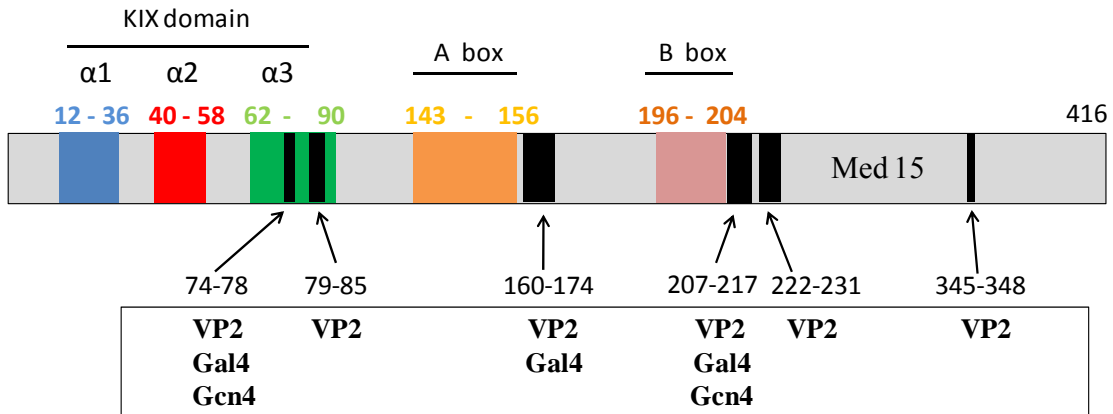


Figure 2.3. Binding sites identified in Med15 for Gal4, Gcn4 and VP2.

The mass spectrometric mapping of binding sites between Med15 and the three activators Gal4, Gcn4, and VP2 relied on the complementary use of MALDI and ESI, which was particularly crucial for VP2 analysis. As summarized in Table 2.2, all VP2 cross-linked products, including Med15 345-348, 74-78, 79-85, 207-217, 222-231, and 160-174, could only be detected and confirmed by MALDI MS and MS/MS. More details are provided in Figure 2.4, in which signals of six potential VP2 cross-linked peptides can be clearly observed in MALDI (top panel) whereas only two potential VP2 cross-linked products, 74-78 and 207-217, are observed in negative ESI MS (bottom panel). No potential cross-linked products were detected in positive ESI MS (middle panel). Interestingly, the utilized VP2 sequence contains 35% acidic residues (6 out of 17) and no basic residues (His, Arg, or Lys), which enhance MALDI response [26, 31]. However, MALDI yielded the most binding information for the VP2 activator. With ESI,

VP2-Med15 cross-linked products were detected only in negative ion mode for which MS/MS analysis is much more complex compared to positive ion mode [32]. For Gcn4 (Figure 2.5), MALDI MS (top panel) provided detection of cross-linked products involving Med15 74-78 whereas positive ESI MS (insets of bottom panel) provided detection of Med15 207-217 cross-linked with Gcn4. Finally, for Gal4 (Figure 2.6), MALDI MS (top panel) provided detection of two Gal4 cross-linked products: Med15 74-78 and 207-217. In addition to these two cross-linked products, the cross-linked peptide 160-174 was detected in positive ESI MS, as shown in the inset of the bottom panel in Figure 2.6.

Table 2.2. Med15 binding sites for activators determined and verified by ESI and MALDI.

Activators	Binding site with Med15	Detected by	Confirmed by
Gal11	V ⁷⁴ AVMR ⁷⁸	ESI, MALDI	ESI-MS/MS; MALDI-MS/MS
	R ¹⁶⁰ QLTPQQQLV ¹⁷⁴ NQMK	ESI	ESI-MS/MS
	L ²⁰⁷ LTPQDMEAAK ²¹⁷	ESI, MALDI	ESI-MS/MS
Gcn4	V ⁷⁴ AVMR ⁷⁸	MALDI	MALDI-MS/MS
	L ²⁰⁷ LTPQDMEAAK ²¹⁷	ESI	ESI-MS/MS
VP16	V ⁷⁴ AVMR ⁷⁸	MALDI	MALDI-MS/MS
	N ⁷⁹ TYNTRK ⁸⁵		
	R ¹⁶⁰ QLTPQQQLV ¹⁷⁴ NQMK		
	L ²⁰⁷ LTPQDMEAAK ²¹⁷		
	I ²²² HQQLLFKAR ²³¹		
A ³⁴⁵ LRK ³⁴⁸			

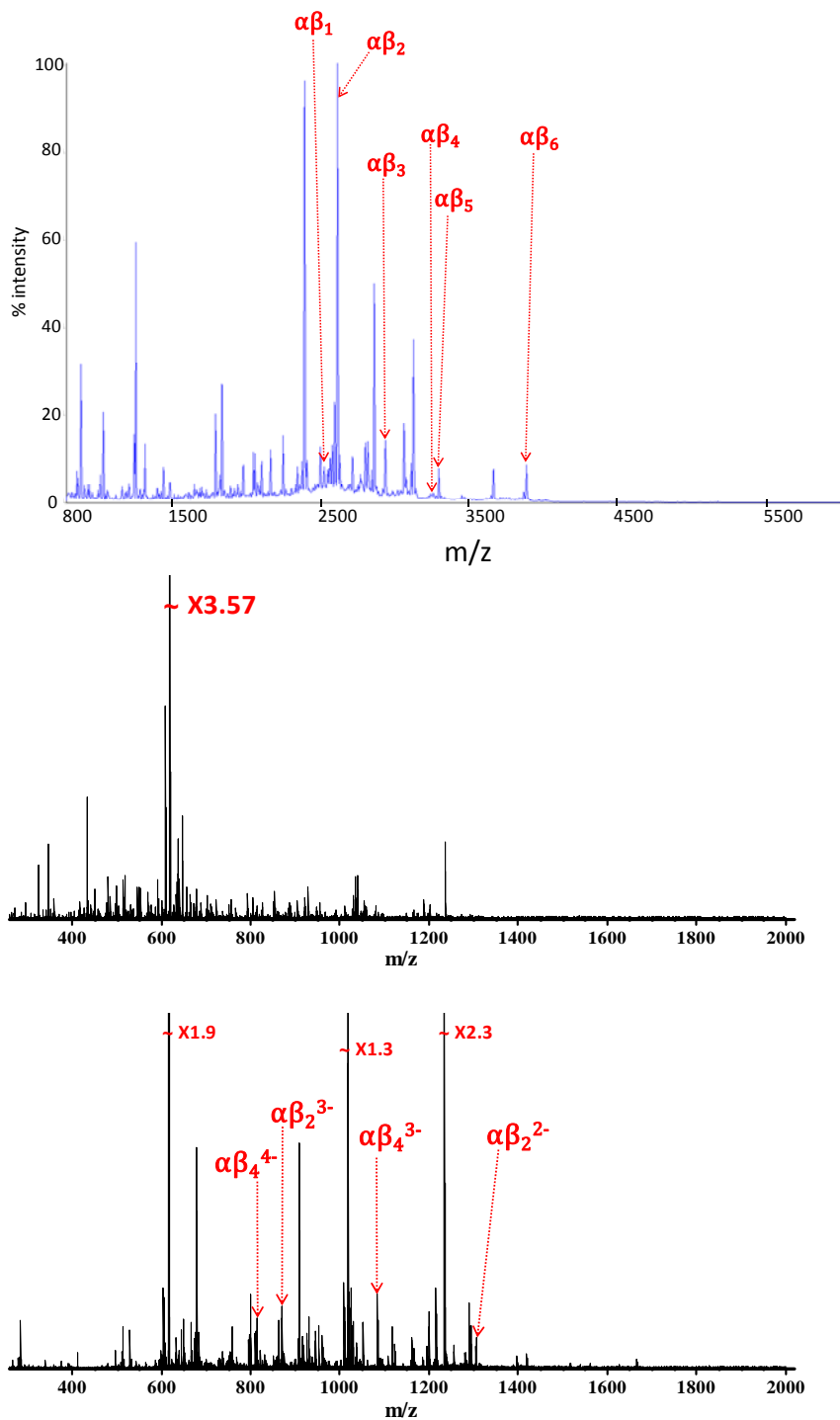


Figure 2.4. MALDI-TOF (top) and ESI FT-ICR MS (positive mode, middle; negative mode, bottom) analysis of VP2/Med15 cross-linked products. Here, α represents the activator VP2, β_1 corresponds to Med15 345-348, β_2 to Med15 74-78, β_3 to Med15 79-

85, β_4 to Med15 207-217, β_5 to Med15 222-231, and β_6 to Med15 160-174. Cross-linked products were verified by MS/MS.

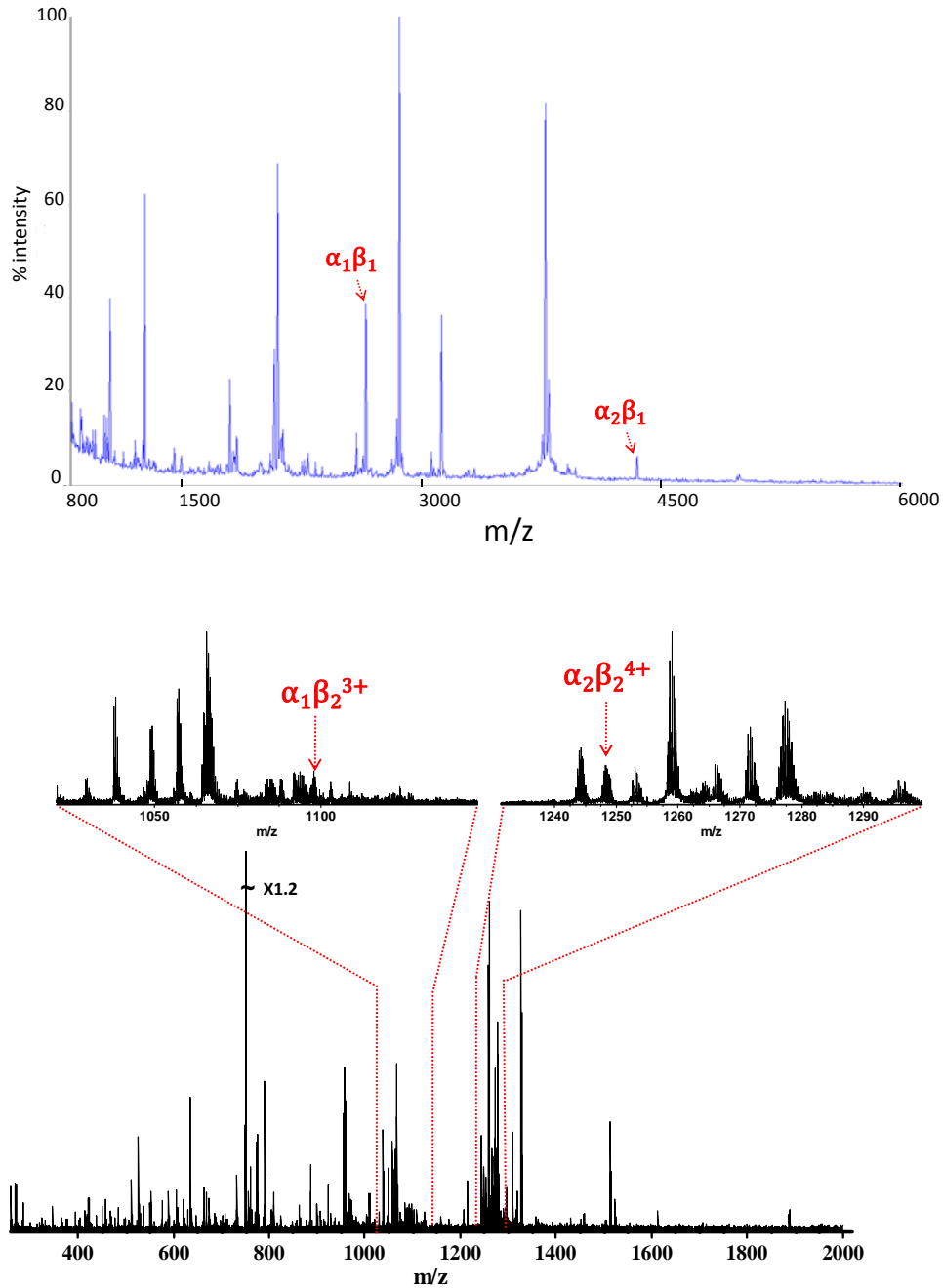


Figure 2.5. MALDI TOF (top) and ESI FT-ICR MS (positive ion mode, bottom) analysis of cross-linked products involving Gcn4 and Med15. Here, α_1 represents the activator

tryptic peptide Gcn4 119-134; α_2 represents Gcn4 105-134, β_1 corresponds to Med15 74-78, and β_2 to Med15 207-217.

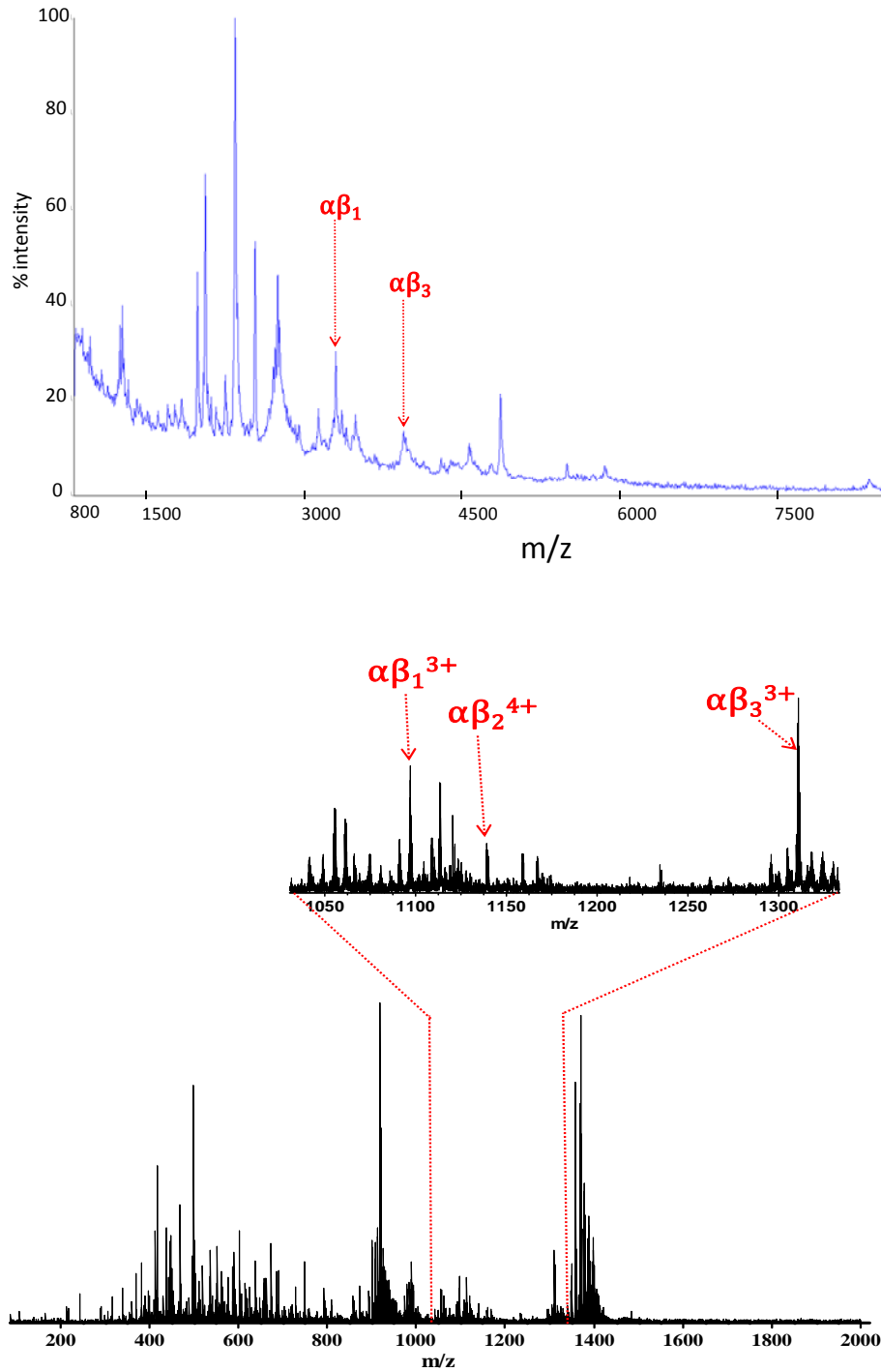


Figure 2.6. MALDI-TOF (top) and ESI FT-ICR MS (positive ion mode, bottom) analysis

of cross-linked products involving Gal4 and Med15. Following photo-cross-linking, samples were subjected to proteolysis and purification as described in the experimental section. Here, α represents the activator Gal4, β 1 corresponds to Med15 74-78, β 2 to Med15 160-174, and β 3 to Med15 207-217.

It should be noted that MALDI and ESI MS can provide cross-linked product candidates but they need to be confirmed by MS/MS. In this work, up to twenty candidates of Gal4, Gcn4, and VP2 cross-linked products with Med15 were observed but several could not be confirmed by MS/MS. Thus, multiplexed MS/MS analyses are crucial to maximize the confirmation. Low-energy CID and MALDI TOF/TOF high-energy CID were both applied and yielded complementary information. As shown in Table 2.2, some cross-linked candidates, including Gal4-Med15 160-174, Gal4-Med15 207-217, and Gcn4-Med15 207-217, could only be confirmed by ESI MS/MS while others, including Gcn4-Med15 74-78 and all six VP2 cross-linked products, were only verified by MALDI TOF/TOF CID.

MALDI TOF/TOF CID (Figure 2.7, top) of VP2-Med15 207-217 produced 14 backbone product ions along both VP2 and Med15 207-217, thereby providing confident confirmation of this cross-linked product. Peaks 1 and 2 in the MALDI TOF/TOF CID spectrum may be assigned as C-S and S-C bond cleavage in the Met side chain or pBpa moiety and are discussed in detail below. Negative ion CID (Fig. 2.7, bottom), on the other hand, produced only uninformative neutral losses from the precursor ions, thus precluding confirmation of the cross-linked product. An example for Gcn4 is shown in Figure 2.8. Here, positive mode ESI CID provided localization of the cross-linking site

between Gcn4 and Med15 to Met²¹³. In addition, 12 backbone cleavages on Gcn4 and their neutral losses (shown in inset) provided confident identification of the cross-linked product. MALDI TOF/TOF CID of the singly protonated form of the same cross-linked species (Fig. 2.8, bottom), on the other hand, showed very limited fragmentation. In addition, observed low-abundance peaks are ill defined, particularly in the higher m/z area shown in the insets. Thus, accurate m/z values could not be obtained. An example for Gal4, the product Gal4-Med15 74-78 is shown in Figure 2.9. Low-energy ESI CID provided 12 backbone cleavages whereas only five were observed in MALDI TOF/TOF CID. However, it should be noticed that MALDI was necessary for confirmation of VP2-Med15 cross-linked species. Similarly, some cross-linked products were only detectable in ESI and were thus limited to low energy CID, as shown in Figure 2.10 for confirmation of the cross-linked product between Gal4 and Med15 160-174.

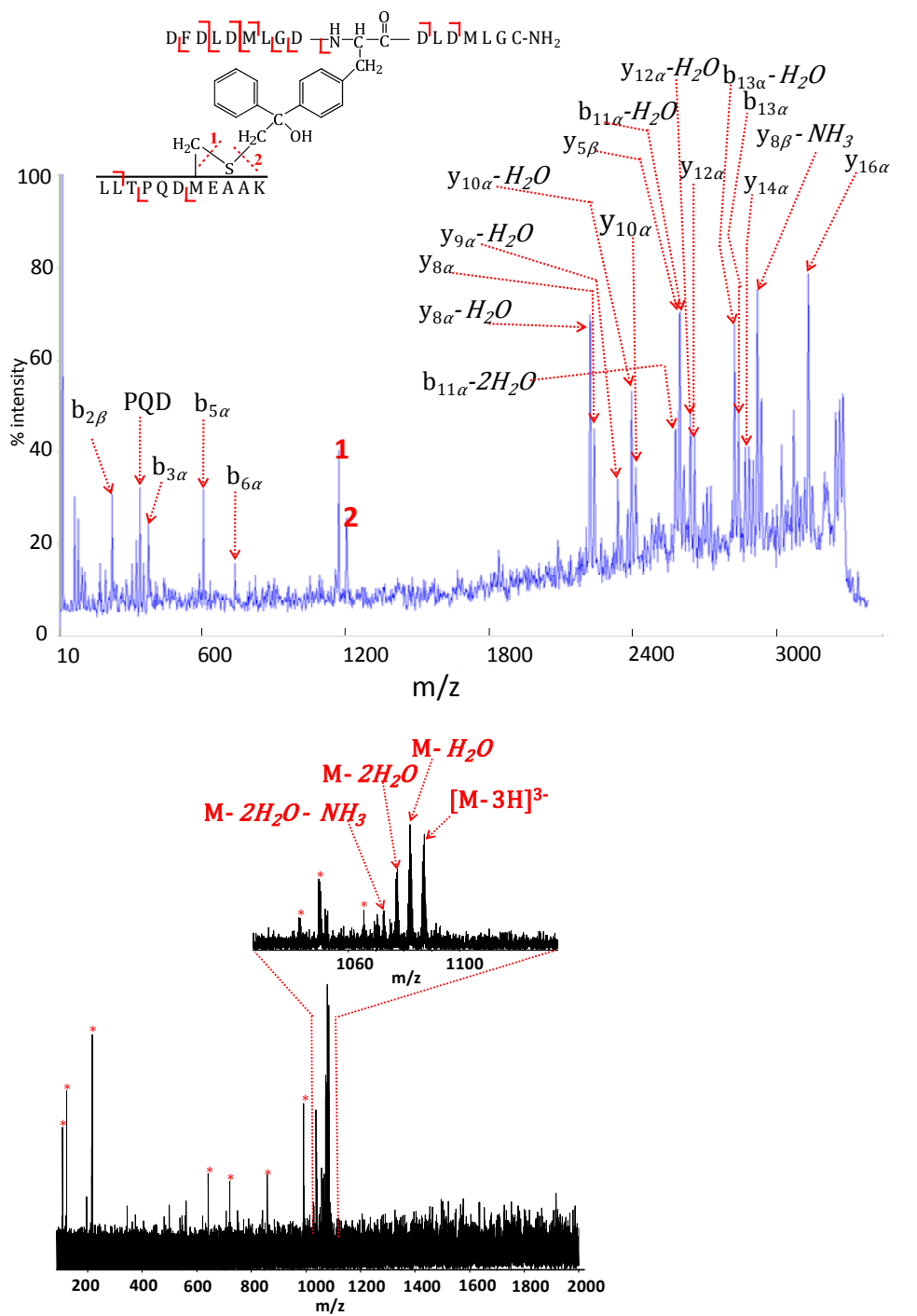
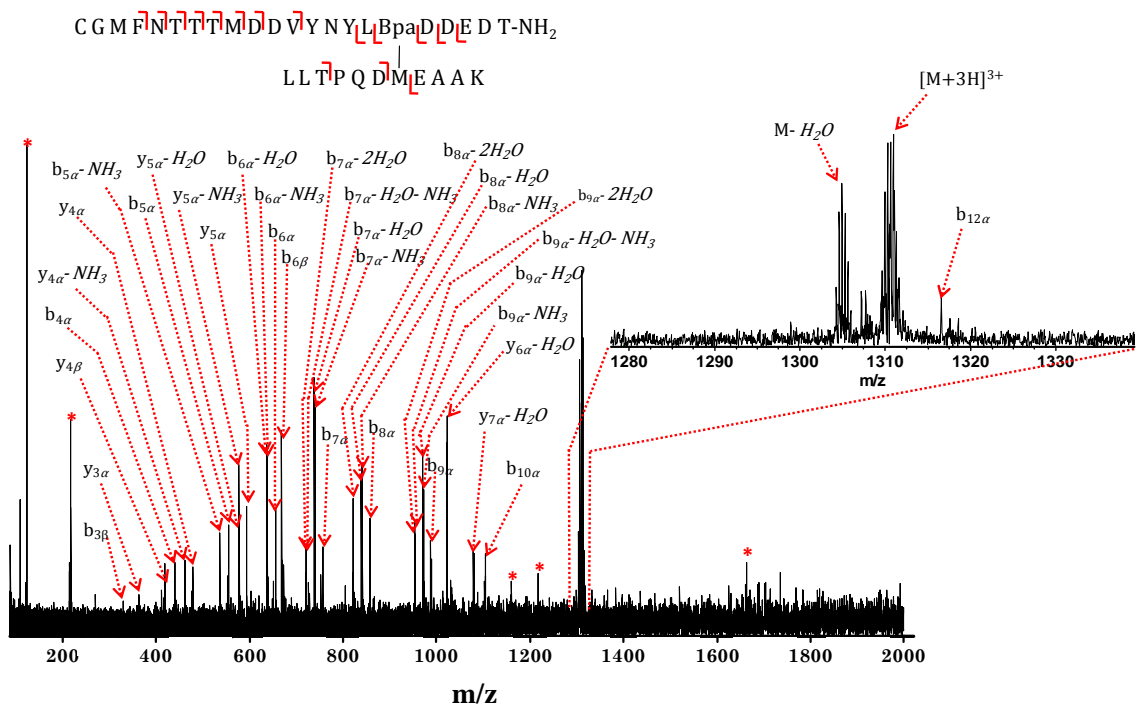


Figure 2.7. MALDI-TOF/TOF CID MS/MS (top) and ESI FT-ICR MS/MS (negative ion low-energy CID, bottom) of a potential cross-linked product: VP2:Med15 207-217. Peaks 1 and 2 can be assigned as C-S bond cleavages, assuming that cross-linking occurred at Met213 in Med15 207-217. In MALDI TOF/TOF CID, extensive peptide

fragmentation is observed but in negative ion mode ESI FT-ICR MS/MS, only neutral losses of water and ammonia were seen, precluding confident verification of this cross-linked product with the latter technique (* = unidentified peaks). Here, α represents VP2 and β corresponds to Med15 207-217.



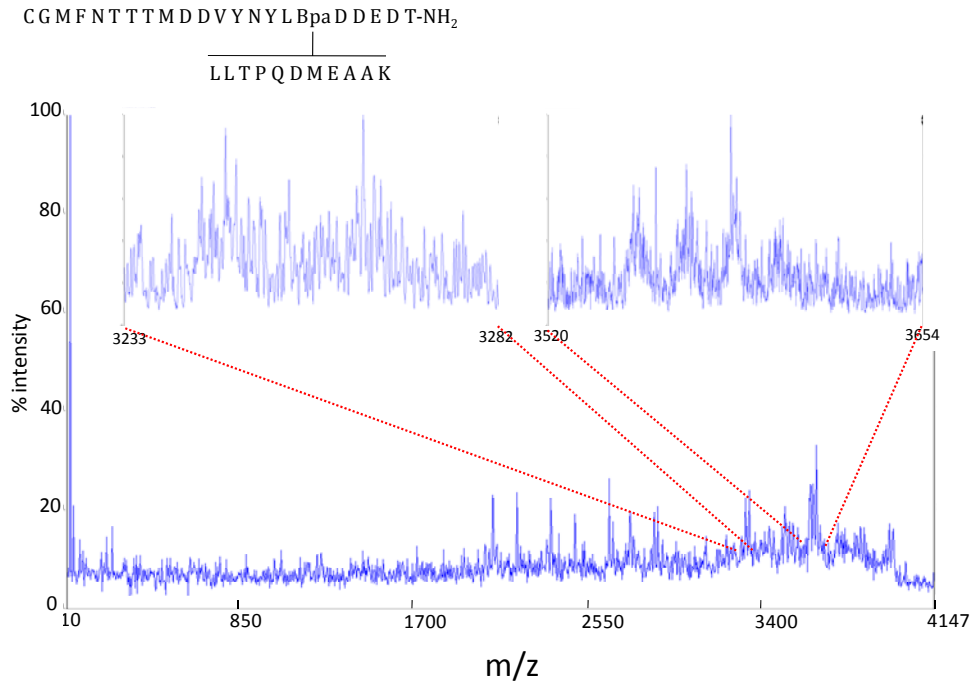


Figure 2.8. ESI FT-ICR MS/MS (positive ion mode, top) and MALDI TOF/TOF high-energy CID MS/MS (bottom) of the potential cross-linked product Gal4:Med15 207-217. A series of backbone cleavages was observed in ESI MS/MS and, based on the fragmentation along the Med15 207-217 peptide backbone, the pBpa cross-linking site can be localized to Met 213. In MALDI TOF/TOF MS/MS, only a limited number of product ion peaks are observed.

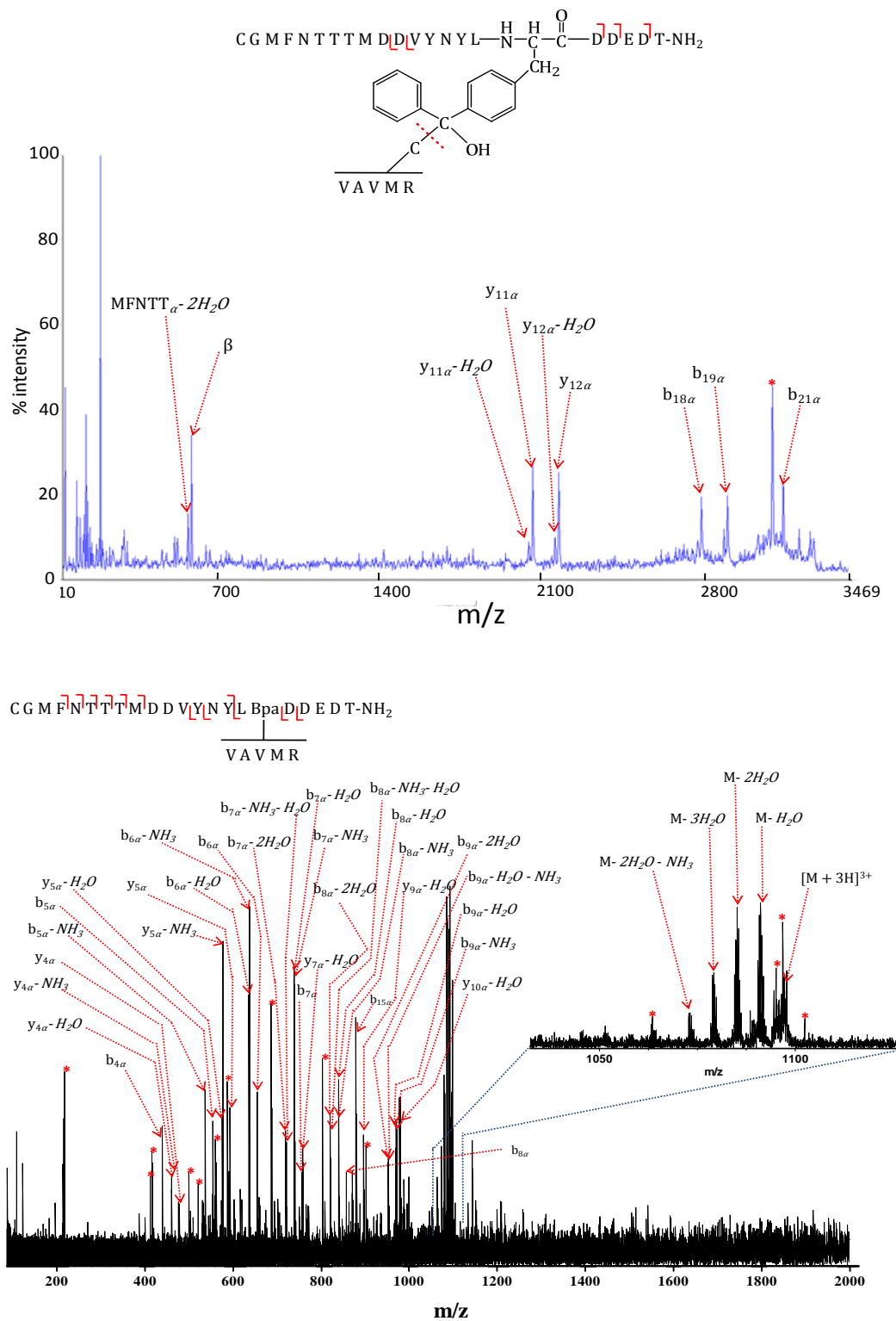


Figure 2.9. MALDI TOF-TOF CID MS/MS (top) and ESI FT-ICR MS/MS (positive ion mode, bottom) of the potential cross-linked product involving Gal4 and Med15 74-78. (β

= free tryptic peptide VAVMR; * = unidentified peak).

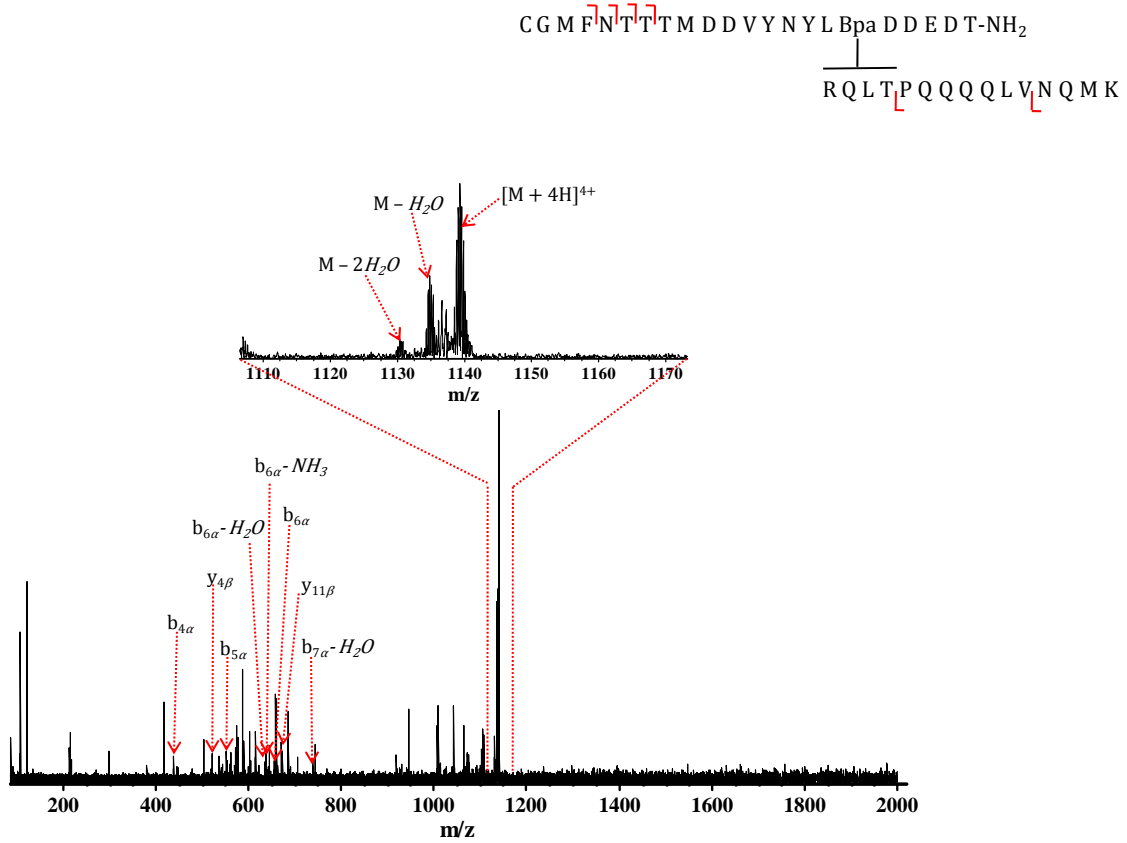


Figure 2.10. ESI FT-ICR MS/MS (positive ion mode) of the potential cross-linked product involving Gal4 and Med15(160-174). Several peaks were not identified, perhaps due to imperfect precursor ion isolation. Here, α represents Gal4 and β corresponds to Med 15(160-174).

MALDI and ESI MS analysis revealed binding sites between Gal4, Gcn4, and VP2 within a few amino acid residues in Med15. In some cases, cross-linking could be localized to one single residue (e.g., Met²¹³ in Med15). It may be noted that most of the Med15 cross-linked peptides, including Med15 74-78 and Med15 207-217, detected for

all three activators, Med15 160-174 for VP2 and Gal4, and Med15 79-85, Med15 222-231, and Med15 345-348 for VP2, contain Met or Arg residues. It has been reported that methyl or methylene groups adjacent to heteroatoms on amino acid side chains are preferable for the pBpa photo-cross-linking reaction and the efficiency of forming photo-cross-linked products relies on the existence of Arg or Met within the reactive region [13]. For Med15 222-231, the C-terminal Arg is not likely involved in the cross-linking reaction because, if so, it would not result in proteolytic cleavage.

Most of the Med15 activator binding sites that were identified and confirmed by ESI and MALDI MS and low- and high-energy CID are located within or close to several regions that were previously predicted to have affinity for activators. For example, residues 74-78 and 79-85 are located within the 62-90 region, which is believed to comprise helix 3 of the Med15 KIX module and an activator binding region [33, 34]. Med15 residues 160-174 and 207-217 are located close to the 143-156 and 196-204 regions, which are homologous to the A and B-boxes of mammalian co-activators that demonstrate activator binding affinity[35].

Further, *in vivo* functional assays were carried out (by Dr. Lum in Prof. Mapp's group) to validate the binding sites found *in vitro*. These results [28] demonstrated that truncation of Med15 (1-186) leads to reduction of activity for Gal4 and VP2. Deletion of Med15 1-345, on the other hand, suppressed the activity of all activators. These results are consistent with findings in this Chapter because, as shown in Figure 2.3, the binding sites of VP2 (residues 74-78, 79-85, 161-174, 207-217, and 222-231), Gal4 (74-78, 160-174, and 207-217), and Gcn4 (74-78, 207-217) are distributed over both deleted regions. In addition, Med15 74-78 may be important for Gal4 activity but not for Gcn4 because

deletion of Med15 1-186 suppressed the activity of Gal4 only. In other words, Med15 207-217 may be the key binding site for Gcn4 activity.

Two papers regarding interaction between Gcn4 and Med15 have been published recently. Herbig et al. reported that no interaction was observed between Gcn4 and Med15 KIX domain (residues 6-90 [36]. This result is inconsistent with the findings in this Chapter but supportive of our discussion (see above) that cross-linked products detected between Med15 74-78 and Gcn4 may not represent behavior *in vivo*. Binding sites revealed by that work include residues 158-238 and 277-368. The former binding site covers Med15 207-217, which was revealed and validated in this Chapter. In the second paper, the B-box in Med15 was believed to be crucial for functional interaction with Gcn4 [37]. In addition, the Med15 KIX domain was revealed to interact directly with Gcn4 as confirmed by NMR analysis [37]. However, this interaction may be redundant due to the random coil motif in the Gcn4 activation domain in solution, which may result in non-functional interactions [37].

2.3.2 Gas-phase cleavage of Bpa photo-crosslinker in MALDI TOF/TOF CID

Notably, abundant product ion peaks corresponding to gas-phase cleavage of the pBpa cross-linker were observed in MALDI TOF/TOF CID spectra. The fragmentation occurred of either the C-S or S-C bond of a Met side chain cross-linked to pBpa (Figure 2.7.), or of a C-C bond (Figure 2.9.) that formed from cross-linking of pBpa to Med15. In the former case, C-S/S-C bond cleavages in MALDI TOF/TOF CID may be explained by analogous C-S/S-C cleavage occurring for peptides with disulfide (SS) bond linkages [38]. The resulting 34 Da doublet occurring in MS/MS spectra (see top panel of Figure 2.7 (peak 1 and 2)) may facilitate the identification of pBpa cross-linked products in

MALDI TOF/TOF CID. For the latter case, C-C bond cleavage results in release of the two cross-linked peptides (yielding the tryptic peptide peak β in Figure 2.9). Such unique fragmentation of pBpa has not been reported in previous sector high-energy CID of pBpa cross-linked peptides [13] and was also absent in our low-energy CID spectra. This unique C-C bond cleavage may also provide a new approach to identify pBpa cross-linked products in MALDI TOF/TOF CID.

2.4 Summary

In conclusion, the combination of photo-cross-linking and multiplexed mass spectrometry provided binding sites of the transcriptional activators, Gal4, Gcn4, and VP2, with the coactivator Med15 at high resolution. In some cases, the binding site can be localized to a single amino acid residue. To our knowledge, this work includes the first application of BP-based photo-cross-linking to yield products with MW up to 5 kDa that could be confirmed by MS and MS/MS. Also, it is the first observation of unique C-S/S-C and C-C bond cleavages in photo-cross-linked products from MALDI TOF/TOF CID. This observation provides a useful tool for identifying BP-based photo-cross-linked products. Complementary use of ESI and MALDI was necessary to maximize the detection of Med15 binding sites. In addition, the combination of low- and high-energy CID provided complementary structural information and was crucial for screening cross-linking product candidates and confirming them. Detected binding sites for Gal4, Gcn4 and VP2 are located at or close to evolutionary conserved regions, including the GACKIX, A and B box motifs, which contain activator binding sites. The multiple binding sites of activators revealed in this work may provide clues for future screening of

small molecules that target activator binding sites and therefore have activatory/inhibitory therapeutic potential.

2.5 References

1. Ptashne, M., How Eukaryotic Transcriptional Activators Work. *Nature*, **1988**, 335, 683-689.
2. Jeong, C.J.; Yang, S.H.; Xie, Y.; Zhang, L.; Johnston, S.A.; Kodadek, T., Evidence that Gal11 protein is a target of the Gal4 activation domain in the mediator. *Biochemistry*, **2001**, 40, 9421-9427.
3. Duncan, S.A.; Navas, M.A.; Dufort, D.; Rossant, J.; Stoffel, M., Regulation of a transcription factor network required for differentiation and metabolism. *Science*, **1998**, 281, 692-695.
4. Li, S.H.; Cheng, A.L.; Zhou, H.; Lam, S.; Rao, M.; Li, H.; Li, X.J., Interaction of Huntington disease protein with transcriptional activator Sp1. *Mol. Cell. Biol.*, **2002**, 22, 1277-1287.
5. Chen, X.; Cheung, S.T.; So, S.; Fan, S.T.; Barry, C.; Higgins, J.; Lai, K.M.; Ji, J.; Dudoit, S.; Ng, I.O.; Van De Rijn, M.; Botstein, D.; Brown, P.O., Gene expression patterns in human liver cancers. *Mol Biol Cell*, **2002**, 13, 1929-1939.
6. Chene, P., Inhibiting the p53-MDM2 interaction: an important target for cancer therapy. *Nat. Rev. Cancer.*, **2003**, 3, 102-109.
7. Pandolfi, P.P., Transcription therapy for cancer. *Oncogene*, **2001**, 20, 3116-3127.
8. Mapp, A.K.; Ansari, A.Z., A TAD further: exogenous control of gene activation. *ACS Chem. Biol.*, **2007**, 2, 62-75.
9. Majmudar, C.Y.; Lum, J.K.; Prasov, L.; Mapp, A.K., Functional specificity of artificial transcriptional activators. *Chem. Biol.*, **2005**, 12, 313-321.
10. Ard, P.G.; Chatterjee, C.; Kunjibettu, S.; Adside, L.R.; Gralinski, L.E.; McMahon, S.B., Transcriptional regulation of the mdm2 oncogene by p53 requires TRRAP acetyltransferase complexes. *Mol. Cell. Biol.*, **2002**, 22, 5650-5661.
11. Park, J.; Kunjibettu, S.; McMahon, S.B.; Cole, M.D., The ATM-related domain of TRRAP is required for histone acetyltransferase recruitment and Myc-dependent oncogenesis. *Genes Dev.*, **2001**, 15, 1619-1624.
12. Jahn, O.; Eckart, K.; Brauns, O.; Tezval, H.; Spiess, J., The binding protein of corticotropin-releasing factor: Ligand-binding site and subunit structure. *Proc. Natl. Acad. Sci. USA*, **2002**, 99, 12055-12060.
13. Jahn, O.; Tezval, H.; Spiess, J.; Eckart, K., Tandem mass spectrometric characterization of branched peptides derived from photoaffinity labeling. *Int. J. Mass spectrom.*, **2003**, 228, 527-540.

14. Ahrends, R.; Kosinski, J.; Kirsch, D.; Manelyte, L.; Giron-Monzon, L.; Hummerich, L.; Schulz, O.; Spengler, B.; Friedhoff, P., Identifying an interaction site between MutH and the C-terminal domain of MutL by crosslinking, affinity purification, chemical coding and mass spectrometry. *Nucleic Acids Res.*, **2006**, *34*, 3169-3180.
15. Dietrich, K.A.; Sindelar, C.V.; Brewer, P.D.; Downing, K.H.; Cremo, C.R.; Rice, S.E., The kinesin-1 motor protein is regulated by a direct interaction of its head and tail. *Proc. Natl. Acad. Sci. USA*, **2008**, *105*, 8938-8943.
16. Dorman, G.; Prestwich, G.D., Benzophenone Photophores in Biochemistry. *Biochemistry*, **1994**, *33*, 5661-5673.
17. Papayannopoulos, I.A., The Interpretation of Collision-Induced Dissociation Tandem Mass-Spectra of Peptides. *Mass Spectrom. Rev.*, **1995**, *14*, 49-73.
18. Wysocki, V.H.; Tsaprailis, G.; Smith, L.L.; Breci, L.A., Special feature: Commentary - Mobile and localized protons: a framework for understanding peptide dissociation. *J. Mass Spectrom.*, **2000**, *35*, 1399-1406.
19. Cech, N.B.; Enke, C.G., Relating electrospray ionization response to nonpolar character of small peptides. *Anal. Chem.*, **2000**, *72*, 2717-2723.
20. Schmidt, A.; Karas, M.; Dulcks, T., Effect of different solution flow rates on analyte ion signals in nano-ESI MS, or: When does ESI turn into nano-ESI? *J. Am. Soc. Mass Spectrom.*, **2003**, *14*, 492-500.
21. Trester-Zedlitz, M.; Kamada, K.; Burley, S.K.; Fenyo, D.; Chait, B.T.; Muir, T.W., A modular cross-linking approach for exploring protein interactions. *J. Am. Chem. Soc.*, **2003**, *125*, 2416-2425.
22. Lamos, S.M.; Krusemark, C.J.; McGee, C.J.; Scalf, M.; Smith, L.M.; Belshaw, P.J., Mixed isotope photoaffinity reagents for identification of small-molecule targets by mass spectrometry. *Angew. Chem. Int. Ed.*, **2006**, *45*, 4329-4333.
23. Majmudar, C.Y., Mechanistic Investigations of Transcriptional Activator Function for the Design of Synthetic Replacements Ph.D. dissertation, University of Michigan. **2008**.
24. Medzihradzky, K.F.; Leffler, H.; Baldwin, M.A.; Burlingame, A.L., Protein identification by in-gel digestion, high-performance liquid chromatography, and mass spectrometry: Peptide analysis by complementary ionization techniques. *J. Am. Soc. Mass Spectrom.*, **2001**, *12*, 215-221.
25. Bodnar, W.M.; Blackburn, R.K.; Krise, J.M.; Moseley, M.A., Exploiting the complementary nature of LC/MALDI/MS/MS and LC/ESI/MS/MS for increased proteome coverage. *J. Am. Soc. Mass Spectrom.*, **2003**, *14*, 971-979.
26. Stapels, M.D.; Barofsky, D.F., Complementary use of MALDI and ESI for the HPLC-MS/MS analysis of DNA-binding proteins. *Anal. Chem.*, **2004**, *76*, 5423-5430.
27. Getie, M.; Schmelzer, C.E.H.; Weiss, A.S.; Neubert, R.H.H., Complementary mass spectrometric techniques to achieve complete sequence coverage of recombinant human tropoelastin. *Rapid Commun. Mass Spectrom.*, **2005**, *19*, 2989-2993.
28. Majmudar, C.Y.; Wang, B.; Lum, J.K.; Hakansson, K.; Mapp, A.K., A high-resolution interaction map of three transcriptional activation domains with a key coactivator from photo-cross-linking and multiplexed mass spectrometry. *Angew.*

- Chem. Int. Ed. Engl.*, **2009**, *48*, 7021-7024.
29. Caravatti, P.; Allemann, M., The Infinity Cell - a New Trapped-Ion Cell with Radiofrequency Covered Trapping Electrodes for Fourier-Transform Ion-Cyclotron Resonance Mass-Spectrometry. *Org. Mass Spectrom.*, **1991**, *26*, 514-518.
 30. Senko, M.W.; Canterbury, J.D.; Guan, S.H.; Marshall, A.G., A high-performance modular data system for Fourier transform ion cyclotron resonance mass spectrometry. *Rapid Commun. Mass Spectrom.*, **1996**, *10*, 1839-1844.
 31. Krause, E.; Wenschuh, H.; Jungblut, P.R., The dominance of arginine-containing peptides in MALDI-derived tryptic mass fingerprints of proteins. *Anal. Chem.*, **1999**, *71*, 4160-4165.
 32. Bowie, J.H.; Brinkworth, C.S.; Dua, S., Collision-induced fragmentations of the (M-H)(-) parent anions of underivatized peptides: An aid to structure determination and some unusual negative ion cleavages. *Mass Spectrom. Rev.*, **2002**, *21*, 87-107.
 33. Thakur, J.K.A., H.; Yang, F.; Pan, S.J.; Fan, X.; Breger, J.; Frueh, D.P.; Gulshan, K.; Li, D.K.; Mylonakis, E.; Struhl, K.; Moye-Rowley, W.S.; Cormack, B.P.; Wagner, G.; Näär, A.M., A nuclear receptor-like pathway regulating multidrug resistance in fungi. *Nature*, **2008**, *452*, 604-609.
 34. Thakur, J.K.; Arthanari, H.; Yang, F.J.; Pan, S.J.; Fan, X.C.; Breger, J.; Frueh, D.P.; Gulshan, K.; Li, D.K.; Mylonakis, E.; Struhl, K.; Moye-Rowley, W.S.; Cormack, B.P.; Wagner, G.; Naar, A.M., A nuclear receptor-like pathway regulating multidrug resistance in fungi. *Nature*, **2008**, *452*, 604-U604.
 35. Kim, D.H.; Kim, G.S.; Yun, C.H.; Lee, Y.C., Functional conservation of the glutamine-rich domains of yeast Gal11 and human SRC-1 in the transactivation of glucocorticoid receptor Tau 1 in *Saccharomyces cerevisiae*. *Mol. Cell. Biol.*, **2008**, *28*, 913-925.
 36. Herbig, E.; Warfield, L.; Fish, L.; Fishburn, J.; Knutson, B.A.; Moorefield, B.; Pacheco, D.; Hahn, S., Mechanism of Mediator Recruitment by Tandem Gcn4 Activation Domains and Three Gal11 Activator-Binding Domains. *Mol. Cell. Biol.*, **2010**, *30*, 2376-2390.
 37. Jedidi, I.; Zhang, F.; Qiu, H.F.; Stahl, S.J.; Palmer, I.; Kaufman, J.D.; Nadaud, P.S.; Mukherjee, S.; Wingfield, P.T.; Jaroniec, C.P.; Hinnebusch, A.G., Activator Gcn4 Employs Multiple Segments of Med15/Gal11, Including the KIX Domain, to Recruit Mediator to Target Genes in Vivo. *J. Biol. Chem.*, **2010**, *285*, 2438-2455.
 38. King, G.J.; Jones, A.; Kobe, B.; Huber, T.; Movadov, D.; Hume, D.L.; Ross, I.L., Identification of disulfide-containing chemical cross links in proteins using MALDI-TOF/TOF-mass spectrometry. *Anal. Chem.*, **2008**, *80*, 5036-5043.

Chapter 3

Gas-Phase Cleavage of Sulfur-Sulfur and Sulfur-Carbon Bonds in Tandem Mass Spectrometry of Peptides Linked by Disulfide-Containing Cross-linkers

3.1 Introduction

Thiol-cleavable cross-linkers (TCCs) are utilized to map interfaces in protein complexes [1, 2] as well as to determine low resolution three-dimensional protein structures [3]. The conventional strategy for identifying tryptic peptides linked by TCCs involves splitting the sample in two. One half of the sample is subjected to disulfide reduction, optionally followed by thiol group alkylation [4] and the other half is not. Comparison of mass spectra of the reduced and unreduced proteolyzed samples reveals potential inter-molecularly cross-linked peptides as they are observed in the unreduced sample but not in the reduced sample. Similarly, putative intra-molecularly cross-linked products demonstrate a mass shift, e.g., +2 Da without alkylation and +57 Da with iodoacetamide alkylation, for the reduced sample. Such sample manipulations prior to mass spectrometry (MS) analysis increase sample consumption and operation time. Efforts have been made to eliminate these shortcomings by performing S-S and C-S bond cleavage in the gas phase by applying tandem MS (MS/MS) techniques. For example,

King et al. utilized high-energy CID on a MALDI TOF/TOF mass spectrometer to identify peptides cross-linked by 3,3'-dithiobis (sulfosuccinimidyl propionate) (DTSSP) [5]. In that work, doublet isotopic clusters separated by 66 Da as well as specific neutral losses allowed identification of dead-end, inter-, and intra-molecularly cross-linked peptide products. However, high-energy CID may not be a suitable approach in all cases, for example it can cause loss of post-translational modifications (PTMs). Also, high-energy CID involves significant ion scattering, which can lower sensitivity. Thus, systematic investigation of the fragmentation behavior of peptides linked by TCCs by alternative MS/MS techniques is of interest for elucidating the optimal approach of gas-phase S-S and C-S bond cleavage in cross-linking applications.

Several MS/MS fragmentation techniques have been shown to effectively cleave S-S and C-S bonds in peptides containing natural disulfide bonds. These techniques include high-energy CID [6], electron capture dissociation (ECD) [7], electron transfer dissociation (ETD) [8, 9], electron detachment dissociation (EDD) [10], 157 nm photodissociation [11], MALDI post-source decay [12], MALDI in-source decay (ISD) [13], and negative ion CID [14] and infrared multiphoton dissociation (IRMPD) [10]. Several hypotheses have been put forth to explain the preferential S-S and C-S bond cleavage occurring following various MS/MS activation approaches with a particular focus on radical-driven fragmentation. For example, in the "hot hydrogen" model of ECD, electron-proton recombination is thought to occur and preferential S-S bond cleavage is considered a result of the high hydrogen atom affinity of the S-S bond [7]. Other models invoke electron capture into the σ^* orbital of the S-S bond, either directly through Coulomb stabilization, or via through bond electron transfer [15, 16]. McLuckey

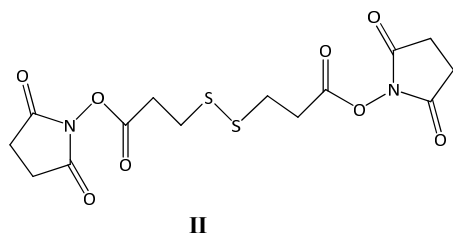
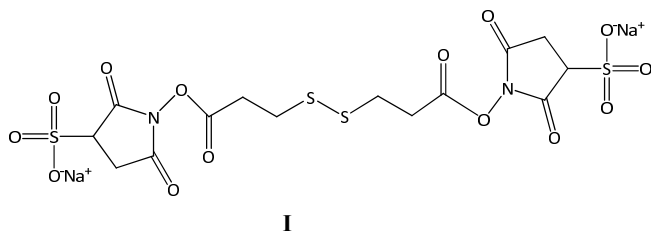
and co-workers [8] argued that hydrogen transfer is unlikely to contribute to S-S bond cleavage in ETD because such cleavages increased when protons were replaced by fixed charges. Disulfide bond cleavage in positive mode low-energy CID is charge state dependent [17]: as the charge state of insulin decreased from +5 to +1, the efficiency of S-S bond cleavage increased with exclusively such cleavage for the +1 charge state.

Gas-phase S-S bond cleavage has also been investigated in MS/MS of metal-adducted peptides. Complexes of singly charged disulfide-containing peptides with sodium and magnesium were found to selectively lose H₂S₂, allowing identification of disulfide bonds [18]. Transitional metals have also been used to facilitate S-S bond rupture in sustained off-resonance irradiation (SORI) CID, which is ineffective for protonated disulfide-containing peptides [19]. Finally, based on the high affinity of gold(I) for sulfur [20], multiply charged S-S bond-containing peptides complexed with gold(I) were shown to undergo selective S-S cleavage in low-energy CID [21].

Activated ion ECD (AI-ECD) is a variant of ECD in which analytes are unfolded through heating either before or after electron irradiation. This strategy can provide greatly enhanced sequence information compared to conventional ECD because product ion pairs that would otherwise be held together through noncovalent interactions are separated [22]. Infrared irradiation is considered to be the preferred approach of activation in AI-ECD due its easy implementation and the avoidance of pressure or temperature increases [23]. To our knowledge, comparison of ECD and AI-ECD for S-S/C-S bond cleavage efficiency has not been reported.

Here, we used the TCCs DTSSP (**I**) and dithiobis (succinimidyl propionate) (DSP) (**II**), to react with model peptides, including α -melanocyte-stimulating hormone (MSH)

and [Lys³]-bombesin (BN), and protein (ubiquitin, proteolyzed after the reaction) to generate a series of inter-molecularly cross-linked peptides (ICPs), referred to as type 2 cross-linked products [24]. Type 1 (intramolecularly cross-linked) and type 2 products are both crucial for providing information on spatial constraints in a protein [24] but only type 2 products can reveal inter-protein interactions and demonstrate separated product ions following S-S/C-S bond cleavages in MS/MS analysis. Fragmentation patterns of these ICPs following a variety of MS/MS activation approaches, including ECD, AI-ECD, negative ion CID, EDD, and MALDI TOF/TOF high-energy CID were carried out in a systematic manner with the aim to find the optimum strategy for gas-phase S-S/C-S bond cleavage in ICPs linked by TCCs. Preferential cleavage of S-S or C-S bonds allows identification of ICPs in a background of non cross-linked peptides.



3.2 Experimental

3.2.1 Reagents and Cross-linking Reactions.

Model peptides MSH (Ac-SYSMEHFRWGKPV-NH₂) and BN (pEQKLGNGWAVGHLM-NH₂) were purchased from Sigma (St. Louis, MO) and used without further purification. DTSSP and DSP were purchased from Pierce (Rockford, IL). For cross-linking reactions, 1 mM of MSH or BN were incubated in bicarbonate buffer (0.1 M, pH 8) with DSP at up to 1:2 peptide to cross-linker molar ratio for 35 minutes at room temperature. The cross-linking reaction was then quenched by adding 1M ammonium bicarbonate to a 50 mM final concentration. Cross-linked products were desalted with C18 Ziptips (Millipore, Billerica, MA) and diluted with either 49.95:49.95:0.1 CH₃CN:H₂O:CH₃COOH or 49.875:49.875:0.25 MeOH:H₂O:NH₄OH for positive or negative ion mode MS analysis, respectively. Ubiquitin (Sigma, St. Louis, MO) was incubated with DTSSP at 1:100 protein to cross-linker molar ratio for 35 minutes in 15 mM HEPES buffer (pH 7.6) at room temperature for 35-45 minutes. After the cross-linking reaction, the protein was denatured by heating (100 °C) for 10 minutes followed by prompt placing on ice. The protein was then digested with trypsin or Glu-C (Promega, Madison, WI) at a 1:50 enzyme to protein ratio for 15-20 hours at 37 °C. The digestion was quenched by adding formic acid to 0.1% final concentration (v/v). The resulting peptides were desalted with C18 Ziptips and diluted with spray solvent as described above for either positive or negative ion mode MS analysis.

3.2.2 Mass Spectrometry and Data Analysis

All experiments involving ECD, AI-ECD, negative ion CID, and EDD were carried out with an actively shielded 7 Tesla Fourier transform ion cyclotron resonance

(Q-FT-ICR) mass spectrometer (Apex-Q, Bruker Daltonics, Billerica, MA). Target analytes were directly infused into an electrospray ionization (ESI) source (Apollo II, Bruker Daltonics) and electrosprayed in positive ion mode for ECD and AI-ECD experiments, and in negative ion mode for EDD and CID experiments at a flow rate of 70 $\mu\text{L}/\text{h}$. A counterflow of hot (200-240 $^{\circ}\text{C}$) nitrogen gas was applied to assist desolvation of ESI droplets. Potential cross-linked products, which were determined by accurate mass, were selected for MS/MS experiments. Precursor ions were accumulated in the first hexapole for 0.1 s, transferred through the mass-selective quadrupole (5-10 m/z isolation window), mass selectively accumulated in the second hexapole for up to 1-2 s, then ions were transferred through high-voltage ion optics, and captured in the ICR cell by dynamic trapping. An indirectly heated hollow dispenser cathode was used to generate an electron beam for electron-based activation. ECD was performed at a bias voltage of negative 0.2-0.8 V and an irradiation time of 50-80 ms. For AI-ECD, all conditions were kept the same as in ECD except that isolated precursor ions were pre-irradiated for 20-100 ms by 10.6 μm photons at 10 W laser power (25 W CO_2 laser, Synrad, Mukilteo, WA). Control experiments for each AI-ECD analysis, in which precursor ions were only irradiated by IR photons, were performed to ensure that pre-IR irradiation did not cause unexpected fragmentation. Negative ion CID of mass-selected cross-linked products was performed in an external collision cell at a collision voltage of 16-25 V. Argon was used as collision gas. EDD was performed at a - 21 V bias voltage for 750-1200 ms. All spectra were acquired with XMASS (version 6.1, Bruker Daltonics) using 512 K data points and summed over 10-66 scans. Data processing was performed with the MIDAS analysis software [25]. For accurate mass determination, external calibration was

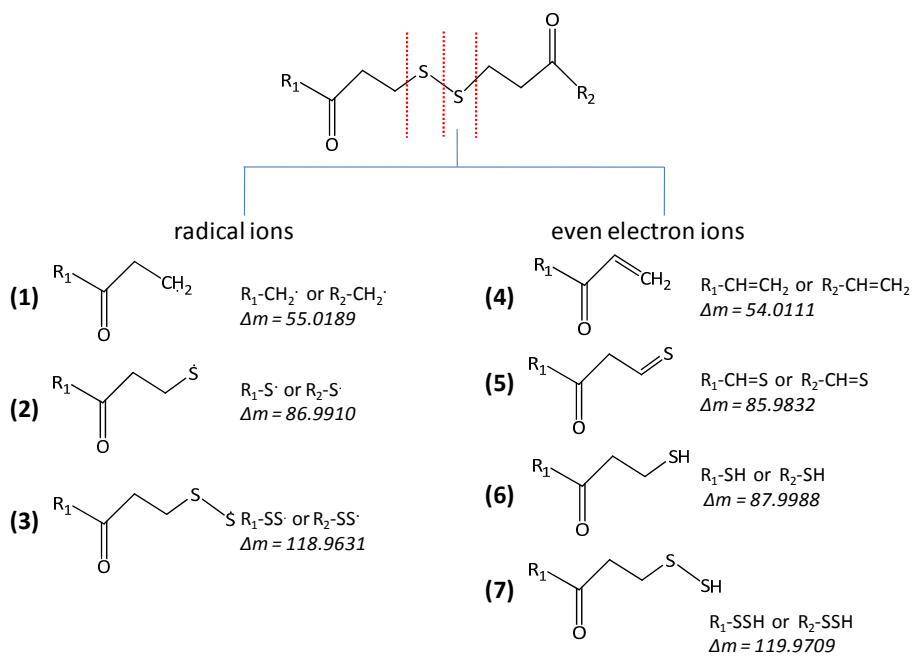
performed with ES tuning mix (Hewlett Packard, Waldbronn, Germany). Internal calibration in EDD was performed by using the calculated masses of precursor and charge reduced ions. These calibrations were based on a two-term frequency-to- m/z calibration equation [26]. For MALDI TOF/TOF analysis, 0.5 μL of alpha cyano-4-hydroxycinnamic acid (CHCA) and 2,5-dihydroxybenzoic acid (DHB) mixture (each 10 mg/mL in 50% acetonitrile, 0.1% TFA) was hand-spotted to 0.5 μL cross-linked peptides onto a 192-well MALDI target and allowed to dry under atmosphere. MALDI mass spectra were acquired on an Applied Biosystems 4800 Proteomics Analyzer in reflector positive ion mode. Peptide masses were acquired up to 4000 Da. Mass spectra were obtained with 2000 laser (Nd-YAG laser operating at 355 nm and 200 Hz) shots. MS/MS spectra were also acquired in positive ion mode. Atmosphere, at a pressure of around 6×10^{-7} torr was used as collision gas with a collision energy of 2 keV.

3.2.3 Nomenclature for ICPs and their fragments in MS and MS/MS spectra

Intermolecularly cross-linked TCC products of MSH and BN are termed MSH-TCC and BN-TCC, respectively. ICPs from ubiquitin proteolysis are referred to as $\alpha_n\text{TCC}\beta_n$ in which α_n represents the peptide with the longest N-terminal stretch before the cross-linking site and β_n represents the other peptide. Here, the ICP pair corresponding to residues 35-51 (GIPPDQQLIFAGKQLE) and 52-64 (DGRTLSDYNIQKE) is termed $\alpha_1\text{TCC}\beta_1$ and for the ICP pair 43-54 (LIFAGKQLEDGR) and 55-72 (TLSDYNIQKESTLHLVLR) is termed $\alpha_2\text{TCC}\beta_2$.

In cases where fragmentation occurs within either chain of the ICPs but does not involve a TCC moiety, the corresponding product ions are referred to in the standard peptide product ion nomenclature but with the subscript α or β (this nomenclature is not

applicable for MSH-TCC and BN-TCC due to their symmetric structures), e.g., $c_{6\beta_1}{}^{'+}$ (from β_1 of α_1 TCC β_1). When fragmentation occurs at a peptide backbone bond with retention of a TCC moiety as well as another intact cross-linked peptide, the corresponding ion is denoted as ion type/R, e.g., z_5^+/R and $z_{3\beta}^+/R$, where R is indicated as MSH, BN, α_1 , α_2 , β_1 , or β_2 . When fragmentation occurs both at the peptide backbone and involves S-S or C-S bond cleavages (structures and abbreviations are shown in Scheme 3.1), the corresponding product ions are labeled as ion type-X where X is an abbreviation referring to types of S-S or C-S bond cleavages as shown in Scheme 3.1.



Scheme 3.1 Structures, nomenclature, and mass increment of product ions observed in this work. R_1 and R_2 are specifically indicated for some peptides.

3.3 Results and Discussion

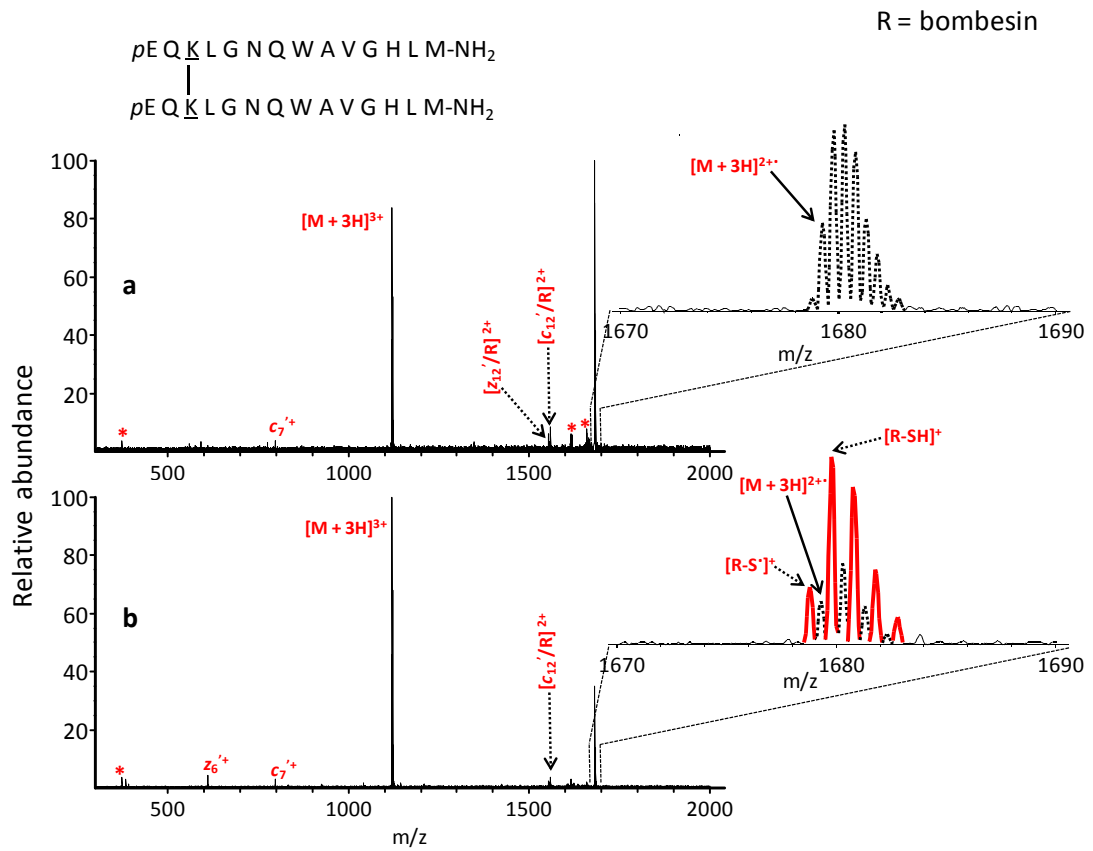
3.3.1 ECD and AI-ECD of TCC products from BN, MSH, and ubiquitin proteolytic peptides

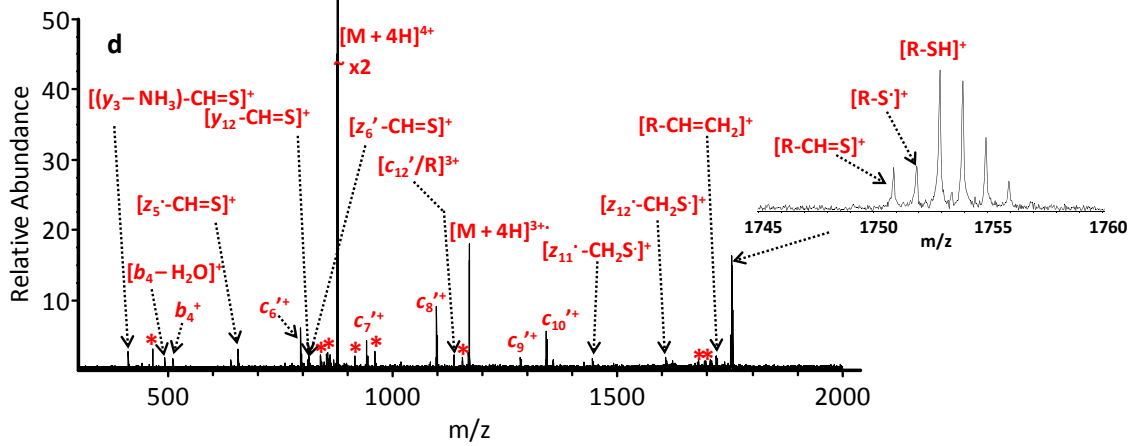
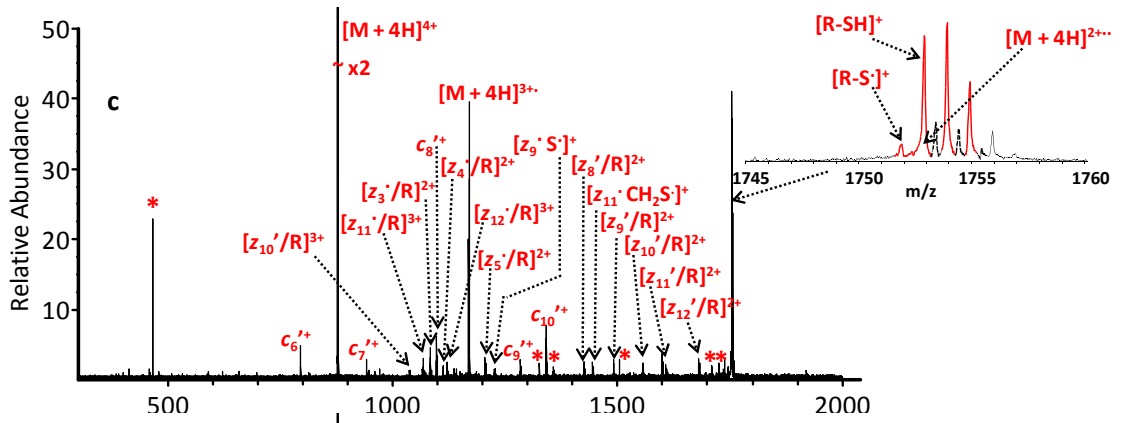
Panels a, c, e, and g in Figure 3.1 show ECD spectra of MSH-TCC, BN-TCC, $\alpha 1\text{TCC}\beta 1$, and $\alpha 2\text{TCC}\beta 2$, respectively. The corresponding AI-ECD spectra are displayed in panels b, d, f, and h, respectively. For triply protonated BN-TCC, very limited fragmentation was seen in both ECD and AI-ECD, consistent with the high m/z value of the precursor ion [27]. In both spectra, an abundant product ion peak is observed at m/z 1680. Zoomed-in views of this peak (insets in Figures 1a and b) show that, in ECD it corresponds to the charge-reduced form of the triply protonated BN-TCC precursor ion whereas, in AI-ECD, it corresponds to a mixture of the charge reduced species ($[M + 3H]^{2+}$) and singly charged products from disulfide cleavage (a mixture of R-S• and R-SH, see Scheme 1 for nomenclature). The occurrence of disulfide cleavage products in AI-ECD indicates that such cleavage occurs in ECD but cannot be detected because noncovalent interactions between the two BN chains prevent product ions from separating [22, 28]. Low abundance product ions from BN backbone cleavage are seen in both ECD and AI-ECD. However, the appearance of only one additional product ion in AI-ECD indicates that S-S bond cleavage is a preferred fragmentation pathway.

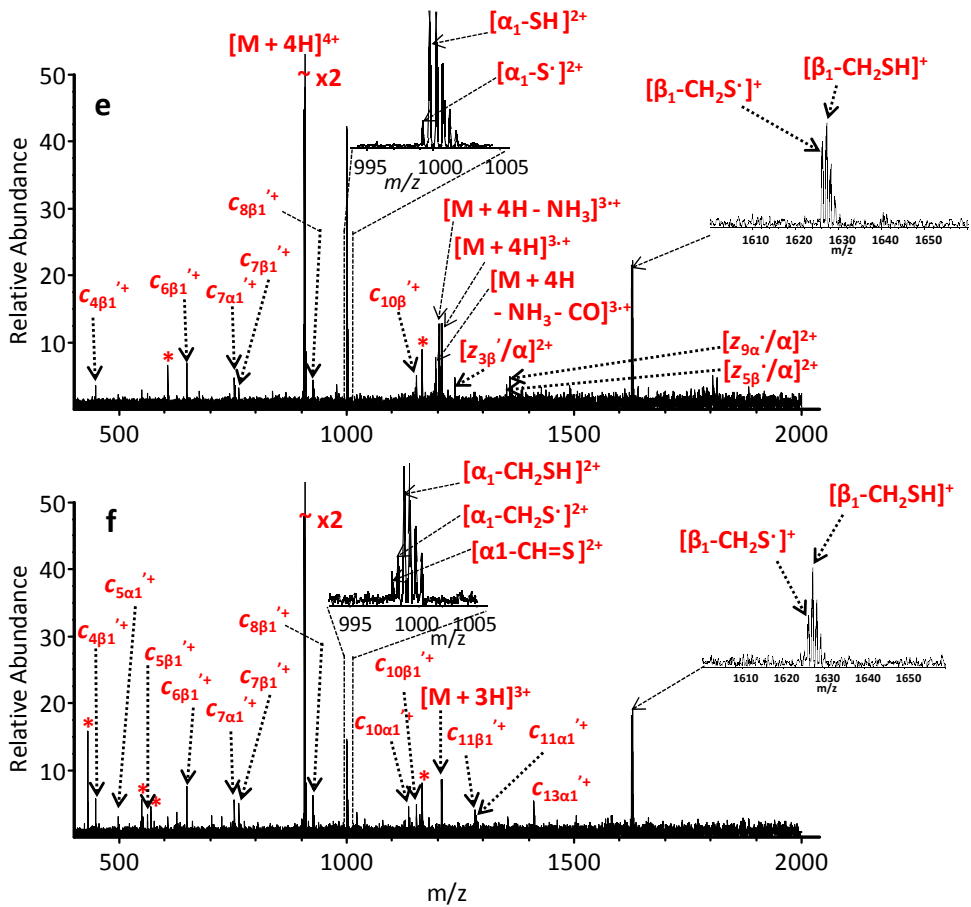
ECD and AI-ECD spectra of quadruply protonated MSH-TCC (Figure 3.1, panels c and d) are clearly different from those of BN-TCC in spite of the similarity in primary structure, including blocked N-termini as well as the number of basic residues. In ECD of MSH-TCC, prominent S-S bond cleavage as well as extensive backbone fragmentation is observed. The insets in Figures 3.1c and d show zoomed-in views of the region around

m/z 1750-1756, clearly demonstrating singly charged ions (highlighted with solid lines) resulting from S-S bond cleavages. Low abundance doubly charge reduced MSH-TCC ($[M + 4H]^{2+}$) is also present in the ECD spectrum (shown by dashed lines). Most backbone fragments in the MSH-TCC ECD spectrum are z -type ions, including $z_3 - z_5$ and $z_8 - z_{12}$, with the TCC moiety and another intact MSH chain. Among those, $z_3 - z_5$ are radical ions whereas $z_8 - z_{12}$ are even-electron species from hydrogen migration [29]. No c' -type ions (also from H rearrangement) were observed. The greatly enhanced ECD fragmentation for MSH-TCC compared to BN-TCC may be explained by the higher charge state, resulting in a lower precursor ion m/z value [27]. Three significant differences were observed between ECD and AI-ECD of MSH-TCC. First, the peak abundance corresponding to S-S bond cleavage (around m/z 1750-1755 as shown in the inset) was lower in AI-ECD compared to ECD alone, suggesting that disulfide bond cleavage is a primary fragmentation pathway subject to secondary fragmentation when the precursor ion is unfolded. Second, the doubly charge reduced $[M + 4H]^{2+}$ species was absent in AI-ECD, indicating that this species from ECD has been subject to covalent bond cleavage but that complementary fragments are held together through noncovalent interactions that are disrupted by the pre-IR irradiation. Several low m/z fragments, including $(y_3^+ - NH_3)-CH=S$, $y_{12}^+ - CH=S$, $z_5^+ - CH=S$, and $b_4^+ / b_4^+ - H_2O$, absent in ECD, appeared in AI-ECD of MSH-TCC. Other peaks unique to AI-ECD include a c_{12}' ion with TCC and another MSH peptide chain as well as a low abundance peak corresponding to C-S bond cleavage. Third, z_3-z_5/R and z_8-z_{12}/R product ion series detected following ECD were not observed in AI-ECD, presumably due to secondary fragmentation.

S-S bond cleavage represents the dominant product ion peaks in both ECD and AI-ECD of $\alpha_1\text{TCC}\beta_1$ and $\alpha_2\text{TCC}\beta_2$ (Figure 3.1, panels e-h). Similar to MSH-TCC, differences were observed in product ion patterns between ECD and AI-ECD. First, neutral losses, including NH_3 and its subsequent CO loss, from the charge reduced, $[\text{M} + 4\text{H}]^{3+}$, species were observed in ECD of $\alpha_1\text{TCC}\beta_1$ and $\alpha_2\text{TCC}\beta_2$ (panels e and g, Figure 3.1) but were absent in the corresponding AI-ECD spectra. Neutral losses of small molecules from charge-reduced species frequently occurs in ECD [30-32] and loss of NH_3 and CO are considered to be specific for Ser/Thr and Asp/Glu, respectively [32] although the presence of these residues does not guarantee the observation of these neutral losses (for example, MSH-TCC studied here has two Ser and one Glu residue). Side chain losses are greatly enhanced in ECD of cyclic peptides compared to linear ones [33]. Thus, structural constraints do play a role in the appearance of neutral losses, which could explain why more unfolded peptides in AI-ECD do not yield these products. Second, backbone fragmentation of $\alpha_1\text{TCC}\beta_1$ and $\alpha_2\text{TCC}\beta_2$ was enhanced in AI-ECD compared to ECD in agreement with previous results [23].







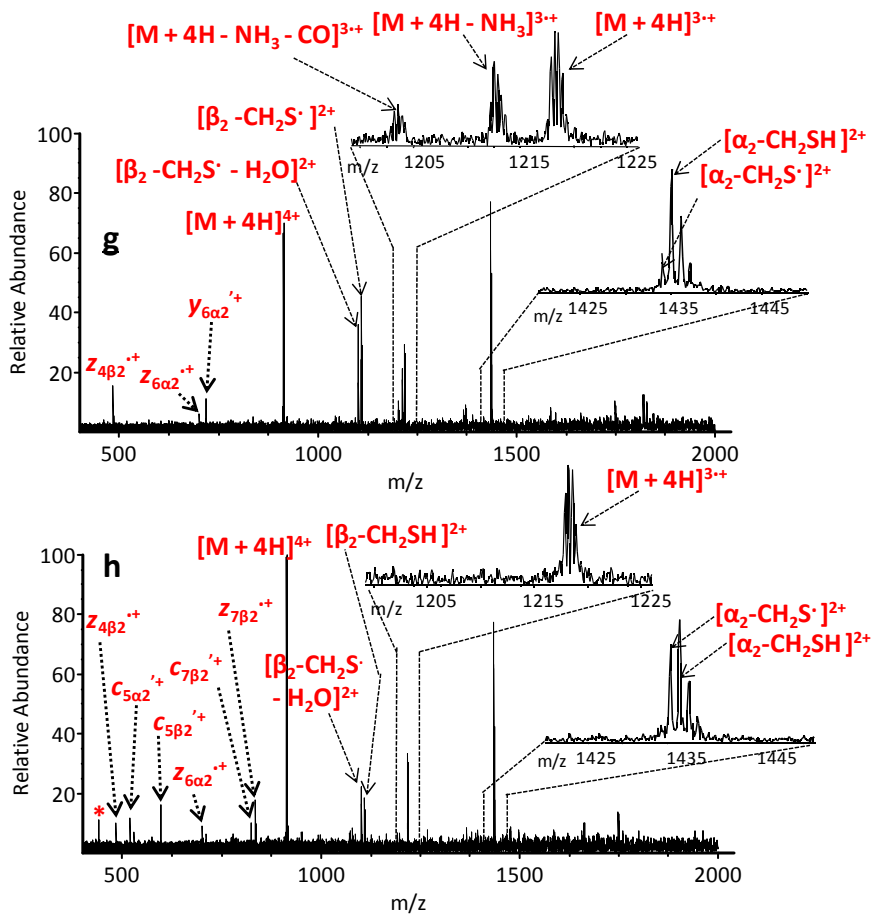


Figure 3.1 ECD and AI-ECD of TCC products from BN (panels a and b), MSH (panels c and d), and ubiquitin; α_1 TCC β_1 (panels e and f), and α_2 TCC β_2 (panels g and h). For BN, S-S bond cleavage was observed in AI-ECD (inset in panel b) but not in ECD alone (inset in panel a). * = unidentified peaks.

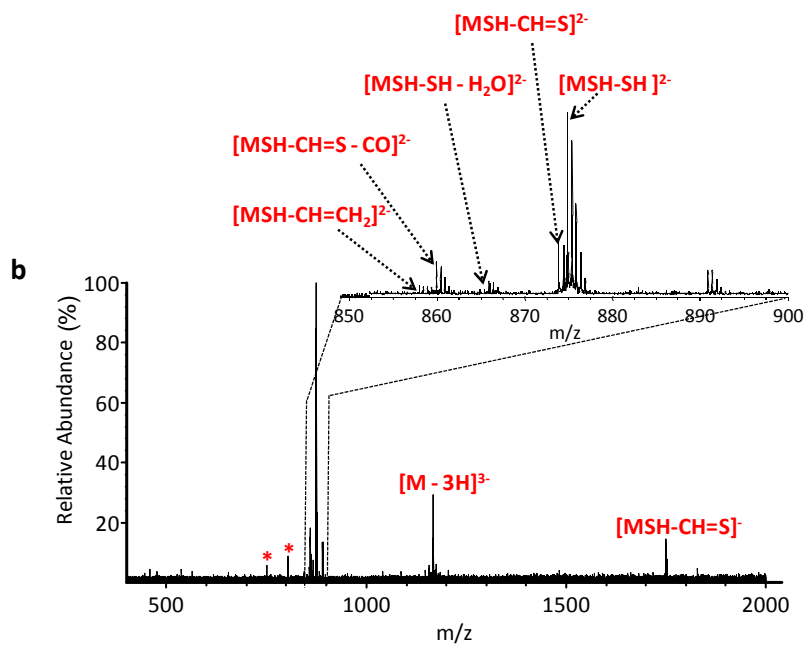
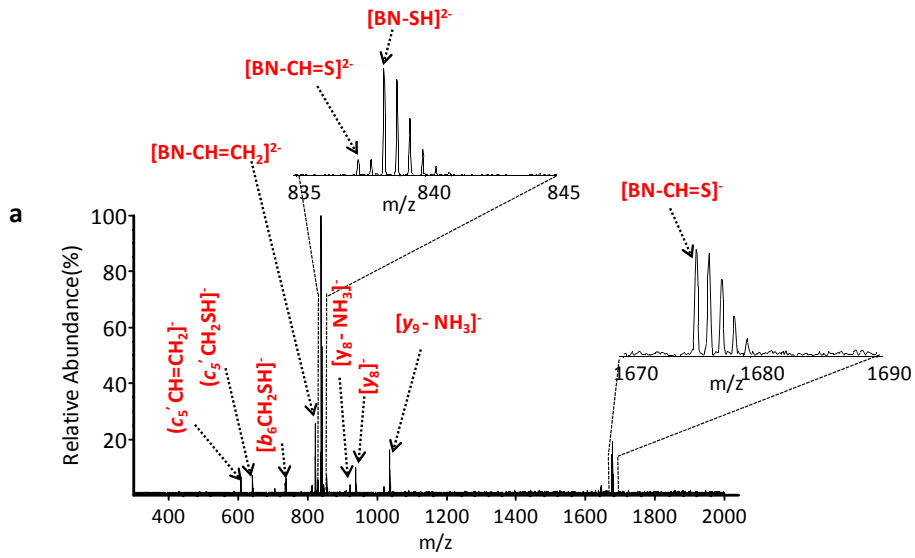
3.3.2 Negative ion CID of BN-TCC, MSH-TCC, α_1 TCC β_1 , and α_2 TCC β_2

Singly deprotonated peptides containing cysteine disulfide bonds have been shown to undergo significant C-S bond cleavage in negative ion CID, including abundant

neutral loss of H_2S_2 and $\text{H}_2\text{S}_2 + \text{CO}_2$ [34]. Preferential S-S and C-S bond cleavages were also reported in negative ion CID by McLuckey and co-workers [14] and similar behavior was observed by Kalli et al. in EDD [10] and negative ion IRMPD [10]. However, to our knowledge, negative ion CID of TCC products has not been explored. Negative ion CID spectra of BN-TCC, MSH-TCC, $\alpha_1\text{TCC}\beta_1$ and $\alpha_2\text{TCC}\beta_2$ are shown in Figures 3.2a to d. Triply deprotonated TCC products of MSH and BN yielded abundant even electron ions corresponding to S-S and C-S bond cleavages, in agreement with previous reports on negative ion IRMPD [10] and CID [14] of disulfide-containing peptides. The major fragmentation pathway corresponded to doubly deprotonated $\text{R-CH}_2\text{SH}$ ($\text{R} = \text{MSH}$ or BN) but R-CH=S and R-CH=CH_2 product ions were also observed. For disulfide-containing peptides, it has been reported that C-S bond cleavage is followed by backbone fragmentation to yield c and z -S type product ions [14]. In our experiments, c and z -S type ions were only observed for BN which showed c_5^- ion formation (c_5^- - CH=CH_2 and c_5^- - CH_2SH) and b_6 ion formation (b_6^- - CH_2SH). These product ions correspond to secondary fragmentation on the C-terminal side of the cross-linked residue (Lys^3). One step BN backbone cleavages, including y_8^- and y_9^- ions, were also observed. Neutral loss of NH_3 was observed for the latter two product ions, presumably because amidated side chains are present in both fragments [35] (Gln^7 in the y_8 ion and $\text{Asn}^6 + \text{Gln}^7$ in the y_9 ion). For triply deprotonated MSH-TCC, neutral losses of water from $\text{MSH-CH}_2\text{SH}$ and CO from MSH-CH=S , were observed. Those losses can be rationalized by the presence of Glu^5 [35, 36] in the sequence.

Unlike the pronounced S-S bond cleavages and modest C-S bond cleavages observed for MSH-TCC and BN-TCC, only weak signals corresponding to S-S and C-S

bond cleavages were observed in negative ion CID of $\alpha_2\text{TCC}\beta_2$ and such fragments were completely absent for $\alpha_1\text{TCC}\beta_1$ (Figure 3.2, panels c and d). Instead, a plentitude of neutral loss peaks, including H_2O , NH_3 , and CH_3CHO losses from precursor ions were observed. These neutral losses can be rationalized due to the presence of Glu and Asp (for water loss), Gln and Asn (for ammonia loss), and Thr (for CH_3CHO loss) [14]



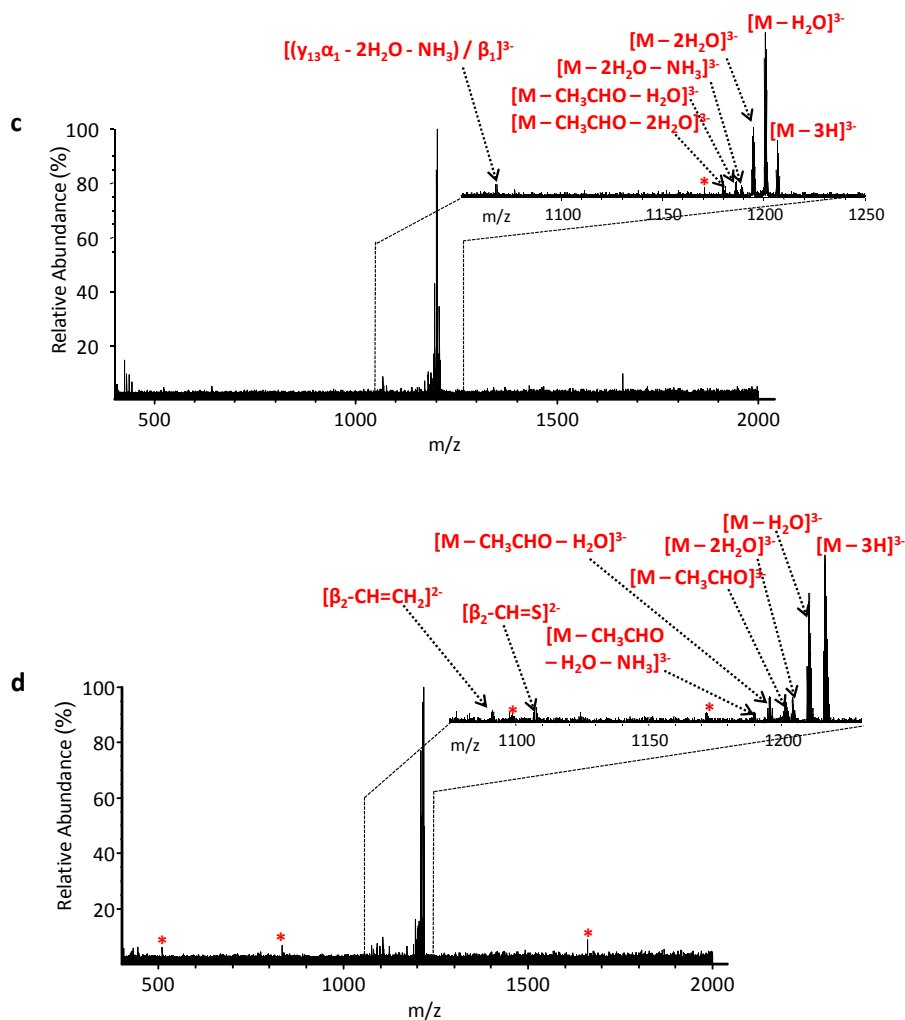


Figure 3.2 . Negative ion CID of TCC products from BN (panel a), MSH (panel b), and ubiquitin; α_1 TCC β_1 (panel c) and α_2 TCC β_2 (panel d). Abundant peaks corresponding to S-S and C-S bond cleavages are observed for BN and MSH but such cleavage is absent for α_1 TCC β_1 . For α_2 TCC β_2 , S-S and C-S bond cleavage is observed but at low abundance. * = unidentified peaks.

3.3.3 EDD of BN-TCC and MSH-TCC

Similar to ECD for positively charged ions, EDD is a radical-driven fragmentation technique but for negative ions [37]. EDD provides more random peptide

backbone cleavages than negative ion CID [38] and retains PTMs [39] as well as higher order structure [40]. EDD typically cleaves C α -C and N-C α backbone bonds in peptides, generating *x/a'* and *c/z'* ions, respectively. *y*-type ions are also observed in EDD [41]. EDD of disulfide-containing peptides demonstrated preferential cleavage of S-S and C-S bonds as well as abundant tryptophan side chain loss [10]. EDD spectra of triply deprotonated MSH-TCC and BN-TCC are shown in Figure 3.3. Unlike their corresponding negative ion CID spectra, fragments corresponding to S-S and C-S bond cleavages are observable but are not dominant. In EDD of BN-TCC, z_6^- is the most abundant product ion with the exception of the charge reduced species, $[M - 3H]^{2-}$. Close inspection of the isotopic cluster of the charge reduced species (see inset) reveals that a mixture of $[M - 3H]^{2-}$ and BN-C=S, with the latter corresponding to S-S bond cleavage, is present. Low abundance contributions from BN-S \cdot and BN-SH can also be assigned.

In EDD of MSH-TCC (Figure 3.3, panel b), doubly deprotonated product ions corresponding to S-S bond cleavage are observed around *m/z* 900 and analogous singly deprotonated ions are observed around *m/z* 1780 (see inset). Product ions resulting from C-S bond cleavage are also observed around *m/z* 1720 as is combined S-S and backbone bond cleavage (to yield z_{11}^- -S \cdot). In addition, backbone product ions from cleavages between Ser¹, Tyr², and Ser³ are seen in the form of $y_{12}^- - H_2O$, y_{11}^- , and $y_{11}^- - NH_3$. However, the dominant EDD product is charge reduction without fragmentation.

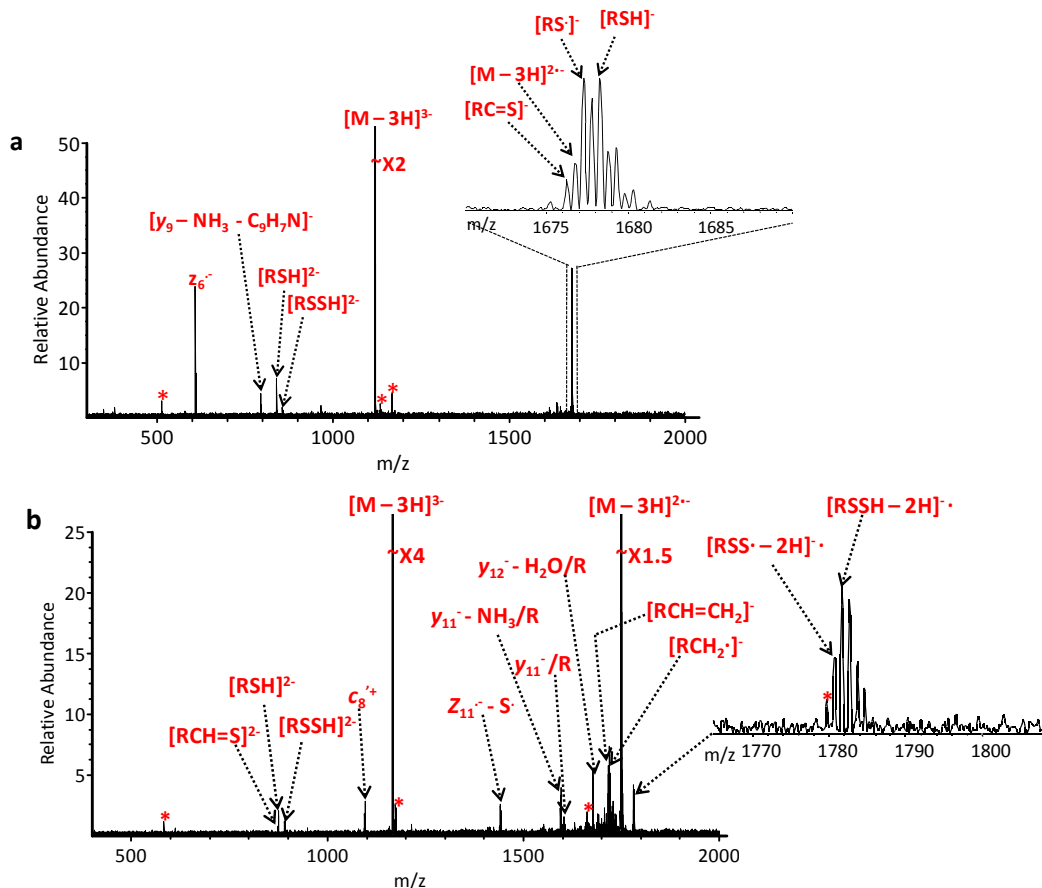


Figure 3.3 EDD of TCC products from BN (panel a) and MSH (panel b). S-S and C-S bond cleavages are observed, along with backbone fragments, including y -, z -, and c -type ions. However, the fragmentation efficiency is low. In EDD of BN-TCC, a y_9 ion with -17 Da (NH_3) and -129 Da mass shift is observed. The latter shift corresponds to neutral loss from the tryptophan side chain, as previously reported [10]. * = unidentified peaks.

3.3.4 MALDI TOF/TOF CID of BN-TCC, MSH-TCC, $\alpha_1\text{TCC}\beta_1$, and $\alpha_2\text{TCC}\beta_2$.

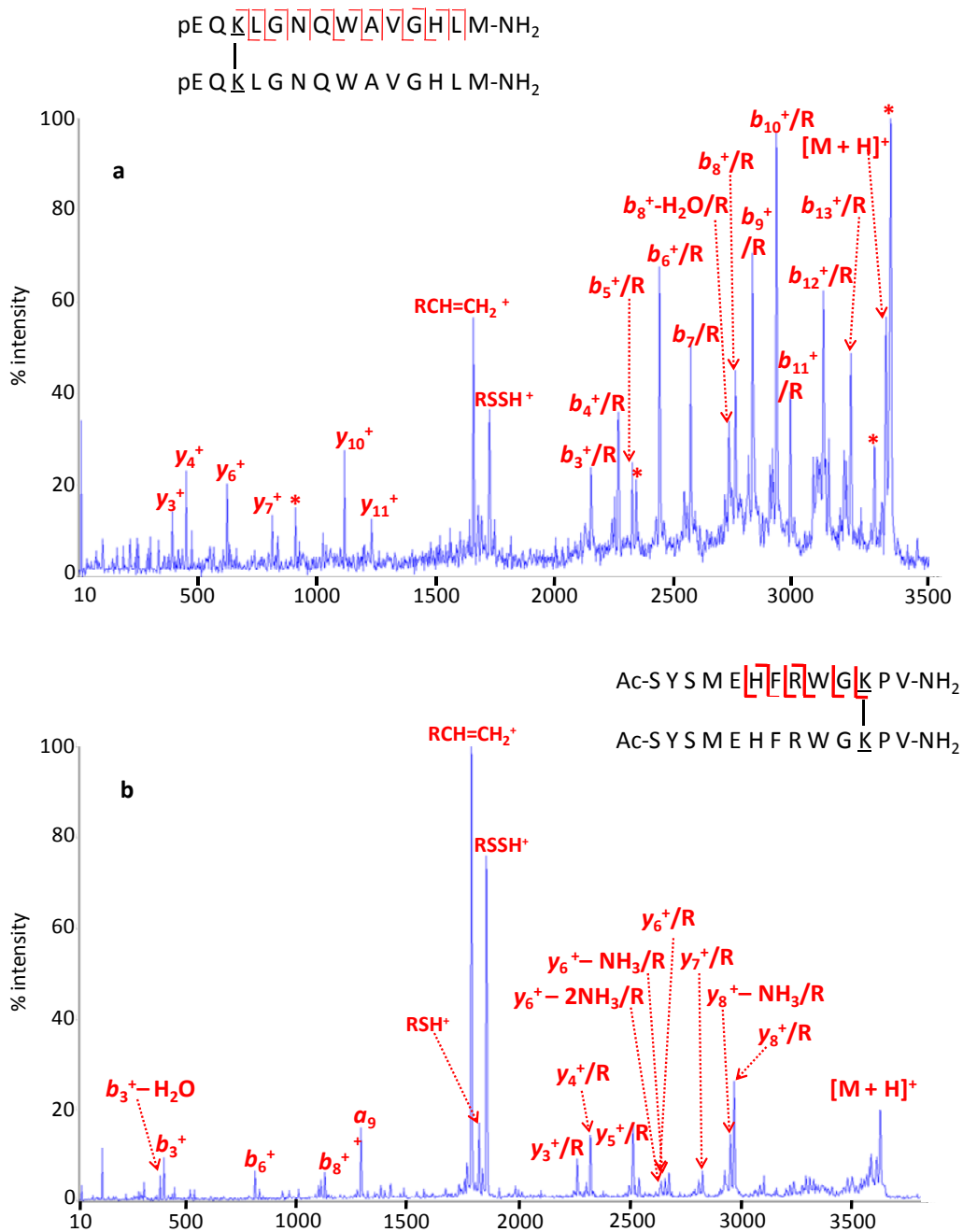
Figure 3.4 shows MALDI TOF/TOF CID of BN-TCC, MSH-TCC, $\alpha_1\text{TCC}\beta_1$, and $\alpha_2\text{TCC}\beta_2$. In agreement with previous observations by King et al.[5], all spectra demonstrate asymmetric C-S bond cleavages, leading to the formation of doublet peaks

differing by 66 Da. Symmetric S-S bond cleavages of low abundance were only observed for MSH-TCC and α_1 TCC β_1 . Unlike the dominant doublet peaks from C-S bond cleavage shown in previous work [5], we observed a variation of signal intensities for the 66 Da doublets.

For MSH-TCC, the 66 Da doublets were the dominant product ions. Low abundance backbone cleavages along with some further neutral NH₃ loss were observed. For BN-TCC, 66 Da doublets were observed but of lower abundance than a series of backbone cleavages. As shown in Figure 3.1a and b, S-S and C-S bond cleavages in ECD of BN-TCC were not observed unless IR irradiation was applied prior to ECD. In MALDI TOF/TOF CID, pre-activation is not required for observation of C-S bond cleavage but backbone cleavages appear more favorable. For α_1 TCC β_1 , C-S bond cleavage resulted in a 66 Da doublet with the α_1 peptide constituting the most abundant peak whereas that from β_1 had a 75% lower abundance. This observation may be due to the more extensive backbone fragmentation of β_1 compared to α_1 . A similar trend was observed in the TOF/TOF CID spectrum of α_2 TCC β_2 in which α_2 yielded an abundant b_{10} product ion and had lower abundance in the C-S bond cleavage doublet. Five backbone cleavages also occurred on β_2 but they are of rather low abundances. The most abundant product ion peak for α_2 TCC β_2 , which is accompanied by subsequent water loss, cannot be unambiguously identified because it represents loss of a C-terminal Arg residue, which is possible for both α_2 and β_2 to yield either $b_{11\alpha}$ or $b_{17\beta}$.

Based on the MALDI TOF/TOF CID spectra of TCC products from BN, MSH, α_1 TCC β_1 , and α_2 TCC β_2 , it may be concluded that backbone fragmentation and C-S bond cleavage are two competing fragmentation channels where favoring of one channel

suppresses the other. Such behavior was not observed in ECD, e.g., no S-S or C-S bond cleavage was observed for BN-TCC without IR irradiation but backbone cleavages were also insignificant. However, it should be noticed that MALDI TOF/TOF CID requires much less precursor signal abundance than ECD or EDD.



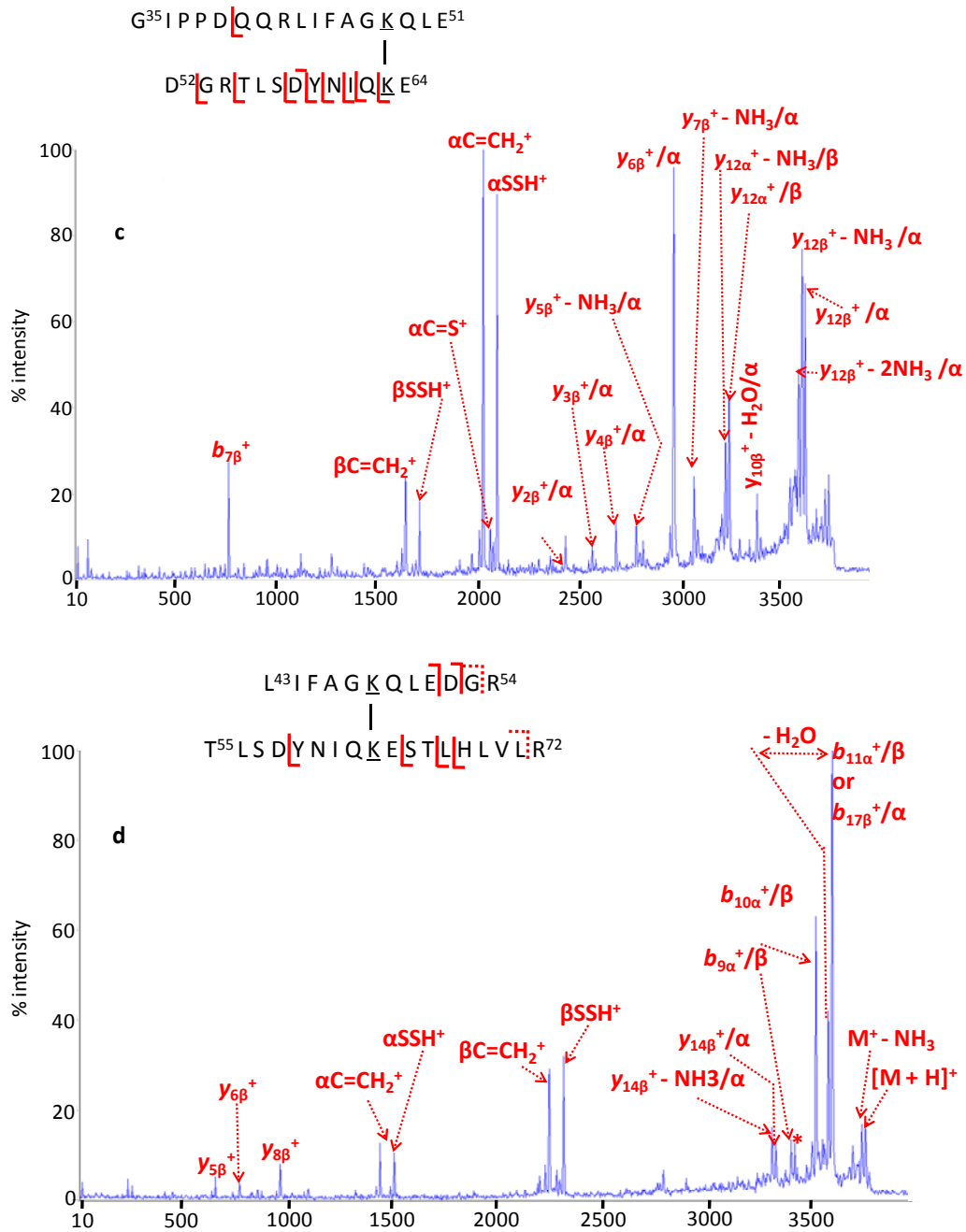


Figure 3.4 MALDI TOF/TOF CID of TCC products from BN (panel a), MSH (panel b), and ubiquitin; α_1 TCC β_1 (panel c) and α_2 TCC β_2 (panel d). Abundant 66 Da doublets resulting from C-S bond cleavages are observed in all cases, along with significant backbone fragmentation. * = unidentified peaks.

3.4 Summary

Based on the presented comparison between ECD, AI-ECD, negative ion CID, EDD, and MALDI TOF/TOF CID for effective and preferential cleavage of S-S and C-S bonds in peptides intramolecularly cross-linked with TCCs, ECD appears to be the superior approach, except for BN-TCC in which IR pre-irradiation, i.e., AI-ECD, was required. Negative ion CID, which yields preferred S-S and C-S bond cleavages for disulfide-containing peptides, did not provide consistent results for S-S and C-S bond cleavages in peptides cross-linked by TCCs. EDD provided S-S and C-S bond cleavages but with low efficiency. Finally, MALDI TOF/TOF CID results in C-S bond cleavage to form a 66 Da doublet without requiring as abundant precursor ions as ECD or EDD. However, backbone fragmentation of ICPs can be more pronounced than C-S bond cleavage, rendering the identification of cross-linked peptides less straightforward. Therefore, we conclude that ECD is a valuable complementary tool to MALDI TOF/TOF CID for identification of ICPs.

3.5 References

1. Bennett, K.L.; Kussmann, M.; Bjork, P.; Godzwon, M.; Mikkelsen, M.; Sorensen, P.; Roepstorff, P., Chemical cross-linking with thiol-cleavable reagents combined with differential mass spectrometric peptide mapping - A novel approach to assess intermolecular protein contacts. *Protein Sci.*, **2000**, *9*, 1503-1518.
2. Davidson, W.S.; Hilliard, G.M., The spatial organization of apolipoprotein A-I on the edge of discoidal high density lipoprotein particles - A mass spectrometry study. *J. Biol. Chem.*, **2003**, *278*, 27199-27207.
3. Peterson, J.J.; Young, M.M.; Takemoto, L.J., Probing alpha-crystallin structure using chemical cross-linkers and mass spectrometry. *Mol. Vision*, **2004**, *10*, 857-866.

4. Gorman, J.J.; Wallis, T.P.; Pitt, J.J., Protein disulfide bond determination by mass spectrometry. *Mass Spectrom. Rev.*, **2002**, *21*, 183-216.
5. King, G.J.; Jones, A.; Kobe, B.; Huber, T.; Movavadov, D.; Hume, D.L.; Ross, I.L., Identification of disulfide-containing chemical cross links in proteins using MALDI-TOF/TOF-mass spectrometry. *Anal. Chem.*, **2008**, *80*, 5036-5043.
6. Bean, M.F.; Carr, S.A., Characterization of Disulfide Bond Position in Proteins and Sequence-Analysis of Cystine-Bridged Peptides by Tandem Mass-Spectrometry. *Anal. Bioanal. Chem.*, **1992**, *201*, 216-226.
7. Zubarev, R.A.; Kruger, N.A.; Fridriksson, E.K.; Lewis, M.A.; Horn, D.M.; Carpenter, B.K.; McLafferty, F.W., Electron capture dissociation of gaseous multiply-charged proteins is favored at disulfide bonds and other sites of high hydrogen atom affinity. *J. Am. Chem. Soc.*, **1999**, *121*, 2857-2862.
8. Gunawardena, H.P.; Gorenstein, L.; Erickson, D.E.; Xia, Y.; McLuckey, S.A., Electron transfer dissociation of multiply protonated and fixed charge disulfide linked polypeptides. *Int. J. Mass Spectrom.*, **2007**, *265*, 130-138.
9. Chrisman, P.A.; Pitteri, S.J.; Hogan, J.M.; McLuckey, S.A., SO₂- electron transfer ion/ion reactions with disulfide linked polypeptide ions. *J. Am. Soc. Mass Spectrom.*, **2005**, *16*, 1020-1030.
10. Kalli, A.; Hakansson, K., Preferential cleavage of S-S and C-S bonds in electron detachment dissociation and infrared multiphoton dissociation of disulfide-linked peptide anions. *Int. J. Mass Spectrom.*, **2007**, *263*, 71-81.
11. Fung, Y.M.E.; Kjeldsen, F.; Silivra, O.A.; Chan, T.W.D.; Zubarev, R.A., Facile disulfide bond cleavage in gaseous peptide and protein cations by ultraviolet photodissociation at 157 nm. *Angew. Chem. Int. Ed.*, **2005**, *44*, 6399-6403.
12. Jones, M.D.; Patterson, S.D.; Lu, H.S., Determination of disulfide bonds in highly bridged disulfide-linked peptides by matrix-assisted laser desorption/ionization mass spectrometry with postsource decay. *Anal. Chem.*, **1998**, *70*, 136-143.
13. Kocher, T.; Engstrom, A.; Zubarev, R.A., Fragmentation of peptides in MALDI in-source decay mediated by hydrogen radicals. *Anal. Chem.*, **2005**, *77*, 172-177.
14. Chrisman, P.A.; McLuckey, S.A., Dissociations of disulfide-linked gaseous polypeptide/protein anions: Ion chemistry with implications for protein identification and characterization. *J. Proteome Res.*, **2002**, *1*, 549-557.
15. Sawicka, A.; Skurski, P.; Hudgins, R.R.; Simons, J., Model calculations relevant to disulfide bond cleavage via electron capture influenced by positively charged groups. *J. Phys. Chem. B*, **2003**, *107*, 13505-13511.
16. Sobczyk, M.; Neff, D.; Simons, J., Theoretical study of through-space and through-bond electron transfer within positively charged peptides in the gas phase. *Int. J. Mass Spectrom.*, **2008**, *269*, 149-164.
17. Wells, J.M.; Stephenson, J.L.; McLuckey, S.A., Charge dependence of protonated insulin decompositions. *Int. J. Mass Spectrom.*, **2000**, *203*, A1-A9.
18. Kim, H.I.; Beauchamp, J.L., Identifying the presence of a disulfide linkage in peptides by the selective elimination of hydrogen disulfide from collisionally activated alkali and alkaline earth metal complexes. *J. Am. Chem. Soc.*, **2008**, *130*, 1245-1257.
19. Mihalca, R.; van der Burgt, Y.E.M.; Heck, A.J.R.; Heeren, R.M.A., Disulfide bond cleavages observed in SORI-CID of three nonapeptides complexed with

- divalent transition-metal cations. *J. Mass Spectrom.*, **2007**, *42*, 450-458.
20. Shaw, C.F., Gold-based therapeutic agents. *Chem. Rev.*, **1999**, *99*, 2589-2600.
 21. Gunawardena, H.P.; O'Hair, R.A.J.; McLuckey, S.A., Selective disulfide bond cleavage in gold(I) cationized polypeptide ions formed via gas-phase ion/ion cation switching. *J. Proteome Res.*, **2006**, *5*, 2087-2092.
 22. Horn, D.M.; Ge, Y.; McLafferty, F.W., Activated ion electron capture dissociation for mass spectral sequencing of larger (42 kDa) proteins. *Anal. Chem.*, **2000**, *72*, 4778-4784.
 23. Lin, C.; Cournoyer, J.J.; O'Connor, P.B., Probing the gas-phase folding kinetics of peptide ions by IR activated DR-ECD. *J. Am. Soc. Mass Spectrom.*, **2008**, *19*, 780-789.
 24. Schilling, B.; Row, R.H.; Gibson, B.W.; Guo, X.; Young, M.M., MS2Assign, automated assignment and nomenclature of tandem mass spectra of chemically crosslinked peptides. *J. Am. Soc. Mass Spectrom.*, **2003**, *14*, 834-850.
 25. Senko, M.W.; Canterbury, J.D.; Guan, S.H.; Marshall, A.G., A high-performance modular data system for Fourier transform ion cyclotron resonance mass spectrometry. *Rapid Commun. Mass Spectrom.*, **1996**, *10*, 1839-1844.
 26. Ledford, E.B., Jr.; Rempel, D.L.; Gross, M.L., Space charge effects in Fourier transform mass spectrometry. Mass calibration. *Anal. Chem.*, **1984**, *56*, 2744-2748.
 27. Kalli, A.; Hakansson, K., Comparison of the electron capture dissociation fragmentation behavior of doubly and triply protonated peptides from trypsin, Glu-C, and chymotrypsin digestion. *J. Proteome Res.*, **2008**, *7*, 2834-2844.
 28. Zubarev, R.A.; Horn, D.M.; Fridriksson, E.K.; Kelleher, N.L.; Kruger, N.A.; Lewis, M.A.; Carpenter, B.K.; McLafferty, F.W., Electron capture dissociation for structural characterization of multiply charged protein cations. *Anal. Chem.*, **2000**, *72*, 563-573.
 29. O'Connor, P.B.; Lin, C.; Cournoyer, J.J.; Pittman, J.L.; Belyayev, M.; Budnik, B.A., Long-lived electron capture dissociation product ions experience radical migration via hydrogen abstraction. *J. Am. Soc. Mass Spectrom.*, **2006**, *17*, 576-585.
 30. Cooper, H.J.; Hudgins, R.R.; Hakansson, K.; Marshall, A.G., Characterization of amino acid side chain losses in electron capture dissociation. *J. Am. Soc. Mass Spectrom.*, **2002**, *13*, 241-249.
 31. Zubarev, R.A.; Kelleher, N.L.; McLafferty, F.W., Electron capture dissociation of multiply charged protein cations. A nonergodic process. *J. Am. Chem. Soc.*, **1998**, *120*, 3265-3266.
 32. Falth, M.; Savitski, M.M.; Nielsen, M.L.; Kjeldsen, F.; Andren, P.E.; Zubarev, R.A., Analytical Utility of Small Neutral Losses from Reduced Species in Electron Capture Dissociation Studied Using SwedECD Database. *Anal. Chem.*, **2008**, *80*, 8089-8094.
 33. Leymarie, N.; Costello, C.E.; O'Connor, P.B., Electron capture dissociation initiates a free radical reaction cascade. *J. Am. Chem. Soc.*, **2003**, *125*, 8949-8958.
 34. Bilusich, D.; Maselli, V.M.; Brinkworth, C.S.; Sanguina, T.; Lebedev, A.T.; Bowie, J.H., Direct identification of intramolecular disulfide links in peptides using negative ion electrospray mass spectra of underivatized peptides. A joint experimental and theoretical study. *Rapid Commun. Mass Spectrom.*, **2005**, *19*,

- 3063-3074.
35. Bilusich, D.;Bowie, J.H., Fragmentations of (M-H)(-) Anions of Underivatised Peptides. Part 2: Characteristic Cleavages of Ser and Cys and of Disulfides and Other Post-Translational Modifications, Together with Some Unusual Internal Processes. *Mass Spectrom. Rev.*, **2009**, *28*, 20-34.
 36. Harrison, A.G., Fragmentation reactions of protonated peptides containing glutamine or glutamic acid. *J. Mass Spectrom.*, **2003**, *38*, 174-187.
 37. Budnik, B.A.; Haselmann, K.F.; Zubarev, R.A., Electron detachment dissociation of peptide di-anions: an electron-hole recombination phenomenon. *Chem. Phys. Lett.*, **2001**, *342*, 299-302.
 38. Haselmann, K.F.; Budnik, B.A.; Kjeldsen, F.; Nielsen, M.L.; Olsen, J.V.; Zubarev, R.A., Electronic excitation gives informative fragmentation of polypeptide cations and anions. *Eur. J. Mass Spectrom.*, **2002**, *8*, 117-121.
 39. Kjeldsen, F.; Silivra, O.A.; Ivonin, I.A.; Haselmann, K.F.; Gorshkov, M.; Zubarev, R.A., C-alpha-C backbone fragmentation dominates in electron detachment dissociation of gas-phase polypeptide polyanions. *Chem. Eur. J.*, **2005**, *11*, 1803-1812.
 40. Mo, J.J.;Hakansson, K., Characterization of nucleic acid higher order structure by high-resolution tandem mass spectrometry. *Anal. Bioanal. Chem*, **2006**, *386*, 675-681.
 41. Anusiewicz, I.; Jasionowski, M.; Skurski, P.; Simons, J., Backbone and side-chain cleavages in electron detachment dissociation (EDD). *J. Phys. Chem. A*, **2005**, *109*, 11332-11337.

Chapter 4

Selective C-I Bond Cleavage in ECD: Prospects for Designing a Novel Chemical Cross-linker and Mechanistic Implications

4.1 Introduction

In the current post-genomic era, the next challenge is to reveal the structure of numerous unknown proteins that are encoded in the vast genome data and understand their biological function and interaction networks. Three classic techniques, X-ray crystallography, nuclear magnetic resonance (NMR) spectroscopy, and electron microscopy (EM) have been applied to reveal protein structure in crystal form (X-ray and EM) or in solution (NMR). Although tremendous achievements have been made, bottlenecks of these techniques exist: they are time-consuming, sometimes require sample amounts up to gram level, and have stringent requirements for sample purity. An alternative approach is to apply chemical cross-linking combined with proteolytic digestion and mass spectrometry (3C-PD-MS) to characterize protein structure and function. This approach provides information about protein-protein interactions [1-6], distance constraints for protein residue pairs, solvent exposure of specific amino acids, and binding sites in protein complexes [7-11]. The main idea behind 3C-PD-MS is to link amino acid pairs covalently and therefore maintain distance constraints for

subsequent analysis. Because identification of cross-linked products relies on mass spectrometric analysis, 3C-PD-MS is an attractive alternative to X-ray crystallography, NMR, and EM by demonstrating great sensitivity, high measurement accuracy, and more lenient requirements for sample purity and amount.

Despite the rather straightforward implementation of 3C-PD-MS, confident detection of cross-linked peptides remains challenging due to the difficulty of differentiating cross-linked peptide signals from unmodified peptides. In addition, signals for cross-linked peptides are often weak or even absent due to ion suppression from more abundant unmodified peptides. Furthermore, the diversity of cross-linked products, including intermolecular, intramolecular, or dead-end cross-linked peptides [12], may also render mass spectra highly complex.

Two main approaches have been established to enhance the detection of cross-linked peptides in MS. One approach is to design a cross-linker with specific enrichment potential [1, 2, 13-18] to isolate cross-linked peptides prior to MS analysis. The other approach involves differentiation of cross-linked peptides from unmodified peptides by designing a cross-linker that is cleavable in either solution (e.g., by a reducing reagent [19, 20]), or the gas phase. Solution-phase cleavage allows identification of cross-linked peptides from comparative analysis of spectra from cleaved and uncleaved samples whereas characteristic fragments from MS/MS, including collision-induced dissociation (CID) [21, 22], infrared multiphoton dissociation (IRMPD) [23], and MALDI TOF/TOF high-energy CID [24] allows direct identification of cross-linked peptides. Gas-phase cleavable cross-linkers may be more promising than solution-phase cleavage because this strategy does not require multiple rounds of MS analysis and comparison of complex

spectra. Therefore, the sample preparation time and required sample amount are reduced.

Since its inception [25], electron capture dissociation (ECD) has become a powerful MS/MS technique for characterizing proteins and peptides. In ECD, low energy electrons (<1 eV) are captured by multiply charged precursor cations, resulting in formation of radical species that undergo N-C_α backbone bond cleavages to generate even-electron *c*-type and radical *z*-type ions [25]. One of the most intriguing features of ECD is the preservation of post-translational modifications (PTMs) [26-30], which allows straightforward localization of PTMs. Many PTMs are highly labile in the gas phase and are preferentially lost in slow-heating MS/MS analysis, including CID and IRMPD. In addition, CID and IRMPD result in peptide backbone amide bond cleavage initiated by mobile protons [31] to yield *b*- and *y*-type product ions. Thus, ECD and CID provide complementary structural information about proteins and peptides of particular importance in peptide *de novo* sequencing [32]. Furthermore, ECD is an ideal MS/MS approach for generating preferential cleavage of disulfide (S-S) bonds [33] although S-S bond cleavage is also observed in other MS/MS approaches, including negative ion CID [34], negative ion IRMPD[35], electron detachment dissociation (EDD) [35], and high-energy CID [24, 36, 37]. Finally, ECD can be used to characterize protein interfaces due to retention of non-covalent interactions [38, 39]. However, to our knowledge, ECD has not yet been applied for differentiating cross-linked peptides from unmodified peptides with the exception of the experiments described in Chapter 3 of this thesis.

Divalent metal ions, including, e.g., Ca²⁺, Mg²⁺, and Co²⁺, have been used to generate multiply charged protein and peptide cations, either stand alone or combined with protonation sites, for ECD analysis. ECD of metal-adducted species may yield

unique fragmentation pathways compared to protonated analytes due to changes in electron capture behavior and gas-phase protein/peptide structure [40-42].

The exact mechanism of ECD is still not unraveled and continues to be under investigation. To date, there are two postulations: first, for peptide ECD [25, 33, 43], electrons are believed to be captured at protonated sites to cause neutralization and formation of a hypervalent radical center with subsequent energy release. A hot hydrogen atom ($H\bullet$) is ejected and can attach to an S-S bond (if present) or to backbone carbonyl groups. This hydrogen migration results in preferential cleavage of S-S bonds or non-selective cleavage of adjacent $N-C_\alpha$ backbone bonds, respectively. This mechanism is referred to as the hot hydrogen model. An alternative theory is the so-called superbase mechanism that was proposed by Turecek and co-workers [44] and by Simons and co-workers [45, 46]. In that theory, electrons are captured directly by backbone amide π^* orbitals to generate a group with high basicity (superbase). Protons are then abstracted from adjacent locations to yield charge neutralization and subsequent $N-C_\alpha$ bond cleavage. In the superbase model, protons do not have to originate from protonated basic sites. Therefore, it explains ECD of metal-adducted peptides. Simons et al. [45, 46] concluded from computational work that 90-99% of electrons are captured at positively charged sites and that 1-10% are directly attached to either S-S σ^* or amide π^* orbitals, assisted by Coulomb stabilization from adjacent positively charged groups. Such stabilization renders direct electron attachment exothermic. Recently, Simons' group proposed that electrons captured by positively charged groups can be released and transferred to S-S or $N-C_\alpha$ bonds for inducing subsequent dissociation [47, 48].

Electron transfer dissociation (ETD) [49] is believed to be analogous to ECD by

sharing a similar mechanism and generating *c*- and *z*-type ions. One favorable characteristic of ETD over ECD is its direct compatibility with radio-frequency based ion storage without needing a magnetic field to confine electrons [50]. Because the electron transfer process in ETD relies on electron donation from radical reagent anions, some factors that influence ECD and ETD dissociation, including cross sections for electron capture/transfer, recombination energies, and the time scales of the electron capture/transfer process, can be different [51]. For example, precursor ions absorb all electron energy in ECD but, in ETD, energy is partitioned between analyte ions and the remaining neutral reagent [48]. In addition, it has been reported that doubly protonated precursor ions yield less backbone fragmentation than their triply protonated counterparts in ECD [52]. In ETD, doubly protonated species generally generate limited fragmentation unless supplementary activation methods, including collisional activation and pre-IR irradiation, are applied [50, 51].

Protein iodination has been widely applied in crystallographic studies as a useful probe with high electron density [53], and as a radio-label for monitoring metabolic reactions, both *in vitro* and *in vivo* [54]. Recently, carbon iodine (C-I) bonds were reported to demonstrate preferential cleavage under 266 nm UV laser irradiation to yield a radical product with unique fragmentation in subsequent CID [55]. By contrast, little is known about carbon-halogen bond cleavage in ECD. Prominent carbon-bromide (C-Br) bond cleavage in ECD was reported by Marshall and co-workers in 2006 [56]. In that work, efficient C-Br cleavage was attributed to direct electron capture by the C-Br bond, or electron transfer from disulfide bonds, which may originally capture the electron. These authors also reported that disulfide bond reduction and alkylation, eliminated

bromide loss in ECD.

Here, a series of standard peptides were iodinated and subjected to CID, MALDI TOF/TOF high-energy CID, ECD, and ETD with the aim to explore the prospect of designing a novel cross-linker with C-I bond that could provide unique iodine loss (125.89 Da) in tandem MS (MS/MS).

4.2 Experimental

4.2.1 Sample Preparation and Iodination Reaction

Melanocyte stimulating hormone (MSH), Lys3-Bombesin (BE), and Arg-Arg-Gastrin Fragment 22-30 (AARF) were purchased from Sigma (St. Louis, MO) and used in without further purification. The sequences of these peptides are shown in Figure 4.1.

Melanocyte stimulating hormone (MSH): Ac-SYSMEHFRWGKPV-NH ₂
Lys3-Bombesin: pEQKLG NQWAVGHLM-NH ₂
Arg-Arg-Gastrin Fragment 22-30 (AARF): RRLEEEEEAYG

Figure 4.1. Sequences of peptides used in this study.

Peptide iodination was carried out according to previous reports [57]. Briefly, peptides were dissolved in 100 mM phosphate buffered saline (PBS), pH 7.2, to a final concentration of 1-3 mM. The peptide MSH was initially dissolved in PBS buffer followed by water (referred to as condition 1) and then water followed by PBS buffer

(condition 2). In both cases, PBS buffer and water was kept at a 1:1 volume ratio. 100 μL peptide solution was mixed with 50 μL of 75 mM NaI and 15 mM I_2 solution. This mixture was incubated at room temperature for ~ 30 minutes followed by addition of 15 μL TFA to quench the reaction and desalting by C_{18} spin column. Desalted samples were diluted to 5 μM for subsequent MS analysis.

Generation of peptide gas-phase calcium adducts depends on ESI spray solvent, amino-acid sequence, and pH value. In the present work, A 1 M calcium chloride (Sigma, St. Louis MO) stock solution was prepared in water (HPLC Grade, Fisher) and then added to iodinated peptide solutions to a final concentration of 30-100 μM .

4.2.2 Mass Spectrometry

CID (to identify the iodination site) and ECD (for iodine loss efficiency (ILE) calculations) were carried out with an actively shielded 7 Tesla Fourier transform ion cyclotron resonance (Q-FT-ICR) mass spectrometer (Apex-Q, Bruker Daltonics, Billerica, MA). Target analytes were directly infused into an ESI source (Apollo II, Bruker Daltonics) and electrosprayed in positive ion mode for CID and ECD analysis at a flow rate of 70 $\mu\text{L}/\text{h}$. A counterflow of hot (200-240 $^\circ\text{C}$) nitrogen gas was applied to assist desolvation of ESI droplets. Potential iodinated products, determined by accurate mass, were selected for MS/MS experiments. Precursor ions were accumulated in the first hexapole for 0.1 s, transferred through the mass-selective quadrupole (5-10 m/z isolation window), mass selectively accumulated in the second hexapole for up to 1-2 s, then ions were transferred through high-voltage ion optics, and captured in the ICR cell by dynamic trapping. An indirectly heated hollow dispenser cathode was used to generate

an electron beam. ECD was performed at a bias voltage of - 0.2-0.8 V and an irradiation time of 50-80 ms. Argon was used as collision gas for CID.

All Apex FT-ICR mass spectra were acquired with XMASS (version 6.1, Bruker Daltonics) using 512 K data points and summed over 10-66 scans. All data were then analyzed with MIDAS software [58]. For accurate mass determination, external calibration was performed with ES tuning mix (Hewlett Packard, Waldbronn, Germany) or by using the calculated masses of precursor ions and charge reduced precursor ions. All calibrations were based on frequency-to-m/z calibration with a two-term calibration equation [59].

For MALDI TOF/TOF analysis, 0.5 μ L of alpha cyano-4-hydroxycinnamic acid (CHCA) and 2,5-dihydroxybenzoic acid (DHB) mixture (each 10 mg/mL in 50% acetonitrile, 0.1% TFA) was hand-spotted to 0.5 μ L iodinated peptides onto a 192-well MALDI target and allowed to dry under atmosphere. MALDI mass spectra were acquired on an Applied Biosystems 4800 Proteomics Analyzer in reflector positive ion mode. Peptide masses were acquired up to 4,000 Da. Mass spectra were obtained with 2,000 laser (Nd-YAG laser operating at 355 nm and 200 Hz) shots. MS/MS spectra were also acquired in positive ion mode. Atmosphere, at a pressure of $\sim 6 \times 10^{-7}$ torr was used as collision gas with a collision energy of 2 keV. Data analysis was performed by MS-Expedite (version 3.0, <http://www.proteomecommons.org>).

For ECD and ETD comparison, data were obtained on a Bruker Solarix 7 Tesla Q-FT ICR mass spectrometer. Details of the ETD implementation have been previously reported [60]. Briefly, the ESI source is modified for coupling with negative ion chemical ionization (nCI) via a split octopole ion guide. Fluoranthene radical anions for

the ETD reaction are generated in an nCI source with methane as CI reagent, and transferred via the split octopole to a hexapole collision cell. ESI-generated triply- or doubly-protonated singly iodinated precursor ions also entered the hexapole for the ETD reaction. Ion accumulation and reaction time were set as 500 and 600 ms, respectively. After the ETD reaction, product ions are transferred to the ICR cell for further analysis. ECD of the same peptides was also performed with the SolariX instrument for comparison. All spectra were acquired with 256 K data points and summed over 66 scans. Data were analyzed with the DataAnalysis software (version 4.0, Bruker Daltonics). In all ECD and ETD experiments (on both the Apex and SolariX instruments), precursor ion depletion was controlled to be ~90% (by comparing precursor ion peak abundance following ECD/ETD with a control experiment in which no MS/MS was performed). ILE calculations were carried out based on equation 1. These calculations were performed by adding all peak abundances involving C-I bond cleavage and the resulting value was divided by the summed abundance of all identifiable ECD product ions. In addition, all peak abundances were normalized to their charge state prior to calculation. For ILE analysis, experiments were performed in triplicate to obtain the average and standard deviation.

$$\frac{\sum(\text{all iodine loss peaks})}{\sum(\text{all ECD fragments})} \times 100\%$$

Equation 1

4.3 Results and Discussion

4.3.1 Selective Iodination of His⁶ or Tyr² in MSH

Following iodination reactions under both condition I and condition II described above, unmodified, singly-, and doubly-iodinated MSH were observed (Figure 4.2). Singly iodinated MSH was selected for MS/MS analysis. Initially, we assumed that iodination would occur mainly on Tyr² because tyrosine is known to be the most reactive amino acid residue [55]. However, because two iodinations were observed, CID was performed to confirm the iodination site in singly iodinated MSH from condition I and condition II, respectively. Interestingly, CID spectra of singly iodinated MSH from condition I (Figure 4.3, panel A) and condition II (panel B) are different in appearance, indicating that different iodination sites were obtained following reaction condition I and II, respectively. The CID spectrum of singly iodinated MSH from condition I contains a series of *y* ions (*y*₆-*y*₁₂) in which *y*₆ and *y*₇ ions are unmodified whereas *y*₈-*y*₁₂ ions contain one iodine. These results lead us to conclude that His⁶, instead of Tyr², is the iodination site in singly iodinated MSH from condition I, although previous reports demonstrated that tyrosine iodination is much faster than that of histidine [61, 62]. Similarly, the CID spectrum of singly iodinated MSH from condition II contained unmodified *y*₆-*y*₁₁ ions but one iodine addition for *y*₁₂, indicating that iodination occurred on Tyr². In both cases, iodination on His⁶ and Tyr² is selective because all major fragment peaks can be attributed to one iodination state.

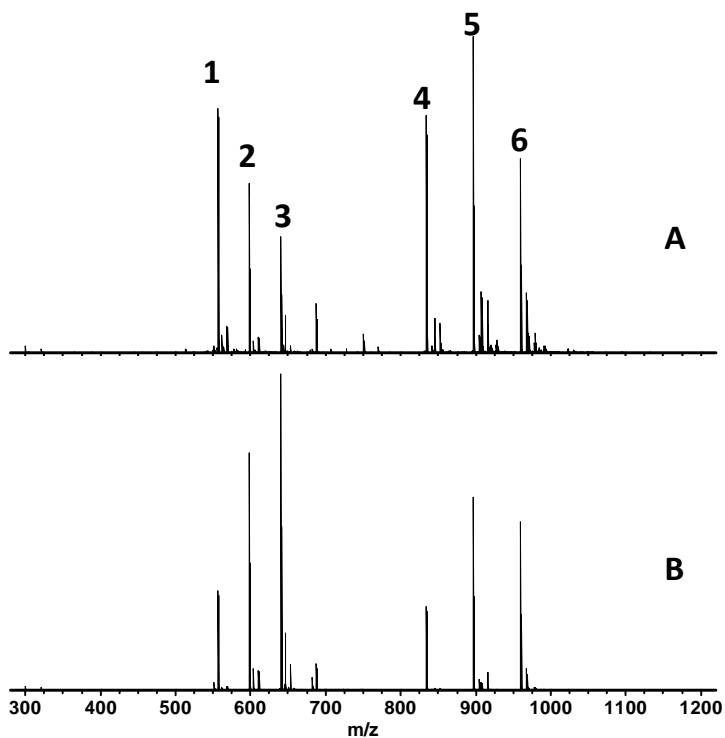


Figure 4.2. Positive ion mode ESI of MSH iodination product from condition I (panel A) and II (panel B). 1-3: triply protonated species; 4-6: doubly protonated species; 1,4: unmodified MSH; 2,5: singly iodinated MSH; 3,6: doubly iodinated MSH.

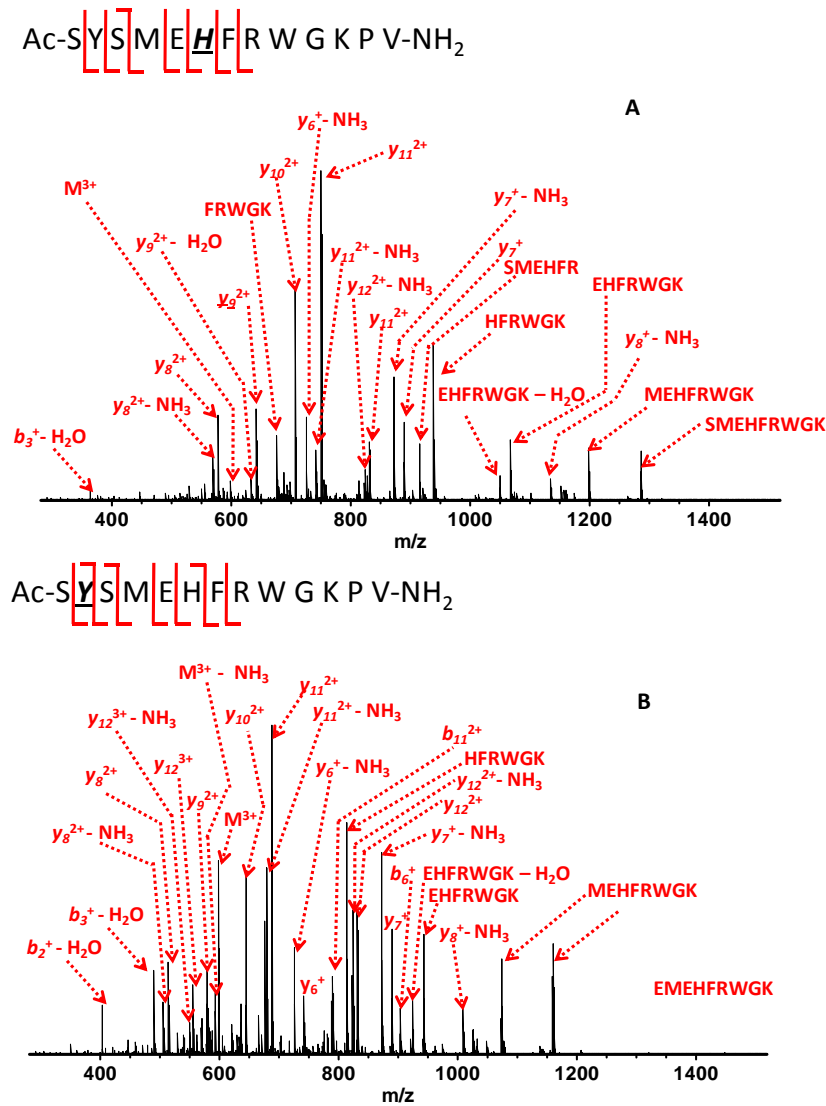


Figure 4.3. From the two different reaction conditions, PBS buffer followed by water (condition I) and the reverse order (condition II), His⁶ (panel A) and Tyr² (panel B) in MSH could be selectively iodinated, respectively, as verified by CID.

4.3.2 C-I Bond Cleavage Behavior in ECD of Doubly and Triply Protonated His⁶- and Tyr²-iodinated MSH

Once selective iodination of His⁶ and Tyr² in MSH had been identified, their triply protonated forms were subjected to ECD and the corresponding spectra are shown in Figure 4.4 (panel A for His⁶-iodinated MSH and panel B for Tyr²-iodinated MSH). Peaks resulting from C-I bond cleavage are observed in both spectra. However, the iodine loss peak for His⁶-iodinated MSH was much more abundant (than that for Tyr²-iodinated MSH, as shown in Figure 4.4 panel A and B. In order to make a fair comparison, quantitative analysis was carried out by calculating the ILEs according to Equation 1. The ILEs from ECD of triply protonated His⁶ and Tyr² iodinated MSH species are shown in Figure 4.5, panel A. A clear difference is observed: 29% for His⁶ iodination and ~8% for Tyr² iodination.

In order to explain the discrepancy in ILEs from triply protonated His⁶ and Tyr² iodinated MSH, we note that His⁶ is a potential protonation site, along with Arg⁸ and Lys¹¹ (the N-terminus of MSH is acetylated), in triply protonated MSH. If His⁶ is protonated, the C-I bond on the same residue will be very close (a few bonds) to a positively charged group. On the other hand, the C-I bond on Tyr² is four residues away from the closest protonation site (His⁶). ECD of doubly protonated singly iodinated MSH was also carried out. Figure 4.5, panel B shows ILEs of doubly protonated His⁶- and Tyr²-iodinated MSH from ECD. Unlike their triply protonated counterparts, ILE values for these two species are rather close: 22% for His⁶-iodinated MSH and 18% for Tyr² iodination. Based on the gas-phase basicity of amino acids, Arg⁸ >> Lys > His [63, 64], Arg⁸ is likely protonated in doubly protonated singly iodinated MSH. The second protonation

site is likely a mixture of His⁶ and Lys¹¹, thus the favorable (for C-I bond cleavage) proton location on His⁶ is less occupied than for the corresponding triply protonated species. In addition, previous reports demonstrated that ECD fragmentation is influenced by the gas-phase conformation of precursor ions [52]. Compared with doubly protonated species, triply protonated species should be more unfolded in the gas phase, prior to ECD, due to Coulomb repulsion, thereby lowering the probability that protonated residues (His⁶, Arg⁸, and Lys¹¹) are located spatially close to the C-I bond of Tyr². Thus, the ILE of Tyr²-iodinated MSH should be lower than that of His⁶-iodinated MSH, consistent with our observations. Doubly protonated species, on the other hand, are more likely to be folded in the gas phase, making it possible for positively charged groups to be located close to the C-I bond in either His⁶ or Tyr². Based on the superbase model for ECD, electron attachment to the C-I bond (and thus subsequent dissociation) is stabilized by adjacent positively charged groups. Thus, His⁶ and Tyr²-iodinated MSH may demonstrate similar ILE values, as observed.

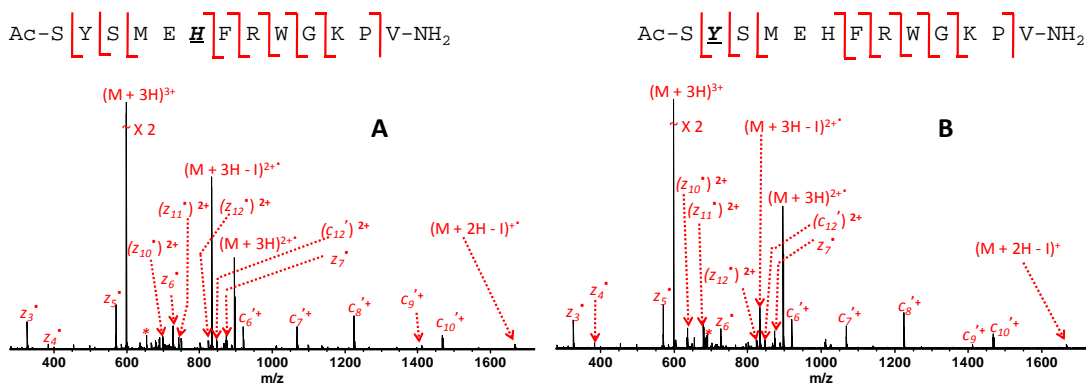


Figure 4.4. ECD of triply protonated His⁶-iodinated MSH (panel A) and Tyr²-iodinated

MSH (panel B). In panel A, the most abundant fragment corresponds to iodine loss. The ratio of this iodine loss peak to the charge reduced species is ~2:1. Here, His⁶ is a likely protonation site, thus positive charge is very close to the C-I bond. In panel B, the most abundant fragment still corresponds to iodine loss but is less abundant than for His⁶-iodinated MSH. The ratio of this iodine loss peak to the charge reduced species is ~1:3. Series of backbone product ions are also observed. In the case of Tyr²-iodinated MSH, the C-I bond is a few residues away from the closest likely positive site (His⁶).

4.3.3 ECD of Ca²⁺-adducted Histidine- and Tyrosine-Iodinated MSH

ECD of doubly charged Ca²⁺-adducted His⁶- and Tyr²-iodinated MSH was also carried out and their ILE values, ~32% for His⁶-iodinated MSH and ~35% for Tyr²-iodinated MSH, respectively, are shown in panel C of Figure 4.5. Based on the hypothesis above (and assuming that the Ca-peptide complex is not zwitterionic), the Ca²⁺ binding site would be crucial for C-I bond cleavage in ECD. There is a glutamic acid residue (Glu⁵) in MSH, which likely is the preferred site for Ca²⁺ coordination: previous work showed that Ca²⁺ binds preferentially to side chains of acidic residues in the gas phase [65], particularly when acidic residues are located in the middle of the sequence [66]. Ca²⁺ binding to Glu⁵ may place a positively charged group close to both His⁶ and Tyr², which may explain the similar ILE values for His⁶- and Tyr²-iodinated MSH in ECD.

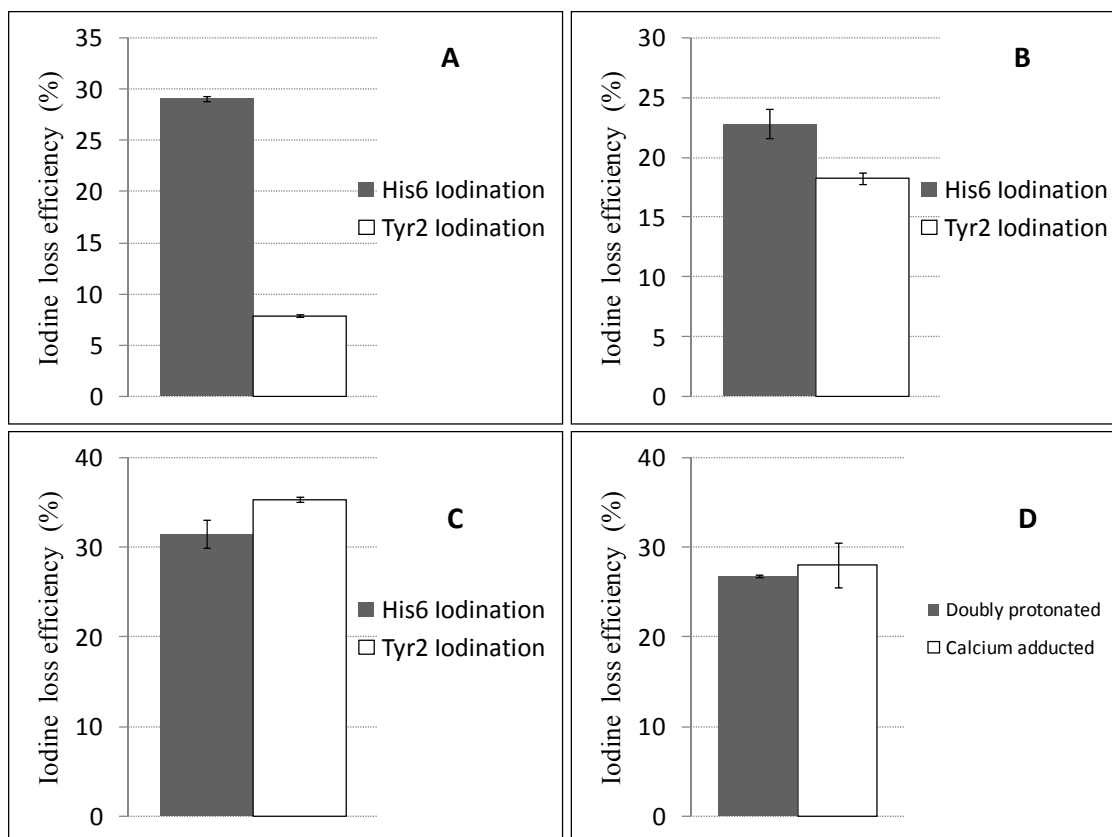


Figure 4.5. ILE of triply protonated His⁶- and Tyr²- iodinated MSH (panel A). His⁶ iodination results in much higher ILE than that of Tyr². ILE of doubly protonated His⁶- and Tyr²-iodinated MSH are shown in panel B. His⁶ iodination results in slightly higher ILE than that of Tyr². Doubly protonated peptides are likely to have more folded gas-phase structures than triply protonated species. Thus, positive charge can be spatially close to the C-I bond in the Tyr²-iodinated species. ILE of doubly charged calcium-adducted His⁶-and Tyr²-iodinated MSH is shown in panel C. A likely calcium binding site is the acidic Glu⁵ residue between His⁶ and Tyr². Thus, positive charge may be close to the C-I bond in either iodinated form. Panel D represents the ILE of doubly protonated and calcium-adducted Tyr¹⁰ doubly iodinated AARF. Doubly protonated peptides may fold in the gas phase, placing the C-I groups on Tyr¹⁰ spatially close to the likely

protonation sites (Arg1-2 near the N-terminus). The Ca^{2+} ion is likely to coordinate to the string of acidic residues N-terminal to Tyr¹⁰.

4.3.4 ECD of Doubly Protonated and Calcium-Adducted Doubly Iodinated AAGF and Singly Iodinated BE

Doubly iodinated AAGF, with both C-I bonds in Tyr¹⁰, was also subjected to ECD. ILEs from ECD of doubly protonated and Ca^{2+} -adducted AAGF are shown in Fig. 5, panel D. The ILEs for the two forms of AAGF are close, 27% for protonated AAGF and 28% for Ca^{2+} -adducted AAGF. The three potential protonation sites in AAGF, i.e., the free N-terminus, and Arg 1-2, are all close to the N-terminus and seven residues away from the C-I bonds on Tyr¹⁰. As discussed above, doubly charged ions may be folded in the gas phase, thereby placing protons spatially close to the C-I bonds in Tyr¹⁰. In the case of Ca^{2+} -adducted AAGF, the Ca^{2+} ion is likely to bind to the string of acidic residues (Glu4-8) [66]. The Ca^{2+} ion may also coordinate to two deprotonated Glu residues in the polyGlu sequence while the N-terminus or Arg1-2 is protonated, i.e., generating a gas-phase zwitterion. A future interesting topic would be to investigate the effect of other metal ions on ILE in ECD of iodinated peptides.

ECD of singly iodinated BE was also performed for which the iodination site is His¹¹. Because the N-terminus of BE is blocked, the most likely protonation sites are Lys² and His¹¹. Thus, based on the findings discussed above, we expected to observe efficient C-I bond cleavage for doubly protonated singly iodinated BE in ECD. The corresponding spectrum is shown in the upper panel of Figure 4.6. As expected, iodine loss corresponded to the most abundant product ion peak. The abundance ratio between

the iodine loss peak and the charge reduced peak is $\sim 4:1$. The ECD spectrum of Ca^{2+} -adducted BE, shown in the lower panel of Figure 4.6, also demonstrates iodine loss but with much lower peak abundance: the abundance ratio to the charge reduced species is 1:3.5. Because there are no acidic residues in BE, Ca^{2+} is likely to chelate to carbonyl oxygens [65] along the peptide backbone, which may not yield a preferential location for efficient C-I bond cleavage.

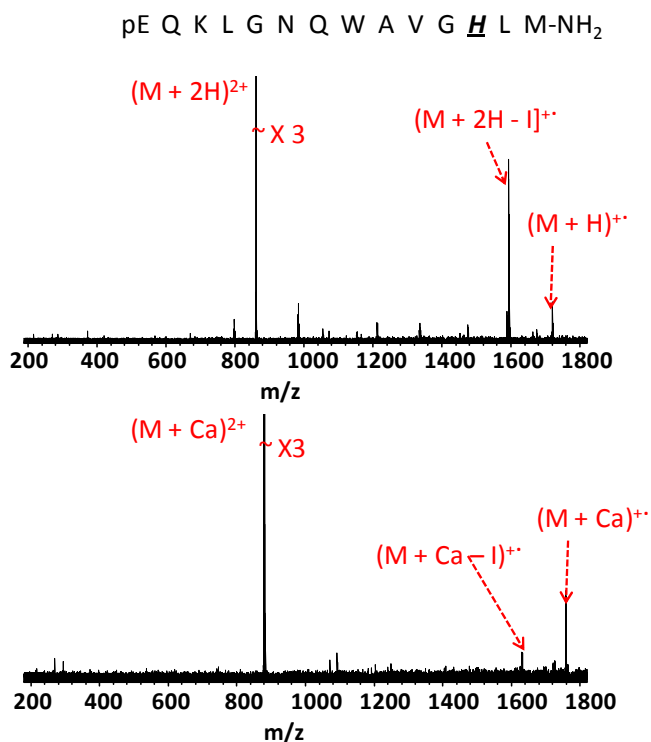


Figure 4.6. ECD of doubly protonated and calcium-adducted His¹²-iodinated bombesin. For the doubly protonated species (top panel), the most abundant fragment corresponds to iodine loss whereas iodine loss is not dominant for the calcium-adducted species (bottom panel). In the doubly protonated species, His¹² is likely protonated, thus placing positive charge close to the C-I bond. In the Ca-adducted species, there is no obvious calcium binding site close to His¹².

4.3.5 C-I Bond Cleavage in ECD: Implications for the ECD Mechanism

The results presented above regarding C-I bond cleavage in ECD provide a chance to refine the theory on the ECD mechanism. Relative to the hot hydrogen model, the superbase mechanism seems superior for interpreting our present results: Coulomb stabilization from an adjacent positively charged group may allow direct electron capture at the C-I bond and subsequently induce C-I bond rupture. Interestingly, the distance between the C-I bond and the positive charge indeed appears to influence ILE. For example, protonation of His⁶ in singly iodinated MSH would place a positive charge only a few bonds away from the C-I bond and thereby yield the observed highly efficient C-I bond cleavage. A similar argument can be made for doubly protonated His¹²-iodinated BE. On the other hand, when the positively charged group is located further away from the C-I bond, for example in the case of triply protonated Tyr²-iodinated MSH, ILE in ECD is lower although still observed. Thus, peptide gas-phase conformation plays a critical role for ILE in ECD because more unfolded peptides are less likely to have positive charge located close to a C-I bond unless the charge is a proton on an iodinated His residue. The experiments involving ECD of Ca-adducted iodinated peptides provided additional support for this hypothesis: when the Ca²⁺ ion was likely to be localized close to a C-I bond, either through bond or through space, abundant C-I bond cleavage was observed.

4.3.6 ETD and ECD Comparison of Doubly and Triply Protonated Histidine and Tyrosine Singly Iodinated MSH

ETD and ECD both generate *c*- and *z*-type ions and are believed to involve similar

fragmentation mechanisms. However, some reports have addressed the differences between ECD and ETD [48, 51]. ILEs of triply protonated His⁶ and Tyr² singly iodinated MSH from ECD and ETD are shown in Figure 4.7. These results demonstrate that C-I bond cleavage is significant in both ECD and ETD. Similar fragmentation patterns were observed in ECD and ETD, including much higher ILE for His⁶ compared to Tyr² iodination, presumably due to the charge on His⁶. However, ETD resulted in a much higher charge reduced peak abundance than ECD and less extensive backbone fragmentation (shown in Figures 4.8-4.11). Although the charge reduced peak abundance was higher in ETD, the ILEs of His⁶ and Tyr² singly iodinated MSH were higher than those from ECD due to the less extensive peptide backbone fragmentation. For triply protonated singly iodinated MSH, His⁶ iodination demonstrated higher ILE value than that from Tyr² iodination in both ECD and ETD.

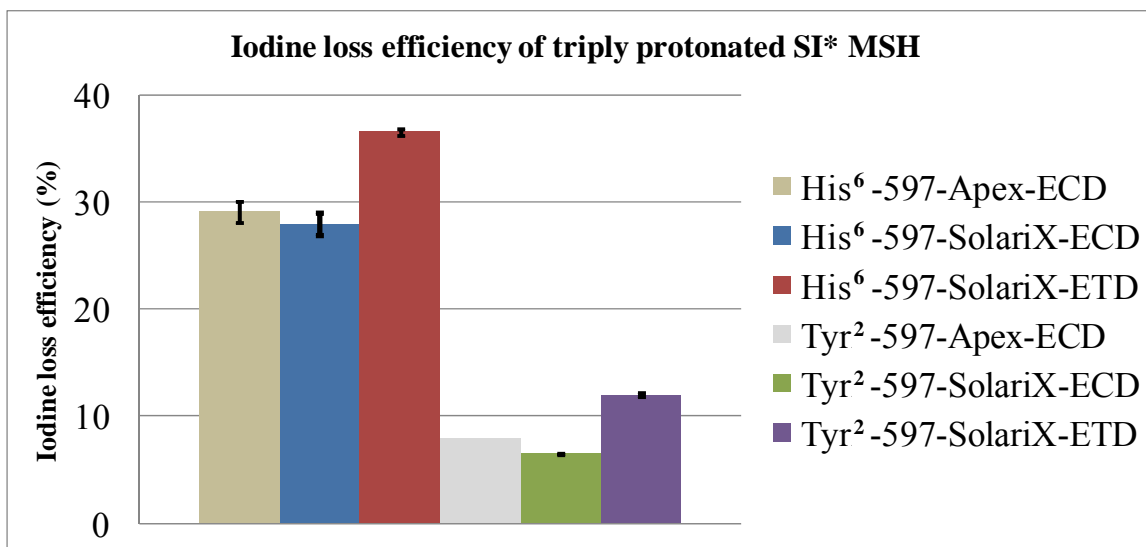


Figure 4.7. ILEs of triply protonated His⁶- and Tyr² singly-iodinated MSH from ECD and ETD on the SolariX FT-ICR instrument. ILEs from ECD on the Apex instrument are

also shown for comparison. Very little variation is seen between ECD on the two instruments. ILEs from ETD are higher than the corresponding values from ECD because ETD results in more abundant charge reduced species and less peptide backbone fragmentation. *SI=singly iodinated

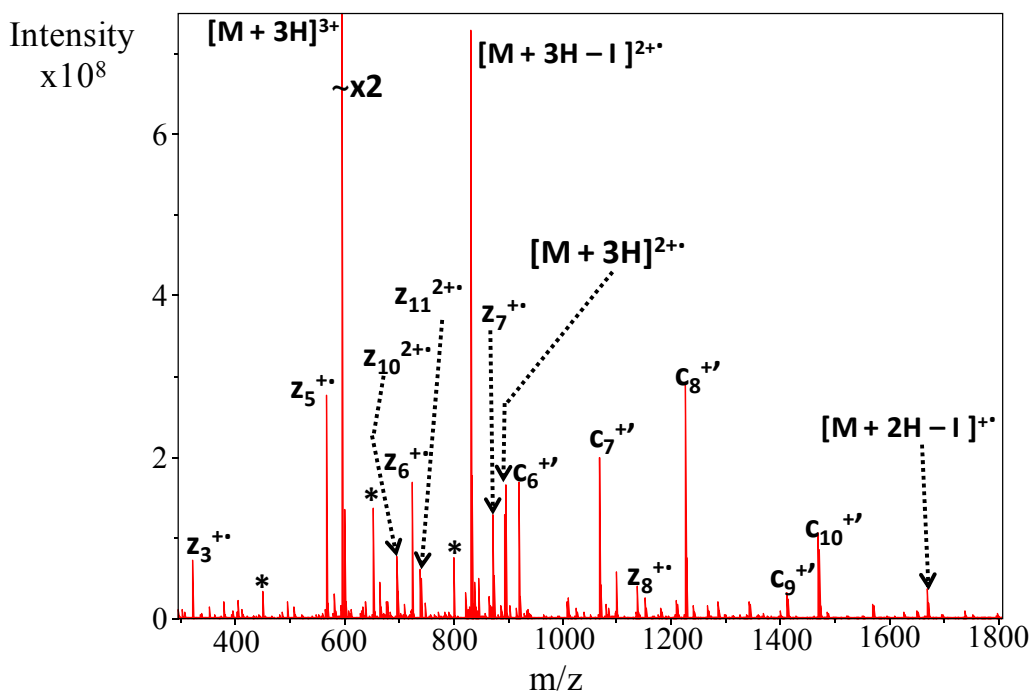


Figure 4.8. ECD of triply protonated His⁶ singly iodinated MSH on a Solarix FT-ICR instrument.

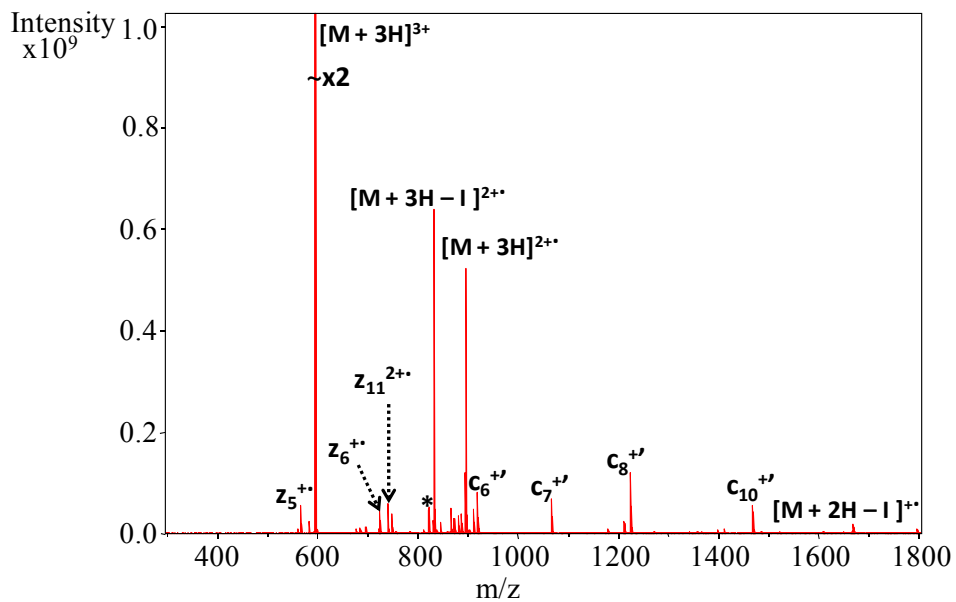


Figure 4.9. ETD of triply protonated His⁶ singly iodinated MSH on a Solarix FT-ICR instrument.

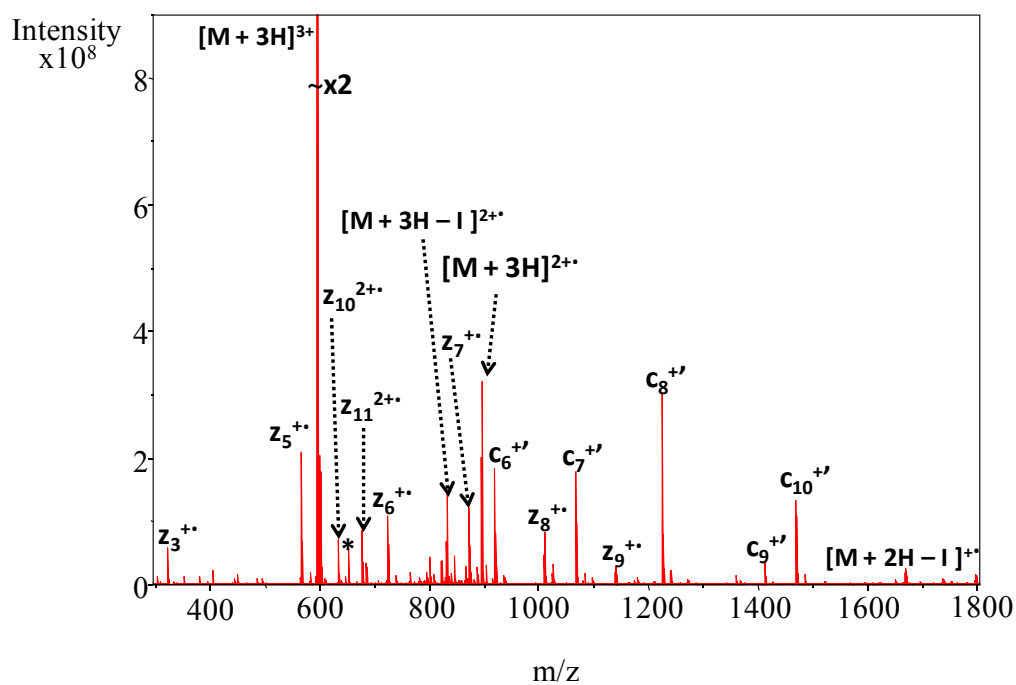


Figure 4.10. ECD of triply protonated Tyr² singly iodinated MSH on a Solarix FT-ICR instrument.

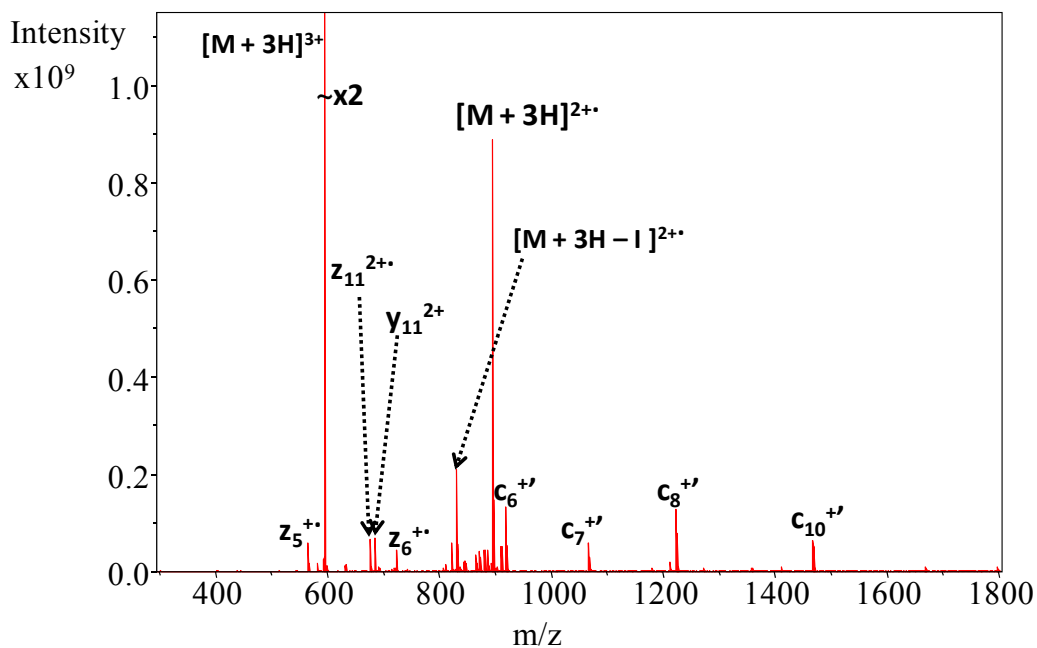


Figure 4.11. ETD of triply protonated Tyr² singly iodinated MSH on a SolariX FT-ICR instrument.

For doubly protonated singly iodinated MSH, as shown in Figure 4.12, no significant difference in ILE value was observed for His⁶ and Tyr² iodination. In addition, unlike the case of triply protonated singly iodinated MSH, ILE values from ECD and ETD of doubly protonated singly iodinated MSH only demonstrated a slight difference. In addition, for triply protonated species, ILEs from the Apex and SolariX instruments were close: 29.1±0.9% vs. 27.9±0.6% for His⁶ and 6.5±0.1%, 7.9%±0.05% for Tyr², respectively, demonstrating interinstrument reproducibility of ECD for C-I bond cleavage. For doubly protonated species, on the other hand, ILEs from Apex and SolariX were more different: 22.8±1.2% vs. 28.7±0.2% for His⁶ and 18.2±0.5% vs. 27.5±0.1% for Tyr², respectively.

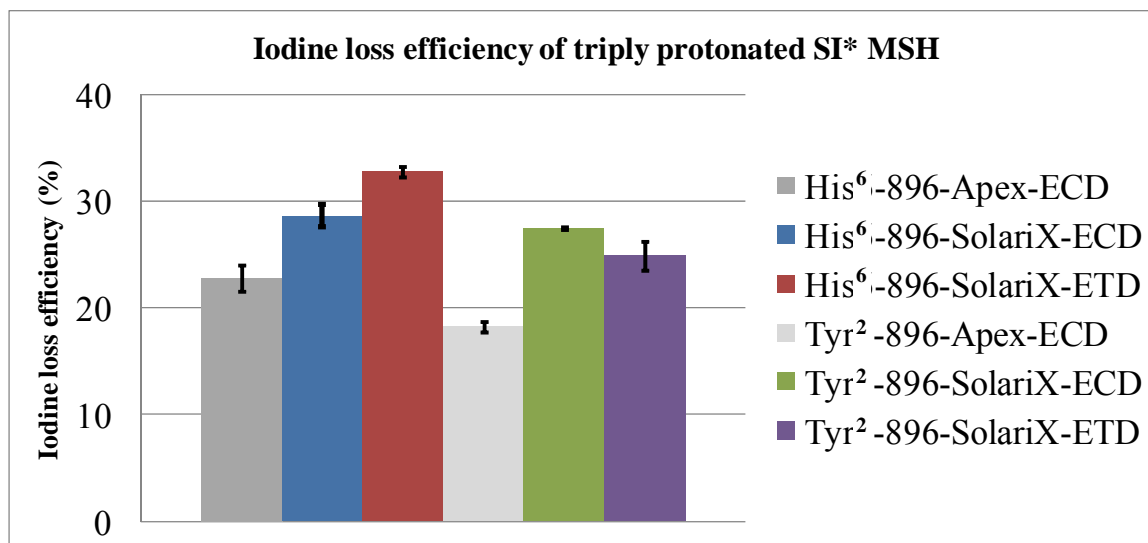


Figure 4.12. ILEs of doubly protonated His⁶- and Tyr² singly-iodinated MSH from ECD and ETD on the SolariX FT-ICR instrument. ILEs from ECD on the Apex instrument are also shown for comparison. The SolariX instrument provided higher ILE values in ECD than the Apex instrument. ILEs from SolariX ECD and ETD are similar. *SI=singly iodinated.

4.3.7 MALDI TOF/TOF CID of His⁶ Singly Iodinated MSH

MALDI TOF/TOF high-energy CID of His⁶ singly iodinated MSH was carried out for comparison to ECD/ETD. The purpose of this comparison was to investigate whether C-I bond cleavage is analogous to C-S and S-S bond cleavage, which is known to preferentially occur in ECD [33], ETD [67] and MALDI TOF/TOF CID [68]. The corresponding spectrum is shown in Figure 4.13. Briefly, a series of *b/y* ions as well as dehydrated internal fragments, are observed but C-I bond cleavage is absent, indicating

that the C-I bond is labile only in ECD/ETD and stable under MALDI TOF/TOF CID.

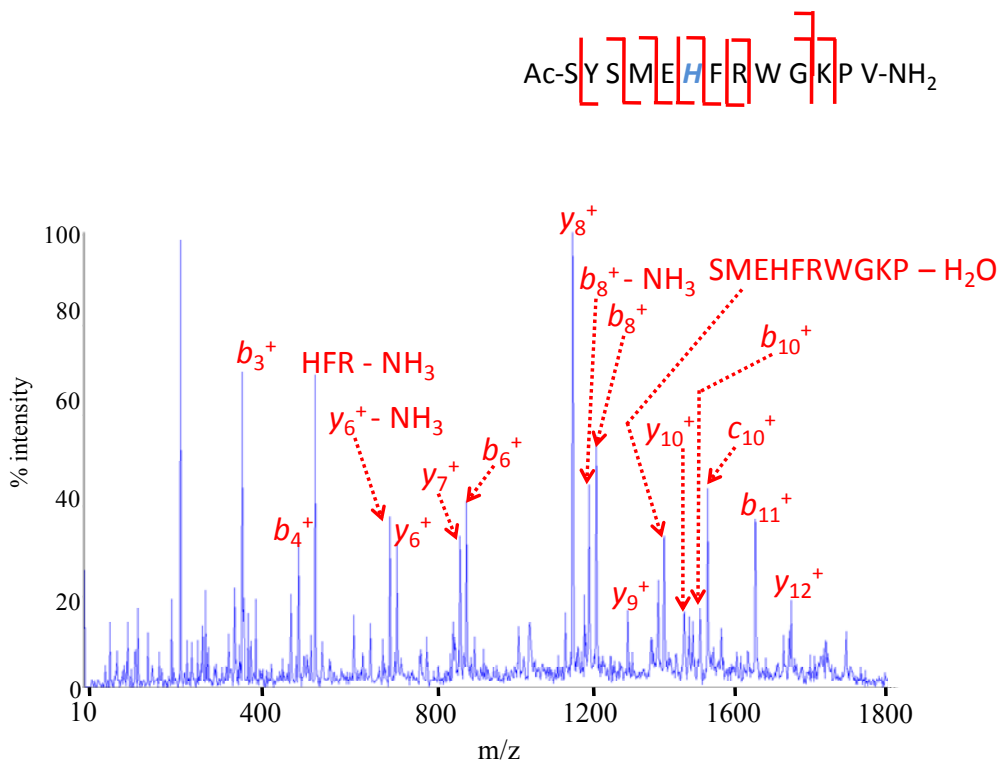


Figure 4.13. MALDI TOF/TOF CID of His⁶ singly iodinated MSH.

4.4 Summary

For the peptide MSH, His⁶ and Tyr² could be selectively iodinated by varying the initial reaction conditions. Iodinated peptides were subjected to ECD and ETD in two different FT-ICR mass spectrometers in their triply- and doubly protonated and calcium-adducted forms. For all iodinated peptides, C-I bond cleavage was observed in both ECD and ETD but with various efficiencies. It appears that proximity between the C-I bond

and a positive charge, either through bond or through space, is necessary for efficient C-I bond cleavage. ECD and ETD on the same instrument (SolariX system) both demonstrate prominent C-I bond cleavage and ILE values from ECD and ETD were close for triply protonated singly iodinated MSH. In addition, ETD produced a more abundant charge reduced species but thus resulted in less backbone fragmentation. Unlike the disulfide bond, which is labile in both ECD and MALDI TOF/TOF high-energy CID, the C-I bond is labile in ECD/ETD only. These results provide a guide to designing a novel cross-linker containing a C-I bond and a fixed positive charge for generation of unique reporter ions (iodine loss). In addition, the C-I bond provides a new target (besides S-S and backbone N-C α bonds) to understand the mechanism of ECD and ETD.

4.5 References

1. Alley, S.C.; Ishmael, F.T.; Jones, A.D.; Benkovic, S.J., Mapping protein-protein interactions in the bacteriophage T4 DNA polymerase holoenzyme using a novel trifunctional photo-cross-linking and affinity reagent. *J. Am. Chem. Soc.*, **2000**, *122*, 6126-6127.
2. Trester-Zedlitz, M.; Kamada, K.; Burley, S.K.; Fenyo, D.; Chait, B.T.; Muir, T.W., A modular cross-linking approach for exploring protein interactions. *J. Am. Chem. Soc.*, **2003**, *125*, 2416-2425.
3. Hino, N.; Okazaki, Y.; Kobayashi, T.; Hayashi, A.; Sakamoto, K.; Yokoyama, S., Protein photo-cross-linking in mammalian cells by site-specific incorporation of a photoreactive amino acid. *Nat. Methods*, **2005**, *2*, 201-206.
4. Tang, X.T.; Munske, G.R.; Siems, W.F.; Bruce, J.E., Mass spectrometry identifiable cross-linking strategy for studying protein-protein interactions. *Anal. Chem.*, **2005**, *77*, 311-318.
5. Baruah, H.; Puthenveetil, S.; Choi, Y.A.; Shah, S.; Ting, A.Y., An engineered aryl azide ligase for site-specific mapping of protein-protein interactions through photo-cross-linking. *Angew. Chem. Int. Ed.*, **2008**, *47*, 7018-7021.

6. Zhang, H.Z.; Tang, X.T.; Munske, G.R.; Tolic, N.; Anderson, G.A.; Bruce, J.E., Identification of Protein-Protein Interactions and Topologies in Living Cells with Chemical Cross-linking and Mass Spectrometry. *Mol. Cell. Proteomics*, **2009**, *8*, 409-420.
7. Mills, J.S.; Miettinen, H.M.; Barnidge, D.; Vlases, M.J.; Wimer-Mackin, S.; Dratz, E.A.; Sunner, J.; Jesaitis, A.J., Identification of a ligand binding site in the human neutrophil formyl peptide receptor using a site-specific fluorescent photoaffinity label and mass spectrometry. *Journal of Biological Chemistry*, **1998**, *273*, 10428-10435.
8. Majmudar, C.Y.; Wang, B.; Lum, J.K.; Hakansson, K.; Mapp, A.K., A high-resolution interaction map of three transcriptional activation domains with a key coactivator from photo-cross-linking and multiplexed mass spectrometry. *Angew. Chem. Int. Ed. Engl.*, **2009**, *48*, 7021-7024.
9. Grintsevich, E.E.; Benchaar, S.A.; Warshaviak, D.; Boonthung, P.; Halgand, F.; Whitelegge, J.P.; Faull, K.F.; Loo, R.R.O.; Sept, D.; Loo, J.A.; Reisler, E., Mapping the cofilin binding site on yeast G-actin by chemical cross-linking. *J. Mol. Biol.*, **2008**, *377*, 395-409.
10. Bich, C.; Bovet, C.; Rochel, N.; Peluso-Iltis, C.; Panagiotidis, A.; Nazabal, A.; Moras, D.; Zenobi, R., Detection of Nucleic Acid-Nuclear Hormone Receptor Complexes with Mass Spectrometry. *J. Am. Soc. Mass Spectrom.*, **2010**, *21*, 635-645.
11. Maly, D.J.; Allen, J.A.; Shokat, K.M., A mechanism-based cross-linker for the identification of kinase-substrate pairs. *J. Am. Chem. Soc.*, **2004**, *126*, 9160-9161.
12. Schilling, B.; Row, R.H.; Gibson, B.W.; Guo, X.; Young, M.M., MS2Assign, automated assignment and nomenclature of tandem mass spectra of chemically crosslinked peptides. *J. Am. Soc. Mass Spectrom.*, **2003**, *14*, 834-850.
13. Kang, S.; Mou, L.Y.; Lanman, J.; Velu, S.; Brouillette, W.J.; Prevelige, P.E., Synthesis of biotin-tagged chemical cross-linkers and their applications for mass spectrometry. *Rapid Commun. Mass Spectrom.*, **2009**, *23*, 1719-1726.
14. Chowdhury, S.M.; Du, X.X.; Tolic, N.; Wu, S.; Moore, R.J.; Mayer, M.U.; Smith, R.D.; Adkins, J.N., Identification of Cross-Linked Peptides after Click-Based Enrichment Using Sequential Collision-Induced Dissociation and Electron Transfer Dissociation Tandem Mass Spectrometry. *Anal. Chem.*, **2009**, *81*, 5524-5532.
15. Sinz, A.; Kalkhof, S.; Hing, C., Mapping protein interfaces by a trifunctional cross-linker combined with MALDI-TOF and ESI-FTICR mass spectrometry. *J. Am. Soc. Mass Spectrom.*, **2005**, *16*, 1921-1931.
16. Yan, F.N.; Che, F.Y.; Rykunov, D.; Nieves, E.; Fiser, A.; Weiss, L.M.; Angeletti, R.H., Nonprotein Based Enrichment Method to Analyze Peptide Cross-Linking in Protein Complexes. *Anal. Chem.*, **2009**, *81*, 7149-7159.
17. Nessen, M.A.; Kramer, G.; Back, J.; Baskin, J.M.; Smeenk, L.E.J.; de Koning, L.J.; van Maarseveen, J.H.; de Jong, L.; Bertozzi, C.R.; Hiemstra, H.; de Koster, C.G., Selective Enrichment of Azide-Containing Peptides from Complex Mixtures. *J. Proteome Res.*, **2009**, *8*, 3702-3711.
18. Ahrends, R.; Kosinski, J.; Kirsch, D.; Manelyte, L.; Giron-Monzon, L.;

- Hummerich, L.; Schulz, O.; Spengler, B.; Friedhoff, P., Identifying an interaction site between MutH and the C-terminal domain of MutL by crosslinking, affinity purification, chemical coding and mass spectrometry. *Nucleic Acids Res.*, **2006**, *34*, 3169-3180.
19. Bennett, K.L.; Kussmann, M.; Bjork, P.; Godzwon, M.; Mikkelsen, M.; Sorensen, P.; Roepstorff, P., Chemical cross-linking with thiol-cleavable reagents combined with differential mass spectrometric peptide mapping - A novel approach to assess intermolecular protein contacts. *Protein Sci.*, **2000**, *9*, 1503-1518.
 20. Back, J.W.; Notenboom, V.; de Koning, L.J.; Muijsers, A.O.; Sixma, T.K.; de Koster, C.G.; de Jong, L.Z., Identification of cross-linked peptides for protein interaction studies using mass spectrometry and O-18 labeling. *Anal. Chem.*, **2002**, *74*, 4417-4422.
 21. Soderblom, E.J.; Goshe, M.B., Collision-induced dissociative chemical cross-linking reagents and methodology: Applications to protein structural characterization using tandem mass spectrometry analysis. *Anal. Chem.*, **2006**, *78*, 8059-8068.
 22. Lu, Y.L.; Tanasova, M.; Borhan, B.; Reid, G.E., Ionic Reagent for Controlling the Gas-Phase Fragmentation Reactions of Cross-Linked Peptides. *Anal. Chem.*, **2008**, *80*, 9279-9287.
 23. Gardner, M.W.; Vasicek, L.A.; Shabbir, S.; Anslyn, E.V.; Brodbelt, J.S., Chromogenic cross-linker for the characterization of protein structure by infrared multiphoton dissociation mass spectrometry. *Anal. Chem.*, **2008**, *80*, 4807-4819.
 24. King, G.J.; Jones, A.; Kobe, B.; Huber, T.; Mouvadov, D.; Hume, D.L.; Ross, I.L., Identification of disulfide-containing chemical cross links in proteins using MALDI-TOF/TOF-mass spectrometry. *Anal. Chem.*, **2008**, *80*, 5036-5043.
 25. Zubarev, R.A.; Kelleher, N.L.; McLafferty, F.W., Electron capture dissociation of multiply charged protein cations. A nonergodic process. *J. Am. Chem. Soc.*, **1998**, *120*, 3265-3266.
 26. Zubarev, R.A., Reactions of polypeptide ions with electrons in the gas phase. *Mass Spectrom. Rev.*, **2003**, *22*, 57-77.
 27. Cooper, H.J.; Hakansson, K.; Marshall, A.G., The role of electron capture dissociation in biomolecular analysis. *Mass Spectrom. Rev.*, **2005**, *24*, 201-222.
 28. Meng, F.Y.; Forbes, A.J.; Miller, L.M.; Kelleher, N.L., Detection and localization of protein modifications by high resolution tandem mass spectrometry. *Mass Spectrom. Rev.*, **2005**, *24*, 126-134.
 29. Garcia, B.A.; Siuti, N.; Thomas, C.E.; Mizzen, C.A.; Kelleher, N.L., Characterization of neurohistone variants and post-translational modifications by electron capture dissociation mass spectrometry. *Int. J. Mass Spectrom.*, **2007**, *259*, 184-196.
 30. Whitelegge, J.P.; Zabrouskov, V.; Halgand, F.; Souda, P.; Bassiliana, S.; Yan, W.; Wolinsky, L.; Loo, J.A.; Wong, D.T.W.; Faull, K.F., Protein-sequence polymorphisms and post-translational modifications in proteins from human saliva using top-down Fourier-transform ion cyclotron resonance mass spectrometry. *Int. J. Mass Spectrom.*, **2007**, *268*, 190-197.
 31. Dongre, A.R.; Jones, J.L.; Somogyi, A.; Wysocki, V.H., Influence of peptide

- composition, gas-phase basicity, and chemical modification on fragmentation efficiency: Evidence for the mobile proton model. *J. Am. Chem. Soc.*, **1996**, *118*, 8365-8374.
32. Horn, D.M.; Zubarev, R.A.; McLafferty, F.W., Automated de novo sequencing of proteins by tandem high-resolution mass spectrometry. *Proc. Natl. Acad. Sci. U. S. A.*, **2000**, *97*, 10313-10317.
 33. Zubarev, R.A.; Kruger, N.A.; Fridriksson, E.K.; Lewis, M.A.; Horn, D.M.; Carpenter, B.K.; McLafferty, F.W., Electron capture dissociation of gaseous multiply-charged proteins is favored at disulfide bonds and other sites of high hydrogen atom affinity. *J. Am. Chem. Soc.*, **1999**, *121*, 2857-2862.
 34. Zhang, M.X.; Kaltashov, I.A., Mapping of protein disulfide bonds using negative ion fragmentation with a broadband precursor selection. *Anal. Chem.*, **2006**, *78*, 4820-4829.
 35. Kalli, A.; Hakansson, K., Preferential cleavage of S-S and C-S bonds in electron detachment dissociation and infrared multiphoton dissociation of disulfide-linked peptide anions. *Int. J. Mass Spectrom.*, **2007**, *263*, 71-81.
 36. Bean, M.F.; Carr, S.A., Characterization of Disulfide Bond Position in Proteins and Sequence-Analysis of Cystine-Bridged Peptides by Tandem Mass-Spectrometry. *Anal. Bioanal. Chem.*, **1992**, *201*, 216-226.
 37. Zhou, J.; Ens, W.; Poppechriemer, N.; Standing, K.G.; Westmore, J.B., Cleavage of Interchain Disulfide Bonds Following Matrix-Assisted Laser-Desorption. *Int. J. Mass Spectrom. Ion Processes*, **1993**, *126*, 115-122.
 38. Xie, Y.M.; Zhang, J.; Yin, S.; Loo, J.A., Top-down ESI-ECD-FT-ICR mass spectrometry localizes noncovalent protein-ligand binding sites. *J. Am. Chem. Soc.*, **2006**, *128*, 14432-14433.
 39. Jackson, S.N.; Dutta, S.; Woods, A.S., The Use of ECD/ETD to Identify the Site of Electrostatic Interaction in Noncovalent Complexes. *J. Am. Soc. Mass Spectrom.*, **2009**, *20*, 176-179.
 40. Kleinnijenhuis, A.J.; Mihalca, R.; Heeren, R.M.A.; Heck, A.J.R., Atypical behavior in the electron capture induced dissociation of biologically relevant transition metal ion complexes of the peptide hormone oxytocin. *Int. J. Mass Spectrom.*, **2006**, *253*, 217-224.
 41. Fung, Y.M.E.; Liu, H.C.; Chan, T.W.D., Electron capture dissociation of peptides metalated with alkaline-earth metal ions. *J. Am. Soc. Mass Spectrom.*, **2006**, *17*, 757-771.
 42. Liu, H.C.; Hakansson, K., Divalent metal ion-peptide interactions probed by electron capture dissociation of trications. *J. Am. Soc. Mass Spectrom.*, **2006**, *17*, 1731-1741.
 43. Zubarev, R.A.; Horn, D.M.; Fridriksson, E.K.; Kelleher, N.L.; Kruger, N.A.; Lewis, M.A.; Carpenter, B.K.; McLafferty, F.W., Electron capture dissociation for structural characterization of multiply charged protein cations. *Anal. Chem.*, **2000**, *72*, 563-573.
 44. Syrstad, E.A.; Turecek, F., Toward a general mechanism of electron capture dissociation. *J. Am. Soc. Mass Spectrom.*, **2005**, *16*, 208-224.
 45. Sobczyk, M.; Anusiewicz, W.; Berdys-Kochanska, J.; Sawicka, A.; Skurski, P.;

- Simons, J., Coulomb-assisted dissociative electron attachment: Application to a model peptide. *J. Phys. Chem. A*, **2005**, *109*, 250-258.
46. Anusiewicz, W.; Berdys-Kochanska, J.; Simons, J., Electron attachment step in electron capture dissociation (ECD) and electron transfer dissociation (ETD). *J. Phys. Chem. A*, **2005**, *109*, 5801-5813.
47. Neff, D.; Smuczynska, S.; Simons, J., Electron shuttling in electron transfer dissociation. *Int. J. Mass Spectrom.*, **2009**, *283*, 122-134.
48. Simons, J., Mechanisms for S-S and N-C-alpha bond cleavage in peptide ECD and ETD mass spectrometry. *Chem. Phys. Lett.*, **2010**, *484*, 81-95.
49. Syka, J.E.P.; Coon, J.J.; Schroeder, M.J.; Shabanowitz, J.; Hunt, D.F., Peptide and protein sequence analysis by electron transfer dissociation mass spectrometry. *Proc. Natl. Acad. Sci. U. S. A.*, **2004**, *101*, 9528-9533.
50. Swaney, D.L.; McAlister, G.C.; Wirtala, M.; Schwartz, J.C.; Syka, J.E.P.; Coon, J.J., Supplemental activation method for high-efficiency electron-transfer dissociation of doubly protonated peptide precursors. *Anal. Chem.*, **2007**, *79*, 477-485.
51. Sohn, C.H.; Chung, C.K.; Yin, S.; Ramachandran, P.; Loo, J.A.; Beauchamp, J.L., Probing the Mechanism of Electron Capture and Electron Transfer Dissociation Using Tags with Variable Electron Affinity. *J. Am. Chem. Soc.*, **2009**, *131*, 5444-5459.
52. Kalli, A.; Hakansson, K., Comparison of the electron capture dissociation fragmentation behavior of doubly and triply protonated peptides from trypsin, Glu-C, and chymotrypsin digestion. *J. Proteome Res.*, **2008**, *7*, 2834-2844.
53. Ghosh, D.; Erman, M.; Sawicki, M.; Lala, P.; Weeks, D.R.; Li, N.Y.; Pangborn, W.; Thiel, D.J.; Jornvall, H.; Gutierrez, R.; Eyzaguirre, J., Determination of a protein structure by iodination: the structure of iodinated acetylxylylan esterase. *Acta Crystallogr., Sect. D*, **1999**, *55*, 779-784.
54. Espuna, G.; Andreu, D.; Barluenga, J.; Perez, X.; Planas, A.; Arsequell, G.; Valencia, G., Iodination of proteins by IPy2BF4, a new tool in protein chemistry. *Biochemistry*, **2006**, *45*, 5957-5963.
55. Ly, T.; Julian, R.R., Residue-specific radical-directed dissociation of whole proteins in the gas phase. *J. Am. Chem. Soc.*, **2008**, *130*, 351-358.
56. Nair, S.S.; Nilsson, C.L.; Emmett, M.R.; Schaub, T.M.; Gowd, K.H.; Thakur, S.S.; Krishnan, K.S.; Balaram, P.; Marshall, A.G., De novo sequencing and disulfide mapping of a bromotryptophan-containing conotoxin by Fourier transform ion cyclotron resonance mass spectrometry. *Anal. Chem.*, **2006**, *78*, 8082-8088.
57. Santrucek, J.; Strohalm, M.; Kadlcik, V.; Hynek, R.; Kodicek, M., Tyrosine residues modification studied by MALDI-TOF mass spectrometry. *Biochem. Biophys. Res. Commun.*, **2004**, *323*, 1151-1156.
58. Senko, M.W.; Canterbury, J.D.; Guan, S.H.; Marshall, A.G., A high-performance modular data system for Fourier transform ion cyclotron resonance mass spectrometry. *Rapid Commun. Mass Spectrom.*, **1996**, *10*, 1839-1844.
59. Ledford, E.B.; Rempel, D.L.; Gross, M.L., Space-Charge Effects in Fourier-Transform Mass-Spectrometry - Mass Calibration. *Anal. Chem.*, **1984**, *56*, 2744-2748.

60. Kaplan, D.A.; Hartmer, R.; Speir, J.P.; Stoermer, C.; Gumerov, D.; Easterling, M.L.; Brekenfeld, A.; Kim, T.; Laukien, F.; Park, M.A., Electron transfer dissociation in the hexapole collision cell of a hybrid quadrupole-hexapole Fourier transform ion cyclotron resonance mass spectrometer. *Rapid Commun. Mass Spectrom.*, **2008**, *22*, 271-278.
61. Miyashita, M.; Yamashita, S., Studies on Iodinated Compounds .6. Separation Characteristics of Iodohistidines on Reversed-Phase High-Performance Liquid-Chromatography. *J. Chromatogr.*, **1989**, *475*, 135-144.
62. Liu, Z.J.; Julian, R.R., Deciphering the Peptide Iodination Code: Influence on Subsequent Gas-Phase Radical Generation with Photo dissociation ESI-MS. *J. Am. Soc. Mass Spectrom.*, **2009**, *20*, 965-971.
63. Harrison, A.G., The gas-phase basicities and proton affinities of amino acids and peptides. *Mass Spectrom. Rev.*, **1997**, *16*, 201-217.
64. Garcia, B.; Ramirez, J.; Wong, S.; Lebrilla, C.B., Thermal dissociation of protonated cyclodextrin-amino acid complexes in the gas phase. *Int. J. Mass Spectrom.*, **2001**, *210*, 215-222.
65. Nemirovskiy, O.V.; Gross, M.L., Determination of calcium binding sites in gas-phase small peptides by tandem mass spectrometry. *J. Am. Soc. Mass Spectrom.*, **1998**, *9*, 1020-1028.
66. Nemirovskiy, O.V.; Gross, M.L., Intrinsic Ca²⁺ affinities of peptides: application of the kinetic method to analogs of calcium-binding site III of rabbit skeletal troponin C. *J. Am. Soc. Mass Spectrom.*, **2000**, *11*, 770-779.
67. Chrisman, P.A.; Pitteri, S.J.; Hogan, J.M.; McLuckey, S.A., SO₂- electron transfer ion/ion reactions with disulfide linked polypeptide ions. *J. Am. Soc. Mass Spectrom.*, **2005**, *16*, 1020-1030.
68. Patterson, S.D.; Katta, V., Prompt Fragmentation of Disulfide-Linked Peptides during Matrix-Assisted Laser-Desorption Ionization Mass-Spectrometry. *Anal. Chem.*, **1994**, *66*, 3727-3732.

Chapter 5

Enhancing the Detection of Chemically Cross-linked Peptides in Mass Spectrometry: Enabling Selective Metal Dioxide- based Enrichment for a Novel Homobifunctional Peptide- based Cross-linker

5.1 Introduction

Chemical cross-linking combined with mass spectrometry (MS) has become a powerful tool for characterizing protein higher order structure and identifying protein-protein interactions. Analysis by MS offers lenient requirements for sample purity, high sensitivity, and high sample throughput.

Detection of cross-linked peptides, however, is challenging because: 1) the cross-linking yield is low and cross-linked products are subjected to ion suppression by the vast excess of unmodified peptides [1]; 2) the formation of intermolecular, intramolecular, and dead-end cross-linked products increases spectral complexity [2]; 3) backbone fragmentation of cross-linked peptides in MS/MS is either the same as for the corresponding unmodified peptides, or involve unknown mass shifts, making differentiation of MS/MS signals from cross-linked peptides and unmodified peptides,

respectively, difficult[3]. In order to solve these challenges, efforts have been made to modify chemical cross-linkers for more facile detection of cross-linked peptides in mass spectrometry.

To differentiate signals from cross-linked peptides and unmodified peptides, two sets of spectra can be recorded for comparison. For example, thiol-cleavable cross-linkers (TCCs) [4] can be used for the cross-linking reaction and the product divided in half. One half undergoes liquid-phase disulfide bond reduction and alkylation and the other half is subjected to analysis without further treatment. Comparison of reduced and unreduced samples will reveal potential cross-linked products. Second, chemical cross-linkers can be designed to generate unique gas-phase cleavage products [5-7]. During MS/MS analysis, precursor ions containing gas-phase cleavable cross-linkers produce characteristic product ions which aid the identification of cross-linked products. Gas-phase cleavable cross-linkers can reduce sample preparation time, required sample amounts, and analysis time.

To eliminate ion suppression by unmodified peptides, enrichment moieties can be incorporated into chemical cross-linkers for selective enrichment prior to MS analysis. One example includes incorporation of a biotin moiety into chemical cross-linkers and application of biotin-avidin affinity purification to separate cross-linked products from non-cross-linked peptides [8, 9]. However, use of biotin-avidin affinity purification presents several problems: 1) There must be enough distance between the biotin group and the two cross-linking reactive groups to minimize interference in the cross-linking reaction. Therefore, a rather long chain, e.g., polyethylene glycol, is typically introduced to isolate the biotin group, which makes cross-linker bulky. The length of this spacer arm

typically exceeds the preferred range (8-15 Å), which can impose undesired influences on the obtained protein structural/interaction information [1]. 2) Strong detergents, including SDS and urea, are typically required to dissociate biotin-avidin interactions. Detergents are not compatible with MS analysis and their removal may be challenging and cause sample loss.

Zirconium dioxide (ZrO₂) and titanium dioxide (TiO₂) enrichment combined with MS have been shown to specifically enhance the detection sensitivity of phosphopeptides [10-12]. Enrichment is accomplished simply by varying solvent pH. Here, we demonstrate the design of a novel phosphate-containing peptide-based homobifunctional cross-linker with the aim of allowing metal dioxide enrichment. Two cross-linker designs were explored. First, a tripeptide with amine reactive groups at both ends and a phosphoserine (pS) residue in the middle was synthesized. Second, a heptapeptide (Ac-pSGGCGGC-NH₂) with pS at the N-terminus was evaluated. For the latter cross-linker, one amine reactive group was located in the middle of the peptide and the other one at the C-terminus.

5.2 Experimental

5.2.1 Cross-linker I

Substance P (subP, with the sequence RPKPQQFFGLM-NH₂) and melanocyte-stimulating hormone (MSH, with the sequence Ac-SYSMEHFRWGKPV-NH₂) were purchased from Sigma (St. Louis, MO) and Genscript (Piscataway, NJ), respectively, and used without further purification. Tryptic peptide mixtures were generated by digesting

400 picomole apomyoglobin and 100 picomole bovine serum albumin (BSA) with 3-4 μL of 100 ng/ μL trypsin (Promega, WI) overnight at 37 °C.

The peptide Ac-CpSC-OH (peptide I, pS indicates phosphoserine) was purchased from Genescript, mixed with thiol-reactive N-[γ -maleimido butyryloxy] succinimide ester (GMBS, from Pierce (Rockford, IL); 4:1 molar ratio), and incubated at room temperature for various time periods (40, 105, and 225 minutes, respectively). The product, Ac-C(GMBS)pSC(GMBS)-OH, which has two amine-reactive N-hydroxysuccinimide (NHS) groups linked to the two cysteines, was then incubated with subP and MSH at room temperature (1 hour) followed by quenching with 3 μL 1 M ammonium bicarbonate and desalting by C₁₈ Ziptip (Millipore, Bedford, MA). SubP and MSH reacted with Ac-C(GMBS)pSC(GMBS)-OH were then treated with TiO₂ and ZrO₂ microtips (Glygen, Columbia, MD). The microtips were acidified/cleaned with 3.3% formic acid. Then, samples were loaded, washed with water, and eluted with 0.2% piperidine. The eluates were dried down and reconstituted in ACN:H₂O (1:1 volume ratio) for MS analysis.

5.2.2 Cross-linker II

The peptide Ac-pSGGCGGC-NH₂ (peptide II) was purchased from Genescript and reacted with GMBS at 4:1 molar ratio. Similar to the reaction for peptide I, two molecular equivalents of GMBS conjugate to one molecular equivalent of peptide II by reducing the maleimide groups in GMBS and linking them to the cysteine thiols. Thus, a homobifunctional cross-linker is produced in which two NHS groups from GMBS are available for further cross-linking. C₁₈Ziptip, ZrO₂, and TiO₂ enrichment was performed

as described for cross-linker 1, except that elution was done with 0.2% piperidine and 1% formic acid was immediately added for pH neutralization.

5.2.3 Mass Spectrometry Analysis

All samples were analyzed with a 7 Tesla ESI-Q-FT ICR mass spectrometer (Bruker, Billerica, MA) in negative ion mode by direct infusion at 70 μ L/h. All data were acquired with XMASS software (version 6.1, Bruker Daltonics) in broadband mode from $m/z = 200$ to 2000 with 512k data points and summed over 10-20 scans. Mass spectra were analyzed with the MIDAS analysis software [13]. When needed, external frequency-to- m/z calibration was performed with a two-term calibration equation [14] using two calibration standards ($m/z = 622.02895$ and 922.00979 , from the calibration mix G2421A, Agilent Technologies, Palo Alto, CA). Peptides and cross-linked products were identified based on accurate mass.

For negative collision induced dissociation (CID), precursor ions were mass-selectively accumulated in a hexapole with a 5-10 m/z quadrupole isolation window and subjected to dissociation with argon gas. The collision voltage was 24 V.

5.3 Results and Discussion

5.3.1 Cross-linker I

The synthesis of cross-linker I is summarized in Figure 5.1. GMBS is a commercially available chemical cross-linker with one amine reactive group (NHS) and one sulfhydryl reactive group (maleimide). One mole of peptide will react with two moles of GMBS to yield the product shown in Figure 5.1. The resulting

homobifunctional cross-linker has one phosphate group (from peptide I) and two amine reactive groups (from GMBS).

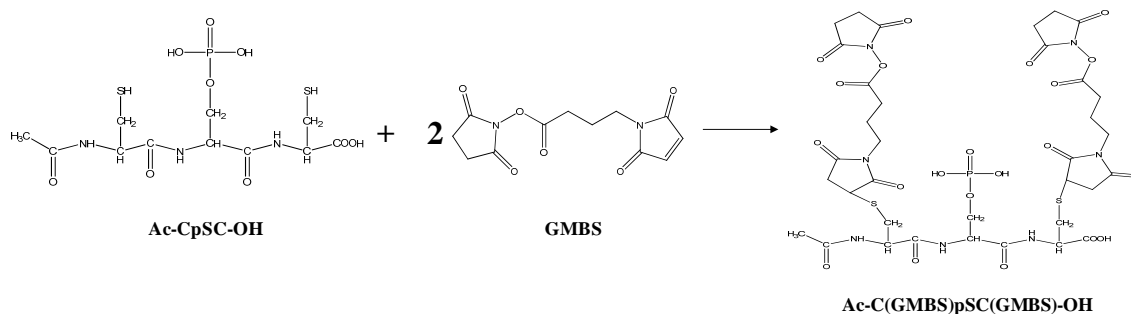


Figure 5.1. Synthesis of cross-linker I.

Cross-linker yield (at 1:4 molar ratio of peptide I and GMBS) as function of reaction time was investigated and the results are shown in Figure 5.2. Reaction times tested for Ac-C(GMBS)pSC(GMBS)-OH formation are 40, 105 and 225 minutes for which the longer time provided the highest cross-linker yield (i.e., transfer of GMBS to both cysteine residues). The yield of the partial cross-linker (transfer to only one cysteine residue) decreases with longer reaction time.

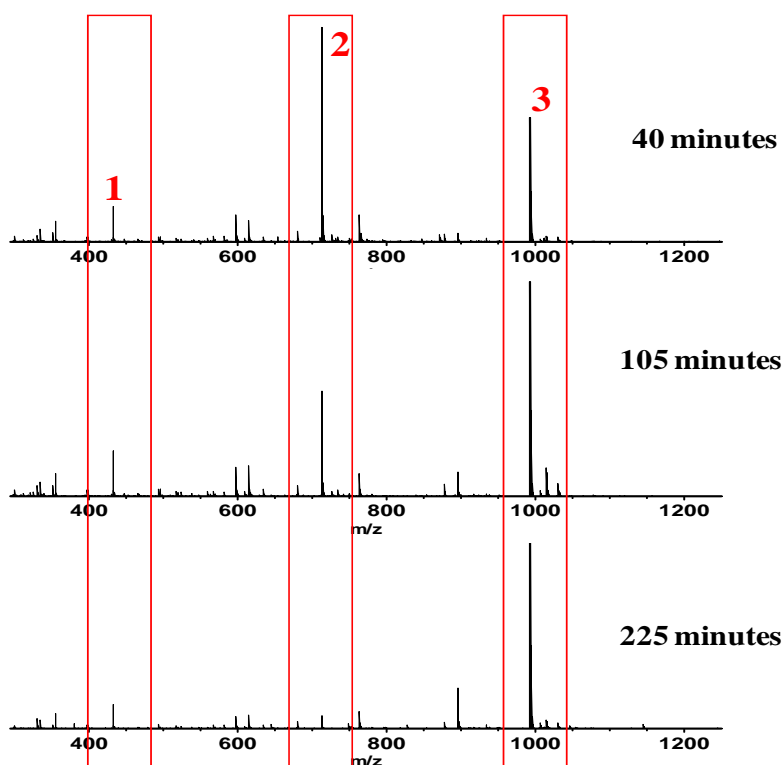


Figure 5.2. Negative ion mode ESI-FT-ICR MS analysis of the yield of cross-linker I at different reaction times. Peptide I and GMBS were mixed at 1:4 molar ratio. 1: unmodified peptide I; 2: partial reaction product with one GMBS attached to peptide I; 3: the cross-linker Ac-C(GMBS)pSC(GMBS)-OH. Peaks 1-3 all correspond to singly charged ions.

Once the cross-linker Ac-C(GMBS)pSC(GMBS)-OH was obtained, it was applied to react with the model peptides subP and MSH. Results from these cross-linking reactions are shown in Figure 5.3. subP contains two amine groups: one at the N-terminus and the other at Lys³. Intra-molecular cross-linking was the major outcome for this peptide (peak2, panel A in Fig. 5.3). MSH, on the other hand, contains only one free amine, at Lys¹¹, because the N-terminus is acetylated. However, inter-molecular cross-

linking was observed for this peptide (peak4, panel B in Fig. 5.3). In addition, because free GMBS was still present (due to the excess amount added to achieve maximum yield of cross-linkers I and II), a product from reaction between free GMBS and MSH was also observed, in which one amine-reactive group from GMBS reacted with Lys¹¹ in MSH (peak 3, panel B). These results provide validation of the activity of the Ac-C(GMBS)pSC(GMBS)-OH cross-linker.

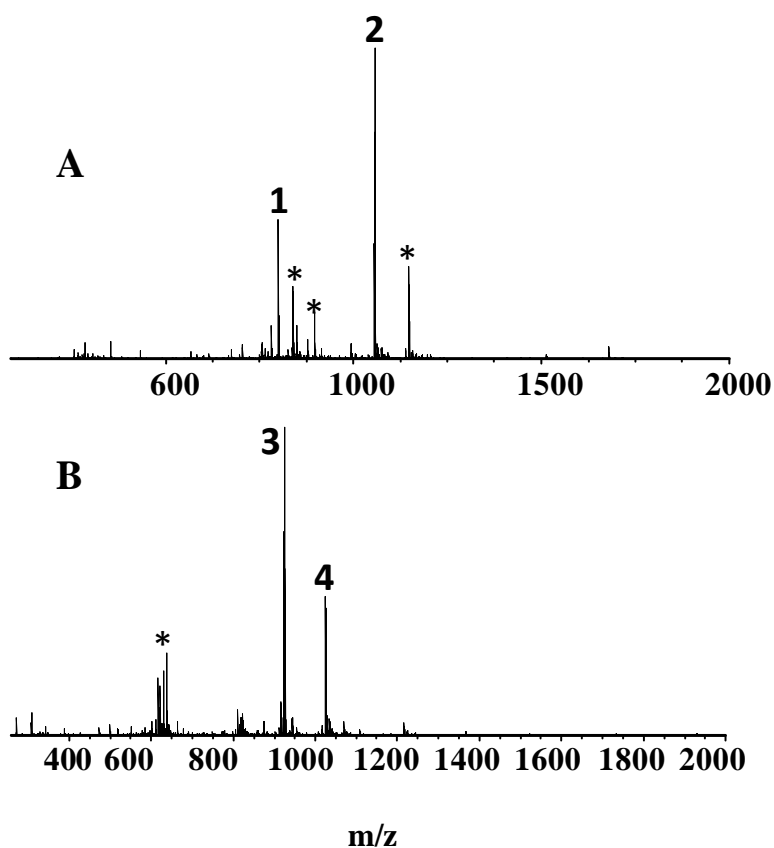


Figure 5.3. Positive ion mode ESI-FT-ICR mass spectra following cross-linking reaction of subP (panel A) and MSH (panel B) with cross-linker I, Ac-C(GMBS)pSC(GMBS)-OH. 1: singly charged un-reacted cross-linker; 2: doubly charged intramolecularly cross-linked subP; 3: doubly charged product from cross-linking of MSH (Lys¹¹) and an amine-

reactive group in free excess GMBS ; 4: quadruply charged intermolecularly cross-linked product of two molecules of MSH; *=unidentified peak.

The subP and MSH cross-linked product solutions were then subjected to TiO_2 and ZrO_2 treatment with or without introducing a background of apomyoglobin tryptic peptides. Contrary to our expectations, inter- and intramolecularly cross-linked products, observed without metal dioxide treatment (as shown in Figure 5.3), were not detected. The result for MSH is shown in Figure 5.4. Here, all observable peaks, including those highlighted within the box, are singly charged and may correspond to solvent or contaminants from the metal dioxide surface. The unsuccessful enrichment of cross-linked products by TiO_2 and ZrO_2 may be attributed to steric effects, which prevent the phosphate group from interacting with the metal dioxide surface. Based on these results, we focused our efforts towards redesigning the cross-linker to facilitate interaction between the phosphate group and the $\text{TiO}_2/\text{ZrO}_2$ surface. This effort resulted in the synthesis of cross-linker II.

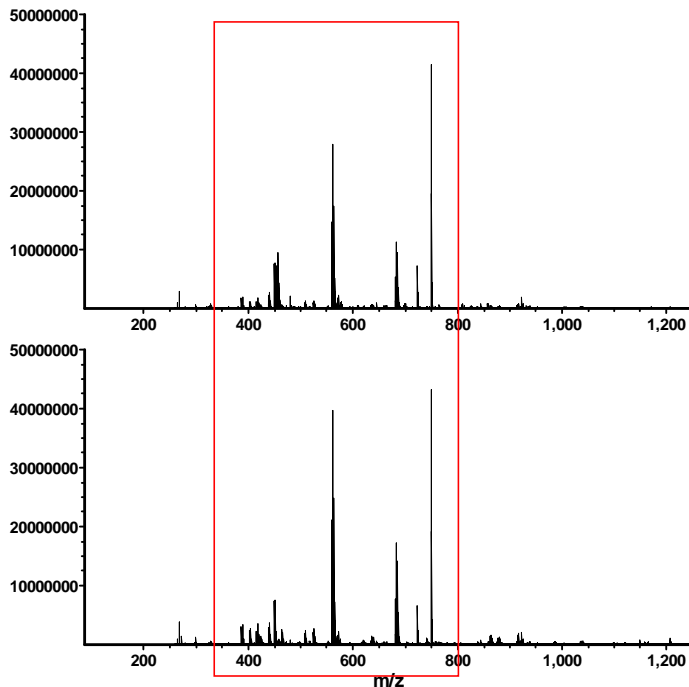


Figure 5.4. ZrO₂ (top) and TiO₂ (bottom) treatment of Ac-C(GMBS)pSC(GMBS)-OH reacted with MSH. The intermolecularly cross-linked product observed without metal oxide treatment (see Figure 5.3) was not detected, perhaps due to steric effects. The highlighted peaks all correspond to singly-charged impurities.

5.3.2 Cross-linker II

The reaction time for maximum yield of cross-linker II was determined to be three hours at a 1:4 molar ratio of peptide II and GMBS at room temperature. The structure of cross-linker II is shown in Figure 5.5. In this structure, the distance between the phosphoserine residue and the two NHS groups is expected to be big enough to prevent steric interference in either intra- or inter-molecular cross-linking, and thereby allow selective binding of cross-linked products to TiO₂/ZrO₂. However, the cross-

linking efficiency of cross-linker II was not satisfactory. For example, intermolecularly cross-linked peptides (e.g., by using MSH) were not generated, however, intramolecularly cross-linked subP was observed.

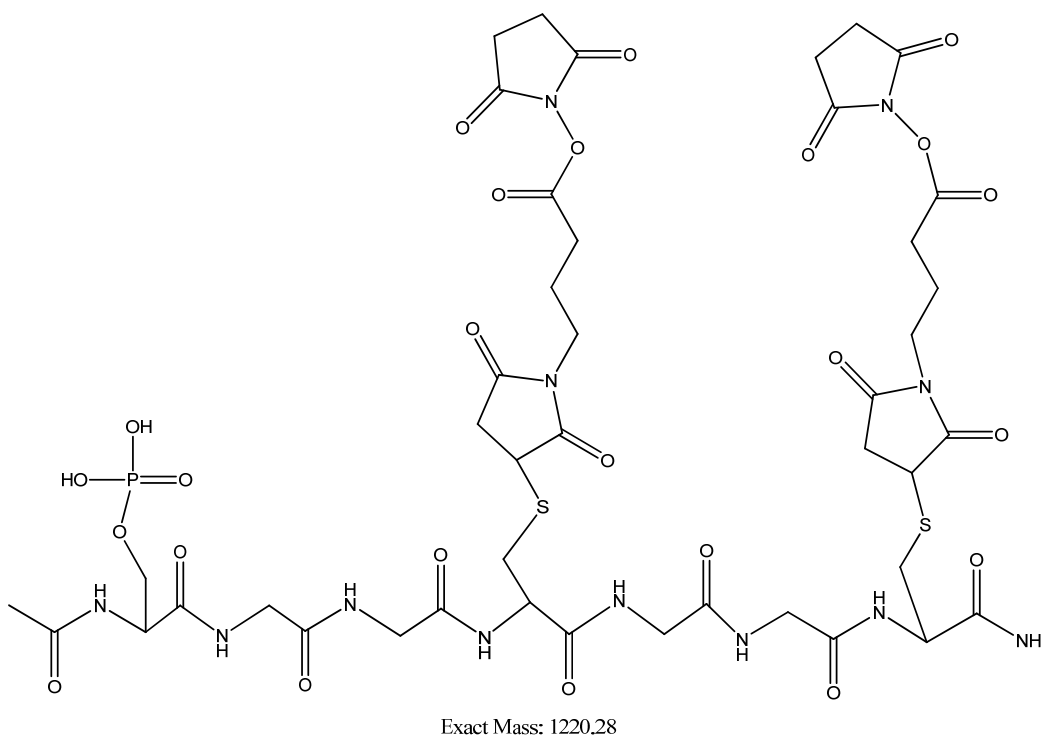


Figure 5.5. Structure of cross-linker II.

SubP intramolecularly cross-linked with this novel cross-linker was spiked into an apomyoglobin tryptic digest and subjected to ZrO₂ and TiO₂ enrichment. Initially, +36 Da mass addition of subP cross-linked product was observed. Further analysis demonstrated that this mass addition can be avoided by manipulating the pH immediately

following the elution process. Therefore, eluted cross-linked product solutions from $\text{TiO}_2/\text{ZrO}_2$ enrichment were promptly neutralized. A comparison of C_{18} Ziptip, ZrO_2 , and TiO_2 treatment of intramolecularly cross-linked subP in an apomyoglobin tryptic digest background is shown in Figure 5.6. Most apomyoglobin tryptic peptides, highlighted in the top panel of Fig. 5.6, were removed by TiO_2 and ZrO_2 treatment, particularly in the case of TiO_2 . By contrast, subP cross-linked product, both in triply- and doubly-deprotonated form (peak 1 and 3, respectively), was detected following TiO_2 and ZrO_2 treatment. A deactivated form of the cross-linker (due to addition of amine groups from ammonium bicarbonate) was also observed and the corresponding structure is shown in Figure 5.7.

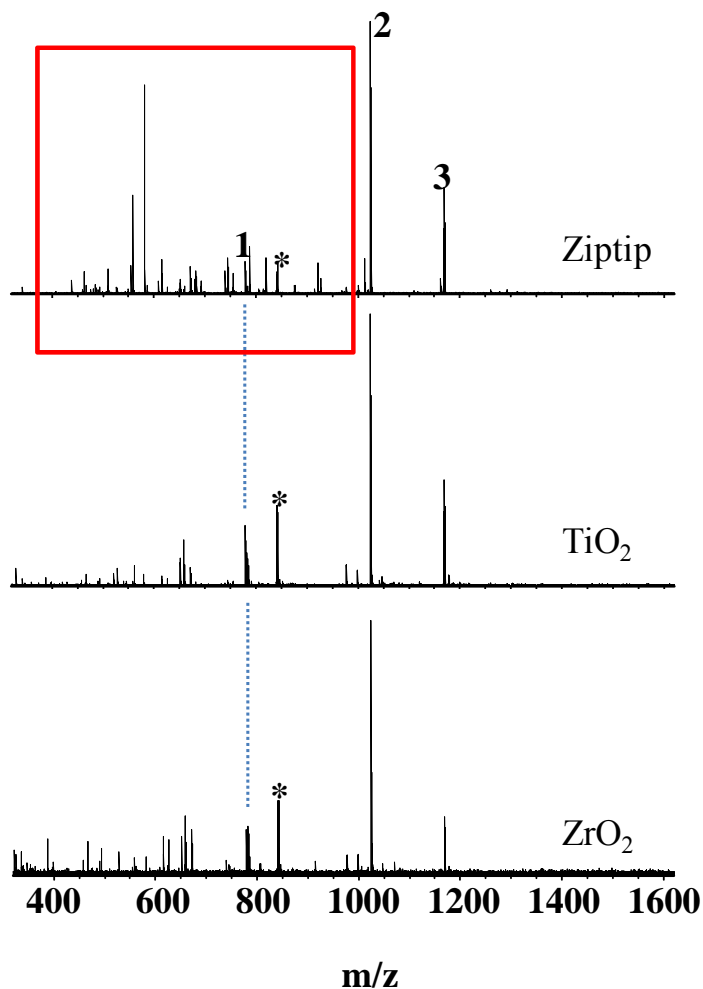


Figure 5.6. Comparison of Ziptip (top), TiO₂ (middle), and ZrO₂ (bottom) treatment of intramolecularly cross-linked product from subP with cross-linker II. 1: triply-deprotonated subP cross-linked product; 2: product (see Fig. 5.7) of reaction between the cross-linker and ammonium bicarbonate; 3: doubly-deprotonated cross-linked subP product. *=unidentified peak.

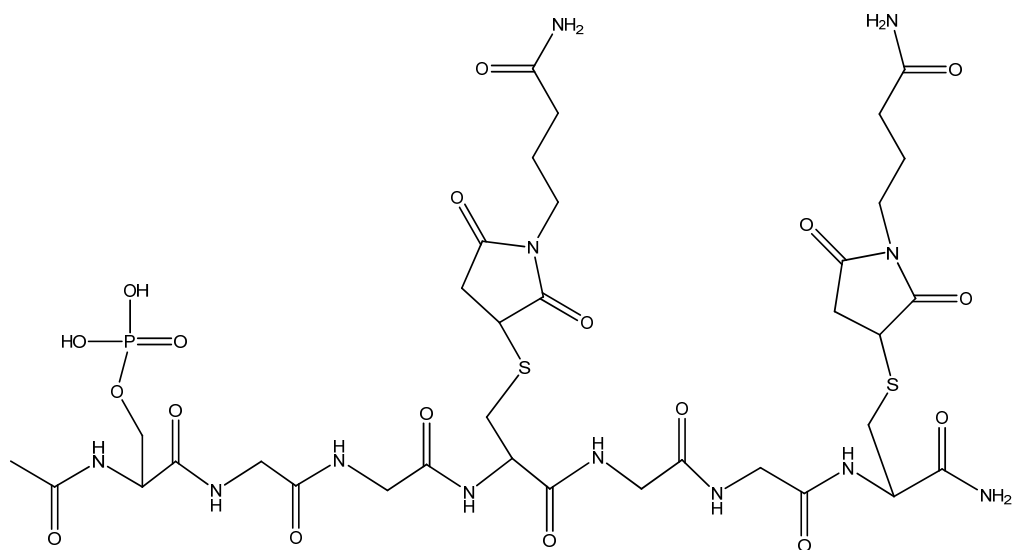


Figure 5.7. Deactivated cross-linker II from reaction with ammonium bicarbonate.

In CID of intramolecularly cross-linked subP (Figure 5.8), C-S bond cleavages on the reduced maleimide moiety were observed whereas neutral loss (- 98 Da) from phosphoserine, ubiquitous in low-energy (positive [15] and negative [16] ion mode) and high-energy CID [17, 18], was absent. Efficient C-S bond cleavage in negative ion CID, along with prominent disulfide bond cleavage, has been previously reported [19]. In CID of subP intramolecularly cross-linked with cross-linker II, heterolytic C-S bond cleavage at both maleimide groups generated the free peptide II (peak 2, Figure 5.8). A peak 34 Da lower can be generated by subsequent C-S bond cleavage, resulting in SH₂ loss, as shown in the scheme in Figure 5.8, to yield a vinyl group on one of the cysteine residues (peak 4 in Fig. 5.8). Alternatively, this species can be generated by direct C-S bond cleavage on the other side of the sulfur. These data reveal that the C-S bond of the reduced maleimide group, at least under certain circumstances, is more labile than the phosphodiester bond in negative ion CID, a phenomenon that, to our knowledge, has not

previously been reported.

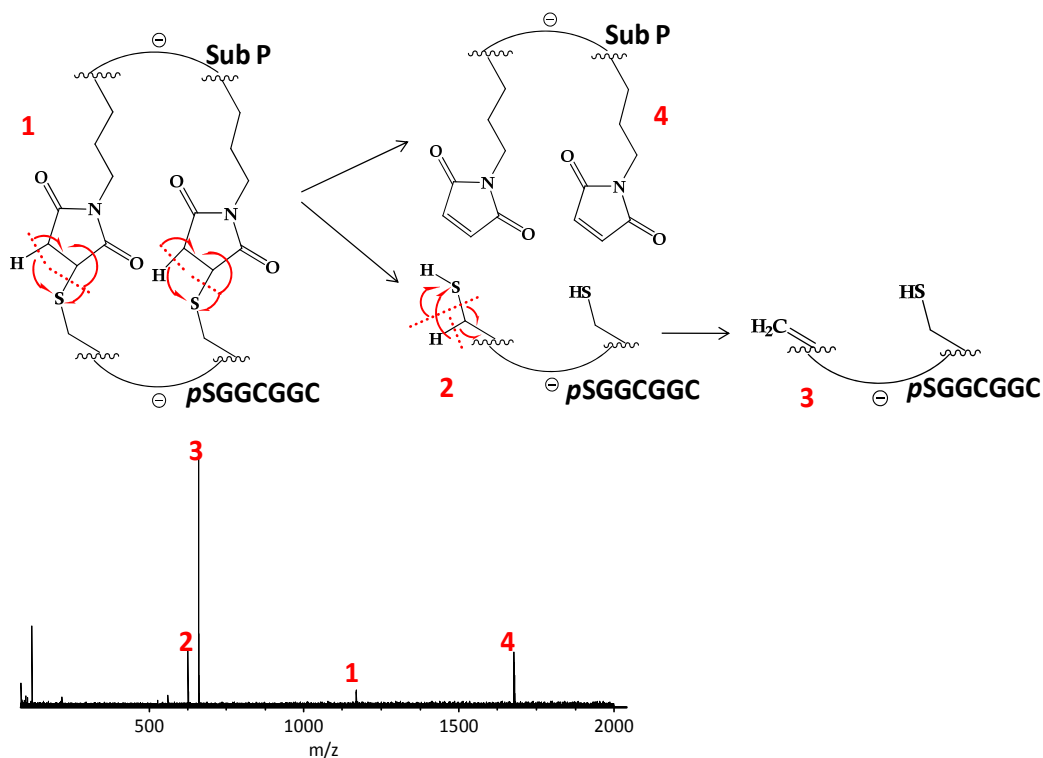


Figure 5.8. Negative ion CID of doubly deprotonated subP cross-linked with cross-linker II (peak 1). C-S bond cleavage on the reduced maleimide group is observed to yield products 2-4 as shown in the upper Scheme. Peaks 2-4 all correspond to singly charged ions.

5.4 Summary

In this Chapter, two peptide-based cross-linkers were designed to include a phosphate group and two amine reactive (NHS) groups. The purpose of adding the phosphate group was to allow cross-linked product enrichment with metal dioxides.

Results show that the distance between the phosphate group and NHS groups is crucial for enrichment. For the smaller cross-linker I, TiO₂/ZrO₂ enrichment was unsuccessful, presumably due to steric effects in which phosphoserine in cross-linked peptides was hindered from interacting with the metal oxide surface. For the large cross-linker II, in which phosphoserine is located further from the two NHS groups, TiO₂/ZrO₂ enrichment for intramolecularly cross-linked subP was demonstrated. However, cross-linker II did not demonstrate intermolecular cross-linking (e.g., for MSH). Future work would focus on further improving the cross-linker design, as discussed in Chapter 8.

5.5 References

1. Sinz, A., Chemical cross-linking and mass spectrometry to map three-dimensional protein structures and protein-protein interactions. *Mass Spectrom. Rev.*, **2006**, *25*, 663-682.
2. Schilling, B.; Row, R.H.; Gibson, B.W.; Guo, X.; Young, M.M., MS2Assign, automated assignment and nomenclature of tandem mass spectra of chemically crosslinked peptides. *J. Am. Soc. Mass Spectrom.*, **2003**, *14*, 834-850.
3. Rinner, O.; Seebacher, J.; Walzthoeni, T.; Mueller, L.; Beck, M.; Schmidt, A.; Mueller, M.; Aebersold, R., Identification of cross-linked peptides from large sequence databases. *Nat. Methods.*, **2008**, *5*, 315-318.
4. Lomant, A.J.; Fairbanks, G., Chemical Probes of Extended Biological Structures - Synthesis and Properties of Cleavable Protein Cross-Linking Reagent [Dithiobis(Succinimidyl-S-35 Propionate). *J. Mol. Biol.*, **1976**, *104*, 243-261.
5. Chowdhury, S.M.; Munske, G.R.; Tang, X.T.; Bruce, J.E., Collisionally activated dissociation and electron capture dissociation of several mass spectrometry-identifiable chemical cross-linkers. *Anal. Chem.*, **2006**, *78*, 8183-8193.
6. Soderblom, E.J.; Goshe, M.B., Collision-induced dissociative chemical cross-linking reagents and methodology: Applications to protein structural characterization using tandem mass spectrometry analysis. *Anal. Chem.*, **2006**, *78*, 8059-8068.
7. Lu, Y.L.; Tanasova, M.; Borhan, B.; Reid, G.E., Ionic Reagent for Controlling the

- Gas-Phase Fragmentation Reactions of Cross-Linked Peptides. *Anal. Chem.*, **2008**, *80*, 9279-9287.
8. Trester-Zedlitz, M.; Kamada, K.; Burley, S.K.; Fenyo, D.; Chait, B.T.; Muir, T.W., A modular cross-linking approach for exploring protein interactions. *J. Am. Chem. Soc.*, **2003**, *125*, 2416-2425.
 9. Ahrends, R.; Kosinski, J.; Kirsch, D.; Manelyte, L.; Giron-Monzon, L.; Hummerich, L.; Schulz, O.; Spengler, B.; Friedhoff, P., Identifying an interaction site between MutH and the C-terminal domain of MutL by crosslinking, affinity purification, chemical coding and mass spectrometry. *Nucleic Acids Res.*, **2006**, *34*, 3169-3180.
 10. Kweon, H.K.; Hakansson, K., Selective zirconium dioxide-based enrichment of phosphorylated peptides for mass spectrometric analysis. *Anal. Chem.*, **2006**, *78*, 1743-1749.
 11. Lubeck, M.; Hartmer, R.; Brekenfeld, A.; Baessmann, C., Combining novel fragmentation and front end enrichment techniques for highly increased sensitivity and selectivity of phosphopeptide detection. *Mol. Cell. Proteomics*, **2005**, *4*, S306-S306.
 12. Cantin, G.T.; Shock, T.R.; Park, S.K.; Madhani, H.D.; Yates, J.R., Optimizing TiO₂-based phosphopeptide enrichment for automated multidimensional liquid chromatography coupled to tandem mass spectrometry. *Anal. Chem.*, **2007**, *79*, 4666-4673.
 13. Senko, M.W.; Canterbury, J.D.; Guan, S.H.; Marshall, A.G., A high-performance modular data system for Fourier transform ion cyclotron resonance mass spectrometry. *Rapid Commun. Mass Spectrom.*, **1996**, *10*, 1839-1844.
 14. Ledford, E.B.; Rempel, D.L.; Gross, M.L., Space-Charge Effects in Fourier-Transform Mass-Spectrometry - Mass Calibration. *Anal. Chem.*, **1984**, *56*, 2744-2748.
 15. Bateman, R.H.; Carruthers, R.; Hoyes, J.B.; Jones, C.; Langridge, J.I.; Millar, A.; Vissers, J.P.C., A novel precursor ion discovery method on a hybrid quadrupole orthogonal acceleration time-of-flight (Q-TOF) mass spectrometer for studying protein phosphorylation. *J. Am. Soc. Mass Spectrom.*, **2002**, *13*, 792-803.
 16. Tholey, A.; Reed, J.; Lehmann, W.D., Electrospray tandem mass spectrometric studies of phosphopeptides and phosphopeptide analogues. *J. Mass Spectrom.*, **1999**, *34*, 117-123.
 17. Annan, R.S.; Carr, S.A., Phosphopeptide analysis by matrix-assisted laser desorption time-of-flight mass spectrometry. *Anal. Chem.*, **1996**, *68*, 3413-3421.
 18. Bennett, K.L.; Stensballe, A.; Podtelejnikov, A.V.; Moniatte, M.; Jensen, O.N., Phosphopeptide detection and sequencing by matrix-assisted laser desorption/ionization quadrupole time-of-flight tandem mass spectrometry. *J. Mass Spectrom.*, **2002**, *37*, 179-190.
 19. Chrisman, P.A.; McLuckey, S.A., Dissociations of disulfide-linked gaseous polypeptide/protein anions: Ion chemistry with implications for protein identification and characterization. *J. Proteome Res.*, **2002**, *1*, 549-557.

Chapter 6

Improved Detection of Ions below m/z 700 with Quadrupole Fractionation (QF) in Hybrid Q-FT-ICR Mass Spectrometry

6.1 Introduction

6.1.1 Linear Quadrupole

The development of the linear quadrupole for mass spectrometric analysis can be traced back to the late 1950s [1]. Since then, the linear quadrupole has also been established as a key component in hybrid mass spectrometers to serve as mass selector [2], ion guide [3], and ion storage device [4]. In addition, the theory concerning ion motion and stability in a linear quadrupole lead to the development of the three-dimensional quadrupole ion trap, which is used in a wide range of applications [5].

Both DC voltage (U) and alternating voltage (with amplitude V_{RF}) are applied to the four rods of a linear quadrupole in a pair wise manner: two opposing quadrupole rods bear the potential $(U + V_{RF}\cos\omega t)$ and the other pair has the potential $-(U + V_{RF}\cos\omega t)$. Ion motion and stability within the quadrupole can be described by the Mathieu equation:

$$\frac{d^2u}{d\xi^2} + [a_u + 2q_u \cos 2\xi]u = 0$$

$$a_x = -a_y = \frac{8zeU}{\omega^2 r_0^2 m}$$

$$q_x = -q_y = \frac{4zeV_{RF}}{\omega^2 r_0^2 m}$$

$$\xi = \frac{\omega t}{2}$$

in which u represents the Cartesian coordinates x or y , z is an integer, e is the elementary charge, r_0 is the radius inscribed by the quadrupole rods, and m is the ion mass.

At specific values of U and V_{RF} , ions of particular m/z values can follow either stable or unstable trajectories within the quadrupole [6]. When the amplitude of an ion trajectory is continuously confined between the quadrupole rods in both the x - and y -direction, the ion can travel through the quadrupole. If U and V_{RF} are such that the ion motion is unstable, ions will collide with the quadrupole rods or exit between them and thus do not make it through the quadrupole [7].

The concept of stable and unstable ion trajectories as function of ion m/z value can be utilized to achieve several goals in mass spectrometry. First, by ramping U and V_{RF} , ions with increasing m/z values can reach the other end of the quadrupole and be detected in an m/z -dependent manner to generate a mass spectrum with a specific m/z range (depending on the initial and final U/V_{RF} values). Here, the quadrupole performs as a mass analyzer [8]. Second, if U and V_{RF} are fixed, only ions within a specific m/z region will undergo stable motion and thus the quadrupole serves as a mass selector, e.g., for subsequent tandem mass spectrometry (MS/MS) experiments. The linear quadrupole can also function in radio frequency (RF)-only mode to serve as an ion guide for a wide m/z range of ions, or, in combination with axial electrodes, as an “ion bottle” for trapping

of ions prior to subsequent MS analysis [9, 10]. The RF-only quadrupole can also be used as a collision cell for confining product ions in MS/MS experiments based on collision induced dissociation (CID) [10] although higher order multipoles are typically preferred for ion storage due to their higher storage capacity and better focusing abilities [11].

6.1.2 Linear Quadrupole and FT-ICR MS

Since the first introduction in 1974 [12], FT-ICR mass spectrometry has become a powerful tool for the detection and characterization of biomolecules by providing sub-ppm mass measurement accuracy [13] and resolving power exceeding 10^6 [14]. The success of FT-ICR MS relies on tremendous advances in various related areas, including the development of the ICR cell [15-18], refining the methods for ion excitation and detection [19-21], the coupling of “soft-ionization” sources including electrospray ionization ESI [22] and matrix-assisted laser desorption/ionization MALDI [23], and the introduction of external ion accumulation in a multipole [24]. The latter development serves three main functions: 1) it alleviates the conflict between the pulsed nature of FT-ICR mass analysis and the continuous ion generation from an ESI source, 2) it allows a high duty cycle to be maintained despite the time requirement for high resolution FT-ICR MS, and 3) it allows efficient transfer and injection of ions from atmospheric pressure into high vacuum.

Interfacing of a linear quadrupole mass filter with an FT-ICR mass analyzer equipped with multipole external ion accumulation extends the latter concept to mass-selective external ion accumulation, which provides further improvements in sensitivity

and dynamic range for ion detection [25]. In addition, the quadrupole can provide external, rapid selection of precursor ions with a specific m/z value for subsequent MS/MS analysis in the ICR cell, e.g., sustained off-resonance irradiation (SORI) CID [26], electron capture dissociation [27], or infrared multiphoton dissociation [28]. Hendrickson *et al.* [29] demonstrated that more compounds can be detected from crude oil by quadrupole fractionation (QF) of an FT-ICR mass spectrum into 30-40 m/z slices by use of an external quadrupole-octopole interface. Similarly, QF has been applied to improve protein detection with signal-to-noise (S/N) ratio increasing from 4 to >200-fold and ~24-fold on average [30]. Further, QF-based FT-ICR analysis has been applied to metabolite detection and shown to increase peak abundances up to five fold [31]. When using external ion accumulation in a multipole, it is important to ensure that ions are accumulated and transferred to the ICR cell without m/z bias. Efforts to understand m/z -related discrimination during external multipole accumulation have been made both experimentally and theoretically [32-34].

In this chapter, we investigated the detection of proteolytic peptides as well as cross-linked peptides by applying the QF approach. Improved detection was observed in both cases, particularly in the low m/z region (350-600). These discoveries are helpful for understanding ion motion in a quadrupole-hexapole interface and provide an option for improving detection of ions with low m/z value.

6.2 Experimental

Horse heart myoglobin, *apo*-myoglobin, and bovine serum albumin (BSA) were

purchased from Sigma (St. Louis, MO) and used without further purification. Trypsin was purchased from Promega (Madison, WI) and chymotrypsin, and GluC were from Sigma. Enzymes were used at either 100 ng/ μ L (trypsin and GluC) or 50 ng/ μ L (chymotrypsin). The temperature for trypsin and GluC digestion was 37 °C and RT was used for chymotrypsin digestion. The time for all digestions was 12-15 h. All proteolysis experiments were quenched by adding 0.1% (v/v) formic acid.

Approximately 300 pmol of BSA was analyzed both with and without incubated with 10 μ L 10mM dithiothreitol (DTT) at 56°C for 1h to achieve disulfide bond reduction. After cooling down to room temperature (RT), the mixture was incubated with 10 μ L 100 mM iodoacetamide (IAA) 1h in the dark at RT for alkylation. Both variants of the protein were digested with 4 μ L 100 ng/ μ L trypsin. *apo*-myoglobin was digested with three different enzymes, including trypsin, chymotrypsin, and GluC. Peptides from the three different types of proteolysis were mixed together. Horse heart myoglobin was chemically cross-linked with bis(sulfosuccinimidyl)suberate (BS3) by mixing protein:cross-linker at a 1:100 molar ratio and reacting at RT for 30 minutes. The reaction was quenched by adding 1M NH_4HCO_3 , the protein was then denatured by heating at 100 °C for ~10 minutes and digested with trypsin for cross-linked peptide detection. Sample concentrations were adjusted to ~0.3 μ M by adding $\text{CH}_3\text{CN}:\text{H}_2\text{O}:\text{HCOOH}$ (49.95:49.95:0.1 volume ratio) for positive ESI mode and $\text{CH}_3\text{CN}:\text{H}_2\text{O}$ (1:1 volume ratio) or $\text{MeOH}:\text{H}_2\text{O}:\text{NH}_4\text{OH}$ (49.9:49.9:0.2 volume ratio) for negative ESI mode. Samples were analyzed on a 7 Tesla ESI-Q-FT-ICR mass spectrometer (Bruker Daltonics, Billerica, MA) at a flow rate of 70 μ L/h. Quadrupole fractionation was performed by collecting spectra from m/z 300 to 1250 at 50 m/z

intervals. Direct infusion (DI) was carried out by maintaining all parameters the same as with QF except for omitting the isolation windows (here, the quadrupole operated in RF-only mode). The number of scans for acquiring spectra was either the same in QF and RF-only analysis, or a larger number was used in DI to proportionally compensate for the extra time needed for QF analysis. For data analysis, only peptides with a monoisotopic peak S/N ratio greater than three were considered. CID was applied, if necessary, to ensure the identity of cross-linked peptides and tryptic peptides. LC/MS of tryptic peptides was performed with an Agilent 1100 HPLC interfaced to the FT-ICR instrument and equipped with a 1 mm×15 cm C₁₈ column.

6.3 Results and Discussion

6.3.1 Improved Detection of Non-cross-linked Peptides by QF

In DI of BSA tryptic peptides without DTT/IAA treatment, 14 peptides were observed after summing three FT-ICR transients. These peptides were identified by accurate mass and confirmed by CID to correspond to a sequence coverage of 22%. Following QF of the same sample with 50 m/z slices and three scans per spectrum (as in DI above), 31 peptides were identified and confirmed by CID, corresponding to a sequence coverage of 41%. The identities of peptides observed in DI and QF analysis are summarized in Table 6.1. 18 more peptides were found with quadrupole fractionation of which 14, as indicated by parentheses in Table 6.1, were detected with a mass less than 700 Da, indicating that QF is particularly valuable for detection of small peptides.

Table 6.1. BSA (without DTT/IAA treatment) tryptic peptides identified in QF and DI analysis, respectively.

Peptides Identified in QF	Peptides Identified in DI
(25-28)	
(37-44)	
66-75	66-75
(152-155)	
(157-160)	
161-167	161-167
169-183	
(223-228)	
(229-232)	
(242-245)	
(246-248)	
249-256	249-256
257-263	257-263
281-285	281-285
319-336	319-336
347-359	
360-371	360-371
402-412	402-412
	413-420
421-433	421-433
(434-436)	
437-451	437-451
438-451	
(452-455)	
(456-459)	
(490-495)	
524-528	524-528
(548-557)	
549-557	549-557
562-568	562-568
(569-580)	
598-607	

For BSA treated with DTT/IAA prior to trypsin digestion, 25 peptides were identified and confirmed by CID in direct infusion analysis whereas 31 peptides were observed with QF. Similar to untreated BSA, DI and QF spectra were both obtained with three scans per spectrum. LC/MS was also carried out for peptide identification.

Identified peptides in DI, QF, and LC/MS are shown in Table 6.2. Example spectra are shown in Figure 6.1, which displays the m/z region of two tryptic peptides with m/z values lower than 450, including $Y^{434}TR^{436}$ (panel a) and $L^{483}CVLHEK^{489}$ (panel b). Both these peptides are undetectable in DI but show observable signals with QF. Two other peptides, $K^{548}QTALVELLK^{557}$ (panel c) and $A^{236}WSVAR^{241}$ (panel d), are observed in both DI and QF modes but with enhanced S/N ratio in the latter case. Among the eight additional peptides identified with quadrupole fractionation, only two were singly protonated ions. The lack of small peptides may be due to losses in the C_{18} Ziptip desalting treatment, which was necessary for the DTT/IAA treated sample. The sequence coverage with DI and QF were 59% and 72%, respectively. The sequence coverage in LC/MS of BSA tryptic peptides following DTT/IAA treatment was 60% (peptides were identified by accurate mass only). The results for DTT/IAA-treated BSA are summarized in Figure 6.2. The sequence coverage obtained from LC/MS is unexpectedly low. This behavior may be due to a non-optimized LC method, including sample amount, column size, elution procedure, and detection parameters. Nevertheless, QF demonstrated an advantage over DI, particularly in the low m/z region.

Table 6.2. BSA (with DTT/IAA treatment) tryptic peptides that identified in QF and DI analysis

Peptides Identified in QF	Peptides Identified in DI	Peptides Identified in LC/MS
35-44	35-44	35-44
		45-65
66-75	66-75	66-75
89-100 (Cys_CAM99)*	89-100 (Cys_CAM99)	89-100 (Cys_CAM99)
106-138 (Cys_CAM125)		
118-138 (Cys_CAM125)	118-138 (Cys_CAM125)	
139-155 (Cys_CAM147)	139-155 (Cys_CAM147)	139-155 (Cys_CAM147)
161-167	161-167	
		168-183
184-204 (Cys_CAM191,192,200)	184-204 (Cys_CAM191,192,200)	
236-241		
249-256	249-256	
264-285	264-285	264-285
286-297 (Cys_CAM288)	286-297 (Cys_CAM288)	286-297 (Cys_CAM288)
298-309 (Cys_CAM301,302)	298-309 (Cys_CAM301,302)	
310-340 (Cys_CAM312,339)	310-340 (Cys_CAM312,339)	310-340 (Cys_CAM312,339)
347-359	347-359	347-359
360-371	360-371	360-371
375-401(Cys_CAM383,384,392)		375-401
402-412	402-412	402-412
413-433		413-433
421-433	421-433	
434-436		
437-451	437-451	437-451
		460-482 (Cys_CAM460,461,471)
469-482 (Cys_CAM471)	469-482 (Cys_CAM471)	
483-489		
499-507 (Cys_CAM499,500)	499-507 (Cys_CAM499,500)	
508-523 (Cys_CAM510)	508-523 (Cys_CAM510)	508-523 (Cys_CAM510)
		534-544 (Cys_CAM537)
529-544 (Cys_CAM537)	529-544 (Cys_CAM537)	
548-557	548-557	548-557
569-580	569-580	569-580
581-597 (Cys_CAM581,582)	581-597 (Cys_CAM581,582)	
598-607	598-607	598-607

*: The reduction and alkylation of given cysteine residue is indicated (e.g. Cys_CAM99: the thiol group on 99th cysteine is reduced and alkylated by applying DTT/IAA)

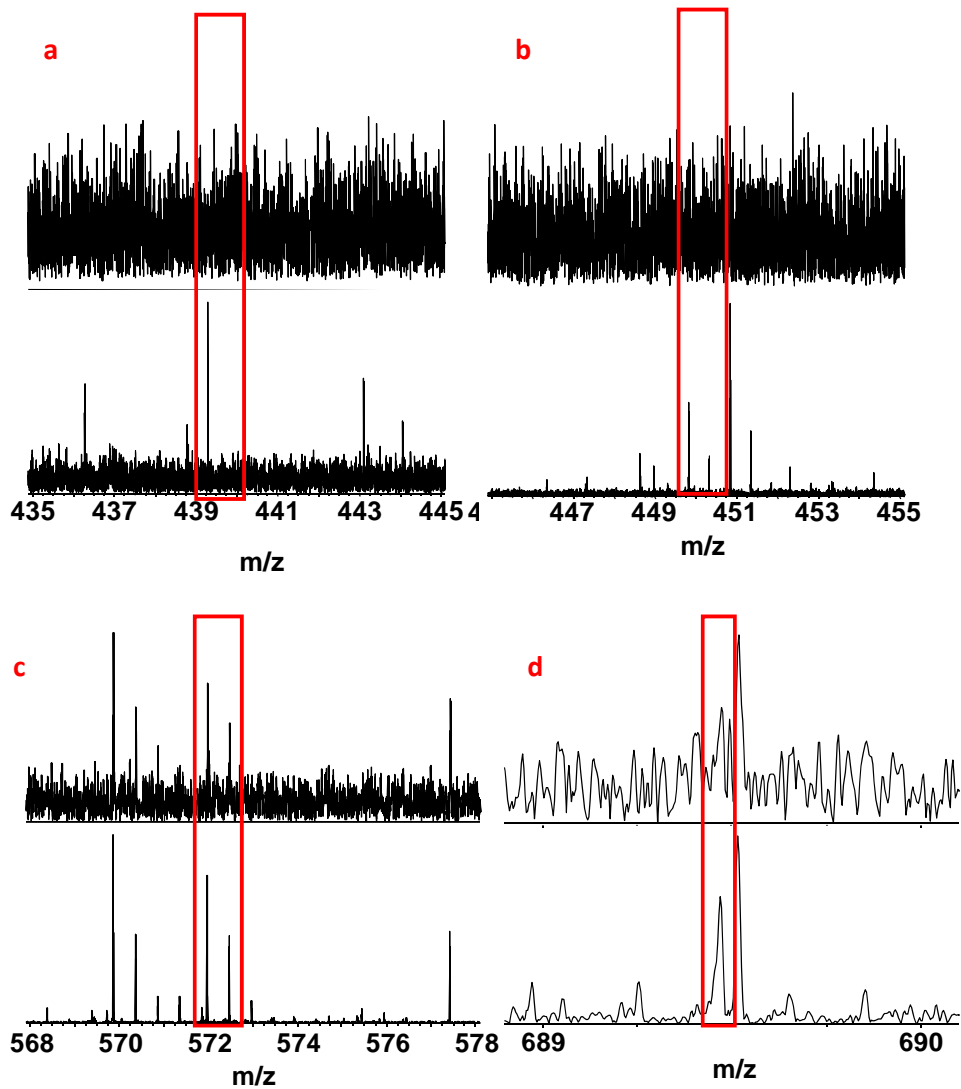


Figure 6.1. Improved BSA tryptic peptide detection by QF (top spectra in each panel) over DI (bottom spectra in each panel). Peptide sequences and charge states are: a) $[Y^{434}\text{-TR}^{436} + H]^+$; b) $[L^{483}\text{-*CVLHEK*^{489} + 2H]^{2+}$; c) $[K^{548}\text{-QTALVELLK}^{557} + 2H]^{2+}$; d) $[A^{236}\text{-WSVAR}^{241} + H]^+$. Modified cysteine residue (from carbamidomethylation) in b) is indicated by italic font and is underlined.

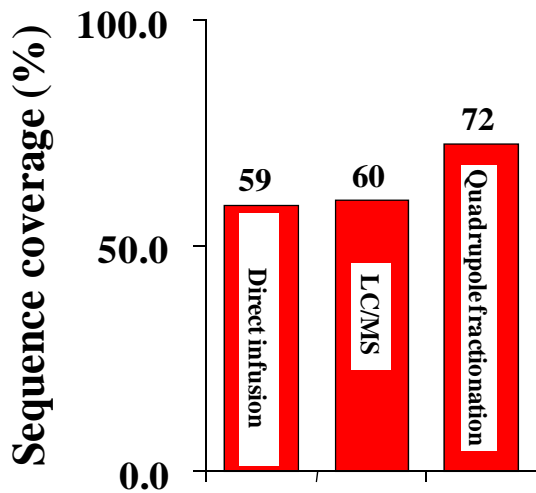


Figure 6.2. Sequence coverage of BSA obtained by DI, LC/MS, and by QF FT-ICR MS analysis.

6.3.2 Improved Detection of Cross-linked Peptides by QF

Cross-linked peptides obtained from reacting BS3 with myoglobin were subjected to DI and QF analysis, respectively. Two intramolecularly cross-linked peptides, SEDLK⁶²K⁶³HGTVVLTALGGILK and NDIAAK¹⁴⁵YK¹⁴⁷ELGFQG, were identified with DI and confirmed by CID. With QF, three more cross-linked species, FK⁴⁷HLK⁵⁰TEAEMK, LFTGHPETLEK⁴²FDK⁴⁵FK, and TEAEMK⁵⁶ASEDLK⁶²K were found based on accurate mass. The two former ones were confirmed by CID but the S/N ratio for the latter one was too low for CID. The corresponding mass spectra are shown in Figure 6.3.

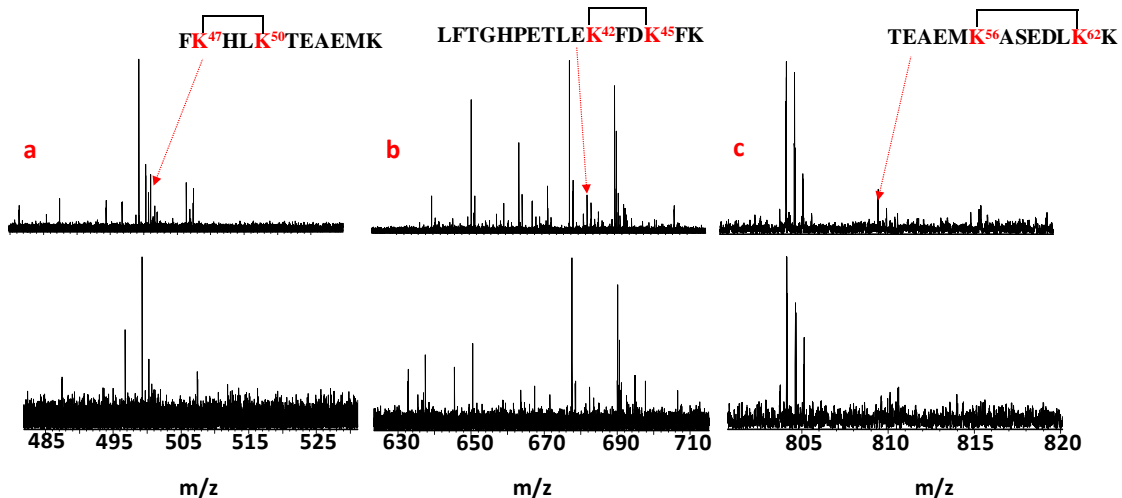


Figure 6.3. Three intramolecularly cross-linked peptides that were observed with QF (top spectra in column a-c) but not in DI (bottom spectra).

Based on the results above, QF can effectively increase S/N ratio and improve ion detection, particularly in the low m/z region (<700). However, it should be pointed out that these spectra were acquired with the same number of scans for QF and DI analysis. Because QF requires more time (n -fold longer than DI where $n =$ the number of m/z regions) than DI, this comparison may not be fair. Allowing additional time for signal averaging in DI analysis (to yield n -fold more scans) may compensate for the difference reported above in terms of S/N ratio between QF and DI. On the other hand, because QF seemed particularly useful in the low m/z region, further analysis of that area was performed, adjusting for the discrepancy in time between QF and DI.

6.3.3 Comparison of QF and DI after Compensating for the Extra Time Needed for QF

In the work presented in this section, QF spectra (in 50 m/z segments) were obtained by averaging three scans whereas DI spectra were acquired with 21 scans over the 350-700 m/z region, which seemed to benefit the most from QF based on the results presented above. Thus, the time taken to perform both experiments was the same. QF and DI spectral acquisition were compared by calculating the ratios of absolute peak abundances between QF and DI spectra. When three scans were used in both QF and DI, the ratio was scaled to compensate for the extra time required for QF. Although S/N ratio is known to increase as the square root of the number of scans [35], our data (see Figure 6.4 for an example) suggest that the absolute peak abundance achieved in DI is proportional to the number of scans (e.g., 2×10^6 for three scans and $\sim 4 \times 10^6$ for six scans). A summary for BSA tryptic peptides is shown in Fig. 6.4, in which most of the peak abundance ratios between 30 vs. three scans scatter around 10.

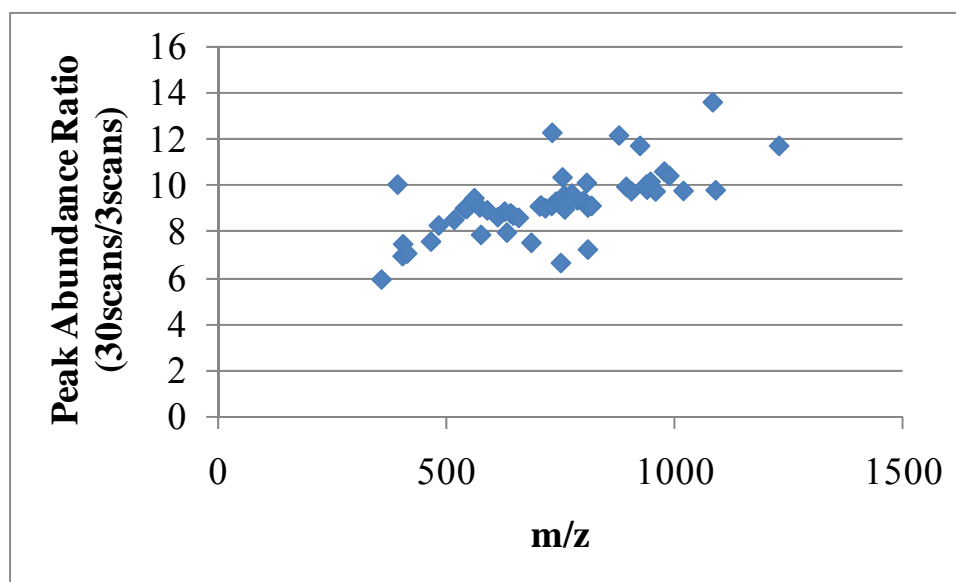


Figure 6.4. Ratios of peak abundances for BSA tryptic peptides from DI spectral acquisition with thirty vs. three scans, respectively.

We first compared QF and DI in positive ESI mode by using a mixture of apomyoglobin peptides from trypsin, chymotrypsin, and Glu C digestion, respectively. These results are shown in Figure 6.5 in which the ratios of peptide peak abundances between QF (three scans) and DI (21 scans) are plotted as function of m/z value. Significant signal enhancements by QF, ranging from 2-9 folds, are shown in the 350-500 m/z region, even when the extra time required for QF was compensated for. The five peptides that benefited the most from QF all have m/z values below 400, confirming that QF is particularly beneficial for low m/z ions.

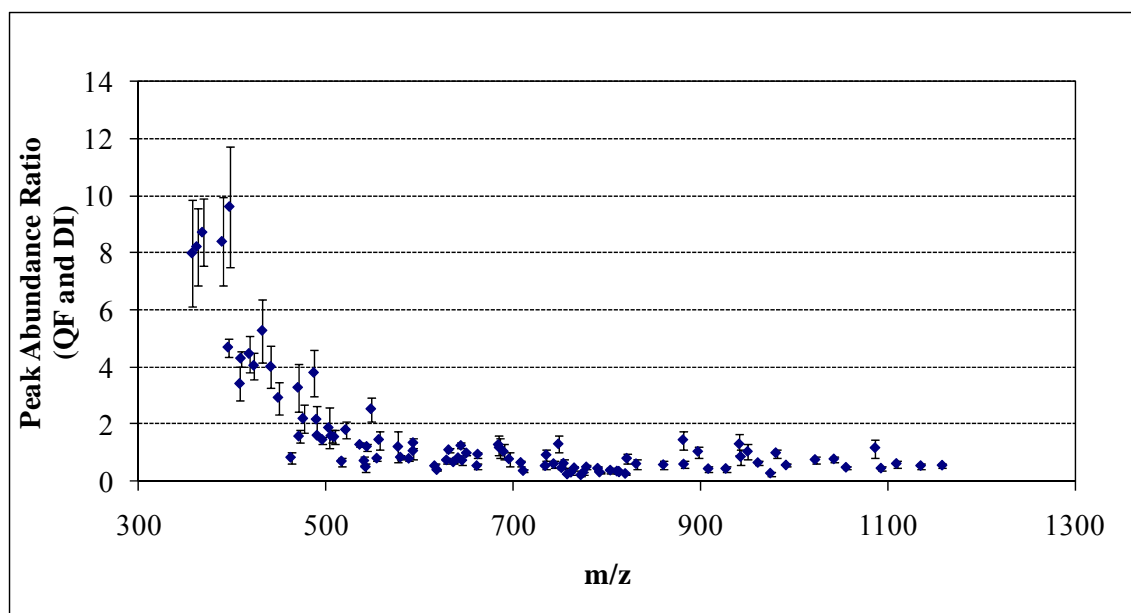


Figure 6.5. Ratio of peak abundances between QF (3 scans) and DI (21 scans) analysis of a peptide mixture in positive ESI mode. The mixture was obtained by digesting apomyoglobin with three enzymes (trypsin, chymotrypsin, and Glu C), respectively, and mixing the resulting peptides. Three replicates were carried out to obtain average and standard deviation.

QF and DI were also compared in negative ESI mode by analyzing the same peptide mixture generated from trypsin, chymotrypsin, and GluC digestion of apomyoglobin (panel A, Figure 6.6) and BSA digested with trypsin after DTT/IAA treatment (panel B, Figure 6.6). Both DI and QF spectra for negative ion mode analysis were obtained with three scans. Similar to positive mode ESI, signal enhancements in QF are observed in the low m/z area (350-600) but the enhancement ratios are lower than those in positive ESI, considering that the extra time required for QF was not compensated for in the negative ion mode experiments. Without compensation (which

biases towards QF, the enhancement ranged from 7-9 fold (for *apo*-myoglobin) and 5-11 fold (for BSA). If absolute peak abundance in negative ion mode is assumed to scale proportionally to the number of scans (as was observed in positive ion mode, Fig. 6.4), the enhancement after compensating for the extra time required for QF (a five-fold difference for the m/z region 350-600) would be 1.4-1.8 fold for myoglobin and 1-2.2 fold for BSA. Based on these calculations, we conclude that QF in negative mode ESI can also achieve signal enhancement but not as significantly as in positive mode ESI.

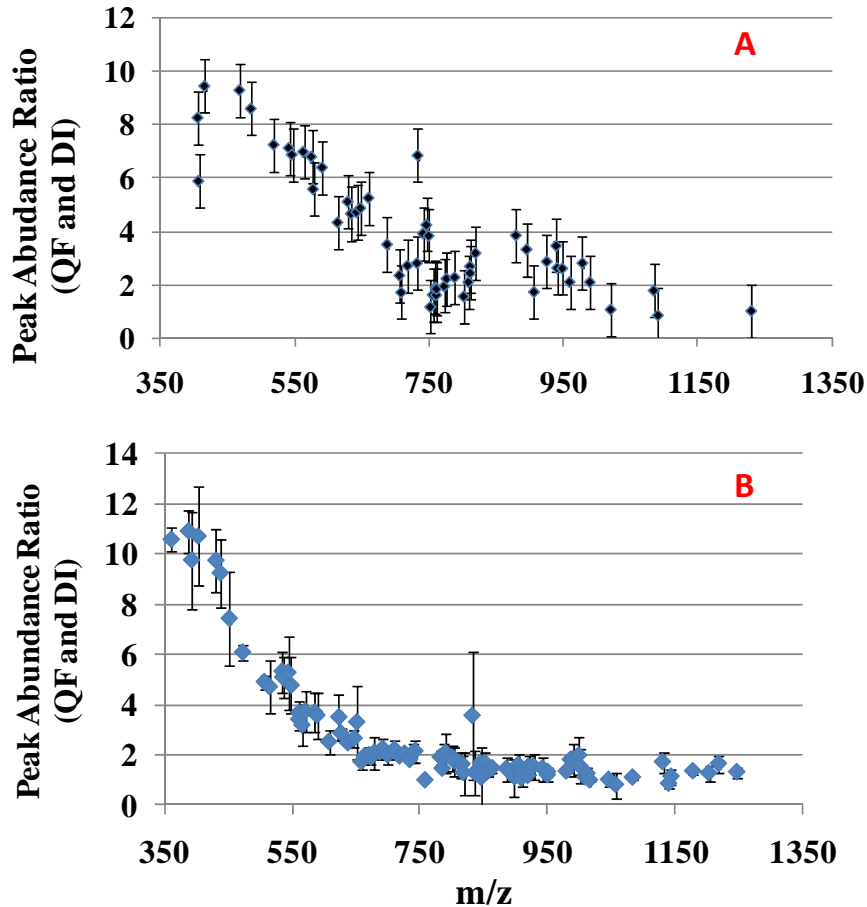


Figure 6.6. Ratio of peak abundances between negative ion mode QF and DI analysis of peptide mixtures obtained from three enzyme (trypsin, chymotrypsin, and Glu C)

digestion of *apo*-myoglobin (panel A) and reduced and alkylated BSA (panel B). Three replicates were carried out to obtain average and standard deviation.

Based on computer simulations and theoretical calculations of ion motion in RF-only multipole ion guides, ion distributions are “onion-like” with multiple cylindrical layers [32, 36]. Ions with higher charge at a specific mass are more radially confined than ions of lower charge. Likewise, at a specific charge, ions of lower mass are more radially confined than ions of higher mass. Thus low charge and high mass ions are more likely to be radially lost [32]. However, the comparison of QF and DI presented here demonstrates that ions with lower m/z values appear to be preferentially lost in DI analysis. This behavior may be explained by axial rather than radial ejection of such species during hexapole storage due to their higher axial kinetic energy. An alternative explanation may be that low m/z ions are radially lost during RF-only quadrupole transmission because they are closer to the low mass cut-off value than higher m/z ions.

6.4 Summary

In this chapter, comparisons between QF and DI detection of proteolytic peptides as well as cross-linked peptides were carried out. Signal enhancements were observed in QF analysis in the low m/z (350-600) region in both positive and negative ESI mode. In positive ion mode, 2-9 fold signal enhancements were obtained with QF after compensating for the 7-fold longer time required for QF (21 scans were used for DI and three scans for each QF slice). In negative ESI mode, lower enhancement, 1-2.2 fold,

was estimated after compensating for the longer time require for DI. These results cannot be explained based on previous computational experiments, which modeled radial oscillations of ions in RF-only multipoles as function of mass and charge. However, low m/z ions may still be axially lost due to their higher axial kinetic energy: in DI analysis, space charge repulsion from trailing higher m/z ions may cause this axial ejection. In QF analysis, space charge repulsion from higher m/z ions can be removed, thus providing a benefit for the detection of low m/z ions. Further studies of ion motion in RF-only and mass-selective quadrupole modes, including computer simulations, would be necessary to explaining the results in this Chapter. Nevertheless, QF is shown to improve ion detection in the low m/z region.

6.5 References

1. Paul, W.; Reinhard, H.P.; Vonzahn, U., Das Elektrische Massensfilter Als Massenspektrometer Und Isotopentrenner. *Z. Phys.*, **1958**, *152*, 143-182.
2. Brubaker, W.M.; Tuul, J., Performance Studies of Quadrupole Mass Filter. *Review of Scientific Instruments*, **1964**, *35*, 1007-&.
3. Iivonen, A.; Saintola, R.; Valli, K., Ion-guide Quadrupole Mass-spectrometer. *Phys. Scr.*, **1990**, *42*, 133-137.
4. Church, D.A., Storage-ring Ion Trap Derived from Linear Quadrupole Radio-frequency Mass Filter. *J. Appl. Phys.*, **1969**, *40*, 3127-&.
5. Douglas, D.J.; Frank, A.J.; Mao, D.M., Linear ion traps in mass spectrometry. *Mass Spectrom. Rev.*, **2005**, *24*, 1-29.
6. Du, Z.H.; Douglas, D.J.; Kononkov, N., Elemental analysis with quadrupole mass filters operated in higher stability regions. *J. Anal. At. Spectrom.*, **1999**, *14*, 1111-1119.
7. Douglas, D.J., Linear Quadrupoles in Mass Spectrometry. *Mass Spectrom. Rev.*, **2009**, *28*, 937-960.
8. Rutherford, S.I., Mass Filter Characteristics of a Quadrupole Analyzer. *J. Vac. Sci.*

- Technol.*, **1965**, 2, 281-&.
9. Dawson, P.H., Performance-Characteristics of an Rf Only Quadrupole. *Int. J. Mass Spectrom. Ion Processes*, **1985**, 67, 267-276.
 10. Campbell, J.M.; Collings, B.A.; Douglas, D.J., A new linear ion trap time-of-flight system with tandem mass spectrometry capabilities. *Rapid Commun. Mass Spectrom.*, **1998**, 12, 1463-1474.
 11. Sudakov, M.; Douglas, D.J., Linear quadrupoles with added octopole fields. *Rapid Commun Mass Spectrom*, **2003**, 17, 2290-2294.
 12. Comisaró, M.B.; Marshall, A.G., Fourier-Transform Ion-Cyclotron Resonance Spectroscopy. *Chem. Phys. Lett.*, **1974**, 25, 282-283.
 13. Conrads, T.P.; Anderson, G.A.; Veenstra, T.D.; Pasa-Tolic, L.; Smith, R.D., Utility of accurate mass tags for proteome-wide protein identification. *Anal. Chem.*, **2000**, 72, 3349-3354.
 14. Marshall, A.G.; Hendrickson, C.L., High-Resolution Mass Spectrometers. *Annu. Rev. Anal. Chem.*, **2008**, 1, 579-599.
 15. Hofstadler, S.A.; Laude, D.A., Isolated Dual Trapped Ion Cell Assembly for Fourier-Transform Ion-Cyclotron Resonance Mass-Spectrometry. *Anal. Chem.*, **1991**, 63, 2001-2007.
 16. Naito, Y.; Fujiwara, M.; Inoue, M., Improvement of the Electric-Field in the Cylindrical Trapped-Ion Cell. *Int. J. Mass Spectrom. Ion Processes*, **1992**, 120, 179-192.
 17. Frankevich, V.; Zenobi, R., Dynamic ion trapping in a cylindrical open cell for Fourier transform ion cyclotron resonance mass spectrometry. *Int. J. Mass spectrom.*, **2001**, 207, 57-67.
 18. Misharin, A.S.; Zubarev, R.A., Coaxial multi-electrode cell ('O-trap') for high-sensitivity detection at a multiple frequency in Fourier transform ion cyclotron resonance mass spectrometry: main design and modeling results. *Rapid Commun Mass Spectrom*, **2006**, 20, 3223-3228.
 19. Comisaró, M.B.; Marshall, A.G., Fourier-Transform Ion-Cyclotron Resonance Spectroscopy. *Chem. Phys. Lett.*, **1974**, 25, 282-283.
 20. Marshall, A.G.; Roe, D.C., Theory of Fourier-Transform Ion-Cyclotron Resonance Mass-Spectrometry .5. Response to Frequency-Sweep Excitation. *J. Chem. Phys.*, **1980**, 73, 1581-1590.
 21. Marshall, A.G.; Wang, T.C.L.; Ricca, T.L., Tailored Excitation for Fourier-Transform Ion-Cyclotron Resonance Mass-Spectrometry. *J. Am. Chem. Soc.*, **1985**, 107, 7893-7897.
 22. Henry, K.D.; Williams, E.R.; Wang, B.H.; McLafferty, F.W.; Shabanowitz, J.; Hunt, D.F., Fourier-Transform Mass-Spectrometry of Large Molecules by Electrospray Ionization. *Proc. Natl. Acad. Sci. U. S. A.*, **1989**, 86, 9075-9078.
 23. Hettich, R.L.; Buchanan, M.V., Investigation of Uv Matrix-Assisted Laser Desorption Fourier-Transform Mass-Spectrometry for Peptides. *J. Am. Soc. Mass Spectrom.*, **1991**, 2, 22-28.
 24. Senko, M.W.; Hendrickson, C.L.; Emmett, M.R.; Shi, S.D.H.; Marshall, A.G., External accumulation of ions for enhanced electrospray ionization Fourier transform ion cyclotron resonance mass spectrometry. *J. Am. Soc. Mass*

- Spectrom.*, **1997**, 8, 970-976.
25. Belov, M.E.N., E.N.; Anderson, G.A.; Udseth, H.R.; Conrads, T.P.; Veenstra, T.D.; Masselon, C.D.; Gorshkov, M.V.; Smith, R.D., Design and performance of an ESI interface for selective external ion accumulation coupled to a Fourier transform ion cyclotron mass spectrometer. *Anal. Chem.*, **2001**, 73, 253-261.
 26. Gauthier, J.W.; Trautman, T.R.; Jacobson, D.B., Sustained Off-Resonance Irradiation for Collision-Activated Dissociation Involving Fourier-Transform Mass-Spectrometry - Collision-Activated Dissociation Technique That Emulates Infrared Multiphoton Dissociation. *Anal. Chim. Acta*, **1991**, 246, 211-225.
 27. Zubarev, R.A.; Kelleher, N.L.; McLafferty, F.W., Electron capture dissociation of multiply charged protein cations. A nonergodic process. *J. Am. Chem. Soc.*, **1998**, 120, 3265-3266.
 28. Little, D.P.; Speir, J.P.; Senko, M.W.; O'Connor, P.B.; McLafferty, F.W., Infrared multiphoton dissociation of large multiply charged ions for biomolecule sequencing. *Anal. Chem.*, **1994**, 66, 2809-2815.
 29. Hendrickson, C.L.Q., J.P.; Emmett, M.R.; Marshall, A.G., Mass-Selective External Ion Accumulation for Fourier Transform Ion Cyclotron Resonance Mass Spectrometry. *49th ASMS Conference on Mass Spectrom and Allied Topics*, **2001**, Chicago, IL, May 27-31, 2001, CD-ROM
 30. Patrie, S.M.; Charlebois, J.P.; Whipple, D.; Kelleher, N.L.; Hendrickson, C.L.; Quinn, J.P.; Marshall, A.G.; Mukhopadhyay, B., Construction of a hybrid quadrupole/Fourier Transform Ion Cyclotron Resonance Mass Spectrometer for versatile MS/MS above 10 kDa. *J. Am. Soc. Mass Spectrom.*, **2004**, 15, 1099-1108.
 31. Southam, A.D.; Payne, T.G.; Cooper, H.J.; Arvanitis, T.N.; Viant, M.R., Dynamic range and mass accuracy of wide-scan direct infusion nanoelectrospray Fourier transform ion cyclotron resonance mass spectrometry-based metabolomics increased by the spectral stitching method. *Anal. Chem.*, **2007**, 79, 4595-4602.
 32. Tolmachev, A.V.; Udseth, H.R.; Smith, R.D., Radial stratification of ions as a function of mass to charge ratio in collisional cooling radio frequency multipoles used as ion guides or ion traps. *Rapid Commun Mass Spectrom*, **2000**, 14, 1907-1913.
 33. Belov, M.E.; Nikolaev, E.N.; Anderson, G.A.; Auberry, K.J.; Harkewicz, R.; Smith, R.D., Electrospray ionization-Fourier transform ion cyclotron mass spectrometry using ion preselection and external accumulation for ultrahigh sensitivity. *J. Am. Soc. Mass Spectrom.*, **2001**, 12, 38-48.
 34. Todd, J.F.J.; Waldren, R.M.; Freer, D.A.; Turner, R.B., The Quadrupole Ion Store (Quistor) .10. Space-Charge and Ion Stability .B. On the Theoretical Distribution and Density of Stored Charge in Rf Quadrupole Fields. *Int. J. Mass Spectrom. Ion Processes*, **1980**, 35, 107-150.
 35. Bayliss, M.A.; Evans, S.; Harris, F.M.; Parry, D.E., A computer-based method to increase the signal-to-noise ratio of negative-ion currents in double-charge-transfer spectroscopy. *Rapid Commun Mass Spectrom*, **1995**, 9, 1502-1506.
 36. March, R.E., An introduction to quadrupole ion trap mass spectrometry. *J. Mass Spectrom.*, **1997**, 32, 351-369.

Chapter 7

Characterization of Enzyme Function and Functional Differentiation in *Curacin A* and *Jamaicamide* Biosynthesis by FTICR MS and IRMPD

7.1 Introduction

Non-ribosomal peptide synthetases (NRPSs) and polyketide synthases (PKSs) are two enzyme families that catalyze the biosynthesis of a large number of natural products with great diversity in chemical structure and pharmacological potential, including antitumor [1], antimicrobial, and immunosuppressant properties [2]. Curacin A (Cur) is a mixed polyketide-nonribosomal peptide (PK-NRP) natural product isolated from the marine cyanobacterium *Lyngbya majuscula* with potential anti-tumor activity [3]. Biosynthesis of Cur relies on the catalysis of PKSs and NRPSs, in which substrates are covalently linked to a serine residue in a carrier protein through a phosphopantetheine (PPant) arm (Figure 7.1). Substrates in NRPS/PKS catalysis are subjected to various chemical reactions (e.g. dehydration and decarboxylation) and undergo chain elongation to form intermediates of increasing length. Eventually, Cur is released.

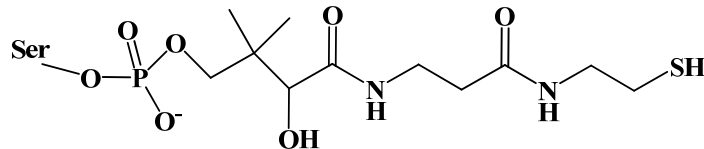


Figure 7.1. Chemical structure of PPant.

Like Cur, jamaicamide (Jam) is a mixed polyketide-nonribosomal peptide (PK-NRP) natural product isolated from the marine cyanobacterium *Lyngbya majuscula*. The structures of Cur and Jam, however, are rather different, as shown in Figure 7.2. Nevertheless, the Cur and Jam biosynthetic pathways have high homology, including dehydratases (ECH_{1s}), decarboxylases (ECH_{2s}), and enoyl reductases (ERs). Therefore, functional determination of enzymes in the Cur and Jam biosynthetic pathways provides key insight into the mechanism of natural product biodiversity. In addition, comparison of analogous enzyme components from the Cur and Jam biosynthetic pathways can provide insights into the evolution and environmentally driven adaptation of these biosynthetic enzymes at the biochemical rather than the genetic level.

In this Chapter, top-down and bottom-up FT-ICR MS and IRMPD experiments were performed to elucidate the functions of a GCN5-related *N*-acetyltransferase (GNAT) in the initiation module of Cur biosynthesis, Cur halogenase (Hal), ECH_{1s}, ECH_{2s}, and ERs from both the Cur and Jam biosynthetic pathways, and a sulfotransferase (ST) and thioesterase (TE) involved in release of mature Cur with a terminal double bond. The presence of Hal is not surprising in the Jam pathway because Jam contains a vinyl chloride group. Halogenation reactions have previously been studied in natural product

biosynthesis [4-7]. However, Cur does not contain a halogen group but intermediate chlorination may be involved in cyclopropane ring formation [4, 8]. Previous work from our group in collaboration with the Sherman lab revealed that Cur ECH₁ and ECH₂ catalyze dehydration and decarboxylation, respectively [9]. ER belongs to the acetyl-CoA NADPH-dependent reductase family and typically reduces α,β C=C bonds [10]. In this Chapter, IRMPD was applied to compare catalytic efficiency of Cur ER and Jam ER.

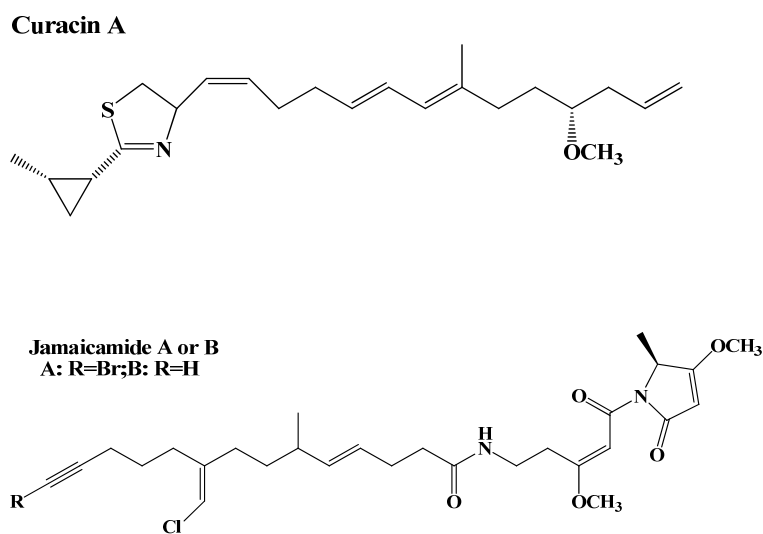


Figure 7.2. Chemical structures of Cur (top) and Jam (bottom).

Furthermore, with the aim to understand the Cur Hal catalytic mechanism based on crystal structures from different ligand binding states, IRMPD was applied to monitor the catalytic efficiency of wild type (WT) Cur Hal as well as a series of site-specific mutants.

acetyl transferase.

7.2.2 FT-ICR MS for Functional Analysis of Proteins from the Cur and Jam Pathways

Trypsin digestion for bottom-up analysis of the AR-GNAT-ACP tridomain was carried out by Dr. Gu. Mass spectrometric analysis was performed with an actively shielded 7 Tesla quadrupole-Fourier transform ion cyclotron resonance (FT-ICR) mass spectrometer (APEX-Q, Bruker Daltonics, Billerica, MA). Target analytes (peptides for the AR-GNAT-ACP tridomain) and intact ACPs for top-down analysis) were diluted with an electrospray solution (1:1 CH₃CN:H₂O with 0.1% HCOOH) and directly infused into an electrospray ionization (ESI) [11] source (Apollo II, Bruker Daltonics) at a flow rate of 70 µL/h and a voltage of - 3.8 kV. A counterflow of hot (240 °C) nitrogen gas was applied to assist desolvation of ESI droplets. For accurate mass determination in top-down analyses, up to 10 picomoles of apomyoglobin (Sigma, St. Louis, MO) was spiked into the ESI solution as internal calibrant. Multiply protonated ions generated from ESI were externally accumulated in a hexapole for 1 s and transferred via high voltage ion optics to the ICR cell for analysis. All data were acquired with XMASS software (version 6.1, Bruker Daltonics) in broadband mode from m/z = 200 to 2000 with 512k data points and summed over 20-30 scans. Mass spectra were analyzed with the MIDAS analysis software [12]. When needed, external frequency-to-m/z calibration was performed with a two-term calibration equation [13] using two calibration standards (m/z = 622.02895 and 922.00979, from the calibration mix G2421A, Agilent Technologies,

Palo Alto, CA). For infrared multiphoton dissociation (IRMPD), precursor ions were mass-selectively accumulated in a hexapole with a 3-5 m/z quadrupole isolation window, transferred to the ICR cell, and irradiated for 100-300 ms by 10.6 μm photons at 10 W laser power (25 W CO₂ laser, Synrad, Mukilteo, WA) for 30-50 scans. Unless specifically mentioned, top-down and IRMPD analyses of ACPs incubated with Cur AR-GNAT-ACP, ECH₁s, ECH₂s, and ERs from Cur and Jam, Cur Hal, and Cur ST and TE were all carried out in a similar manner.

7.2.3. IRMPD-based Quantification of Cur ER, Jam ER, and Cur Hal Catalytic Efficiency

The nomenclature and chemical structures of substrates and products from Hal, ECH₁, ECH₂, and ER catalysis are shown in Figure 7.4.

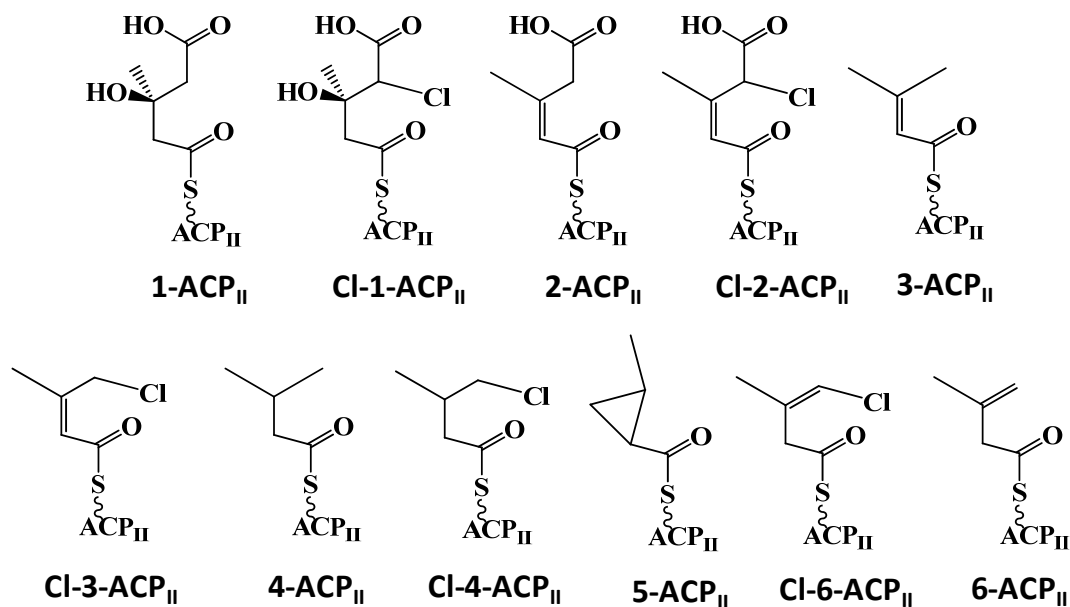


Figure 7.4. Nomenclature and chemical structures for substrates and products for Hal, ECH₁, ECH₂, and ER catalysis.

For ER analysis, the +12 charge state of ACP_{II}-bound intermediates was selected for IRMPD (mixture of substrate and product for saturation reactions and mixture of internal standard and product for cyclopropanation, as described below). Peak abundances of PPant ejection products generated by IRMPD [14] were measured to quantify the yields of Cur/Jam ER catalyzed α,β C=C saturation and cyclopropanation as function of reaction time. In a similar but time-independent approach, IRMPD peak abundances were measured to determine the catalytic efficiencies of wild type and mutant Cur Hal. However, for Hal, the entire charge state distribution was used for IRMPD.

For ER analysis, the ratio of PPant ejection products with a two Dalton mass difference (i.e., corresponding to unsaturated substrate and reduced product) was calculated from the abundance of n and $n + 2$ peaks with the $n + 2$ peak abundance adjusted by subtracting the calculated abundance for the second isotopic peak of the substrate. For the cyclopropanation reaction, an internal standard (**4**-ACP_{II}) was added to ensure unbiased precursor ion isolation of both ACP-bound product and the species used for relative quantification (**4**-ACP_{II} is only two Da heavier than the product from cyclopropanation (**5**-ACP_{II}), i.e., these two ions are only 0.2 m/z units apart in the +12 charge state (similar to substrate and product in saturation reactions) whereas the ACP_{II}-bound substrate, Cl-**3**-ACP, is 34 Da heavier than its cyclopropanation product and thus separated by 2.8 m/z units in the +12 charge state). An isolation window of 5 m/z units was used. IRMPD-based quantification methods were validated by mixing ACP_{II}-bound substrate and product at known ratios and performing IRMPD.

For Cur Hal analysis, IRMPD PPant ejection ions for the product and substrate

are observed at m/z 439.12 and 405.16, respectively. The peak abundance ratio of these two ejection products was used to estimate substrate (**1**-ACP_{II}) to product (Cl**1**-ACP_{II}) conversion efficiency in Cur Hal catalysis. Here, a single chlorine atom addition to the substrate is unlikely to influence ESI efficiency of the ACP-bound intermediate. Time course experiments were also carried out with WT Cur Hal as well as with single amino acid mutants, monitoring the IRMPD product ions at m/z 405 and 439.

7.3 Results and Discussion

7.3.1 Functional analysis of GNAT in the initiation module of CurA biosynthesis

Trypsin digested AR-GNAT-*holo*-ACP was characterized by FT-ICR and IRMPD. Here, AR refers to an N-terminal adaptor domain of unknown function. As shown in Figure 7.5, the PPant-modified 469-484 tryptic peptide (row B in Fig. 7.5) with the sequence ALMEMGIESLELLELR (containing Ser⁴⁷⁷, the known PPant loading site) was observed. By contrast, only the *apo*-peptide was observed for AR-GNAT-*apo*-ACP (row A in Fig. 7.5). PPant ejection from the AR-GNAT-*holo*-ACP active site peptide was observed in IRMPD (spectrum not shown). The observed and calculated masses of these tryptic peptides and their PPant ejection ions are listed in Table 7.1, bottom.

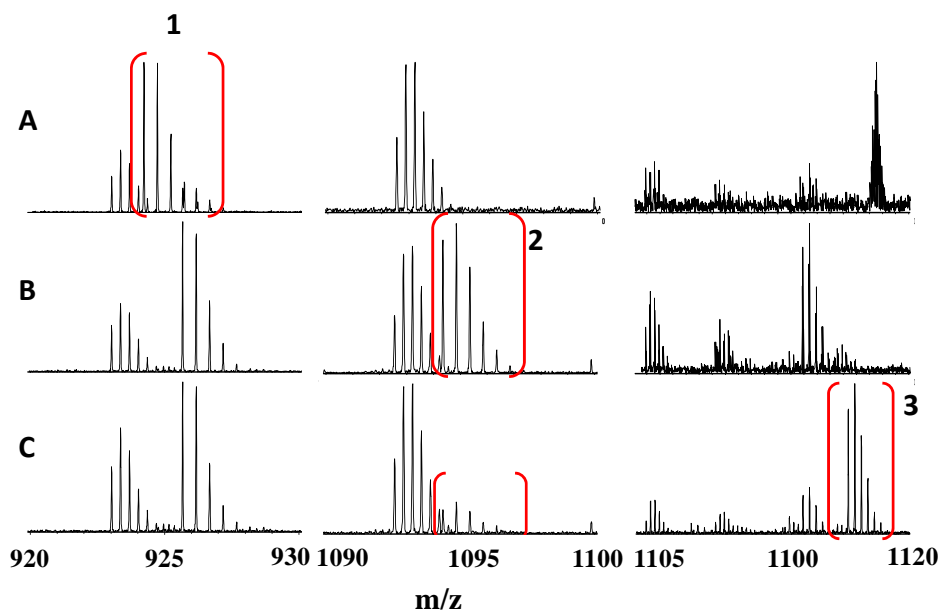


Figure 7.5. Partial FT-ICR mass spectra of trypsin digested AR-GNAT-ACP in *apo*- (row A) and *holo* form (row B) and after incubation with malonyl-CoA (row C). An unmodified doubly protonated peptide (469-484) and its modified counterpart (PPant loaded) were observed at position 1 and 2, respectively. Acetyl transfer product was observed in position 3.

Table 7.1. Precursor and PPant ejection ions observed in FT-ICR MS and IRMPD of *apo*- and *holo*-ACP before and after incubation with AR-GNAT-*apo*-ACP and acetyl- or malonyl-CoA, and of NH₂-ACP after incubation with AR-GNAT-*apo*-ACP and acetyl-CoA (top), and of the trypsin digested AR-GNAT-*apo/holo*-ACP tridomain before and after incubation with malonyl-CoA.

ACP samples				
ACP	ESI-FT-ICR-MS		IRMPD (PPant ejection product)	
	Obs. avg. mass	Calc. avg. mass	Obs. [M+H] ⁺	Calc. [M+H] ⁺
<i>apo</i> -ACP	10820.7	10821.1		
<i>holo</i> -ACP	11160.9	11160.7	261.128	261.127
acetyl-S-ACP	11202.5	11202.7	303.138	303.137
NH ₂ -ACP	11144.5	11144.7	244.166	244.166
acetyl-NH-ACP	11186.4	11186.7	NO	NO
AR-GNAT-ACP trypsin digestion samples				
[469-484 +2H] ²⁺	ESI-FT-ICR-MS		IRMPD (PPant ejection product)	
	Obs. mass	Calc. mass	Obs. [M+H] ⁺	Calc. [M+H] ⁺
<i>apo</i> -ACP	1845.97	1845.95		
<i>holo</i> -ACP	2186.05	2186.04	261.128	261.127
acetyl-ACP	2228.06	2228.05	303.138	303.137

The GNAT enzyme superfamily performs diverse functions in prokaryotes and eukaryotes by transferring an acetyl group to a primary amine at a specific step in diverse biosynthetic pathways [15]. In this Chapter, GNAT was revealed to transfer an acetyl group to a thiol group. This unprecedented function of GNAT was revealed by FT-ICR MS. As shown in Figure 7.6, acetyl transfer to *holo*-ACP-SH (PPant has free terminal thiol group) occurs following incubation with acetyl-CoA and AR-GNAT-*apo*-ACP: a product ion peak can be clearly observed at the + 42 Da position (acetyl transfer) relative to the substrate peak. AR-GNAT-*apo*-ACP can also perform its classical function, i.e.,

transferring an acetyl group to *holo*-ACP-NH₂ (in which the terminal SH group in PPant is replaced by an NH₂ group) but at low efficiency: in the right column of Figure 7.6, only trace amount of acetyl-NH-ACP is observed in the *m/z* area of + 42 Da. Acetyl-S-ACP, observed after incubation with AR-GNAT-*apo*-ACP (left column in Fig. 7.6) was subjected to IRMPD and the corresponding PPant ejection ion is shown in Figure 7.7. For acetyl-NH-ACP, the precursor ion signal was too weak for IRMPD. The observed and calculated masses of *apo*- *holo*- and acetyl-loaded ACPs and their PPant ejection ions are listed in Table 7.1, top.

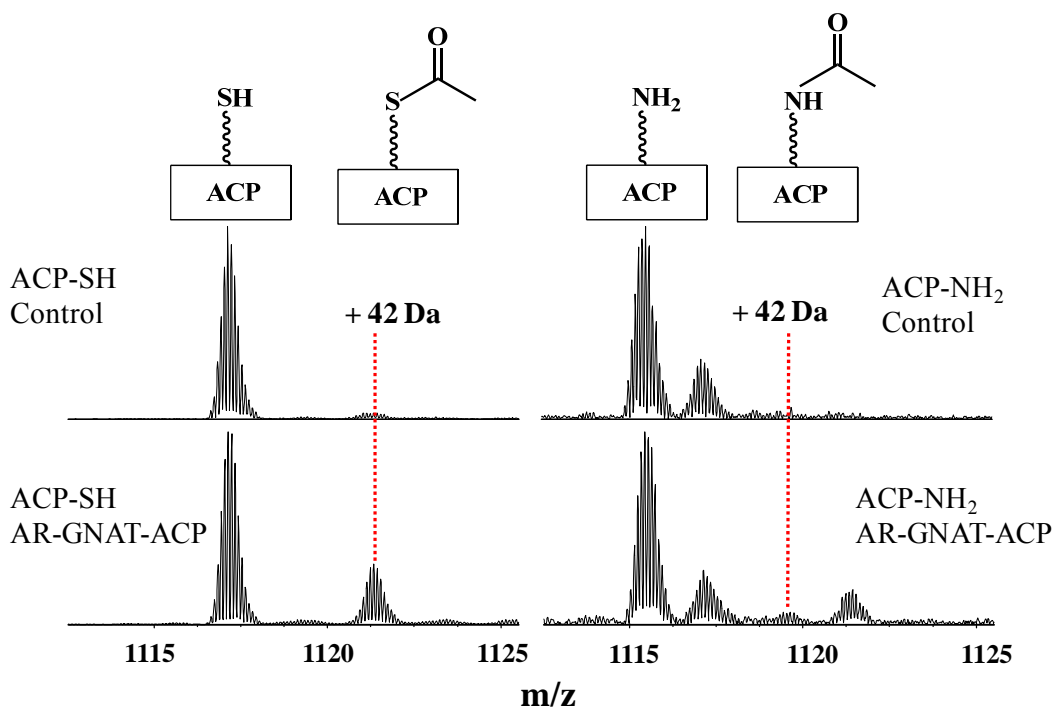


Figure 7.6. Partial FT-ICR mass spectra of *holo*-ACP-SH (left) and *holo*-ACP-NH₂ (right) incubated with the AR-GNAT-*apo*-ACP tridomain in the presence of malonyl-CoA. Acetyl transfer to *holo*-ACP-SH can be readily observed whereas no significant signal is seen for the NH₂ counterpart.

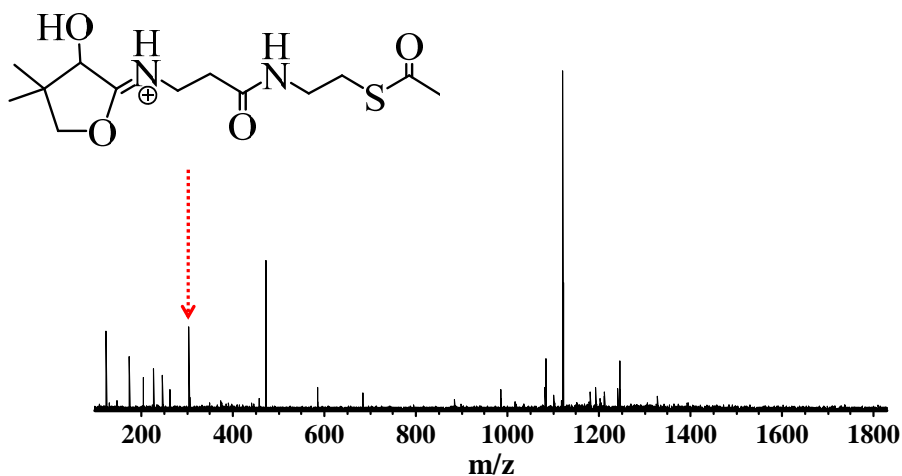


Figure 7.7. IRMPD of the acetyl transfer product of *holo*-ACP-SH. The indicated PPant ejection ion was observed.

FT-ICR MS and IRMPD also revealed that the Cur GNAT has decarboxylation function: after incubating *holo*-ACP with either acetyl-CoA or malonyl-CoA and AR-GNAT-*apo*-ACP, the same product, acetyl-*holo*-ACP, was observed (as shown in Figure 7.8). Because acetyl-CoA and malonyl-CoA differ by one carboxyl group in their chemical structures, AR-GNAT-*apo*-ACP must catalyze decarboxylation along with acetyl transfer. Similar results were observed on the peptide level, as shown in row C, Figure 7.5. Here, acetyl addition was observed in the AR-GNAT-*holo*-ACP tridomain after incubation with malonyl-CoA, demonstrating the occurrence of decarboxylation. In addition, the AR domain is important for effective acetyl transfer. As shown in Figure 7.8,

GNAT-ACP without AR provides much lower acetyl transfer yield than AR-GNAT-ACP.

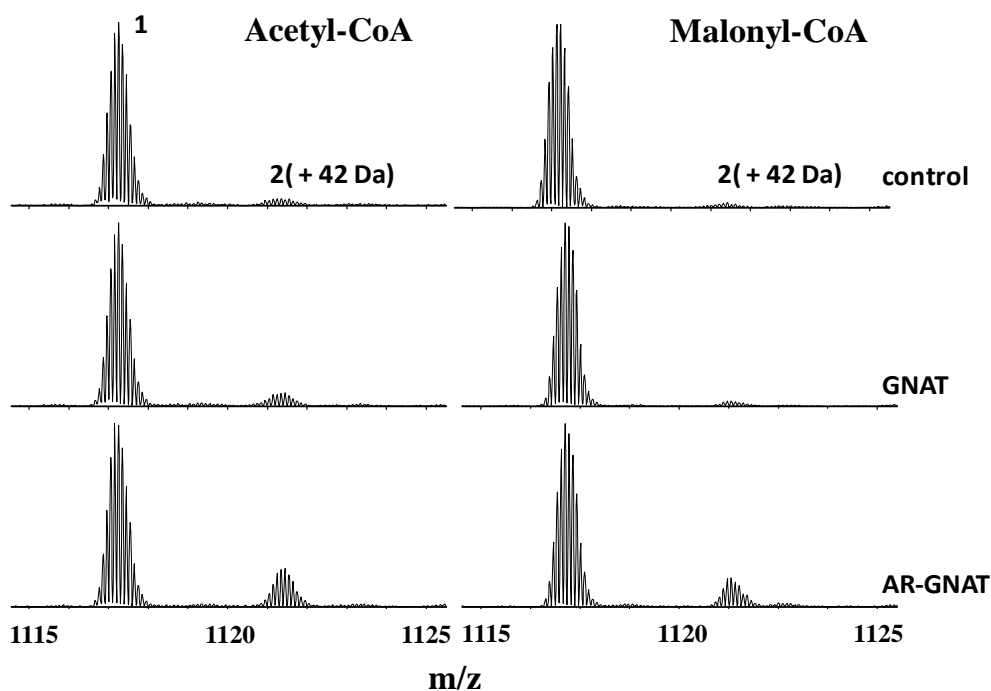


Figure 7.8. FT-ICR MS comparison of the acetyl transfer efficiency of GNAT-*apo*-ACP didomain and GNAT monodomain from acetyl- and malonyl-CoA, respectively. The substrate and product are *holo*-ACP (1) and acetyl-*holo*-ACP (2), respectively.

7.3.2 Functional determination of Cur Hal, ECH₁s, ECH₂s, and ERs from Cur and Jam

Top-down FT-ICR MS analysis of reaction products from Cur Hal, ECH₁, ECH₂, and ER catalysis is shown in Figure 7.9. Incubation of 1-ACP_{II} with Cur ECH₁ and Cur

ECH₂ resulted in dehydration and decarboxylation, respectively. When Cur ER and NADPH were added, a +2 Da shift relative to the decarboxylation product (**3**-ACP_{II}) was observed to yield **4**-ACP_{II}. This reaction represents the canonical ER function of reducing α,β C=C bonds. Reduction was confirmed by IRMPD (Table 7.2, PPant ejection ion from **4**-ACP_{II}).

Cur Hal was confirmed to catalyze mono-chlorination (**1**-ACP_{II} to Cl-**1**-ACP_{II}), as shown in Figure 7.9. The chlorinated product (Cl-**1**-ACP_{II}) was incubated with Cur ECH₁, ECH₂ and ER in a similar manner as described for **1**-ACP_{II} above. As expected, successive dehydration and decarboxylation was observed when ECH₁ and ECH₂ were present. However, when Cur ER and NADPH were added along with ECH₁ and ECH₂, the expected saturation product was absent and a peak with the same m/z value as **4**-ACP_{II} was observed, indicating elimination of chlorine and possible formation of **5**-ACP_{II}, containing the cyclopropyl ring. The structures of **4**-ACP_{II} and **5**-ACP_{II} were confirmed by the Sherman and Wipf groups based on synthesis of authentic standards and GC-MS. This discovery reveals that Cur ER not only keeps the canonical function of reducing α,β C=C bond but also evolved the unprecedented function of catalyzing a cyclopropanation reaction.

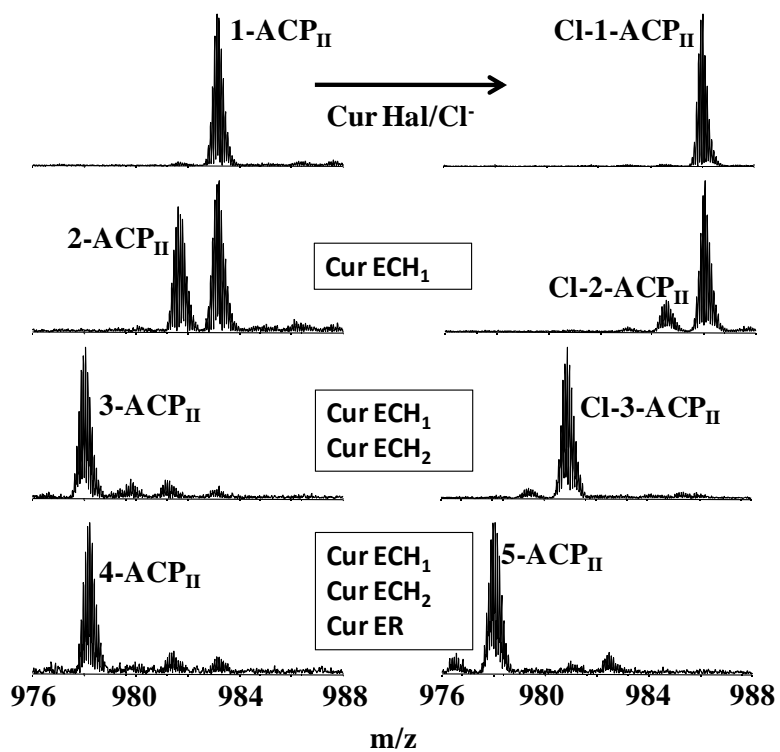
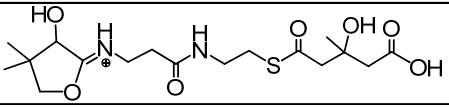
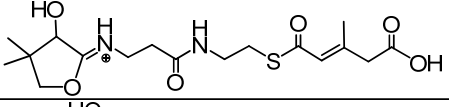
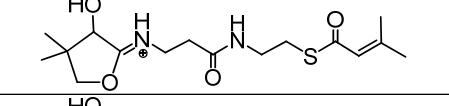
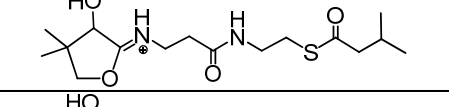
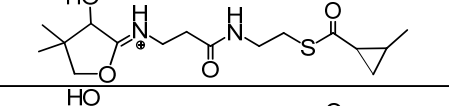
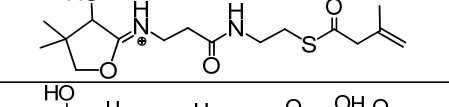
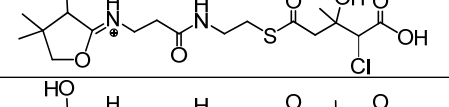
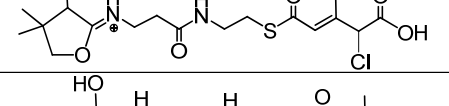
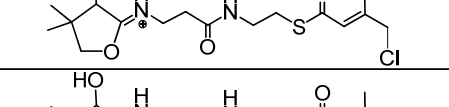
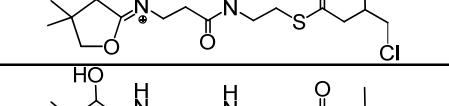
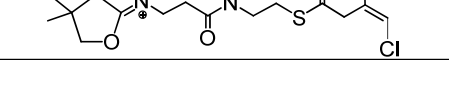


Figure 7.9. FT-ICR MS analysis of 1-ACP_{II} and Cl-1-ACP_{II} after incubation with different combinations of Cur ECH₁, ECH₂, and ER/NADPH.

Table 7.2. ESI FT-ICR MS and IRMPD analysis of various ACP_{II} products.

ACP _{II} samples	ESI-FT-ICR MS		IRMPD	Calculated Mass [M + H] ⁺	Observed Mass [M + H] ⁺
	Calculated Mass (avg.)	Observed Mass (avg.)	Structures of PPant ejection ions		
apo-ACP _{II}	11300.8	11300.7			
1-ACP _{II}	11785.9	11785.9		405.170	405.174
2-ACP _{II}	11767.9	11767.9		387.159	387.164
3-ACP _{II}	11723.9	11723.9		343.169	343.174
4-ACP _{II}	11725.9	11725.9		345.185	345.190
5-ACP _{II}	11723.9	11723.9		343.169	343.169
6-ACP _{II}	11723.9	11723.9		343.169	343.163
Cl-1-ACP _{II}	11819.9	11819.8		439.131	439.128
Cl-2-ACP _{II}	11801.9	11802.0		421.120	421.110
Cl-3-ACP _{II}	11757.9	11757.9		377.130	377.140
Cl-4-ACP _{II}	11759.9	11759.8		379.146	379.156
Cl-6-ACP _{II}	11757.9	11757.8		377.130	377.141

Masses are in Daltons.

Subsequent experiments were carried out to investigate the function of ECH₁, ECH₂ and ER from Jam, as shown in Figure 7.10. Compared to Cur ER, incubation of Cl-**3**-ACP_{II} (from reaction with Cur ECH₁ and ECH₂) with Jam ER and NADPH did not produce **5**-ACP_{II} but Cl-**4**-ACP_{II} (with a +2 Da shift relative to Cl-**3**-ACP_{II}), indicating that Jam ER has the canonical α,β C=C reduction function and does not catalyze cyclopropanation. Furthermore, the function of Jam ER seems redundant in the Jam pathway. As shown in Figure 7.11, the product from incubation of Cl-**1**-ACP_{II} with Jam ECH₁ and ECH₂ has different behavior than the product from incubation of Cl-**1**-ACP_{II} with Cur ECH₁ and ECH₂: the former product does not undergo further reaction (i.e., reduction of cyclopropyl formation) when incubated with either Cur or Jam ER. IRMPD of products from incubation of Cl-**1**-ACP_{II} or **1**-ACP_{II} with Jam ECH₁ and ECH₂ also showed that addition of Jam ER and NADPH did not change the peak abundance at the n + 2 position of the PPant ejection ion (corresponding to C=C bond reduction) relative to the monoisotopic peak (n) (Figure 7.11). The structure of the product from incubation of **1**-ACP_{II} with Jam ECH₁ and ECH₂ was confirmed by GC-MS involving synthesized authentic standards [16] to have β,γ C=C bond (**6**-ACP_{II}), thus Cl-**6**-ACP_{II} has a vinyl chloride moiety which cannot be introduced by Cur or Jam ER. Therefore, the function of Jam ER (for α,β C=C reduction) is redundant in the Jam biosynthetic pathway.

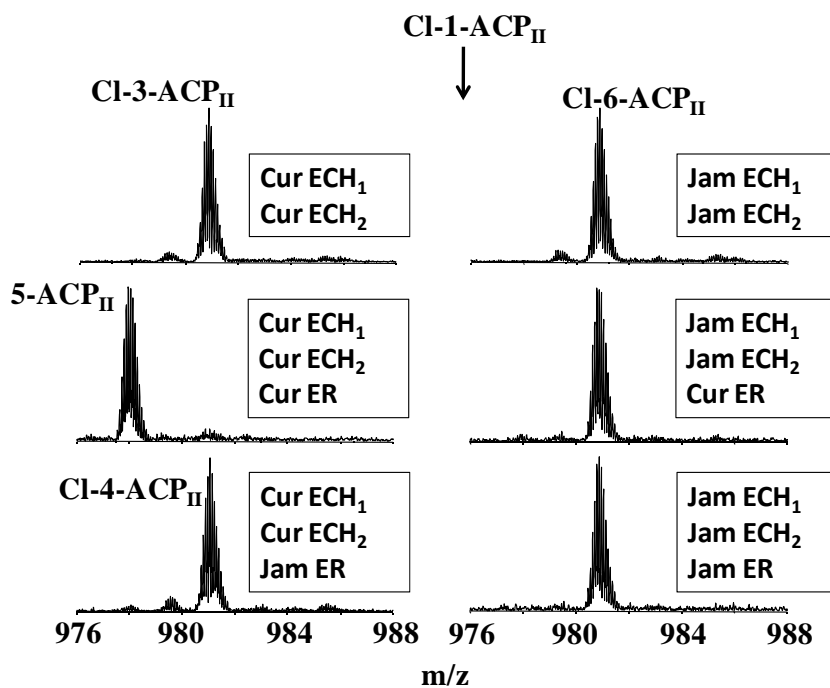


Figure 7.10. FT-ICR MS analysis of Cl-1-ACP_{II} incubated with ECH₁, ECH₂, and ER from Cur or Jam.

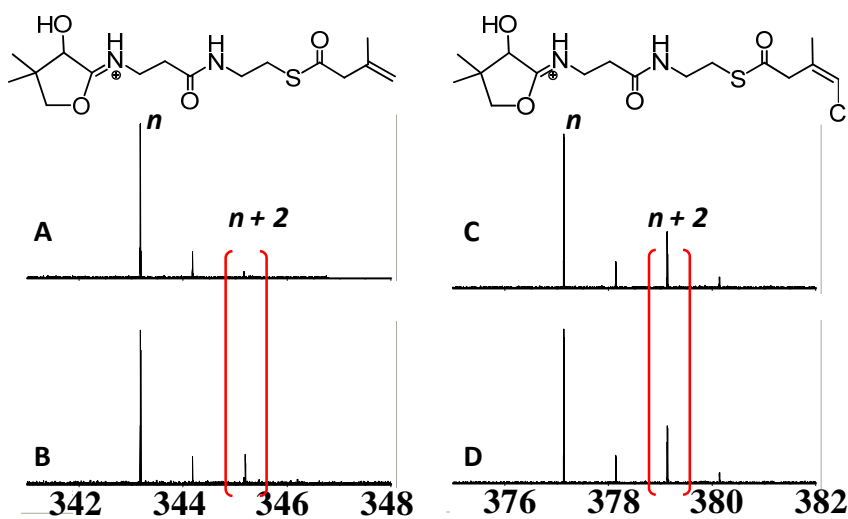


Figure 7.11. IRMPD of products from 1-ACP_{II} (panels A and B) and Cl-1-ACP_{II} (panels

C and D) incubated with Jam ECH₁ and ECH₂ (panels A and C) and Jam ECH₁, ECH₂, and ER (panels B and D). No significant change in peak abundance at the n + 2 position relative to the corresponding unsaturated PPant ejection ion was seen for Cl-**1**-ACP_{II}.

7.3.3 Functional differentiation of ERs from Cur and Jam

As mentioned above, Cur ER shows the unprecedented function of catalyzing a cyclopropanation reaction. At the same time, Cur ER and Jam ER have both demonstrated the canonical function of saturating α,β C=C bond. Thus, we explored the interesting comparison of Cur ER and Jam ER catalytic efficiencies for cyclopropanation and saturation, respectively, by FT-ICR MS.

The α,β C=C saturation, (e.g., by converting Cl-**3**-ACP_{II} to Cl-**4**-ACP_{II}) does not affect ESI efficiency and the products and substrates have similar charge states distributions. Therefore, a single protein charge state can be selected for analysis [17]. In this Chapter, quantification based on a single charge state (+12) selected for fragmentation is shown (see below) to yield identical results as subjecting the entire charge state distribution to IRMPD. Thus, we focused on the +12 charge state for IRMPD analysis. For Cur ER cyclopropanation, quantification of **5**-ACP_{II} was achieved by using **4**-ACP_{II} as an internal standard. No desaturation product of **4**-ACP_{II} was detected to interfere with the **5**-ACP_{II} measurement. Relative catalytic yield can be obtained by measuring the ratio of the PPant ejection ions from ACP_{II}-related species with a two Dalton mass difference, i.e., peaks n and n+2, respectively.

Before comparing the catalytic efficiencies of ERs from Cur and Jam, the

IRMPD-based quantification method was validated by analyzing a series of known mixtures of ER-related substrates/products or internal standard/product pairs, including 3-ACPII/4-ACPII, Cl-3-ACPII/Cl-4-ACPII, and 4-ACPII (used as internal standard)/5-ACPII. As shown in Figure 7.11, all three pairs show good agreement (linearity) between the known ratio and the IRMPD measurement. A linear dynamic range of 2-80% is demonstrated.

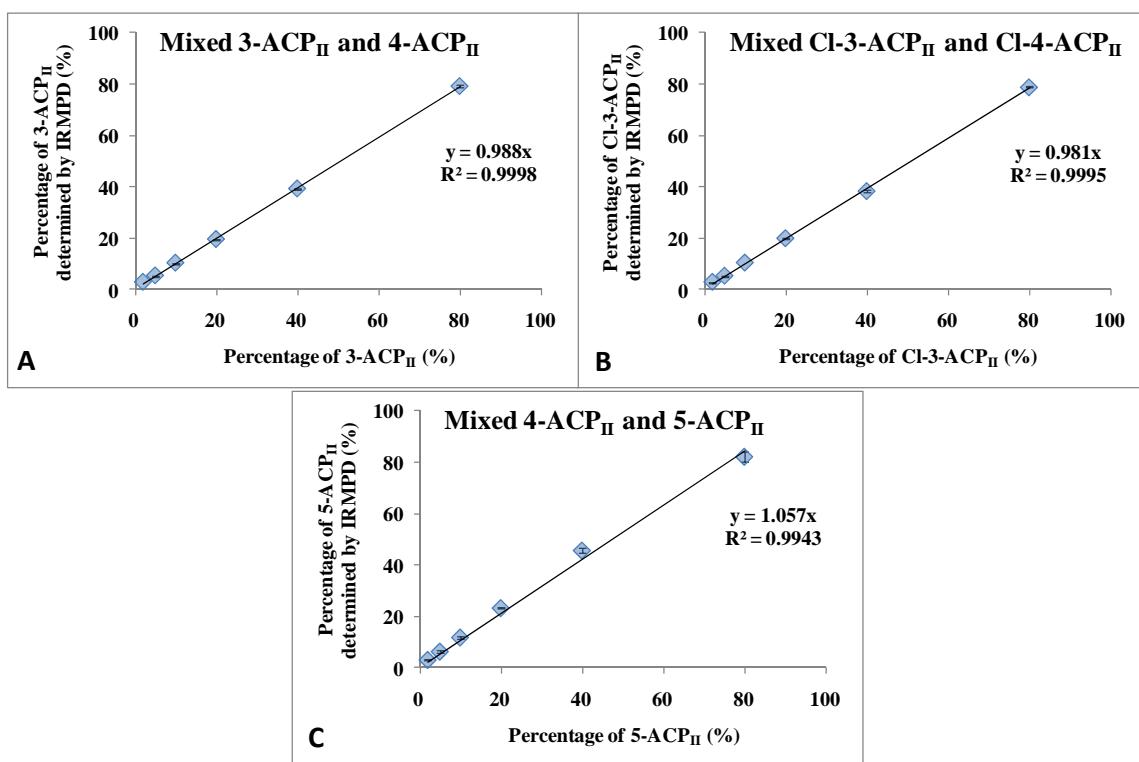


Figure 7.12. 3-ACPII/4-ACPII (panel A), Cl-3-ACPII/Cl-4-ACPII (panel B), and 4-ACPII/5-ACPII (panel C) were mixed at known ratios and quantified by IRMPD. Each measurement was performed in triplicate to obtain a standard deviation.

After validating the IRMPD-based quantification method, time-course studies of

catalytic efficiencies were performed, as shown in Figure 7.13. These data demonstrate that Jam ER saturation of α,β C=C is much faster (by ~240-fold) than that of Cur ER saturation under identical experimental conditions. Jam ER has retained a canonical α,β C=C reduction function and so has Cur ER but with lower efficiency. In addition, Cur ER has gained the unprecedented ability for cyclopropanation of a chlorinated substrate (by the upstream Cur Hal). These results provide unique insights into functional group diversity in secondary metabolites.

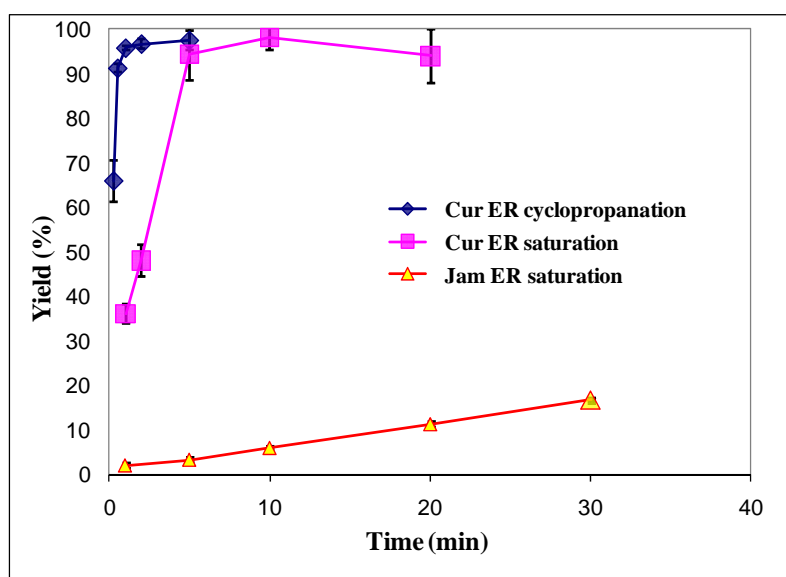


Figure 7.13. Catalytic efficiencies for cyclopropanation and saturation of Cur and Jam ERs. All time-course studies were performed in triplicate under the same reaction conditions.

7.3.4 Application of IRMPD to reveal crucial residues for Cur Hal catalysis

Chlorination assay (from 1-ACP_{II} to Cl-1-ACP_{II}) was developed by Dr. Gu from

Sherman's lab. Briefly, the chlorination reaction was carried out in a 110 μ L mixture containing 5 μ M Hal, 10 mM Tris-HCl (pH 7.8), 100 μ M fresh $\text{Fe}(\text{NH}_4)_2(\text{SO}_4)_2$, 25 μ M **1-ACP_{II}**, and 1 mM α -ketoglutarate. The mixture was incubated at 24 °C for 10 min and the reaction was quenched by adding 20 μ L formic acid. HPLC (Source 15RPC column from GE Healthcare with linear gradient from 30% to 70% CH_3CN) was then applied to purify the product for subsequent MS analysis. Based on the crystal structure of Cur Hal obtained by the Smith group, selected residues were mutated to elucidate substrate recognition and binding of chloride and α KG. IRMPD was applied to monitor PPant ejection ions from the substrate (**1-ACP_{II}**, m/z 405) and product (**Cl-1-ACP_{II}**, m/z 439) of the Hal reaction and thereby evaluate the Cur Hal catalytic efficiency. The corresponding results are shown in Figure 7.14. Wild type Cur Hal showed ~82% relative yield. A conservative substitution, Leu112 to Ile, provided a similar value, 72%. Replacement of Arg241 and Arg247, which are basic residues and believed to anchor α KG to the Cur Hal active site,[18], with Ala rendered **Cl-1-ACP_{II}** almost undetectable, indicating nearly complete functional loss of Cur Hal. Substituting Ser 120, which was believed to bind Cl^- via hydrogen bonding, and Ser132, which connects to the Cur Hal active site through a hydrogen bond, with Ala had similar effects as the arginine mutations. Mutation of residues in the active site lid resulted in loss of Cur Hal function to various extents. Among these mutations, the largest functional loss, up to 20 fold, was observed for K50, K54, and Y68. Ala substitution of Ser44 and K48 resulted in 4-6 fold functional loss, indicating that those residues may influence the catalysis indirectly.

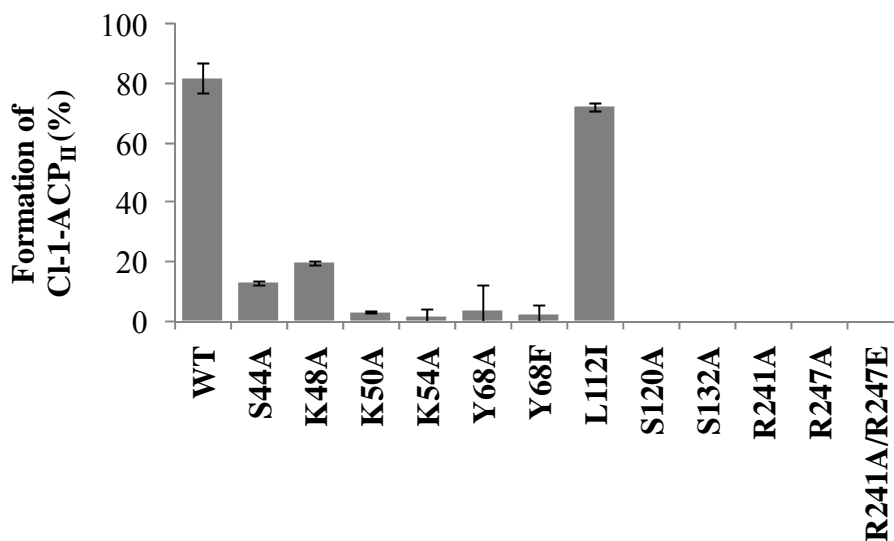


Figure 7.14. Catalytic efficiencies of WT Cur Hal and site-specific Hal mutants from IRMPD-based quantification.

7.3.5 Characterization of products from ST and TE catalysis in the termination module of CurA biosynthesis

The Cur chain termination, which involves formation of an unusual terminal olefin (Figure 7.2), was also studied, as shown in Figure 7.15. After treating *holo*-ACP_{III} (**1**-ACP_{III}, see Fig. 7.14) with ST in the presence of adenosine 3'-phosphate 5'-phosphosulfate (row C), a product with +80 Da shift was observed, indicating addition of an SO₃⁻ group to form **2**-ACP_{III}. When **1**-ACP_{III} was treated with ST and TE, a product with a -256 Da shift (ACP_{III} tethered to PPant with a free SH group, denoted as **3**-ACP_{III}) was observed. Combined with other data from the Sherman lab, addition of an SO₃⁻ group is believed to occur on **1**-ACP_{III} (catalyzed by ST) to form **2**-ACP_{III} followed by

product release (by the TE) involving decarboxylative chain termination to form **3-ACP_{III}** [19]. Because sulfate groups are highly labile in the gas phase, IRMPD was unable to differentiate between **1-ACP_{III}** and **2-ACP_{III}**, which generated the same PPant ejection ion.

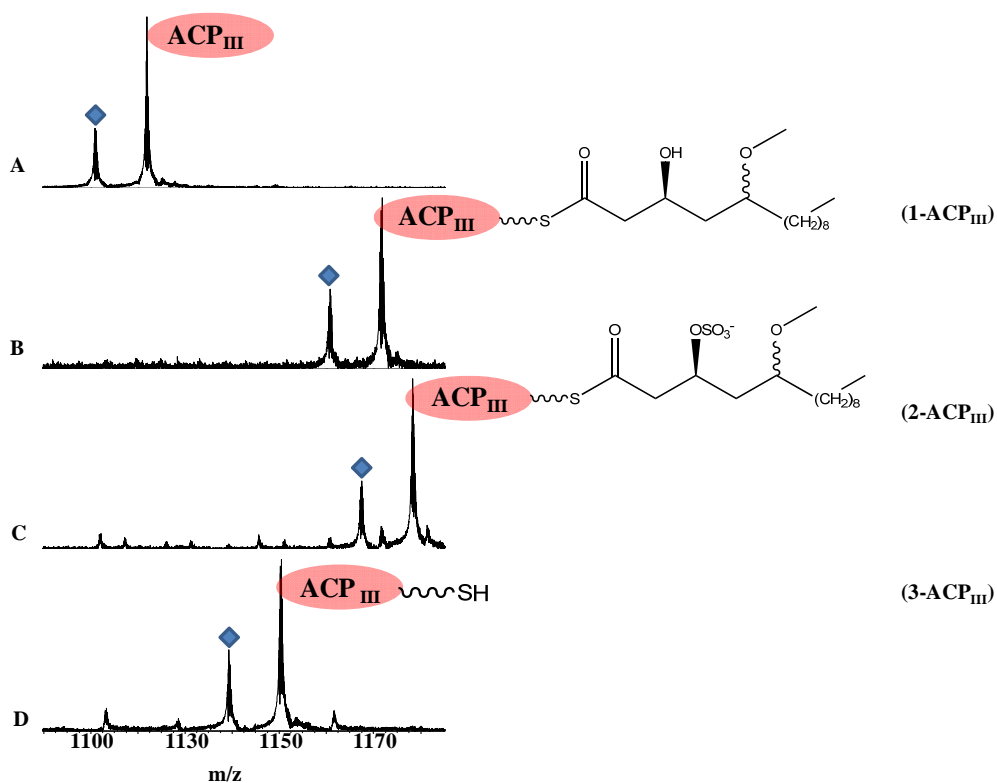


Figure 7.15. FT-ICR MS analysis of *apo*-ACP_{III} (A), *holo*-ACP_{III} (B), and *holo*-ACP_{III} incubated with ST (C), and ST + TE (D). Peaks labeled with diamonds in A-D correspond to ACP_{III} lacking an N-terminal methionine relative to the heavier form of ACP_{III}.

7.4 Summary

In this Chapter, FT-ICR MS was successfully applied to characterize enzymatic

reactions in the Cur and Jam biosynthetic pathways. There are two main approaches to reach that goal. First, top-down analysis can provide accurate mass of substrate and product and enzyme function can be revealed from observed mass shifts. For example, -18 Da shift indicates dehydration and + 80 Da shift may correspond to SO_3^- group addition. Second, IRMPD can be applied to investigate and confirm reaction mechanisms due to generation of specific PPant ejection ions. In addition, substrate and product structural information generally remains on PPant ejection ions and, therefore, simplifies characterization of substrates and products. For example, C=C saturation, which only causes a 2 Da mass difference, can be successfully characterized and differentiated by IRMPD whereas it is difficult to decipher in a top-down approach..

FT-ICR MS and IRMPD revealed that Cur GNAT has the unprecedented function of transferring an acetyl group to a free thiol group, instead of the canonical amine group. The N-terminal AR domain is important for this novel function of GNAT. In addition, the Cur GNAT displays bifunctional activity by also catalyzing decarboxylation.

ECH_1 and ECH_2 from Cur and Jam appear at first glance to both catalyze dehydration ($\text{ECH}_{1\text{s}}$) and decarboxylation ($\text{ECH}_{2\text{s}}$) based on accurate mass shifts. However, further analysis involving both FT-ICR MS and other approaches, such as GC-MS and organic synthesis, revealed that ECH_1 and ECH_2 from Cur generate a product with α,β C=C moiety whereas Jam ECH_1 and ECH_2 yield β,γ C=C. The function of Cur Hal was revealed to involve formation of mono-chlorinated product. Coupled with Cur Hal, ECH_1 , and ECH_2 , Cur ER was revealed to have the unprecedented function of catalyzing cyclopropanation. At the same time, Cur ER still retains the canonical function of the ER enzyme family to reduce α,β C=C bond. The saturation function of

Jam ER is redundant in Jam biosynthesis because the formation of β,γ C=C and vinyl chlorination are catalyzed by upstream enzymes (Hal, ECH₁ and ECH₂).

The catalytic efficiencies of Cur ER cyclopropanation and Cur and Jam ER saturation were also evaluated. IRMPD results showed that Cur ER catalyzes cyclopropanation much faster, ~240 fold, than saturation. Jam ER can still efficiently catalyze a saturation reaction. We applied a similar strategy to explore the catalytic efficiency of Hal following a series of site-specific mutations. Finally, FT-ICR MS was applied to investigate the sequential addition and release of SO₃⁻ on ACP_{III}, catalyzed by ST and TE, respectively, thereby providing insight into the decarboxylative chain termination, which results in a terminal olefin, in the Cur biosynthetic pathway.

7.5 References

1. Wipf, P.; Reeves, J.T.; Balachandran, R.; Day, B.W., Synthesis and biological evaluation of structurally highly modified analogues of the antimitotic natural product curacin A. *J. Med. Chem.*, **2002**, *45*, 1901-1917.
2. Schwecke, T.; Aparicio, J.F.; Molnar, I.; Konig, A.; Khaw, L.E.; Haydock, S.F.; Oliynyk, M.; Caffrey, P.; Cortes, J.; Lester, J.B.; Bohm, G.A.; Staunton, J.; Leadlay, P.F., The Biosynthetic Gene-Cluster for the Polyketide Immunosuppressant Rapamycin. *Proc. Natl. Acad. Sci. U. S. A.*, **1995**, *92*, 7839-7843.
3. Chang, Z.X.; Sitachitta, N.; Rossi, J.V.; Roberts, M.A.; Flatt, P.M.; Jia, J.Y.; Sherman, D.H.; Gerwick, W.H., Biosynthetic pathway and gene cluster analysis of curacin A, an antitubulin natural product from the tropical marine cyanobacterium *Lyngbya majuscula*. *J. Nat. Prod.*, **2004**, *67*, 1356-1367.
4. Vaillancourt, F.H.; Yeh, E.; Vosburg, D.A.; O'Connor, S.E.; Walsh, C.T., Cryptic chlorination by a non-haem iron enzyme during cyclopropyl amino acid biosynthesis. *Nature*, **2005**, *436*, 1191-1194.
5. Vaillancourt, F.H.; Yin, J.; Walsh, C.T., SyrB2 in syringomycin E biosynthesis is a

- nonherne Fe-II alpha-ketoglutarate- and O-2-dependent halogenase. *Proc. Natl. Acad. Sci. U. S. A.*, **2005**, *102*, 10111-10116.
6. Galonic, D.P.; Vaillancourt, F.H.; Walsh, C.T., Halogenation of unactivated carbon centers in natural product biosynthesis: Trichlorination of leucine during barbamide biosynthesis. *J. Am. Chem. Soc.*, **2006**, *128*, 3900-3901.
 7. Flatt, P.M.; O'Connell, S.J.; McPhail, K.L.; Zeller, G.; Willis, C.L.; Sherman, D.H.; Gerwick, W.H., Characterization of the initial enzymatic steps of barbamide biosynthesis. *J. Nat. Prod.*, **2006**, *69*, 938-944.
 8. Vaillancourt, F.H.; Yeh, E.; Vosburg, D.A.; Garneau-Tsodikova, S.; Walsh, C.T., Nature's inventory of halogenation catalysts: Oxidative strategies predominate. *Chem. Rev.*, **2006**, *106*, 3364-3378.
 9. Gu, L.C.; Jia, J.Y.; Liu, H.C.; Hakansson, K.; Gerwick, W.H.; Sherman, D.H., Metabolic coupling of dehydration and decarboxylation in the curacin A pathway: Functional identification of a mechanistically diverse enzyme pair. *J. Am. Chem. Soc.*, **2006**, *128*, 9014-9015.
 10. Nordling, E.; Jornvall, H.; Persson, B., Medium-chain dehydrogenases/reductases (MDR) - Family characterizations including genome comparisons and active site modelling. *Eur. J. Biochem.*, **2002**, *269*, 4267-4276.
 11. Iglesias, A.H.; Santos, L.F.A.; Gozzo, F.C., Collision-Induced Dissociation of Lys-Lys Intramolecular Crosslinked Peptides. *J. Am. Soc. Mass Spectrom.*, **2009**, *20*, 557-566.
 12. Senko, M.W.; Canterbury, J.D.; Guan, S.H.; Marshall, A.G., A high-performance modular data system for Fourier transform ion cyclotron resonance mass spectrometry. *Rapid Commun. Mass Spectrom.*, **1996**, *10*, 1839-1844.
 13. Ledford, E.B.; Rempel, D.L.; Gross, M.L., Space-Charge Effects in Fourier-Transform Mass-Spectrometry - Mass Calibration. *Anal. Chem.*, **1984**, *56*, 2744-2748.
 14. Dorrestein, P.C.; Bumpus, S.B.; Calderone, C.T.; Garneau-Tsodikova, S.; Aron, Z.D.; Straight, P.D.; Kolter, R.; Walsh, C.T.; Kelleher, N.L., Facile detection of acyl and peptidyl intermediates on thiotemplate carrier domains via phosphopantetheinyl elimination reactions during tandem mass spectrometry. *Biochemistry*, **2006**, *45*, 12756-12766.
 15. Vetting, M.W.; de Carvalho, L.P.S.; Yu, M.; Hegde, S.S.; Magnet, S.; Roderick, S.L.; Blanchard, J.S., Structure and functions of the GNAT superfamily of acetyltransferases. *Arch. Biochem. Biophys.*, **2005**, *433*, 212-226.
 16. Gu, L.; Wang, B.; Kulkarni, A.; Geders, T.W.; Grindberg, R.V.; Gerwick, L.; Hakansson, K.; Wipf, P.; Smith, J.L.; Gerwick, W.H.; Sherman, D.H., Metamorphic enzyme assembly in polyketide diversification. *Nature*, **2009**, *459*, 731-735.
 17. Gordon, E.F.; Mansoori, B.A.; Carroll, C.F.; Muddiman, D.C., Hydrophobic influences on the quantification of equine heart cytochrome c using relative ion abundance measurements by electrospray ionization Fourier transform ion cyclotron resonance mass spectrometry. *J. Mass Spectrom.*, **1999**, *34*, 1055-1062.
 18. Khare, D.W., B.; Gu, L.; Razelun, J.; Sherman, D.H.; Gerwick, W.H.; Håkansson, K.; and Smith, J.L., Conformational Switch Triggered by α -Ketoglutarate in a

- Halogenase of Curacin A Biosynthesis. *Proc. Natl. Acad. Sci.*, **2010**, in press.
19. Gu, L.; Wang, B.; Kulkarni, A.; Gehret, J.J.; Lloyd, K.R.; Gerwick, L.; Gerwick, W.H.; Wipf, P.; Hakansson, K.; Smith, J.L.; Sherman, D.H., Polyketide decarboxylative chain termination preceded by o-sulfonation in curacin a biosynthesis. *J. Am. Chem. Soc.*, **2009**, *131*, 16033-16035.

Chapter 8

Summary and Prospects for Future Studies

8.1 Summary and Conclusion

8.1.1 The Goals of the Dissertation

Mass spectrometry (MS) combined with chemical cross-linking has become a promising technique to characterize protein structure at low resolution and protein-protein interactions. Advantages provided by MS include high sample throughput, high sensitivity, and lenient requirements for sample purity. Coupled with proteolysis and liquid chromatography (LC), large protein complexes with molecular weights up to 670 kDa have been characterized [1].

However, efficient identification of cross-linked peptides remains challenging. Difficulties include: 1) how to generate MS signals for cross-linked peptides; and 2) how to differentiate such signals from peaks corresponding to unmodified peptides. For the first challenge, cross-linked peptides suffer from low cross-linking yield and ion suppression by the large excess of unmodified peptides. The chemical cross-linking yield can be improved by controlling reaction conditions, including the molar ratio of sample and cross-linker, pH value, and modification of reactive groups [2]. LC/MS can be applied to alleviate the ion suppression effect but is unable to completely solve this

problem because a number of unmodified peptides may still co-elute with cross-linked peptides and thereby influence their ionization efficiencies. In addition, optimizing the separation of cross-linked peptides from unmodified peptides in LC is time and sample consuming. For the second challenge, cross-linked peptide signals are difficult to differentiate from those of unmodified peptides in MS/MS because product ions from cross-linked peptides can be either the same as for the corresponding non-cross-linked peptides, or carry “mystery” mass shifts. Such mass shifts are difficult to identify because all possible combinations of proteolytic peptides need to be considered, representing a significant computational problem [3].

To solve the first problem, affinity tags can be incorporated into cross-linkers to allow selective enrichment. To date, biotin is the most commonly used and commercially available affinity tag, however, biotin must be sufficiently distant from the reactive groups to minimize interferences. Therefore, long chain, e.g., polyethylene glycol, chains [4], are typically introduced to isolate the biotin group, which makes the cross-linker bulky. In addition, the length of this spacer arm normally exceeds the preferred range of 8-15 Å [2, 5], which may influence the acquisition of meaningful information on protein structure and interactions [2]. In addition, detergents are typically required to dissociate biotin-avidin interactions and removal of detergents prior to MS analysis may be challenging and cause sample loss. For the second problem, gas-phase cleavable cross-linkers, which display unique fragmentation patterns in MS/MS analysis, can be utilized. This strategy has been implemented with IR irradiation [6, 7], UV irradiation [8], or CID [9-13] to produce characteristic so called “reporter ions” [9], which provide identification of cross-linked products.

One of main purposes of this thesis is to explore efficient detection of cross-linked peptides in MS analysis, which includes: 1) designing cross-linker with novel enrichment potential, 2) investigating optimal MS/MS approaches to induce efficient gas-phase fragmentation of cross-linked peptides with disulfide bond linkage, and 3) study the C-I bond cleavage under ECD with the aim to design the cross-linker with unique mass loss in MS/MS analysis. The other goal for this thesis is to apply chemical cross-linking, MS and MS/MS techniques to reveal protein-protein interaction, enzyme function, and enzyme function differentiation.

8.1.2 Summary of Experimental Results

In this thesis, interactions between gene transcriptional activators and co-activator (mediator) 15 were characterized. In some cases, the binding site could be localized to a single amino acid residue. The successful mapping of such *in vitro* protein-protein interactions relied on the complementary use of multiplexed MS and MS/MS techniques. Incorporation of a redox-sensitive biotin tag into transcriptional activators containing a photo-cross-linking group was also important. Notably, C-C and C-S bond cleavages in the photo-cross-linker moiety were observed in MALDI TOF/TOF CID. In some cases, such cleavages resulted in free mediator tryptic peptides. To our knowledge, this unique fragmentation behavior in MALDI TOF/TOF CID has not previously been reported.

A novel peptide-based cross-linker was synthesized by incorporating an N-terminal phosphate group and two amine reactive groups in the middle and at the C-terminus, respectively. This cross-linker demonstrated amine reactivity and an intramolecularly cross-linked product could be selectively enriched by TiO₂ and ZrO₂.

Compared with biotin-based enrichment, which typically involves MS-unfriendly salts and detergents, selective enrichment of phosphate-containing cross-linked product by metal dioxides can be achieved simply by changing the pH.

Fragmentation patterns of peptides chemically cross-linked with disulfide bond-containing cross-linkers were investigated in ECD, EDD, negative ion CID, and MALDI TOF/TOF CID. The purpose of this project was to find an optimal gas-phase cleavage approach to facilitate selective identification of cross-linked peptides. Results demonstrated that combined use of ECD and MALDI TOF/TOF CID would provide efficient S-S and C-S bond cleavages in the cross-linker.

Highly selective C-I bond cleavage in ECD and ETD was observed. Data also demonstrated that a through-bond or through-space proximate positively charged group can facilitate and enhance C-I bond cleavage. These results provide a guide to designing novel cross-linkers, for which the unique mass of iodine loss (125.9 Da) would be helpful to differentiate cross-linked peptide signals in MS/MS analysis. In addition, these discoveries provide an additional model to understand the ECD/ETD mechanisms.

Quadrupole fractionation (QF) was revealed to achieve better detection of proteolytic peptides, particularly in the low m/z region (<700) than direct infusion (DI) mode. These results cannot be explained based on previous computational experiment, in which ions with higher m/z value were believed to have larger radius for radial stratification in RF-only multipoles and are more likely to lose [14]. Results in this thesis demonstrated that low m/z ions may still be axially lost due to the space charge repulsion from trailing higher m/z ions in DI analysis. Space charge repulsion can be removed in

QF analysis and therefore the detection of low m/z ions is improved. Further studies of ion motion in RF-only and mass-selective quadrupole would be necessary to explain the results in this Chapter.

Finally, FT-ICR MS and IRMPD were applied to characterize the function of enzymes from the *curacin A* and *Jamaicamide* biosynthetic pathways. Furthermore, IRMPD was applied to estimate catalytic efficiencies for several enzymes in both pathways. These results provide insights into the evolution and environmentally driven adaptation of these enzymes at the biochemical rather than genetic level.

8.2 Prospects for Future Studies

8.2.1 Photo-cross-linking and Mass Spectrometry

As discussed in Chapter 2, *in vitro* photo-cross-linking combined with multiplexed MS, MS/MS analyses, and avidin purification was successfully applied to characterize protein-protein interactions *in vitro*. Ideally, these methods should be extendable to *in vivo* analysis of protein complexes in their native environment. Incorporation of the photo-cross-linker p-benzoyl phenyl alanine (pBpa) into target protein *in vivo* by substituting endogenous residues can be achieved by genetic engineering [15, 16]. However, addition of an enrichment moiety to such cross-linkers would be highly challenging. Incorporation of single or tandem enrichment tags, including polyhistidine and biotin, has been reported [17, 18] but it will only enrich the undigested complex and not proteolytic cross-linked products. Formaldehyde-mediated protein cross-linking can also be applied *in vivo* [19]. However, this method is limited to

the identification of protein subunits in a protein complex and does not provide precise binding sites [20]. In addition, formaldehyde has a very short spacer arm (~about 2 Å) and will only cross-link residues that are in very close proximity [21]. Future directions in this area should focus on the design of specific unnatural amino acids that contain both cross-linking and enrichment moieties. For example, pBpa may be modified to introduce an alkyne group, which can be used for alkyne-azido “click” purification [22]. Once such unnatural amino acids are incorporated into target protein complexes, they could undergo cross-linking reaction and be subsequently enriched, particularly following proteolysis. In addition, such a method could be combined with other tags (e.g., histidine or biotin) to achieve purification of target protein complexes prior to proteolysis. Thus, the chance of observing cross-linked peptides should be enhanced.

8.2.2 Fragmentation Patterns of Cross-linked Peptides with Disulfide Bond Linkage

In Chapter 3, fragmentation patterns of cross-linked peptides with disulfide bond (S-S) linkage were investigated. S-S and C-S bond cleavages in various MS/MS approaches were the main focus of that study. Based on the results from ECD, EDD, negative ion CID, and MALDI TOF/TOF CID, the first and last of these MS/MS approaches were considered to be the optimal combination for inducing efficient S-S/C-S bond rupture and thereby aid the identification of S-S cross-linked peptides.

One remaining question is the preference of C-S cleavage vs. S-S cleavage. For example, in that work, efficient C-S bond cleavages were observed in MALDI TOF/TOF high energy CAD. On the other hand, efficient S-S bond cleavage is observed in ECD.

Because S-S and C-S bonds have similar dissociation energies [23], it would be interesting to further examine this phenomenon.

8.2.3 Design of a Novel Cross-linker with Metal Dioxide Enrichment Potential or Unique Fragmentation Pattern

In Chapter 5, efforts were discussed to design a peptide-based cross-linker with $\text{TiO}_2/\text{ZrO}_2$ enrichment potential. A phosphate group was positioned at the peptide N-terminus whereas two amine-reactive (N-hydroxysuccinimide (NHS)) groups were placed in the middle and at the C-terminus, respectively. The spatial distance between the phosphate group and the two NHS groups should be long enough to allow selective binding of the phosphate to $\text{TiO}_2/\text{ZrO}_2$. However, the observed enrichment efficiency was not ideal, which may be attributed to the branched nature of the cross-linker. In addition, only intramolecularly cross-linked peptides were observed for this cross-linker and efforts to obtain intermolecularly cross-linked species from model peptides and standard proteins were unsuccessful. To solve these problems, two amine-reactive groups need to be placed at both ends of a linear molecule with fixed length. A phosphate group could be incorporated by extending a branch at the middle of such a linear molecule. The length of that branch should be long enough to allow metal dioxide enrichment. Based on this idea, a potential design was developed by Prof. Larsen at the University of Michigan. The proposed structure, in which the phosphate group is incorporated via a PEG chain, is shown in Figure 8.1. The length of the PEG chain can be easily varied. In addition, the PEG chain can modulate the water solubility of the cross-linker.

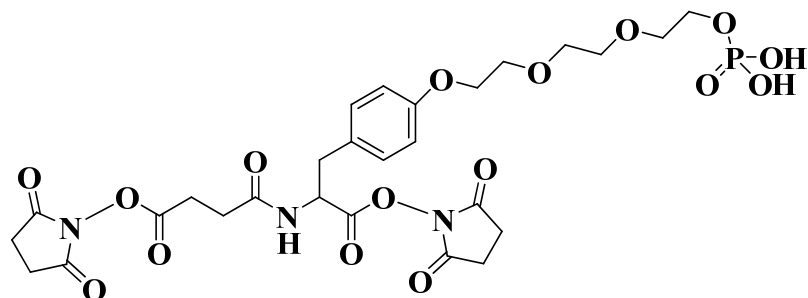


Figure 8.1. A novel cross-linker design suggested by Prof. Larsen.

In Chapter 4, C-I bond cleavage in ECD was examined. It was concluded that an adjacent positive charge, either through bond or through space, is required to obtain efficient C-I bond cleavage. This conclusion is very important for designing a novel cross-linker with a gas-phase labile C-I bond. The release of an iodine atom in MS/MS analysis yield a unique mass loss (125.9), which can facilitate differentiation of cross-linked peptide signals from those of unmodified peptides. Similar to the design of a phosphate-containing cross-linker, the iodine-based cross-linker can be designed as a linear molecule with amine-reactive groups at both ends. In addition, a fixed charged group and a C-I moiety can be placed in the middle of the backbone. Numerous reports have demonstrated the design and synthesis of such linear cross-linkers with reactive groups at both ends [10, 12, 24]. Further, incorporation of a fixed charge group into a cross-linker has also been reported [12]. Comparison of C-I bond cleavage in ECD and 266 nm UV laser irradiation would also be interesting. As mentioned in Chapter 4, the charge-directed C-I bond cleavage observed in ECD appears to be best explained by the “Utah-Washington” model for ECD [25, 26]. Such effects, however, should be absent under 266 nm UV irradiation. Therefore, C-I photodissociation may be more reliable

than that from ECD.

8.2.4 Study of Quadrupole Fractionation Mechanisms

As shown in Chapter 6, signal enhancements were observed in quadrupole fractionation (QF) analysis in the low m/z (i.e., 350-600) region in both positive and negative ESI mode. These results contradict previous computational analysis, which modeled radial oscillations of ions in RF-only multipoles as functions of mass and charge [14]. Higher m/z ions have higher radial oscillation radii and are therefore more likely to be radially lost. We concluded that space charge repulsion from trailing higher m/z ions may cause axial ejection of lower m/z ions. In QF analysis, space charge repulsion from higher m/z ions is removed, thus providing a benefit for the detection of low m/z ions. Further studies of ion motion in RF-only and mass-selective quadrupole modes, including computer simulations and analysis of different sample types (e.g., metabolites with m/z values below 700), would be necessary to explain the results in this Chapter.

8.2.5 MS/MS-based Approach to Study Enzyme Catalytic Efficiency

Results in Chapter 7 demonstrate that IRMPD can be applied to reveal enzyme catalytic efficiency. Spectral complexity is greatly reduced by selective cleavage of the reactive group off a carrier protein (PPant ejection). This method can be generalized as an MS/MS-based approach to estimate the relative ratio between substrate and product if: 1) the reaction occurs at a specific site in a protein (e.g., the PPant arm discussed in Chapter 7) and that region can be selectively cleaved in MS/MS; 2) the reaction does not result in big changes in ionization efficiency; and 3) the product can be purified for subsequent analysis. This MS/MS-based approach can be applied for time-course studies,

or for comparing the catalytic efficiency of related enzymes.

8.3 References

1. Chen, Z.A.; Jawhari, A.; Fischer, L.; Buchen, C.; Tahir, S.; Kamenski, T.; Rasmussen, M.; Lariviere, L.; Bukowski-Wills, J.C.; Nilges, M.; Cramer, P.; Rappsilber, J., Architecture of the RNA polymerase II-TFIIF complex revealed by cross-linking and mass spectrometry. *EMBO J.*, **2010**, *29*, 717-726.
2. Sinz, A., Chemical cross-linking and mass spectrometry to map three-dimensional protein structures and protein-protein interactions. *Mass Spectrom. Rev.*, **2006**, *25*, 663-682.
3. Rinner, O.; Seebacher, J.; Walzthoeni, T.; Mueller, L.; Beck, M.; Schmidt, A.; Mueller, M.; Aebersold, R., Identification of cross-linked peptides from large sequence databases. *Nat. Methods.*, **2008**, *5*, 315-318.
4. Fujii, N.; Jacobsen, R.B.; Wood, N.L.; Schoeniger, J.S.; Guy, R.K., A novel protein crosslinking reagent for the determination of moderate resolution protein structures by mass spectrometry (MS3-D). *Bioorg. Med. Chem. Lett.*, **2004**, *14*, 427-429.
5. Collins, C.J.; Schilling, B.; Young, M.L.; Dollinger, G.; Guy, R.K., Isotopically labeled crosslinking reagents: Resolution of mass degeneracy in the identification of crosslinked peptides. *Bioorg. Med. Chem. Lett.*, **2003**, *13*, 4023-4026.
6. Gardner, M.W.; Vasicek, L.A.; Shabbir, S.; Anslyn, E.V.; Brodbelt, J.S., Chromogenic cross-linker for the characterization of protein structure by infrared multiphoton dissociation mass spectrometry. *Anal. Chem.*, **2008**, *80*, 4807-4819.
7. Petrotchenko, E.V.; Xiao, K.H.; Cable, J.; Chen, Y.W.; Dokholyan, N.V.; Borchers, C.H., BiPS, a Photocleavable, Isotopically Coded, Fluorescent Cross-linker for Structural Proteomics. *Mol. Cell. Proteomics*, **2009**, *8*, 273-286.
8. Yang, L.; Tang, X.T.; Weisbrod, C.R.; Munske, G.R.; Eng, J.K.; von Haller, P.D.; Kaiser, N.K.; Bruce, J.E., A Photocleavable and Mass Spectrometry Identifiable Cross-Linker for Protein Interaction Studies. *Anal. Chem.*, **2010**, *82*, 3556-3566.
9. Tang, X.T.; Munske, G.R.; Siems, W.F.; Bruce, J.E., Mass spectrometry identifiable cross-linking strategy for studying protein-protein interactions. *Anal. Chem.*, **2005**, *77*, 311-318.
10. Soderblom, E.J.; Goshe, M.B., Collision-induced dissociative chemical cross-linking reagents and methodology: Applications to protein structural characterization using tandem mass spectrometry analysis. *Anal. Chem.*, **2006**, *78*, 8059-8068.
11. Chowdhury, S.M.; Munske, G.R.; Tang, X.T.; Bruce, J.E., Collisionally activated

- dissociation and electron capture dissociation of several mass spectrometry-identifiable chemical cross-linkers. *Anal. Chem.*, **2006**, *78*, 8183-8193.
12. Lu, Y.L.; Tanasova, M.; Borhan, B.; Reid, G.E., Ionic Reagent for Controlling the Gas-Phase Fragmentation Reactions of Cross-Linked Peptides. *Anal. Chem.*, **2008**, *80*, 9279-9287.
 13. King, G.J.; Jones, A.; Kobe, B.; Huber, T.; Mouvadov, D.; Hume, D.L.; Ross, I.L., Identification of disulfide-containing chemical cross links in proteins using MALDI-TOF/TOF-mass spectrometry. *Anal. Chem.*, **2008**, *80*, 5036-5043.
 14. Tolmachev, A.V.; Udseth, H.R.; Smith, R.D., Radial stratification of ions as a function of mass to charge ratio in collisional cooling radio frequency multipoles used as ion guides or ion traps. *Rapid Commun Mass Spectrom*, **2000**, *14*, 1907-1913.
 15. Rigaut, G.; Shevchenko, A.; Rutz, B.; Wilm, M.; Mann, M.; Seraphin, B., A generic protein purification method for protein complex characterization and proteome exploration. *Nat. Biotechnol.*, **1999**, *17*, 1030-1032.
 16. Suchanek, M.; Radzikowska, A.; Thiele, C., Photo-leucine and photo-methionine allow identification of protein-protein interactions in living cells. *Nat. Methods*, **2005**, *2*, 261-267.
 17. Nishio, K.; Iwamoto-Kihara, A.; Yamamoto, A.; Wada, Y.; Futai, M., Subunit rotation of ATP synthase embedded in membranes: α or β subunit rotation relative to the c subunit ring. *Proc. Natl. Acad. Sci. U. S. A.*, **2002**, *99*, 13448-13452.
 18. Nittis, T.; Guittat, L.; LeDuc, R.D.; Dao, B.; Duxin, J.P.; Rohrs, H.; Townsend, R.R.; Stewart, S.A., Revealing Novel Telomere Proteins Using in Vivo Cross-linking, Tandem Affinity Purification, and Label-free Quantitative LC-FTICR-MS. *Mol. Cell. Proteomics*, **2010**, *9*, 1144-1156.
 19. Orlando, V.; Strutt, H.; Paro, R., Analysis of chromatin structure by in vivo formaldehyde cross-linking. *Methods*, **1997**, *11*, 205-214.
 20. Toews, J.; Rogalski, J.C.; Clark, T.J.; Kast, J., Mass spectrometric identification of formaldehyde-induced peptide modifications under in vivo protein cross-linking conditions. *Anal. Chim. Acta*, **2008**, *618*, 168-183.
 21. Sutherland, B.W.; Toews, J.; Kast, J., Utility of formaldehyde cross-linking and mass spectrometry in the study of protein-protein interactions. *J. Mass Spectrom.*, **2008**, *43*, 699-715.
 22. Diaz, D.D.; Rajagopal, K.; Strable, E.; Schneider, J.; Finn, M.G., "Click" chemistry in a supramolecular environment: Stabilization of organogels by copper(I)-catalyzed azide-alkyne [3+2] cycloaddition. *J. Am. Chem. Soc.*, **2006**, *128*, 6056-6057.
 23. Franklin, J.L.; Lumpkin, H.E., Some C-S, H-S and S-S Bond Strengths by the Electron Impact Method. *J. Am. Chem. Soc.*, **1952**, *74*, 1023-1026.
 24. Liu, F.; Goshe, M.B., Combinatorial Electrostatic Collision-Induced Dissociative Chemical Cross-linking Reagents for Probing Protein Surface Topology. *Anal. Chem.*, **2010**, *82*, 6215-6223.
 25. Syrstad, E.A.; Turecek, F., Toward a general mechanism of electron capture dissociation. *J. Am. Soc. Mass Spectrom.*, **2005**, *16*, 208-224.

26. Sobczyk, M.; Anusiewicz, W.; Berdys-Kochanska, J.; Sawicka, A.; Skurski, P.; Simons, J., Coulomb-assisted dissociative electron attachment: Application to a model peptide. *J. Phys. Chem. A*, **2005**, *109*, 250-258.